Australian Tropical Cyclones: The Response to Climate Change and the Effects on Water Quality in the Great Barrier Reef

By
Chelsea L. Parker
B. Sc. Physical Geography, University of Bristol, 2010
Sc. M. Geological Sciences, Brown University, 2014

A Dissertation Submitted in Partial Fulfilment of the Requirements for the Degree of Doctor of Philosophy in the Department of Earth, Environmental, and Planetary Sciences at Brown University

Providence, Rhode Island
May 2017

This dissertation by Chelsea L. Parker is accepted in its present form by the Department of Earth, Environmental, and Planetary Sciences as satisfying the dissertation requirement for the degree of Doctor of Philosophy.

Date _______________ ___________________________________
Amanda H. Lynch, Advisor

Recommended to the Graduate Council

Date_______________ ___________________________________
Jung-Eun Lee, Reader

Date_______________ ___________________________________
John F. Mustard, Reader

Date_______________ ___________________________________
Timothy D. Herbert, Reader

Date_______________ ___________________________________
James M. Done, Reader

Approved by the Graduate Council

Date_______________ ___________________________________
Andrew G. Campbell, Dean of the Graduate School

CURRICULUM VITAE

Chelsea L. Parker

Brown University
Department of Earth, Environmental, and Planetary Sciences
Institute at Brown for Environment and Society
85 Waterman Street, Providence, RI 02912
Chelsea_Parker@brown.edu, 508-287-2527

Education

Ph.D.	Earth, Environmental, and Planetary Sciences, Brown University Advisor: Amanda Lynch Thesis Title: 'Australian Tropical Cyclones: The Response to Climate Change and the Effects on Water Quality in the Great Barrier Reef'	May 2017
M.Sc.	Geological Sciences, Brown University Advisor: Amanda Lynch Thesis Title: 'Factors Affecting the Trajectory and Intensification of Tropical Cyclone Yasi'	May 2014
BTEC	Business and Technology Education Council, U.K. Advanced Diploma in Tropical Habitat Conservation, Thesis Title: 'The Species Diversity, Abundance, and Distributions of Nudibranch sp. as an indicator of the Ecosystem and Community Health and Environmental Quality'	April 2011
B. Sc.	Physical Geography, University of Bristol, U.K. Advisor: Joy Singarayer Honors Dissertation: 'Future changes to Ocean Biogeochemistry and the fate of North Atlantic Cold-Water Coral Reefs'	June 2010

First-Authored Publications

Parker, C.L., Lynch, A.H., Mooney, P.A. (2017) "Factors Affecting the Trajectory and Intensification of Tropical Cyclone Yasi (2011)". Atmospheric Research **http://doi.org/10.1016/j.atmosres.2017.04.002**.

Parker, C. L., Lynch, A. H., Spera, S. A., and Spangler, K. R.: "The Relationship between Tropical Cyclone Activity, Nutrient Loading, and Algal Blooms over the Great Barrier Reef" Biogeosciences Discussion, **doi:10.5194/bg-2017-23**. And *in Review* for Biogeosciences, 2017.

Parker, C.L., Bruyère, C.L., Mooney, P.A., "The Response of Tropical Cyclone Characteristics to Projected Climate Change in Northeast Australia". *Submitted to* Climate Dynamics

Conference Proceedings

Parker, C.L., Lynch, A.H., Tsukernik, M., Arbetter, T.E. (June 2013) “Evaluating WRF-ARW v3.4.1 Simulations of Tropical Cyclone Yasi”. *Extended Abstract.* From NCAR’s 14th Annual WRF User’s Workshop.

First Author Presentations

2016

Invited Seminar by the Research Computing Centre, University of Queensland, Australia.
“The Response of Tropical Cyclone Characteristics to Projected Climate Change in Northeast Australia through WRF simulations and Pseudo Global Warming Technique.”
Presentation at the 17th Annual WRF Users' Workshop, Boulder, CO.
“The Response of Tropical Cyclone Characteristics to Projected Climate Change in Northeast Australia through WRF simulations and Pseudo Global Warming Technique.”
Lunch Bunch at Brown University Department of Earth, Environmental, and Planetary Sciences.
“The Relationship between Tropical Cyclones and Algal activity over the Great Barrier Reef and Projected Responses to Climate Change.”
Presentation at AMS 32nd Conference on Hurricanes and Tropical Meteorology, San Juan, PR.
“The Response of Land-falling Tropical Cyclone Characteristics to Projected Climate Change in Northeast Australia.”
Presentation at AMS 14th Symposium on Coastal Environment, 96th AMS Annual Meeting, New Orleans, LA. “Investigating the Relationships between Tropical Cyclones, Sediment Loading, and Algal Blooms over the Great Barrier Reef.”

2014

Poster at the 2014 AGU Fall Meeting, San Francisco, CA.
“Factors affecting the Intensity and Trajectory of Tropical Cyclone Yasi (February 2011).”
Poster at NCAR’s 15th Annual WRF User’s Workshop, Boulder, CO.
“Factors affecting the Intensity and Trajectory of Tropical Cyclone Yasi.”
Poster at 26th Conference on Weather Analysis and Forecasting / 22nd Conference on Numerical Weather Prediction, 94th AMS Annual Meeting, Atlanta, GA.
“Numerical Weather Modelling of the Factors affecting the Rapid Intensification of Tropical Cyclone Yasi.”

2013

Presentation at NCAR’s 14th Annual WRF User’s Workshop, Boulder, CO.
“Evaluating WRF-ARW v3.4.1 Simulations of Tropical Cyclone Yasi.”
Lunch Bunch at Brown University Department of Earth, Environmental, and Planetary Sciences.
“Tropical Cyclones and Coral Reef Ecosystems.”
Poster at NCSE's 13th National Conference on Science, Policy, and the Environment: Disasters and Environment, Washington D.C. “Sensitivity of Coral Reef Ecosystems to Tropical Cyclones: a case study with Cyclone Yasi.”

Grants and Fellowships

Institute at Brown for Environment and Society Graduate Fellowship 2015-2016

National Center for Atmospheric Research Visitor Grant 2015

Institute at Brown for Environment and Society Research Grant 2014

Brown University Center of Environmental Studies Research Grant 2012

Awards and Honors

First Place Student Oral Presenter award for Presentation, 2016
14th Symposium on the Coastal Environment, 96th AMS Annual Meeting.

Student award and honourable mention for Poster, 2014
26th Conference on Weather Analysis and Forecasting /
22nd Conference on Numerical Weather Prediction, 94th AMS Annual Meeting

Teaching, Mentoring, and Work Experience

Teaching Assistant — *Brown University*
Weather and Climate, Instructor: Dr. Meredith Hastings — Spring 2015
Climate and Climate Change, — Fall 2013
Instructors: Dr. Amanda Lynch, Dr. Leah VanWey
Gave several guest lectures; ran exam review sessions; ran lab sessions; mentored students on final projects; held office hours; devised several assignments; graded all assignments and exams.

Guest Lecturer — *Brown University*
Global Water Cycle, Instructor: Dr. Jung Eun Lee — Spring 2015, 2017

Teaching Outreach — *Vartan Gregorian*
Elementary Science Teacher — 2015-2016
Created and taught weekly science lessons that align with the Next Generation Science Standards to classroom of 3rd-6th graders with learning disabilities

Mentoring — *Brown University*
Mentor and Thesis Reader — Spring 2015
Rebecca Payne, undergraduate Senior Thesis in Geology:
'Response of Precipitation Seasonality to Extreme Changes in Climate Using an Idealized GCM'.

Work Experience
Scientific Research Assistant — *Frontier*
The Fiji Marine Conservation Project organized by — 2011
The Society for Environmental Exploration, U.K.

Intern — *Real Time Architecture*
Organized through the China Recruitment Ltd and — 2011
China Consulting Ltd Asia Internship Program, Shanghai

Services

Reviewer — 2013-present
Weather and Forecasting, Journal of Applied Meteorology and Climatology, Journal of Hydrometeorology

Diversity Working Group, Brown University 2014-present

One of the founders and active members of a student lead initiative to improve inclusion and graduate student diversity in the department. Met with University Deans to discuss diversity and outreach; created, submitted, and implemented financial budgets; designed departmental posters, brochures, newsletters; and ran an outreach booth at a major conference.

Faculty Representative, Brown University 2015-2016

Attended faculty meetings and acted as an advocate for the graduate student body and a liaison between graduate students and faculty members. Implemented and updated graduate student wiki page, created and implemented graduate student exit survey.

First Year Graduate Mentor, Brown University 2014-2016

Provided one-on-one mentoring to incoming first-year graduate students. Held monthly meetings and attended organized activities.

Member 2013-present

American Geophysical Union; American Meteorological Society; European Geosciences Union; Graduate Women In Science and Engineering; Earth Science Women's Network

Skills

Scientific Programming: Shell scripting, Unix, Python, NCL (NCAR Command Language), Matlab, Kaleidagraph, R, STATA, ENVI, ArcGIS, Microsoft Office Suite.

Modeling Expertise: (NCAR) Weather Research and Forecasting Model, (NCAR) Community Earth System Model.

Spoken Languages: fluent French; fluent conversational Cantonese; intermediate Spanish; intermediate Mandarin.

Certifications: PADI Rescue Diver

ACKNOWLEDGEMENTS

Firstly, I would like to thank my advisor and my committee. I started out my graduate career at Brown in an Environmental Studies Masters program, that now no longer exists. My advisor Amanda Lynch took me on as her student, offered to transfer me into the Department of Earth, Environmental and Planetary Sciences, and saw the potential in me to pursue a Ph.D. Amanda allowed and encouraged me to pursue my own interests and always pushed me out of my comfort zone, resulting in an interdisciplinary Ph.D. program. Working with Amanda made me learn to be the independent and self-motivated scientist that I am today. Above all, Amanda supported my travel for research and conferences, from places such as Boulder and Australia. I made great progress intellectually and professionally during those trips, and I doubt I would have achieved this thesis without those experiences.

Over the years, my committee has provided excellent guidance and structure. Thanks to Jung-Eun Lee for all her support and encouragement, and always being available to listen and discuss research. Jack Mustard always asked tough but helpful questions, and taught me how to juggle the complex schedules of professors. Tim Herbert always helped me to look at the bigger picture and forwards in my career. And thanks to Jon Witman, for providing an interdisciplinary voice on my committee over the last 3 years and keeping me on track with ecosystem dynamics. I also have to thank James Done for extensive guidance and research discussions, and support during my visits to the National Center for Atmospheric research. And a big thank you to him for agreeing to be my outside reader and travelling to Rhode Island for my defense.

There are many other wonderful scientists that I need to thank for helping me to produce this thesis. Thank you to Greg Holland for his openness and frankness when discussing research and future career prospects. He hosted me at NCAR and provided the original introduction to the Regional Climate Group there. The Group supported me professionally, academically, and personally. I learned an unbelievable amount during my time with the group and was able to make large strides towards completing my thesis chapters with their support. I particularly need to thank Cindy Bruyère and James Done for taking me under their wings and acting as excellent mentors and project advisors. Additionally, I would like to thank Priscilla Mooney for the many hours she spent helping me to develop the methodology of climate model downscaling, as well as many Skype meetings while writing papers together. She has been an immensely supportive and helpful collaborator.

I would also like to thank Henry Johnson, and Todd Arbetter for countless hours of technical help. Henry made numerous disc spaces available for me to fill with data and regularly backed up all my data without being asked, to save me from disaster. Todd sat with me for hours on end to figure out WRF, learn Python, and derive wave dynamics equations. I will never forget his help, and the modeling and coding that went into this thesis would not have been possible without him.

Now, to thank my friends. My best friend Jenny Mayo has been there for me and listened to me every day. She has really ridden the roller coaster of grad school with me and I am amazed she has still decided to start a PhD program now. Thank you to Dido

Penny, Janica Chavda, and all my close friends at home who have filled my holidays with fun, and motivated me to get through graduate school.

I moved to the U.S. without knowing anyone, and my great friends that I have known throughout my time at Brown: Becca Keane, Brianna Craft, Miguel Segura, Maya Wei, Masha Tsukernik, Will Daniels, Will Longo, Samantha Bova, and Rachel Lupien have been great supports and sounding boards for my science, but also filled my free time with laughter, explorations around Providence, and amazing outdoor adventures.

I am also indebted to my office mates. Keith Spangler has been the greatest lab mate, from indulging my complaints, to teaching me about U.S. politics, and to always being on hand for grammatical correction. He has made me a better writer and a more informed person. Steph Spera has truly been my rock throughout graduate school, and my go to for all scientific, professional, personal, or emotional help. We went through this journey together and I definitely could not have done this without her, though perhaps maybe we would have finished our theses a little faster if we had not been officemates!

The most important acknowledgements I have saved for last, my family. Thank you to my parents Hasina and Martin Parker who have worked so hard their whole lives to get me where I am today. While taking the path of a Ph.D. in Earth Science is wildly different from their own experiences, they have supported all of my decisions and endeavors without question. They have made every effort to still be my support system despite the distance between us, and have been so flexible in to travelling to see me all the time. I am sure that the completion of this thesis is just as much of a sigh of relief for them.

Finally, as I have demonstrated, this thesis required the help and input of many people, but it was really my partner Dan Moriarty who got me to the finish line. He has continually supported me, talked me down from giving up on graduate school, gave me a better work-life balance, served as an in-house copy editor, and even adjusted his career to help me through the final stages of my thesis. Watching him navigate his thesis and the end of graduate school has given me so much experience and paved the way for me to follow. And thank you to the whole Moriarty family who made me a part of their family, giving me unconditional love and support, and making me finally feel at home in the U.S.

TABLE OF CONTENTS

INTRODUCTION

Coral reefs are tropical, marine ecosystems supported by coral organisms and are some of the most productive and diverse ecosystems on Earth (Moberg and Folke 1999). Although they only cover 0.1-0.5% of the ocean surface (Copper 1994; Spalding and Grenfell 1997), coral reefs are considered the most diverse marine habitat (Knowlton et al. 2010) and support a third of all marine fish species (McAllister 1991). They also supply over tens of millions of people with food, raw materials, recreation, coastal protection, and aesthetic and cultural benefits (Moberg and Folke 1999).

The Great Barrier Reef (GBR) is the world's largest coral reef system (Hughes et al. 2015). The GBR Marine Park covers an area of 350,000 km^2, extends more than 2,300 km along Australia's northeastern coast, and includes 600 islands (GBR Marine Park Authority 2017; Stoeckl et al. 2011). The GBR Marine Park is home to a diverse array of ecosystems including over 3000 individual coral reefs, 600 hard and soft coral species, and 1600 fish species. The present reef structure may be up to 8,000 years old (GBR Marine Park Authority 2017) and was added to the World Heritage List in 1981. The park annually generates approximately AUS$5.7 billion to the Australian economy and 69,000 full-time-equivalent jobs (Deloitte Access Economics 2013). This economical service is derived primarily from tourism, recreation, and fishing activities (Stoeckl et al. 2011). Additionally, the GBR Marine Park provides regulating services such as nutrient cycling and barrier protection from storm activity (Oxford Economics 2009). Lastly, the GBR Marine Park possesses cultural importance for a number of Aboriginal Australian and Torres Strait Islander peoples (Great Barrier Reef Marine Park Authority 2006).

Corals are the foundation species that support and structure reef ecosystems. Despite the Marine Park, World Heritage listing, and some protection efforts, the GBR has lost half of its coral cover over the past 40 years (Bellwood et al. 2004; Brodie and Waterhouse 2012; GBR Marine Park Authority 2014) and is estimated to lose another 5-10% by 2022 if there is no intervention (De'ath et al. 2012). This decline is a consequence of cumulative impacts and compounding pressures from local- and global-scale stressors. Globally, the dominant driver is anthropogenic climate change where rising sea levels 'drown' reefs (Grigg et al. 2002), ocean acidification reduces calcification rates and coral growth (De'ath et al. 2009; GBR Marine Park Authority 2014; Silverman et al. 2014), and increasing temperatures cause widespread coral bleaching and die off events (notably in 1998, 2002 [Berkelmans et al. 2004], and 2016 [Ainsworth et al. 2016; Hoegh-Guldberg and Ridgway 2016; Hughes et al. 2017]). Locally, anthropogenic risks include unsustainable fishing, dredging, agricultural runoff, coastal development and industrialization, and an expanding fossil-fuel industry (Hughes et al. 2015), all of which result in reduced water quality and a greater dominance of macroalgae. These drivers have sharply increased since the industrial revolution. Land clearing and land-use change have increased the volume of sediments, nitrogen, and phosphorus delivered to the lagoon since European settlement by up to a factor of 10 (Furnas et al. 2003; Brodie et al. 2013). Fish biomass has already decreased by 80% in fishing zones within the Marine Park (GBR Marine Park Authority 2014). Under current policies, these human drivers will continue to increase rapidly: the coastal population is predicted to double to 10 million by 2050 (Australian Bureau of Statistics 2013); and there are new plans for a 60-year development of the world's largest coal port at the edge of the GBR World Heritage Area (Hughes et al. 2015).

Tropical cyclones are the focus of this dissertation because they represent a very interesting disturbance to coral reef ecosystems. Tropical cyclones (TCs) are natural phenomena and a local-scale disturbance to the GBR. However, the characteristics of cyclones are likely to be affected by global, anthropogenic climate change (Walsh et al. 2016). In this way, TCs are the mechanistic bridge across both local and global scales. Primary consequences of TCs include breakage of coral assemblages from wind and wave kinetic energy (Done 1992; Puotinen 2007; Fabricius et al. 2008); and salinity-induced stress, coral bleaching, and die off from heavy rainfall (Smith and Buddermeier 1992; Sweatman et al. 2007). A secondary consequence is reduced water quality from increased concentrations of suspended sediments, colored dissolved organic matter, nutrients, pesticides, and herbicides in the water column through either wind-driven re-suspension of sediments and nutrients to the surface waters (Furnas 1989; Marra et al. 1990; Larcombe and Carter 2004; Wolanksi et al. 2005), or nutrient and sediment loading driven by rainfall-induced runoff and river discharge (Davies and Eyre 2005; Mitchell et al. 2005; Stieglitz 2005; Hoegh-Guldberg et al. 2011; Brodie 2012). Poor water quality inhibits photosynthesis in the benthic coral organisms (Devlin and Schaffelke 2009), decreases calcification rates (Devlin and Schaffelke 2009), increases competition with surface phytoplankton and algal activity (Fraser and Currie 1996; Furnas et al. 2005; Brodie et al. 2010), and causes smothering, resulting in coral bleaching and mortality (Anthony and Fabricius 2000; Fabricius and Wolanski 2000). This TC-induced poor water quality has been linked with outbreaks of Crown of Thorns starfish, which feed on corals and can greatly reduce reef cover (Brodie et al. 2005; Fabricius et al. 2010).

TCs can interact with and compound the aforementioned anthropogenic pressures. The combined effect of these stressors reduces coral cover and ecosystem function. As coral cover declines, reef complexity and rugosity decline, and the ecosystem supports a lower density of fish (Hoegh-Guldberg et al. 2007). These declines negatively affect both commercial and recreational fishing, the tourism industry, and ecosystem function. Campbell and Swan (2016) predict a decline of 175,000 tourists from China, the U.K., and the U.S.A. alone if the bleaching from 2016 persists, resulting in a ~AUS$1 billion loss per year. Furthermore, the functional efficiency of the reefs as a storm barrier will decrease (Hoegh-Guldberg et al. 2007). Coastal areas will therefore be exposed to un-attenuated storm surge and wind and wave action. Together, the stressors will continue to reduce the resilience of the GBR ecosystems and their ability to withstand future disturbances, resulting in a negative feedback cycle.

Throughout this thesis, I build a suite of tools to model TC characteristics in a regime of global warming and understand the implications of these findings for reef environments. First, I use remote sensing techniques to examine the relationship between tropical cyclone activity and GBR water quality. Then, I use regional numerical modelling techniques to develop an appropriate methodology to simulate tropical cyclone cases that affect the northeastern coastline of Australia. This refined model set up is then utilized to simulate and assess the change in damaging tropical cyclone characteristics with climate perturbation. This thesis uniquely explores both the relationship between tropical cyclones and the GBR environment, and the dynamical response of cyclones to climate change. The results provide critical information that could inform management and mitigation efforts for the GBR against future stressors. Furthermore, the findings of this thesis could also be extrapolated to the future of other reef environments globally that face a similar combination of stressors.

Chapter One presents a novel exploration of the relationship between tropical cyclone activity and water quality over the GBR Marine Park area. We use the remotely-sensed 8-day Moderate Resolution Imaging Spectroradiometer (MODIS) chlorophyll *a* product (as a proxy for water quality), meteorological data, and statistical techniques to examine whether significant causal mechanisms for cyclone induced water quality change can be detected over the extent of the GBR surface waters over a 10-year period. Our results demonstrate that chlorophyll *a* concentrations increase over reef environments at 8 and 16 days after tropical cyclone presence in the area. Our findings show that wind speed in isolation only increases minimum levels of chlorophyll *a*, and rainfall and translation speed reduce the measures of water quality (such as the average and maximum chlorophyll *a*) that negatively affect the reef ecosystem. Therefore, we conclude that the primary driver of water quality reduction is nutrient and sediment loading from cyclone-induced rainfall, river discharge, and coastal inundation from storm surge. The extent of water quality degradation is principally governed by the size of the tropical cyclone system and the total area affected by tropical cyclone conditions given the role of nutrient loading via rainfall and coastal inundation. Chapter 1 is published as a discussion paper and under review in *Biogeosciences* (Parker et al. 2017a).

Chapter Two provides a detailed analysis of the sensitivity of the simulated trajectory, intensification, and translation speed of Tropical Cyclone Yasi (2011) in the Weather Research and Forecasting (WRF) model for Advanced Research (WRF-ARW) version 3.4.1. This work improves the simulation of intense tropical cyclone events that affect the Queensland coastline of Australia at a horizontal grid spacing of 12km, to facilitate future regional climate studies. To assess the ensemble of simulations, we devised a new skill score to summarize the deviations from observations at landfall. The results demonstrated simulation sensitivity to initial condition resolution and the need for a new initialization dataset, and a strong sensitivity to cumulus schemes, with a trade-off between trajectory and intensity simulation accuracy. The deviations resulted from the differences in the trigger functions and the representation of shallow convection over the tropical ocean between the schemes. We also found that improving the accuracy of the sea surface temperature boundary condition data by correcting a newly discovered sea surface temperature lag in a reanalysis data or using a higher resolution dataset used can improve the simulation. Higher resolution data sets that can capture steep sea surface temperature gradients and include increased temperatures, increase relative vorticity and intensity of the simulated system. Chapter 2 is under a second round of review in *Atmospheric Research* after initial acceptance with revisions (Parker et al. 2017b).

Chapter Three addresses how characteristics of intense tropical cyclones that affect the Queensland coastline of Australia will respond to climate change. Here, we focus on the relative changes in damaging characteristics such as intensity, trajectory, rainfall, translation speed, and size in the three most recent intense systems that affected the area. We used WRF-ARW v.3.4.1 (set up as tested in Chapter 2), and the future climate downscaled from the Community Earth System Model through a pseudo global warming technique. This technique required the calculation of a climate change delta of the difference between the monthly averaged climate from the present day (1976 to 2005) and the future climate simulated from the 8.5 Representative Concentration Pathway (2071-2100). Results demonstrate a consistent response of increasing intensity (both reduced central pressures and increased wind speeds). The responses of other characteristics were variable. The smallest and weakest case could undergo the greatest change, with the largest proportional increase in intensity and rainfall, and a 40% size increase. We found that the monthly steering flow deltas steered the April case equatorward and increased the translation speed, but shifted the January and February cases poleward with little change to the translation speed. The results highlight the sensitivity of tropical cyclone development and characteristics to the boundary conditions of the environment and therefore climatic change. The findings also demonstrate the importance of case study based approaches for investigating the response of tropical cyclones to climate change. Chapter 3 is recently submitted to *Climate Dynamics*.

Chapter Four synthesizes results from Chapters 1 and 3 and the current understanding in the literature of how tropical cyclones may respond to climate change in the western South Pacific and the implications for the Great Barrier Reef. I discuss that total TC frequency will likely decrease, but the number of intense TCs will increase in the western South Pacific. Additionally, maximum intensity and TC-associated rainfall and storm surge will increase with climate change. Damage to the GBR will therefore be augmented through amplified breakage and dislodgement and reductions in water quality. These discussions suggest that local policy and mitigation efforts should work to improve water quality in the GBR and protection of the ecosystems to strengthen natural reef resilience to stressors (such as cyclones) that cannot be controlled. Future work could expand to examine storm surge height and stream gauge data to further assess the mechanisms of TC-induced water quality reduction and better inform mitigation efforts. The chapter demonstrates there is still uncertainty surrounding the change to TC genesis location, trajectory, translation speed, and size with climate change. Therefore, future work should focus on the changes to these characteristics and on improving the prediction of the steering flow, sea surface temperature, and the El Niño Southern Oscillation in the future environment. The chapter also reveals the need for further case study based approaches with a larger sample size to identify the trends and outliers of TC response to climate change.

The **Methodology** section following Chapters one to four, provides greater detail about the Weather Research and Forecasting model utilized in this thesis. The section provides a description of the additional steps and simulations that were required to facilitate this research work.

References

Ainsworth, T. D., Heron, S. F., Ortiz, J. C., Mumby, P. J., Grech, A., Ogawa, D., ... & Leggat, W. (2016). Climate change disables coral bleaching protection on the Great Barrier Reef. Science, 352(6283), 338-342.

Anthony, K. R., & Fabricius, K. E. (2000). Shifting roles of heterotrophy and autotrophy in coral energetics under varying turbidity. Journal of experimental marine biology and ecology, 252(2), 221-253.

Australian Bureau of Statistics, Australian Demographic Statistics, (2013) "Queensland Government Population Projections 2013 edn" http://go.nature.com/ceQlpg

Bellwood, D. R., Hughes, T. P., Folke, C., & Nyström, M. (2004). Confronting the coral reef crisis. Nature, 429(6994), 827-833.

Berkelmans, R., De'ath, G., Kininmonth, S., & Skirving, W. J. (2004). A comparison of the 1998 and 2002 coral bleaching events on the Great Barrier Reef: spatial correlation, patterns, and predictions. Coral reefs, 23(1), 74-83.

Brodie, J. E., Kroon, F. J., Schaffelke, B., Wolanski, E. C., Lewis, S. E., Devlin, M. J., ... & Davis, A. M. (2012). Terrestrial pollutant runoff to the Great Barrier Reef: an update of issues, priorities and management responses. Marine Pollution Bulletin, 65(4), 81-100.

Brodie, J., & Waterhouse, J. (2012). A critical review of environmental management of the 'not so Great'Barrier Reef. Estuarine, Coastal and Shelf Science, 104, 1-22.

Brodie, J., Fabricius, K., De'ath, G., & Okaji, K. (2005). Are increased nutrient inputs responsible for more outbreaks of crown-of-thorns starfish? An appraisal of the evidence. Marine pollution bulletin, 51(1), 266-278.

Brodie, J., Schroeder, T., Rohde, K., Faithful, J., Masters, B., Dekker, A., ... & Maughan, M. (2010). Dispersal of suspended sediments and nutrients in the Great Barrier Reef lagoon during river-discharge events: conclusions from satellite remote sensing and concurrent flood-plume sampling. Marine and Freshwater Research, 61(6), 651-664.

Brodie, J., Waterhouse, J., Schaffelke, B., Kroon, F., Thorburn, P., Rolfe, J., ... & Warne, M. (2013). Land use impacts on Great Barrier Reef water quality and ecosystem condition. Reef Water Quality Protection Plan Secretariat.

Campbell, R., & Swann, T. (2016). Great barrier bleached. http://apo.org.au/node/64933

Copper, P. (1994). Ancient reef ecosystem expansion and collapse. Coral reefs, 13(1), 3-11.

Davies, P. L., & Eyre, B. D. (2005). Estuarine modification of nutrient and sediment exports to the Great Barrier Reef Marine Park from the Daintree and Annan River catchments. Marine Pollution Bulletin, 51(1), 174-185.

De'ath, G., Lough, J. M., & Fabricius, K. E. (2009). Declining coral calcification on the Great Barrier Reef. Science, 323(5910), 116-119.

De'ath, G., Fabricius, K. E., Sweatman, H., & Puotinen, M. (2012). The 27–year decline of coral cover on the Great Barrier Reef and its causes. Proceedings of the National Academy of Sciences, 109(44), 17995-17999.

Deloitte Access Economics (2013), Economic contribution of the Great Barrier Reef, Great Barrier Reef Marine Park Authority, Townsville. http://elibrary.gbrmpa.gov.au/jspui/handle/11017/2996

Devlin, M., & Schaffelke, B. (2009). Spatial extent of riverine flood plumes and exposure of marine ecosystems in the Tully coastal region, Great Barrier Reef. Marine and Freshwater Research, 60(11), 1109-1122.

Done, T. J. (1992). Effects of tropical cyclone waves on ecological and geomorphological structures on the Great Barrier Reef. Continental Shelf Research, 12(7), 859-872.

Emanuel, K. A. (1991). The theory of hurricanes. Annual Review of Fluid Mechanics, 23(1), 179-196.

Fabricius, K. E., & Wolanski, E. (2000). Rapid smothering of coral reef organisms by muddy marine snow. Estuarine, Coastal and Shelf Science, 50(1), 115-120.
Fabricius, K. E., De'Ath, G., Puotinen, M. L., Done, T., Cooper, T. F., & Burgess, S. C. (2008). Disturbance gradients on inshore and offshore coral reefs caused by a severe tropical cyclone. Limnology and Oceanography, 53(2), 690-704.
Fabricius, K. E., Okaji, K., & De'Ath, G. (2010). Three lines of evidence to link outbreaks of the crown-of-thorns seastar Acanthaster planci to the release of larval food limitation. Coral Reefs, 29(3), 593-605.
Fraser, R. H., & Currie, D. J. (1996). The species richness-energy hypothesis in a system where historical factors are thought to prevail: coral reefs. American Naturalist, 138-159.
Furnas, M. M. (1989, January). Cyclonic disturbance and a phytoplankton bloom in a tropical shelf ecosystem. In Red Tides: Biology, Environmental Science and Toxicology. Proceedings of the First International Symposium on Red Tides held November 10-14, 1987, in Takamatsu, Kagawa Prefecture, Japan-pages: 273-276. Elsevier Science Publishing Co., Inc.
Furnas, M. M. (2003). Catchments and corals: terrestrial runoff to the Great Barrier Reef. Australian Institute of Marine Science & CRC Reef Research Centre.
Furnas, M., Mitchell, A., Skuza, M., & Brodie, J. (2005). In the other 90%: phytoplankton responses to enhanced nutrient availability in the Great Barrier Reef Lagoon. Marine pollution bulletin, 51(1), 253-265.
Great Barrier Reef Marine Park Authority (2017). Facts About the Great Barrier Reef. [Accessed online 18 March 17] http://www.gbrmpa.gov.au/about-the-reef/facts-about-the-great-barrier-reef
Great Barrier Reef Marine Park Authority. (2006). "Fact Sheet No. 4 – Aboriginal and Torres Strait Islander People and the Great Barrier Reef. Region". [Accessed Online 18 Mar. 17]https://web.archive.org/web/20070614223725/http://www.gbrmpa.gov.au/__data/assets/pdf_file/0009/2142/Fact_Sheet_04_IPLU.pdf
Great Barrier Reef Marine Park Authority. (2014) "Great barrier reef outlook report 2014." http://elibrary.gbrmpa.gov.au/jspui/handle/11017/2855
Grigg, R., Grossman, E., Earle, S., Gittings, S., Lott, D., & McDonough, J. (2002). Drowned reefs and antecedent karst topography, Au'au Channel, SE Hawaiian Islands. Coral Reefs, 21(1), 73-82.
Hoegh-Guldberg, O., & Ridgway, T. (2016). Coral bleaching hits great barrier reef as global temperatures soar. Green Left Weekly, (1090), 10.
Hoegh-Guldberg, O., Andréfouët, S., Fabricius, K., Diaz-Pulido, G., Lough, J., Marshall, P., & Pratchett, M. S. (2011). Vulnerability of coral reefs in the tropical Pacific to climate change. Vulnerability of tropical Pacific fisheries and aquaculture to climate change. Secretariat of the Pacific Community, Noumea, 251-296.
Hoegh-Guldberg, O., Mumby, P. J., Hooten, A. J., Steneck, R. S., Greenfield, P., Gomez, E., ... & Knowlton, N. (2007). Coral reefs under rapid climate change and ocean acidification. Science, 318(5857), 1737-1742.
Hughes et al. (2017). "Global warming and recurrent mass bleaching of corals" Nature, In press doi:10.1038/nature21707
Hughes, T. P., Day, J. C., & Brodie, J. (2015). Securing the future of the Great Barrier Reef. Nature Climate Change, 5(6), 508-511.
Knowlton, N., Brainard, R. E., Fisher, R., Moews, M., Plaisance, L., & Caley, M. J. (2010). Coral reef biodiversity. Life in the World's Oceans: Diversity Distribution and Abundance, 65-74.
Larcombe, P., & Carter, R. M. (2004). Cyclone pumping, sediment partitioning and the development of the Great Barrier Reef shelf system: a review. Quaternary Science Reviews, 23(1), 107-135.

Marra, J., Bidigare, R. R., & Dickey, T. D. (1990). Nutrients and mixing, chlorophyll and phytoplankton growth. Deep Sea Research Part A. Oceanographic Research Papers, 37(1), 127-143.

McAllister, D.E., 1991. What is the status of the world's coral reef fishes? Sea Wind 5, 14–18

Mitchell, C., Brodie, J., & White, I. (2005). Sediments, nutrients and pesticide residues in event flow conditions in streams of the Mackay Whitsunday Region, Australia. Marine Pollution Bulletin, 51(1), 23-36.

Moberg, F., & Folke, C. (1999). Ecological goods and services of coral reef ecosystems. Ecological economics, 29(2), 215-233.

Oxford Economics. (2009). Valuing the effects of Great Barrier Reef bleaching. Great Barrier Reef Foundation, Brisbane.

Parker, C. L., Lynch, A. H., Spera, S. A., and Spangler, K. R. (2017a): The Relationship between Tropical Cyclone Activity, Nutrient Loading, and Algal Blooms over the Great Barrier Reef, Biogeosciences Discuss., doi:10.5194/bg-2017-23, in review, 2017.

Parker, C.L., Lynch, A.H., Mooney, P.A. (2017b) "Factors Affecting the Trajectory and Intensification of Tropical Cyclone Yasi (2011)". Atmospheric Research. http://doi.org/10.1016/j.atmosres.2017.04.002

Puotinen, M. L. (2007). Modelling the risk of cyclone wave damage to coral reefs using GIS: a case study of the Great Barrier Reef, 1969–2003. International Journal of Geographical Information Science, 21(1), 97-120.

Silverman, J., Schneider, K., Kline, D. I., Rivlin, T., Rivlin, A., Hamylton, S., ... & Caldeira, K. (2014). Community calcification in Lizard Island, Great Barrier Reef: A 33year perspective. Geochimica et Cosmochimica Acta, 144, 72-81.

Smith, S. V., & Buddemeier, R. W. (1992). Global change and coral reef ecosystems. Annual Review of Ecology and Systematics, 23, 89-118.

Spalding, M. D., & Grenfell, A. M. (1997). New estimates of global and regional coral reef areas. Coral Reefs, 16(4), 225-230.

Stieglitz, T. (2005). Submarine groundwater discharge into the near-shore zone of the Great Barrier Reef, Australia. Marine Pollution Bulletin, 51(1), 51-59.

Stoeckl, N., Hicks, C. C., Mills, M., Fabricius, K., Esparon, M., Kroon, F., ... & Costanza, R. (2011). The economic value of ecosystem services in the Great Barrier Reef: our state of knowledge. Annals of the New York Academy of Sciences, 1219(1), 113-133.

Sweatman, H., Thompson, A., Neale, S., & Thomson, D. (2006). 5. Inshore Coral Reefs Monitoring.

Walsh, K. J., McBride, J. L., Klotzbach, P. J., Balachandran, S., Camargo, S. J., Holland, G., ... & Sugi, M. (2016). Tropical cyclones and climate change. Wiley Interdisciplinary Reviews: Climate Change, 7(1), 65-89.

Wolanski, E., Fabricius, K., Spagnol, S., & Brinkman, R. (2005). Fine sediment budget on an inner-shelf coral-fringed island, Great Barrier Reef of Australia. Estuarine, Coastal and Shelf Science, 65(1), 153-158.

CHAPTER ONE

THE RELATIONSHIP BETWEEN TROPICAL CYCLONE ACTIVITY, NUTRIENT LOADING, AND ALGAL BLOOMS OVER THE GREAT BARRIER REEF

CHELSEA L. PARKER[1,2], AMANDA H. LYNCH[1,2], STEPHANIE A. SPERA[1,2], AND KEITH R. SPANGLER[1,2]

[1]Department of Earth, Environmental, and Planetary Sciences, Brown University, Providence RI 02912, USA
[2] Institute at Brown for Environment and Society, Brown University, Providence RI 02912, USA

Published as a discussion article in its current form
and under review in:
Biogeosciences
doi:10.5194/bg-2017-23

Abstract

The Great Barrier Reef, the world's largest coral reef ecosystem, is subject to many environmental stressors. This study utilizes remotely sensed Moderate Resolution Imaging Spectroradiometer (MODIS) chlorophyll *a* concentration data to explore statistically significant relationships between local-scale tropical cyclone disturbance and relative water quality between 2004-2014. The study reveals that tropical cyclone activity reduces water quality at 8- and 16-day time lags. Relationships suggest that at early stages (during and just after cyclone activity) algal response is induced primarily through wind-driven sediment re-suspension. However, wind speed in isolation only increases minimum levels of chlorophyll *a*, rather than mean or extreme upper values. At greater time lags (16-day), it is suggested that nutrient runoff from rainfall (and perhaps storm surge) increase phytoplankton activity, leading to detrimental ecological effects. The analyses systematically demonstrate the dominance of tropical cyclone size on mean and extreme values of chlorophyll *a* during and after tropical cyclone activity (at 0-, 8-, and 16-day time lags). Both the total area affected and the area from which nutrients can be extracted have more impact on chlorophyll *a* concentrations than either the duration or intensity of the cyclone. Findings indicate that efforts to reduce nutrient and sediment leaching into the reef lagoon from the Queensland coastal lands need to be continued and improved. This will be particularly important in the context of climate change, since tropical cyclone frequency, dynamics and characteristics are likely to change.

1 Introduction

Spanning 350,000 km^2 in area and extending more than 2,300 km along Australia's northeastern coast, the Great Barrier Reef Marine Park encompasses the world's largest coral reef ecosystem (Great Barrier Reef Marine Park Authority 2011; Stoeckl et al. 2011). The Great Barrier Reef Marine Park is home to over 3000 coral reefs and 1600 fish species, and was added to the World Heritage List in 1981. The park annually generates approximately AUS$5.7 billion of value added and 69,000 full-time-equivalent jobs for Australia's economy (Deloitte Access Economics 2013).

Despite protection efforts, the Great Barrier Reef Marine Park is still subject to many local- and global-scale stressors associated with a myriad of negative impacts and long-term consequences. Global, long-term pressures include ocean warming and acidification, resulting in coral bleaching, dissolution, and loss of sensitive reef builders, reduced species richness and abundance, and loss of ecosystem function. This study focuses on the local-scale disturbance of tropical cyclones and the resultant water quality degradation in the Great Barrier Reef. Such disturbances decrease reef system resilience in the face of larger-scale and longer-term stressors.

Tropical cyclones can reduce water quality over the reef environment by increasing concentrations of suspended sediments, colored dissolved organic matter, nutrients, pesticides, and herbicides in the water column through several possible mechanisms: (1) wind-driven re-suspension of sediments (in water columns < 50m in depth), (2) nutrient and sediment loading driven by rainfall-induced runoff and river discharge. An overview of the pathways for the two primary mechanisms is demonstrated in Figure 1.

Initially, the chlorophyll *a* concentration in surface waters may respond to the reduced water quality following tropical cyclone activity through the wind-driven re-suspension mechanism. As the tropical cyclone moves over the reef lagoon, the intense wind and wave energy can re-suspend benthic sediments (Marra et al. 1990; Larcombe and Carter 2004; Wolanksi et al. 2005) with an associated pulse of nutrients from lagoon and reef pore water (Furnas 1989). The re-suspension and resulting nutrient pulse occurs during tropical cyclone passage, and the surface phytoplankton and algal activity respond to the nutrients now available in the surface waters, causing an increase in chlorophyll *a* detection within few days (Furnas 1989). The response in surface chlorophyll *a* levels should be detectable by remote sensing instruments within 10 days of the wind activity in the lagoon area (Subrahmanyam et al. 2002; Lin et al. 2003; Zheng and Tang 2007; Siswanto et al. 2008). Although remotely sensed chlorophyll *a* concentrations in turbid coastal waters may be confounded by an concurrent influx of total suspended sediments (e.g. Gitelson et al. 2008; Gordon and Morel 2012), it can be inferred that a positive bias in chlorophyll *a* measurements during times with heavy sediment loading would still indicate reduced water quality over the reefs and be collinear with the promotion of chlorophyll *a*.

As the tropical cyclone makes landfall, the coastal land is inundated with convective rain and storm surge. Heavy rain can be sustained for significant distances inland, even as the cyclone weakens. This heavy rainfall results in large river discharges from the Great Barrier Reef catchment into the lagoon, resulting in high concentrations of nutrients and sediment loads (Stieglitz 2005; Brodie 2012b). These nutrients and sediments arise primarily from fertilizer leaching and enhanced erosion (Brodie 2012b).

Recent trends in land use can exacerbate these issues. Approximately 40% of the Great Barrier Reef catchment area has been cleared of natural vegetation (Furnas 2003), and the concentrations of inputs have increased as the density and extent of new land-cover types and activities increase (Hutchings et al. 2005; Kroon et al. 2012). Thus, the Great Barrier Reef lagoon is subject to loading events (Davies and Eyre 2005; Mitchell et al. 2005; Hoegh-Guldberg et al. 2011), with inputs being derived from industrial activity, urban areas, sewage treatment, and agriculture on the coastal lands. Following the tropical cyclone event, nutrient and sediment loading degrades water quality and promotes an increase in phytoplankton and algal activity, increasing the detected surface chlorophyll *a* concentrations.

The time taken for rivers to discharge to the lagoon remains an open question in this area, owing to the variability of river flow as a function of storm characteristics, basin and catchment geometry and bathymetry, land use, and antecedent conditions. Gong et al. (2007) found that tropical cyclone storm surge retreat to the lagoon may take roughly 3-4 days after a storm event in North Carolina, United States. Alexander et al. (2001) suggested that rainfall runoff from catchment to lagoon can take roughly one week in parts of Queensland, Australia. The travel time from river mouth to reef lagoon alone requires 1-2 days (Brodie et al. 2010). This sparse evidence leads to expectations that the chlorophyll *a* response to the rainfall discharge would occur at least several days after landfall.

The reduction of water quality through the input of nutrients and sediments through these mechanisms has a negative effect on reef organisms. Sediments and herbicides can inhibit photosynthesis in the benthic coral organisms, causing resource limitation to the phototropic organisms (Devlin and Schaffelke 2009). Nutrients (e.g., particulate nitrogen and phosphorus) can decrease calcification rates (Devlin and Schaffelke 2009), leading to skeletal defects and reproductive impairment (Brodie et al. 2010). Furthermore, an increase in surface photosynthesis through increasing phytoplankton and algal activity (Furnas et al. 2005) can outcompete typical benthic reef producers and builders below (Fraser and Currie 1996; Brodie et al. 2010). The increase in organic matter provided by the phytoplankton is, in turn, cycled through the marine food web and the by-products are deposited on the reef benthic communities, resulting in a number of harmful effects including coral bleaching and mortality through coral smothering (Anthony and Fabricius 2000; Fabricius and Wolanski 2000). Over time, re-occurrence of these long-lasting episodes of degraded water quality can reduce coral species richness (Fabricius and De'ath 2004; Fabricius 2005) and lead to a shift from a coral-dominated to a macroalgal-dominated ecosystem (Fabricius and De'ath 2004; Devlin and Schaffelke 2009; Brodie et al. 2010). This phase shift can cause further mortality of corals and reef organisms (McClanahan et al. 2005; Smith et al. 2006) and would no longer support high biodiversity or provide the same ecosystem services; furthermore, resilience to future disturbances and stressors can be reduced following this phase shift (Lapointe 1997; McCook 1999).

1.1 Remote Sensing of Chlorophyll *a*

Chlorophyll *a* is the pigment used by phytoplankton and algae to photosynthesize. Because phytoplankton abundance responds quickly to changes in nutrient availability (typically within 24 hours of nutrient increase; Örnólfsdóttir et al. 2003), chlorophyll *a* concentrations are frequently used as a proxy for phytoplankton biomass and nutrient status in surface waters (Dekker et al. 2006; Furnas et al. 2005; Brodie et al. 2007). Given that chlorophyll *a* is correlated with suspended particulate nitrogen, phosphorus, and other solids in the water column (Fabricius and De'ath 2004; Udy et al. 2005), the Great Barrier Reef Marine Park Authority frequently uses chlorophyll *a* concentrations to monitor and assess the water quality and health of the reef (Brodie and Furnas 1994; Brodie et al. 1997, 2007; Furnas and Brodie 1996; Steven et al. 1998). To explore whether there is a relationship between tropical cyclone activity and water quality over the Great Barrier Reef, chlorophyll *a* concentration data collected over the entire reef expanse and several tropical cyclone seasons are required. Because *in situ* measurements on this spatiotemporal scale are unavailable, we use remotely sensed chlorophyll *a* concentration products to determine and analyze the water quality over ten years across the whole Great Barrier Reef. This approach has been successfully employed in other long-term water quality case studies in a variety of coastal locations, such as in the Chesapeake Bay (Harding and Perry 1997), the Black Sea (Yunev et al. 2002), and the Basque coastal area (Novoa et al. 2012).

Suspended sediments and dissolved organic matter can lead to inaccuracies in remotely sensed chlorophyll *a* estimates in coastal waters (i.e., "Case 2" waters, in contrast to open ocean areas known as "Case 1" waters) when applying global, optical algorithms (e.g., Gordon and Morel 2012; Wang and Shi 2007; Gitelson et al. 2009; and Odermatt et al. 2012). However, it has been demonstrated that remotely sensed data from the Moderate Resolution Imaging Spectroradiometer (MODIS) are applicable for analysis of coastal waters (Zibordi et al. 2006), and the chlorophyll *a* product can be used to accurately estimate suspended algal activity in coastal areas (Hu 2009). Previous studies have successfully used MODIS chlorophyll *a* data products to analyze chlorophyll changes in other nearshore environments following case study tropical cyclone events (e.g., near Hainan Island; Zheng and Tang 2007; and in the northwest Pacific; Kawai and Wada 2011). Furthermore, Udy et al. (2005) demonstrated that MODIS chlorophyll *a* data follow a similar trend to *in situ* Great Barrier Reef chlorophyll *a* measurements. That said, MODIS-derived chlorophyll *a* measurements can be problematic in coastal waters during times of high suspended sediment (Gitelson et al. 2008), as would be expected in times of cyclone activity (Larcombe and Carter 2004; Wolanksi et al. 2005). While augmented suspended sediment concentrations may lead to an overestimation of chlorophyll *a* values, the presence of suspended sediments in the water column reduces clarity and has negative consequences for reef organisms (Russ and McCook 1999; Birrell et al. 2005, Devlin and Schaffelke 2009). The sediments also lead to favorable conditions for phytoplankton growth, given the associated increased nutrient load (Zheng and Tang 2007). In that context, while not unambiguous, positive changes in measured chlorophyll *a* concentrations uniquely represent degraded water quality across the Great Barrier Reef. To account for the potential overestimation of the effects of cyclone activity on chlorophyll *a*, and to ensure our results our robust, this study also considers the relative difference in chlorophyll *a* concentrations at time lags after tropical cyclone activity, at which time total suspended sediment concentrations in the surface waters may have declined (Brodie et al. 2010).

The median chlorophyll *a* concentration is 0.56 mg m^{-3} globally (Boyce et al. 2010) and ~ 0.46 mg m^{-3} for the Great Barrier Reef (De'ath et al. 2010). However, there are both temporal and spatial variations in these concentrations. Seasonally, summer values in the Great Barrier Reef average around 0.6 mg m^{-3}, while winter values are roughly 0.3 mg m^{-3} (De'ath 2007). Geographically, concentrations in the south and central Great Barrier Reef are approximately 0.54 mg m^{-3}, but only about 0.23 mg m^{-3} in the Far North (Brodie et al. 2007). There is additionally a cross-shelf gradient from 1 mg m^{-3} inshore to 0.25 mg m^{-3} offshore (Furnas and Brodie 1996). Although Great Barrier Reef chlorophyll *a* concentrations are considered to be low, relative to the 1-13 mg m^{-3} concentrations in other coastal regions (such as the Gulf of Mexico (Miller and McKee 2004)), water quality degradation from land-based runoff is a major threat to the sensitive environments of the Great Barrier Reef (Haynes and Michalek-Wagner 2000; Haynes et al. 2007; Great Barrier Reef Marine Park Authority 2014).

Previous studies have assessed the spatial and temporal patterns of flood plumes in the Great Barrier Reef lagoons (Devlin 2001; Devlin et al. 2013) and the effect of terrestrial nutrient runoff on the coral organisms specifically (Devlin and Brodie 2005; Wooldridge et al. 2006). In this study, we explore whether a relationship between tropical cyclone activity and relative water quality can be detected over the entire Great Barrier Reef when accounting for all tropical cyclone and tropical storm activity between 2004-2014. We use statistical tests to address whether significant relationships can be diagnosed at these large temporal and spatial scales between chlorophyll *a* concentrations across the Great Barrier Reef and tropical cyclone activity and the specific characteristics of wind, rainfall, size, and translation speed. We additionally analyze the water quality at different time lags to the tropical cyclone activity to investigate the relative dominance of the tropical cyclone mechanisms for reducing water quality.

2 Methods

2.1 Remotely Sensed Data

MODIS is a multiband imaging spectrometer that was launched by NASA in 2002 on board the Aqua satellite platform. The Aqua satellite is in a sun-synchronous, near-polar orbit at a 705-km altitude, which allows the MODIS instrument to image the entire Earth every one to two days. MODIS provides quantitative data on global ocean bio-optical properties to examine oceanic factors that affect global change and to assess the role of oceans in the global carbon cycle, as well as other biogeochemical cycles (Ocean Biology Processing Group 2003).

We used the 0.041˚ (~4.6 km at the equator), 8-day Level 3 Aqua MODIS Chlorophyll *a* concentration product processed by the NASA Ocean Color Team (Ocean Biology Processing Group 2003). MODIS is an optical sensor and, as such, its ability to collect data can be inhibited by sun glint, inter-orbit gaps, ice, low ambient light, and clouds. Cloud interference presents a considerable impediment when using this product to analyze the relationship between tropical cyclone activity and surface chlorophyll *a* concentrations, as tropical cyclone activity intrinsically brings cloud cover. By averaging the cloud-free acquisitions at each pixel over an 8-day period, the 8-day product is more robust to these sources of error.

Chlorophyll *a* concentration is calculated using radiative transfer equations, and the product is derived from the OCI Algorithm (Ocean Biology Processing Group 2003). The algorithm is based on methods developed for the Coastal Zone Color Scanner program (Gordon and Clark 1980) and has been refined and adapted for MODIS bands (Carder et al. 2003). This adaptation has also improved the accuracy of the chlorophyll *a* estimates in coastal (i.e., Case 2) waters (Carder et al. 2003).

All data composited between 1 January and 15 May (tropical cyclone season for north-eastern Australia) for the years from 2004 to 2014 were downloaded for analysis. We analyzed each global 8-day composite over the Great Barrier Reef region delimited using Geographic Information Systems (GIS) and a shapefile from the Great Barrier Reef Marine Park Authority. The area extends from 10.7°S to 24.6°S and covers an area of 347,192 km^2 (Figure 2).

2.2 Meteorological Data

We used meteorological data for the independent variables in our statistical analyses, including tropical cyclone presence or absence. Tropical cyclone presence or absence was determined for every 8-day period using the coordinate locations of storms recorded in the Operational Data for each tropical cyclone season from 2004 to 2014 (Australian Bureau of Meteorology 2014a). For the predictor variables of activity, we included all events from a tropical low to Category 5 storm. The total number of events in the study period is 43, with an annual maximum of seven events and an annual average of four events (Figure 3). Some events bridge more than one 8-day time period, and so there are ~57 time slices that include tropical cyclone activity (depending on the lag time analyzed). However, a number of these events overlap in time, and so are unlikely to produce a unique chlorophyll *a* response.

We also tested the tropical cyclone characteristics from the Cyclone Damage Potential (CDP) dataset (Holland et al. 2016; see also: Done et al. 2015) for each tropical cyclone that occurred during our study period. The CDP dataset includes 6-hourly maximum wind speeds, translation speed of the system, and radius of 64-knot wind data (i.e., storm size) for tropical cyclone events of Category 1 (on the Saffir-Simpson Scale) or greater (~15 distinct tropical cyclone events and ~22 time periods with tropical cyclone activity > category 1, depending on the time lag being analyzed). We used this dataset to identify tropical cyclone events affecting the Great Barrier Reef area between March 2004 and early April 2014 (the dates available for this dataset), and then calculated the maxima and means of the maximum wind speeds, translation speeds, and tropical cyclone sizes for each 8-day period to be used as the tropical cyclone characteristics predictor variables of chlorophyll *a* concentrations.

Daily coastal weather data during our study period were retrieved from the Australian Bureau of Meteorology weather stations at Lockhart River Airport, Cairns Aero, Townsville Aero, Mackay M.O., Gladstone Airport, and Gladstone Radar (Australian Bureau of Meteorology 2014b) (locations depicted with stars on Figure 2). We calculated the maximum and average daily rainfall total, wind speed, and wind gust over each 8-day period when a tropical cyclone was present in the area. We used the coastal meteorological data to infer the relative importance of the mechanisms for delivering nutrients to the surface lagoon waters during a tropical cyclone event by examining the relative significance and correlation of rainfall and wind activity to chlorophyll *a*.

2.3 Statistical Techniques

Using only the pixels that had data in the 8-day composite, we calculated the minimum (MIN), mean, 90th percentile (90 PCT), 95th percentile (95 PCT), and maximum (MAX) of chlorophyll *a* in each 8-day time step over the whole of the Great Barrier Reef. We then calculated the proportion of pixels that exceeded a level of 1 mg m^{-3} (% > 1mg m^{-3}) over the study region for each 8-day period. This value is roughly double the threshold suggested by De'ath and Fabricius (2010) for maintaining high coral richness and low macroalgal cover. Pixels in excess of 1 mg m^{-3} indicate a strong potential for damaging effects on the reef environment. These metrics of chlorophyll *a* concentrations represent the dependent variables of analysis, as we sought to determine whether, and to what extent, different tropical cyclone characteristics influence these concentration metrics. Since tropical cyclones are extreme events and hence rare by definition, we found it important to include a range of descriptive statistics that reflect the spread of the data (e.g., minimum, mean, upper percentiles, and maximum), so that outliers are properly accounted for.

We then assessed separate bivariate and (where applicable) multivariate relationships between each of these descriptive statistics of chlorophyll *a* and each of the meteorological independent variables using the following statistical methods (Table 1):

(1) Student's two-sample T-tests to identify significant differences in chlorophyll *a* concentrations between pixels with and without tropical cyclone activity in the Great Barrier Reef; (2) multivariate one-way ANOVA to estimate the extent to which tropical cyclone characteristics can explain the variance in chlorophyll *a* concentrations, and which characteristics are significant; and (3) single-factor and piece-wise linear regressions to explore the relationships between chlorophyll *a* concentrations and tropical cyclone size, maximum wind speed, translation speed, coastal rainfall, coastal wind, and coastal gust speeds.

We conducted the statistical analyses for several 8-day time lag increments, based on the available 8-day MODIS composites. For this analysis, the time-lag increments (relative to meteorological data) are referred to as follows: the "no-lag" increment refers to the MODIS composite collected concurrently with the meteorological data over an 8-day period; the "8-day lag" refers to the MODIS composite analyzed against meteorological data from the preceding 8-day period. Other lag increments (16-day, 24-day, 32-day) follow a similar pattern. Statistical analyses were first performed for no-lag data, then repeated for 8-day, 16-day, 24-day, and 32-day lag periods in order to infer possible causal mechanisms between tropical cyclone and phytoplankton activity in the coastal lagoon. We also estimated the response time of the phytoplankton to the tropical cyclone activity, the time of maximum phytoplankton growth and lowest water quality, and the temporal extent of the effect of tropical cyclone activity on the chlorophyll *a* concentrations.

Critical to the interpretation of the mechanisms governing water quality change is the recognition that if the peak remotely sensed chlorophyll *a* response was found during the time of tropical cyclone activity or shortly thereafter (roughly 1 week or less, given results from Subrahmanyam et al. 2002; Lin et al. 2003; Siswanto et al. 2008), then we could infer that the phytoplankton activity was primarily excited by the wind-driven re-suspension mechanism. If, however, the peak response was not detected within this short lag (roughly ~1 week), then it is more likely that the rainfall inundation and river discharge was the dominant mechanism for providing nutrients to augment phytoplankton activity (in the context of results from Alexander et al. 2001 see Figure 1).

2.4 Hypothesized Relationships

As the tropical cyclone passes over the reef and coastal lagoon (0-8 day time lag), it can be hypothesized that wind speeds have a positive correlation with chlorophyll *a* (especially the mean and extreme values) due to re-suspension of benthic sediments and nutrient pulses from pore waters (Furnas 1989). During this period in which wind-driven re-suspension dominates, a negative relationship would be detected between translation speed and chlorophyll *a*. If a tropical cyclone moves more slowly across the Great Barrier Reef lagoon, then the region experiences tropical cyclone wind conditions for a longer duration, allowing for increased re-suspension of sediments. However, the inverse may also be possible, where chlorophyll *a* is positively correlated with tropical cyclone translation speed because an increased translation speed increases the ground-relative wind speed, in turn promoting sediment and associated nutrient re-suspension and a concomitant phytoplankton response. A positive correlation of tropical cyclone size with chlorophyll *a* can be hypothesized: as tropical cyclone size increases, the total area that sediments can be re-suspended from the wind action increases. At this time scale, strong correlations between rainfall and chlorophyll *a* measures may be unlikely given the time required for flow through the catchment to the lagoon.

After the tropical cyclone makes landfall, elevated phytoplankton mass due to the wind-suspended nutrient loading may persist (Lin et al. 2003). However, we hypothesize that a higher magnitude response will be more closely correlated with the cyclone characteristics that control the ensuing rainfall inundation and river discharge mechanism. At the time scale of 8-day and 16-day lags, a significant positive correlation between rainfall and chlorophyll *a* would persist, whereby rainfall transports nutrients and sediments to the Great Barrier Reef lagoon through increased runoff and river discharge. These increases would result in more chlorophyll *a* detected in the lagoon. The influence of rainfall on chlorophyll *a* may be stronger than wind speed at this timescale, since wind-driven re-suspension only occurs during tropical cyclone passage over the lagoon. We also anticipate a negative influence of translation speed on chlorophyll *a*. Maximum potential rainfall in a location affected by tropical cyclone activity is typically inversely proportional to the system's translation speed (Elsner and Kara 1999) and faster forward motion reduces the risk of devastating floods (Elsner and Kara 1999). A positive relationship between tropical cyclone size and chlorophyll *a* is expected, particularly at the mean and extreme upper values. As tropical cyclone size increases, the total catchment area exposed to heavy rainfall typically increases and the storm surge and coastal flood inundation volumes also increase (Irish et al. 2008). Subsequently, the positive correlation between these physical effects and nutrient and sediment loading to the Great Barrier Reef lagoon also intensify, ultimately resulting in reduced water quality.

3 Results and Discussion

The spatial distribution of chlorophyll *a* concentrations over the summer season in the 10-year study period is given in Figure 4 to contextualize the analysis that follows. The average chlorophyll *a* in Figure 4a shows a cross-shelf gradient similar to that reported in Furnas and Brodie (1996), with at least 1 mg m^{-3} average concentrations in the coastal lagoons and around some of the southern reef atolls and decreasing away from the coastline. Extreme water quality reductions are evident (yellow to brown colors, Figure 4b) in lagoons associated with larger urban centers such as the Cairns to Townsville lagoon, and the Gladstone lagoon, all of which have maximum values far exceeding the 1 mg m^{-3} threshold. The Far North region is often considered the most pristine area of the Great Barrier Reef for water quality (De'ath and Fabricius 2010). However, our results demonstrate that the lagoon just south of Lockhart also has elevated chlorophyll *a* and the water quality is a cause for concern for reef health in this location. Although this lagoon does not border a dense urban area, the Far North region is known for cattle grazing, sugarcane agriculture, and tropical fruit horticulture (Agricultural Land Audit 2013); hence, nutrients and pesticides leached from these areas during times of tropical cyclone activity and heavy rain exacerbate the reduction in water quality.

3.1 Tropical Cyclone Activity

Our analysis demonstrates a significant influence of tropical cyclone activity on water quality in the Great Barrier Reef. In particular, we found a statistically significant elevation in chlorophyll *a* concentrations at 8-day and 16-day lags after tropical cyclone activity. At no lag and lags longer than 16 days, no statistically significant elevations were observed. The peak differences occur at an 8-day time lag (Table 2). Specifically, mean values of chlorophyll *a* were systematically greater when a tropical cyclone was present in the preceding 8-day period, with median values increasing by about 9% from ~0.47 mg m^{-3} with no tropical cyclone and ~0.51 mg m^{-3} with tropical cyclone and a large increase in the spread of the data during tropical cyclone presence (Figure 5a). More striking, though, is the pattern for the extreme upper values of chlorophyll *a* measures at the 16-day time lag where maximum values are significantly elevated (Figure 5b). The Student's T-test confirms that a significant difference of 8.06 mg m^{-3} exists between these means (Table 2). Augmented phytoplankton response is therefore still detected over two weeks after the passage of the tropical cyclone. This peak in chlorophyll *a* concentrations at both 8- and 16-day time lags following tropical cyclone activity concurs with the findings of Alexander et al. (2001), suggesting that the process of nutrient and sediment delivery from catchment discharge is the dominant mechanism for reduced water quality. If the effect had been significant from no time lag to an 8-day lag, then this would have been indicative of a more immediate wind-driven re-suspension mechanism dominance (see again Lin et al. 2003). Preliminary results, then, suggest an influence of tropical cyclone activity on chlorophyll *a* arising from the secondary consequences of terrestrial flooding.

3.2 Wind-Driven Re-suspension (No Lag and 8-Day Lag)

To explore the discrete mechanisms by which tropical cyclone activity affects Great Barrier Reef water quality, we looked more closely at the relationship between specific tropical cyclone characteristics and chlorophyll *a* concentrations. During tropical cyclone activity and just after (no-lag and 8-day lag), tropical cyclone characteristics collectively are found to be significantly related to the variance of chlorophyll *a* concentrations in the Great Barrier Reef, with tropical cyclone size as the dominant characteristic influencing water quality. During the tropical cyclone event (no lag), storm characteristics explain 55-65% of the chlorophyll *a* measures, particularly the mean, upper percentiles, and proportion of pixels that exhibit exceedance of water quality threshold (% > 1 mg m^{-3}), as indicated by the multivariate analysis of variance (see Table 3 for ANOVA results). While tropical cyclone wind speed significantly accounts for up to 14% of the predictive power of this model for the mean and 90^{th} percentile of chlorophyll *a*, neither translation speed nor rain proportions are significant in this timeframe (Table 3). Therefore, at this timescale, the re-suspension mechanism accounts for a larger portion of the detected change in chlorophyll *a* than rainfall runoff and river discharge. The tropical cyclone size dominates the model and significantly accounts for up to 60% of the predictive power (Table 3). This suggests that the total area affected by tropical cyclone conditions is the most influential characteristic for altering the chlorophyll *a* concentration at this timescale.

Contrary to the hypothesis, there are few significant direct relationships between tropical cyclone wind speed and chlorophyll *a* dependent variables during tropical cyclone activity (no lag and 8-day lag), except for minimum chlorophyll *a* values over the Great Barrier Reef (Table 5a, b). The only significant positive correlations are between tropical cyclone wind speed and minimum chlorophyll *a* at an 8-day time lag (r^2=0.262, p=0.018; see Table 5b), and between the minimum chlorophyll *a* and average weather station gust speed recorded at no time lag (r^2 = 0.135, p=0.007; Figure 6a). This suggests that increased tropical cyclone and coastal recorded wind speeds only affect minimum and background values of chlorophyll *a*. While *greater* wind speeds would result in the re-suspension of benthic substrates and pore water nutrients (Furnas 1989), the Great Barrier Reef lagoon is known to be a naturally nutrient-limited ecosystem (Furnas 2003; Furnas et al. 2005; Dekker et al. 2006). Hence, the concentration of re-suspended nutrients and the corresponding phytoplankton response would both be small. These findings support earlier results that Great Barrier Reef water quality is unlikely to be influenced by static or re-suspended concentrations of sediments, nutrients, or pollutants already in reef environments (Furnas 2003).

During the 0- and 8-day lag increments relative to tropical cyclone activity, we do not find any statistically significant relationship between tropical cyclone translation speed and chlorophyll *a* (Table 5a, b and Figure 7a, b). Neither the duration of exposure to tropical cyclone winds nor increased ground-relative wind speed exhibit a strong influence at this timescale. The weak response of the chlorophyll *a* to the wind speed characteristic may explain the lack of response to translation speed, since the rate at which the tropical cyclone travels primarily influences the experienced wind speed intensity and duration.

During the passage of the tropical cyclone (no lag), tropical cyclone size has a strong positive influence on chlorophyll *a* concentrations, as reflected in measures of mean, top decile, and proportion of area exceeding the 1 mg m^{-3} threshold for water quality (Table 5a; Figure 8a). Note the appearance of clustering on either side of a potential breakpoint at ~35 km radius in Figure 8a. This cluster pattern is also present in the relationship between cyclone size and other chlorophyll *a* measures at no lag. We tested piece-wise regressions considering the individual clusters, which do not yield significant relationships between tropical cyclone size and chlorophyll *a*. However, we can infer that the positive correlation in the overall data may be driven by the difference between the clusters, if they are representing a physically realistic breakpoint. At no time lag, the relationship between tropical cyclone size and chlorophyll *a* may not be directly continuous, but could be categorical, whereby larger tropical cyclones (>35 km) lead to increased measures of chlorophyll *a* than smaller tropical cyclones (<35 km). More data is required to differentiate between the continuous or categorical positive correlation. Regardless, increasing tropical cyclone size increases the total area that nutrients can be extracted from by tropical cyclone conditions (such as wind speed). The data therefore suggest that total area affected by tropical cyclone conditions is more important than the magnitude of the duration and intensity of the exposure of the Great Barrier Reef to tropical cyclone wind conditions.

The positive correlations between chlorophyll *a* and tropical cyclone size (and the dominance of this characteristic) are maintained at the 8-day time lag (see Table 5b). However, the positive correlations are weaker. For example, the correlations with the chlorophyll *a* mean and the % of pixels > 1 mg m^{-3} are reduced to r^2=0.185 (Table 5b) and r^2=0.2705 (Table 5b, Figure 8b) respectively. This is also reflected in the multivariate ANOVA where, collectively, the tropical cyclone characteristics no longer significantly explain the variance in the chlorophyll *a* at the 8-day time lag. This diminished influence suggests that this time period (8-day lag) is the transition point from the wind-resuspension mechanism to the rainfall runoff and river discharge mechanism. Thus, increasing the tropical cyclone size at this 8-day time lag does increase the area affected by tropical cyclone conditions, but these conditions do not necessarily produce the largest nutrient and chlorophyll *a* response at this timescale. Further analysis to identify the exact timing of the change in mechanisms would require data at an increased temporal resolution which is beyond the scope of this study.

3.3 Rainfall-River Discharge Mechanism (16 Day Lag)

More than two weeks after the passage of the tropical cyclone over the coastal lagoon (16-day lag), we again find that tropical cyclone characteristics are significantly related to the variance of chlorophyll *a* concentrations in the Great Barrier Reef: not only through tropical cyclone size, but also through translation speed and rainfall at this time lag. The analysis of variance shows that the maxima of the characteristics at this time period significantly account for 42-53% of the variance in the mean, 95th percentile, and proportion of area that exceeds 1 mg m^{-3} of chlorophyll *a* (see Table 4 for ANOVA results at 16-day lag). The predictive power is split between size, rainfall, and translation speed, which significantly account for up to 29%, 24%, and 16%, respectively (Table 4). This suggests that at this time lag, storm surge (governed by tropical cyclone size and translation speed) and the catchment inundation (governed by rainfall and tropical cyclone size) cause a greater amount of change in the surface chlorophyll *a* concentrations than wind speed, which does not significantly account for any of the chlorophyll *a* variance (Table 4).

Over two weeks after tropical cyclone activity (16-day lag), single-factor regressions demonstrate that tropical cyclone wind speeds yield few significant correlations with chlorophyll *a*. Additionally, the positive correlation with minimum values is no longer detected at this longer time lag (Table 5c; Figure 6b,c). This suggests that wind speed and associated benthic re-suspension no longer excite a response of phytoplankton activity over the Great Barrier Reef 16 days after a cyclone emerges in the area.

We do not find the hypothesized negative correlation with translation speed. There are in fact positive correlations between tropical cyclone translation speed and the maximum values of chlorophyll *a* at a 16-day time lag (r^2=0.2268, p=0.029 Table 5c, Figure 7c). While the literature suggests that the contribution of nutrients to the lagoon from storm surge retreat is likely minor, the findings here could suggest that increasing translation speed increases coastal erosion from storm surge leading to sediment and nutrient loading into the lagoon. The literature suggests that translation speed and storm surge inundation are inversely correlated (Peng et al. 2004; Weisberg and Zheng 2006). However, the suggested inverse relationship may be non-linear (Irish and Resio 2010) and the sensitivity of storm surge to translation speed varies greatly between cases (Peng et al. 2004). Resonance may occur for certain tropical cyclone translation speeds (Rego and Li 2009), whereby increasing translation speed increases peak surge heights by up to

40% (Rego and Li 2009). Despite flooding a narrower section of the coast, a tropical cyclone with an increased translation speed would move quickly across the shoreline, generating higher surges (Rego and Li 2009). The increase in surge height and associated coastal zone erosion may result in augmented nutrient and sediment leaching from the area affected and thus increased water quality deterioration and phytoplankton response after the inundation water has retreated back to the lagoon. This hypothesis accounts for the positive correlations between tropical cyclone translation speed and the maximum values of chlorophyll *a* at a 16-day time lag, and also explains the lack of correlation with the proportion of the area negatively affected (% > 1 mg m^{-3}) (Table 5c), since the area inundated would be smaller with increased translation speed. In Figure 7, there appears to be a breakpoint in the data, such that there are two clusters of data on either side of tropical cyclone translation speed ~12 km h^{-1}. We have tested a piece-wise regression considering each individual cluster; however, that approach does not yield a significant relationship between tropical cyclone translation speed and chlorophyll *a*.

There are stronger single-factor positive correlations between tropical cyclone-associated rainfall and chlorophyll *a* concentrations than with wind speed at 8- and 16-day time lags (Figures 9b,c compared to Figures 6b,c). This relationship is most pronounced for the extreme chlorophyll *a* values. While the lag time of river discharge following a tropical cyclone event depends on many factors, the data here suggest that it takes one-to-two weeks for the rainfall recorded along the coastline to move through the catchments, leach nutrients and sediments into the rivers and tributaries, and transport and deposit them in the Great Barrier Reef lagoon, where the phytoplankton response to this influx can be detected by the MODIS satellite. Rainfall runoff and river discharge at these time scales have stronger influences on the chlorophyll *a* extreme values (and therefore water quality) than wind-driven re-suspension. The correlations found with rainfall were weaker than anticipated; it may be necessary to include catchment-integrated rainfall and stream flow data to fully explore the rainfall runoff mechanism, which is beyond the scope of this study.

At the 16-day lag, tropical cyclone size (radius) still strongly influences chlorophyll *a* measures such as mean, extreme values, and the proportion of pixels > 1 mg m^{-3} (see Figure 8c for the secondary peak in the correlation with % pixels > 1 mg m^{-3} at 16-day time lag). As tropical cyclone size increases, the total area from which nutrients and sediments can be leached increases. Storm surge and coastal flood inundation volume increases (Irish et al. 2008), and the total coastal area exposed to heavy rainfall also increases. Subsequently, the positive correlations between these physical effects and nutrient and sediment loading would intensify, ultimately resulting in increased chlorophyll *a*, particularly the extreme values. Given the relationships found between tropical cyclone characteristics and chlorophyll *a* at this time lag (16 days), we can infer that the rainfall runoff, river discharge, coastal inundation, and nutrient loading are the main mechanisms affecting the water quality over the Great Barrier Reef, and that the re-suspension mechanism no longer has a role in reducing water quality (Figure 1).

Although some of the correlation values are relatively small, the p-values demonstrate their significance in these processes. Furthermore, a singular tropical cyclone characteristic, size, can account for up to 30-45% of the variability in the surface water chlorophyll *a* concentration. In contrast to Brodie et al. (2012a), which demonstrates that the residence time of nutrients and sediments is on the order of a few weeks in the Great Barrier Reef lagoon, we have found no systematic response of the chlorophyll *a* to tropical cyclone-related weather at timescales longer than 16 days. We find that the wind-driven re-suspension mechanism only contributes to raising minimum values of chlorophyll *a* in the Great Barrier Reef during and just after the tropical cyclone activity, and that the mean and extreme values which degrade the water quality for the reef environment appear to be governed primarily by the catchment inundation and river discharge mechanism through tropical cyclone size and, to a lesser extent, translation speed and rainfall at a 16-day lag. However, it is important to note that any external nutrients and sediments brought to the Great Barrier Reef through storm surge and rainfall runoff that are not biologically utilized during the wet season may persist in the lagoon into the dry season (Brodie et al. 2012a). These latent nutrients may then be re-suspended in the water column through the wind-driven mechanisms during any high-wind event in the dry season, causing an unusual phytoplankton response for the dry season (Brodie and Furnas 1996; Devlin et al. 2001; Udy et al. 2005). In this way, tropical cyclone activity during the wet summer season may still act to reduce water quality in the dry season.

4 Conclusions

The results of this study demonstrate that tropical cyclone activity significantly reduces water quality over the Great Barrier Reef at 8- and 16-day time lags. During and just after the passage of the tropical cyclone (no lag and 8-day lag), the wind-driven re-suspension pathway is the dominant mechanism for inducing a phytoplankton response. However, wind speed in isolation only increases minimum levels of chlorophyll *a* and has no significant effect on the mean or extreme upper values. As such, it may serve to slightly reduce the water quality and render the area more vulnerable to subsequent negative impacts of runoff. At 16-day time lags, we find a positive influence of tropical cyclone translation speed and coastal rainfall on the mean and extremes of chlorophyll *a* concentration, but no relationship with wind speed. Hence, we suggest that the mechanisms of rainfall runoff, river discharge, and coastal inundation retreat are the dominant factors in reducing water quality in the Great Barrier reef at this time lag. The resulting elevations in mean and extreme measures of chlorophyll *a* may ultimately lead to negative effects for the coral organisms and ecosystems. These results are consistent with the proposed mechanism in the literature in which an influx of nutrients and sediments from enhanced erosion and fertilizer loss from the catchment (Brodie et al. 2012b) is drives reduced water quality and elevated phytoplankton activity (Furnas 2003). The mechanism of re-suspension only redistributes the minimal nutrients already in the nutrient-limited ecosystem, which increases minimum chlorophyll *a* values at an immediate timescale, but is insufficient to cause a more notable reduction in the water quality. The positive correlations between rainfall and chlorophyll *a* were weak, and hence our results do not adequately explain the rainfall runoff and river discharge mechanism. In future work, it will be necessary to include catchment-integrated rainfall, stream flow, and wave height data with increased temporal resolution to fully explore the partitioning of the re-suspension, rainfall runoff, river discharge and coastal inundation runoff mechanisms, and the time scales at which these occur.

Our analyses have systematically demonstrated the dominance and significance of tropical cyclone size (radius) in influencing means and extremes of chlorophyll *a* in addition to the proportion of pixels that exceed 1 mg m^{-3}. These effects were observed during the lifecycle of the tropical cyclone, as well as at 8- and 16-day lags. As tropical cyclone size increases, so too do the measures of chlorophyll *a*. Results suggest that the total area affected and area that nutrients can be extracted from is more important than the duration and intensity of the exposure to tropical cyclone conditions such as wind speed and rainfall.

Our findings support policy recommendations for the reduction of runoff, erosion, fertiliser loss, and nutrient and sediment leaching into the reef lagoon from the Queensland coastal lands, such as the Reef Water Quality Protection Plan (Department of Premiers and Cabinet 2013) and the Paddock to Reef program (Department of Premiers and Cabinet 2013). Our results demonstrate that urban and agricultural areas in catchments that drain into the Great Barrier Reef lagoon need to be particularly vigilant in reducing leaching as urbanization and agricultural intensification continue to affect the reef ecosystem, despite increased awareness of its impacts on the reef ecosystems (see Brodie et al. 2012b for an overview of management responses to nutrient loading of the Great Barrier Reef). These measures will be particularly important in the face of climate change, where global pressures such as ocean warming and acidification are likely to increase, resulting in further coral bleaching, dissolution, and reduced ecosystem resilience to disturbances such as tropical cyclones (Hughes et al. 2003; Hoegh-Guldberg et al. 2007; Pandolfi et al. 2011). Furthermore, while tropical cyclone response to climate change is still an active area of inquiry, it has been suggested that the frequency of intense tropical cyclones (Category 4 and 5) and their associated wind speeds, power dissipation, and damage will increase with rising global temperatures (Bender et al. 2010; Knutson et al. 2010; Done et al. 2012; Holland and Bruyère 2013; Knutson et al. 2013). The results of this study demonstrate that the change to tropical cyclone size with climate change has the potential to influence future water quality of the Great Barrier Reef. Although the size response to climate change is inconclusive thus far in the scientific literature, it has been suggested that tropical cyclone-associated precipitation will increase with climate change (Knutson et al. 2013). Finally, increasing tropical cyclone precipitation would provide a potential increase in nutrient leaching through the rainfall runoff and river discharge mechanism and subsequent increases in phytoplankton response and reductions in water quality. In summary, these relationships suggest that tropical cyclone size and precipitation following landfall are the most critical characteristics to assess in future scenario-building for reef resilience.

Data Availability

The Aqua MODIS Level 3 Chlorophyll *a* 4km gridded data set is available at:

https://oceancolor.gsfc.nasa.gov/cgi/l3

The tropical cyclone activity in the area can be retrieved from the Australian Bureau of Meteorology Database of past tropical cyclone tracks:

http://www.bom.gov.au/cyclone/history/

The tropical cyclone characteristic data is described in Holland et al. 2016 and Done et al. 2015

The coastal weather station data can be retrieved from the Australian Bureau of Meteorology Weather Station Directory: http://www.bom.gov.au/climate/data/stations/

Analysis was carried out with ENVI, ArcGIS, STATA version 14.1, and R version 3.3.0.

Author Contributions

C. Parker designed the overall study. C. Parker and S. Spera designed the remote sensing and GIS analysis techniques. K. Spangler aided data organization and design of statistical analysis techniques. C. Parker carried out all analysis and produced all figures. A. Lynch, S. Spera, and K. Spangler contributed to the interpretation of findings. C. Parker prepared the manuscript with contributions from all co-authors.

Acknowledgements

The authors would like to thank Daniel P. Moriarty III for copy editing, and James Done and Greg Holland at the National Center for Atmospheric Research (Boulder, CO) for advice and their Cyclone Damage Potential dataset. We also acknowledge the Bureau of Meteorology Australia for providing tropical cyclone data, coastal weather station wind speed and rainfall data, and NASA Ocean Color group for the gridded surface chlorophyll *a* concentration product from the MODIS satellite.

This work was partially supported by a research award from the Institute at Brown for Environment and Society.

References

Agricultural Land Audit (2013). Agricultural land audit - current pasture production - Far North Queensland. Online http://www.daf.qld.gov.au/environment/ag-land-audit Accessed [May 2016].

Alexander, J., Fielding, C. R., Wakefield, S. J., George, M. T., & Cottnam, C. F. (2001). Fluvial geochemistry through a short-duration, tropical-cyclone induced discharge event in the Burdekin River and Hann Creek, North Queensland, Australia. Aquatic Geochemistry, 7(4), 275-293.

Anthony, K. R., & Fabricius, K. E. (2000). Shifting roles of heterotrophy and autotrophy in coral energetics under varying turbidity. Journal of experimental marine biology and ecology, 252(2), 221-253.

Australian Bureau of Meteorology (2014a). Database of past tropical cyclone tracks. [http://www.bom.gov.au/cyclone/history/]. Accessed April 2014.

Australian Bureau of Meteorology (2014b). Weather Station Directory. [http://www.bom.gov.au/climate/data/stations/]. Accessed May 2014.

Bender, M. A., Knutson, T. R., Tuleya, R. E., Sirutis, J. J., Vecchi, G. A., Garner, S. T., & Held, I. M. (2010). Modeled impact of anthropogenic warming on the frequency of intense Atlantic hurricanes. Science, 327(5964), 454-458.

Boyce, D. G., Lewis, M. R., & Worm, B. (2010). Global phytoplankton decline over the past century. Nature, 466(7306), 591-596.

Birrell, C. L., McCook, L. J., & Willis, B. L. (2005). Effects of algal turfs and sediment on coral settlement. Marine Pollution Bulletin, 51(1), 408-414.

Brodie, J. E., Kroon, F. J., Schaffelke, B., Wolanski, E. C., Lewis, S. E., Devlin, M. J., ... & Davis, A. M. (2012b). Terrestrial pollutant runoff to the Great Barrier Reef: an update of issues, priorities and management responses. Marine Pollution Bulletin, 65(4), 81-100.

Brodie, J. J., Furnas, M. M., Stevens, A., Trott, L. L., Pantus, F. F., & Wright, M. M. (1997, January). Monitoring chlorophyll in the Great Barrier Reef lagoon: trends and variability. In Proceedings of the 8th International Coral Reef Symposium, Panama, 24-29 June 1996-pages: 1: 797-802. Smithsonian Tropical Research Institute.

Brodie, J., & Furnas, M. (1994). Long term monitoring programs for eutrophication and the design of a monitoring program for the Great Barrier Reef. In Proceedings of the 7th International Coral Reef Symposium (Vol. 1, pp. 77-84).

Brodie, J., De'Ath, G., Devlin, M., Furnas, M., & Wright, M. (2007). Spatial and temporal patterns of near-surface chlorophyll a in the Great Barrier Reef lagoon. Marine and Freshwater Research, 58(4), 342-353.

Brodie, J., Schroeder, T., Rohde, K., Faithful, J., Masters, B., Dekker, A., ... & Maughan, M. (2010). Dispersal of suspended sediments and nutrients in the Great Barrier Reef lagoon during river-discharge events: conclusions from satellite remote sensing and concurrent flood-plume sampling. Marine and Freshwater Research, 61(6), 651-664.

Brodie, J., Wolanski, E., Lewis, S., & Bainbridge, Z. (2012a). An assessment of residence times of land-sourced contaminants in the Great Barrier Reef lagoon and the implications for management and reef recovery. Marine pollution bulletin, 65(4), 267-279.

Carder, K. L., Chen, F. R., Lee, Z., Hawes, S. K., & Cannizzaro, J. P. (2003). MODIS ocean science team algorithm theoretical basis document. ATBD, 19(Version 7), 7-18.

Davies, P. L., & Eyre, B. D. (2005). Estuarine modification of nutrient and sediment exports to the Great Barrier Reef Marine Park from the Daintree and Annan River catchments. Marine Pollution Bulletin, 51(1), 174-185.

De'ath, G., & Fabricius, K. (2010). Water quality as a regional driver of coral biodiversity and macroalgae on the Great Barrier Reef. Ecological Applications, 20(3), 840-850.

De’ath, G. (2007) The spatial, temporal and structural composition of water quality of the Great Barrier Reef, andindicators of water quality and mapping risk. Unpublished report to the Marine and Tropical Sciences Research Facility. Reef and Rainforest Research Centre Limited, Cairns (71pp.)

Dekker, A., Marks, A., Qin, Y., & Oubelkheir, K. (2006). Chlorophyll and suspended sediment assessment in a macrotidal tropical estuary adjacent to the Great Barrier Reef: spatial and temporal assessment using remote sensing. CRC Coastal Zone Estuary and Waterway Management.

Deloitte Access Economics (2013), Economic contribution of the Great Barrier Reef, Great Barrier Reef Marine Park Authority, Townsville.

Department of Premiers and Cabinet, (2013). Paddock to Reef Integrated Monitoring, Modelling and Reporting Program, Reef Water Quality Protection Plan, 2013-2018. Queensland Department of Premiers and Cabinet. The State of Queensland and the Commonwealth of Australia. www.reefplan.qld.gov.au.

Department of Premiers and Cabinet, (2013). Reef Water Quality Protection Plan, 2013, For the Great Barrier Reef World Heritage Area and adjacent catchments. Queensland Department of Premiers and Cabinet. The State of Queensland and the Commonwealth of Australia. www.reefplan.qld.gov.au.

Devlin, M. J., & Brodie, J. (2005). Terrestrial discharge into the Great Barrier Reef Lagoon: nutrient behavior in coastal waters. Marine Pollution Bulletin, 51(1), 9-22.

Devlin, M., & Schaffelke, B. (2009). Spatial extent of riverine flood plumes and exposure of marine ecosystems in the Tully coastal region, Great Barrier Reef. Marine and Freshwater Research, 60(11), 1109-1122.

Devlin, M., Waterhouse, J., Taylor, J., & Brodie, J. E. (2001). Flood plumes in the Great Barrier Reef: spatial and temporal patterns in composition and distribution. Great Barrier Reef Marine Park Authority.

Devlin, M. J., Da Silva, E. T., Petus, C., Wenger, A., Zeh, D., Tracey, D., ... & Brodie, J. (2013). Combining in-situ water quality and remotely sensed data across spatial and temporal scales to measure variability in wet season chlorophyll-a: Great Barrier Reef lagoon (Queensland, Australia). Ecological Processes, 2(1), 31.1

Done, J. M., Holland, G. J., Bruyère, C. L., Leung, L. R., & Suzuki-Parker, A. (2012). Modeling high-impact weather and climate: lessons from a tropical cyclone perspective. NCAR/TN-490+ STR, p 28.[Available online at http://nldr. library. ucar. edu/repository/collections/TECH-NOTE-000-000-000-854].

Done, J. M., PaiMazumder, D., Towler, E., & Kishtawal, C. M. (2015). Estimating impacts of North Atlantic tropical cyclones using an index of damage potential. Climatic Change, 1-13.

Elsner, J. B., & Kara, A. B. (1999). Hurricanes of the North Atlantic: Climate and society. Oxford University Press.

Fabricius, K. E. (2005). Effects of terrestrial runoff on the ecology of corals and coral reefs: review and synthesis. Marine pollution bulletin, 50(2), 125-146.

Fabricius, K. E., & De'Ath, G. (2004). Identifying ecological change and its causes: a case study on coral reefs. Ecological Applications, 14(5), 1448-1465.

Fabricius, K. E., & Wolanski, E. (2000). Rapid smothering of coral reef organisms by muddy marine snow. Estuarine, Coastal and Shelf Science, 50(1), 115-120.

Fraser, R. H., & Currie, D. J. (1996). The species richness-energy hypothesis in a system where historical factors are thought to prevail: coral reefs. American Naturalist, 138-159.

Furnas, M. M. (1989, January). Cyclonic disturbance and a phytoplankton bloom in a tropical shelf ecosystem. In Red Tides: Biology, Environmental Science and Toxicology. Proceedings of the First International Symposium on Red Tides held November 10-14,

1987, in Takamatsu, Kagawa Prefecture, Japan-pages: 273-276. Elsevier Science Publishing Co., Inc.
Furnas, M. M. (2003). Catchments and corals: terrestrial runoff to the Great Barrier Reef. CRC/AIMS, Townsville, Australia.
Furnas, M. M., & Brodie, J. J. (1996). Current status of nutrient levels and other water quality parameters in the Great Barrier Reef. Downstream Effects of Land Use-pages: 9-21.
Furnas, M., Alongi, D., McKinnon, D., Trott, L., & Skuza, M. (2011). Regional-scale nitrogen and phosphorus budgets for the northern (14 S) and central (17 S) Great Barrier Reef shelf ecosystem. Continental Shelf Research, 31(19), 1967-1990.
Furnas, M., Mitchell, A., Skuza, M., & Brodie, J. (2005). In the other 90%: phytoplankton responses to enhanced nutrient availability in the Great Barrier Reef Lagoon. Marine pollution bulletin, 51(1), 253-265.
Gitelson, A. A., Dall'Olmo, G., Moses, W., Rundquist, D. C., Barrow, T., Fisher, T. R., ... & Holz, J. (2008). A simple semi-analytical model for remote estimation of chlorophyll-a in turbid waters: Validation. Remote Sensing of Environment, 112(9), 3582-3593.
Gitelson, A. A., Gurlin, D., Moses, W. J., & Barrow, T. (2009). A bio-optical algorithm for the remote estimation of the chlorophyll-a concentration in case 2 waters. Environmental Research Letters, 4(4), 045003.
Gong, W., Shen, J., & Reay, W. G. (2007). The hydrodynamic response of the York River estuary to Tropical Cyclone Isabel, 2003. Estuarine, Coastal and Shelf Science, 73(3), 695-710.
Gordon, H. R., & Clark, D. K. (1980). Remote sensing optical properties of a stratified ocean: an improved interpretation. Applied Optics, 19(20), 3428-3430.
Gordon, H. R., & Morel, A. Y. (2012). Remote assessment of ocean color for interpretation of satellite visible imagery: A review (Vol. 4). Springer Science & Business Media.
Great Barrier Reef Marine Park Authority (2011), Impacts of tropical cyclone Yasi on the Great Barrier Reef: a report on the findings of a rapid ecological impact assessment, July 2011, Great Barrier Reef MPA, Townsville.
Great Barrier Reef Marine Park Authority (2014), Great Barrier Reef Outlook Report 2014, Great Barrier Reef MPA, Townsville.
Halford, A., Cheal, A. J., Ryan, D., & Williams, D. M. (2004). Resilience to large-scale disturbance in coral and fish assemblages on the Great Barrier Reef. Ecology, 85(7), 1892-1905.
Harding Jr, L. W., & Perry, E. S. (1997). Long-term increase of phytoplankton biomass in Chesapeake Bay, 1950-1994. Marine Ecology Progress Series, 157, 39-52.
Haynes, D., & Michalek-Wagner, K. (2000). Water quality in the Great Barrier Reef World Heritage Area: past perspectives, current issues and new research directions. Marine Pollution Bulletin, 41(7), 428-434.
Haynes, D., Brodie, J., Waterhouse, J., Bainbridge, Z., Bass, D., & Hart, B. (2007). Assessment of the water quality and ecosystem health of the Great Barrier Reef (Australia): conceptual models. Environmental Management, 40(6), 993-1003.
Hoegh-Guldberg, O., Andréfouët, S., Fabricius, K., Diaz-Pulido, G., Lough, J., Marshall, P., & Pratchett, M. S. (2011). Vulnerability of coral reefs in the tropical Pacific to climate change. Vulnerability of tropical Pacific fisheries and aquaculture to climate change. Secretariat of the Pacific Community, Noumea, 251-296.
Hoegh-Guldberg, O., Mumby, P. J., Hooten, A. J., Steneck, R. S., Greenfield, P., Gomez, E., ... & Knowlton, N. (2007). Coral reefs under rapid climate change and ocean acidification. Science, 318(5857), 1737-1742.
Holland, G., & Bruyère, C. L. (2013). Recent intense hurricane response to global climate change. Climate Dynamics, 1-11.

Holland, G., J. M. Done, M. Ge, and R. Douglas. (2016) An Index for Cyclone Damage Potential. 32nd Conference on Hurricanes and Tropical Meteorology, 17 – 22 April 2016 San Juan, PR

Hu, C. 2009. A novel ocean color index to detect floating algae in the global oceans. Remote Sensing of Environment 113 pp.2118-2129

Hughes, T. P., Baird, A. H., Bellwood, D. R., Card, M., Connolly, S. R., Folke, C., ... & Lough, J. M. (2003). Climate change, human impacts, and the resilience of coral reefs. Science, 301(5635), 929-933.

Hughes, T., Szmant, A. M., Steneck, R., Carpenter, R., & Miller, S. (1999). Algal blooms on coral reefs: what are the causes?. Limnology and Oceanography, 44(6), 1583-1586.

Hutchings, P., Haynes, D., Goudkamp, K., & McCook, L. (2005). Catchment to reef: water quality issues in the Great Barrier Reef Region—an overview of papers. Marine Pollution Bulletin, 51(1), 3-8.

Irish, J. L., & Resio, D. T. (2010). A hydrodynamics-based surge scale for hurricanes. Ocean Engineering, 37(1), 69-81.

Irish, J. L., Resio, D. T., & Ratcliff, J. J. (2008). The influence of storm size on hurricane surge. Journal of Physical Oceanography, 38(9), 2003-2013.

Kawai, Y., & Wada, A. (2011). Detection of cyclone-induced rapid increases in chlorophyll-a with sea surface cooling in the northwestern Pacific Ocean from a MODIS/SeaWiFS merged satellite chlorophyll product. International journal of remote sensing, 32(24), 9455-9471.

Knapp, K. R., Kruk, M. C., Levinson, D. H., Diamond, H. J., and Neumann, C. J., (2010). "The International Best Track Archive for Climate Stewardship (IBTrACS): Unifying tropical cyclone best track data." Bull. Amer. Meteorol. Soc., 91, 363-376.

Knutson, T. R., McBride, J. L., Chan, J., Emanuel, K., Holland, G., Landsea, C., ... & Sugi, M. (2010). Tropical cyclones and climate change. Nature Geoscience, 3(3), 157-163.

Knutson, T. R., Sirutis, J. J., Vecchi, G. A., Garner, S., Zhao, M., Kim, H. S., ... & Villarini, G. (2013). Dynamical downscaling projections of twenty-first-century Atlantic hurricane activity: CMIP3 and CMIP5 model-based scenarios. Journal of Climate, 26(17), 6591-6617.

Kroon, F. J., Kuhnert, P. M., Henderson, B. L., Wilkinson, S. N., Kinsey-Henderson, A., Abbott, B., ... & Turner, R. D. (2012). River loads of suspended solids, nitrogen, phosphorus and herbicides delivered to the Great Barrier Reef lagoon. Marine pollution bulletin, 65(4), 167-181.

Lapointe, B. E. (1997). Nutrient thresholds for bottom-up control of macroalgal blooms and coral reefs. Limnol. Oceanogr, 44, 1586-1592.

Larcombe, P., & Carter, R. M. (2004). Cyclone pumping, sediment partitioning and the development of the Great Barrier Reef shelf system: a review. Quaternary Science Reviews, 23(1), 107-135.

Lin, I., Liu, W. T., Wu, C. C., Wong, G. T., Hu, C., Chen, Z., ... & Liu, K. K. (2003). New evidence for enhanced ocean primary production triggered by tropical cyclone. Geophysical Research Letters, 30(13).

Marra, J., Bidigare, R. R., & Dickey, T. D. (1990). Nutrients and mixing, chlorophyll and phytoplankton growth. Deep Sea Research Part A. Oceanographic Research Papers, 37(1), 127-143.

McClanahan, T. R., Steneck, R. S., Pietri, D., Cokos, B., & Jones, S. (2005). Interaction between inorganic nutrients and organic matter in controlling coral reef communities in Glovers Reef Belize. Marine Pollution Bulletin, 50(5), 566-575.

McCook, L. J. (1999). Macroalgae, nutrients and phase shifts on coral reefs: scientific issues and management consequences for the Great Barrier Reef. Coral reefs, 18(4), 357-367.

Miller, R. L., & McKee, B. A. (2004). Using MODIS Terra 250 m imagery to map concentrations of total suspended matter in coastal waters. Remote sensing of Environment, 93(1), 259-266.

Mitchell, C., Brodie, J., & White, I. (2005). Sediments, nutrients and pesticide residues in event flow conditions in streams of the Mackay Whitsunday Region, Australia. Marine Pollution Bulletin, 51(1), 23-36.

Novoa, S., Chust, G., Froidefond, J. M., Petus, C., Franco, J., Orive, E., ... & Borja, A. (2012). Water quality monitoring in Basque coastal areas using local chlorophyll-a algorithm and MERIS images. Journal of Applied Remote Sensing, 6(1), 063519-1.

Ocean Biology Processing Group. 2003. MODIS Aqua Level 3 Global Daily Mapped 4 km Chlorophyll a. Ver. 6. PO.DAAC, CA, USA. Dataset accessed [YYYY-MM-DD]. [https://podaac.jpl.nasa.gov] [http://oceancolor.gsfc.nasa.gov/].

Odermatt, D., Gitelson, A., Brando, V. E., & Schaepman, M. (2012). Review of constituent retrieval in optically deep and complex waters from satellite imagery. Remote sensing of environment, 118, 116-126.

Örnólfsdóttir, E. B., Lumsden, S. E., & Pinckney, J. L. (2004). Phytoplankton community growth-rate response to nutrient pulses in a shallow turbid estuary, Galveston Bay, Texas. Journal of plankton research, 26(3), 325-339.

Ouzounov, D., Savtchenko, A., Leptoukh, G., Zhou, B., Ostrenga, D., Deroo, C., & Gonzalez, L. (2004). GES DAAC tools for accessing Terra and Aqua MODIS data. Advances in Space Research, 33(7), 1109-1113.

Pandolfi, J. M., Connolly, S. R., Marshall, D. J., & Cohen, A. L. (2011). Projecting coral reef futures under global warming and ocean acidification. Science, 333(6041), 418-422.

Peng, M., Xie, L., & Pietrafesa, L. J. (2004). A numerical study of storm surge and inundation in the Croatan–Albemarle–Pamlico Estuary System. Estuarine, Coastal and Shelf Science, 59(1), 121-137.

Price, J. F. (1981). Upper ocean response to a hurricane. Journal of Physical Oceanography, 11(2), 153-175.

Rego, J. L., & Li, C. (2009). On the importance of the forward speed of hurricanes in storm surge forecasting: A numerical study. Geophysical Research Letters, 36(7).

Russ, G. R., & McCook, L. J. (1999). Potential effects of a cyclone on benthic algal production and yield to grazers on coral reefs across the central Great Barrier Reef. Journal of Experimental Marine Biology and Ecology, 235(2), 237-254.

Siswanto, E., Ishizaka, J., Morimoto, A., Tanaka, K., Okamura, K., Kristijono, A., & Saino, T. (2008). Ocean physical and biogeochemical responses to the passage of Typhoon Meari in the East China Sea observed from Argo float and multiplatform satellites. Geophysical research letters, 35(15).

Smith, J. E., Shaw, M., Edwards, R. A., Obura, D., Pantos, O., Sala, E., ... & Rohwer, F. L. (2006). Indirect effects of algae on coral: algae-mediated, microbe-induced coral mortality. Ecology letters, 9(7), 835-845.

Steven, A. D. L., Pantus, F., Brooks, D., & Trott, L. (1998). Long-term chlorophyll monitoring in the Great Barrier Reef Lagoon: status report 1, 1993-1995. Great Barrier Reef Marine Park Authority.

Stieglitz, T. (2005). Submarine groundwater discharge into the near-shore zone of the Great Barrier Reef, Australia. Marine Pollution Bulletin, 51(1), 51-59.

Subrahmanyam, B., Rao, K. H., Srinivasa Rao, N., Murty, V. S. N., & Sharp, R. J. (2002). Influence of a tropical cyclone on chlorophyll-a concentration in the Arabian Sea. Geophysical Research Letters, 29(22).

Udy, J., Gall, M., Longstaff, B., Moore, K., Roelfsema, C., Spooner, D. R., & Albert, S. (2005). Water quality monitoring: a combined approach to investigate gradients of change in the Great Barrier Reef, Australia. Marine Pollution Bulletin, 51(1), 224-238.

Walsh, S. M. (2010). Ecosystem-scale effects of nutrients and fishing on coral reefs. Journal of Marine Biology, 2011.

Wang, M., & Shi, W. (2007). The NIR-SWIR combined atmospheric correction approach for MODIS ocean color data processing. Optics Express, 15(24), 15722-15733.

Weisberg, R. H., & Zheng, L. (2006). Hurricane storm surge simulations for Tampa Bay. Estuaries and Coasts, 29(6), 899-913.

Wolanski, E., Fabricius, K., Spagnol, S., & Brinkman, R. (2005). Fine sediment budget on an inner-shelf coral-fringed island, Great Barrier Reef of Australia. Estuarine, Coastal and Shelf Science, 65(1), 153-158.

Wooldridge, S., Brodie, J., & Furnas, M. (2006). Exposure of inner-shelf reefs to nutrient enriched runoff entering the Great Barrier Reef Lagoon: Post-European changes and the design of water quality targets. Marine Pollution Bulletin, 52(11), 1467-1479.

Yunev, O. A., Vedernikov, V. I., Basturk, O., Yilmaz, A., Kideys, A. E., Moncheva, S., & Konovalov, S. K. (2002). Long-term variations of surface chlorophyll a and primary production in the open Black Sea. Marine ecology progress series, 230, 11-28.

Zheng, G. M., & Tang, D. (2007). Offshore and nearshore chlorophyll increases induced by typhoon winds and subsequent terrestrial rainwater runoff. Marine Ecology Progress Series, 333, 61-74.

Zibordi, G., F. Me ́lin, and J.-F. Berthon (2006), Comparison of SeaWiFS, MODIS and MERIS radiometric products at a coastal site, Geophys. Res. Lett., 33, L06617, doi:10.1029/2006GL025778.

Tables

Independent Variable	Dependent Variables	Time Range	Statistical Test
Tropical Cyclone Presence / Absence	minimum, mean, 90th percentile, 95th percentile, maximum, and %>1mgm^{-3}	All dates	Students two-sample T-test
Tropical Cyclone Size	minimum, mean, 90th percentile, 95th percentile, maximum, and %>1mgm^{-3}	When tropical cyclone > Cat 1 present	Single factor and piece-wise linear regression
Tropical Cyclone Maximum Wind	minimum, mean, 90th percentile, 95th percentile, maximum, and %>1mgm^{-3}	When tropical cyclone > Cat 1 present	Single factor regression
Tropical Cyclone Translation Speed	minimum, mean, 90th percentile, 95th percentile, maximum, and %>1mgm^{-3}	When tropical cyclone > Cat 1 present	Single factor and piece-wise linear regression
Weather Station Rainfall	minimum, mean, 90th percentile, 95th percentile, maximum, and %>1mgm^{-3}	When tropical cyclone > Cat 1 present; When any tropical cyclone present; All dates	Single factor regression
Weather Station Wind and Gust Speed	minimum, mean, 90th percentile, 95th percentile, maximum, and %>1mgm^{-3}	When tropical cyclone > Cat 1 present; When any tropical cyclone present; All dates	Single factor single factor regression
Tropical Cyclone Wind, Size, Translation Speed, Coastal Rain	minimum, mean, 90th percentile, 95th percentile, maximum, and %>1mgm^{-3}	When tropical cyclone > Cat 1 present	Multivariable ANOVA

Table 1: The independent and dependent variables, the time range that was used, and the statistical tests that were used to assess the relationships between the variables.

	Chlorophyll *a* Difference (mg m^{-3}) (p value)				
Presence/ Absence	**0 day lag**	**8 day lag**	**16 day lag**	**24 day lag**	**32 day lag**
Minimum	0.0015 (0.49)	0.0005 (0.83)	0.0002 (0.93)	-0.0033 (0.13)	**-0.0045 (0.04)**
Mean	0.0327 (0.27)	**0.0658 (0.02)**	0.0087 (0.76)	0.0237 (0.42)	-0.1344 (0.65)
90^{th} percentile	0.0118 (0.90)	**0.1998 (0.02)**	0.0283 (0.75)	0.0760 (0.40)	-0.0426 (0.64)
95^{th} percentile	0.1122 (0.40)	**0.3567 (0.01)**	0.0344 (0.79)	0.1743 (0.19)	0.0437 (0.74)
%pixels > 1mg m^{-3}	0.0377 (0.97)	1.5813 (0.09)	0.2923 (0.76)	1.0454 (0.27)	0.1769 (0.85)
Maximum	2.4533 (0.27)	**7.0814 (0.01)**	**8.0624 (0.003)**	2.8324 (0.30)	2.0229 (0.46)

Table 2: The T-test results of the difference between chlorophyll *a* dependent variables given whether a tropical cyclone was present or absent over the reef at varying time lags (calculated by present – absent). The significant results are in bold.

		Proportion of variance (%)			
	R^2	Mean Radius	Mean Translation Speed	Mean Wind	Mean Rain
Minimum	0.099	3.532	0.049	0.002	4.740
Mean	***0.568****	***51.055***	2.459	***12.434***	6.655
90th percentile	***0.651****	***60.239***	1.269	***14.489***	5.253
95th percentile	***0.609****	***48.329***	7.353	8.718	6.785
%pixels > 1mg m^{-3}	***0.548****	50.550	0.611	12.380	6.875
Maximum	0.323	3.532	23.761	0.691	10.011

Table 3: The results of the multivariate ANOVA with the averages of tropical cyclone characteristics over the time period as predictor variables and the chlorophyll *a* measures as the dependent variables at no lag. If the ANOVA overall model is significant (p-value is <0.05), the ANOVA r^2 (second column) is given in bold, italic with a star. The proportions that the characteristics account for in the predictive model are given in the subsequent columns. If the relationship is significant (p <0.05) then the percentage is given in bold, italics. The tropical cyclone size significantly accounts for the largest proportion of the predictive power.

		Proportion of variance (%)			
	R^2	**Max Radius**	**Max Translation Speed**	**Max Wind**	**Max Rain**
Minimum	***0.424****	2.052	1.513	14.390	***23.572***
Mean	***0.526****	***25.679***	***14.427***	2.540	***20.181***
90th percentile	0.393	22.828	10.991	4.661	13.218
95th percentile	***0.528****	***25.095***	***15.953***	2.757	***19.891***
%pixels > 1mg m^{-3}	***0.497****	***29.432***	9.822	3.048	12.586
Maximum	0.326	1.814	26.775	2.492	9.159

Table 4: The results of the multivariable ANOVA with the maximums of tropical cyclone characteristics over the time period as predictor variables and the chlorophyll *a* measures as the dependent variables at 16 day lag. If the ANOVA overall model is significant (p-value is <0.05), the ANOVA r^2 (second column) is given in bold, italic with a star. The proportions that the characteristics account for in the predictive model are given in the subsequent columns. If the relationship is significant (p <0.05) then the percentage is given in bold, italics. The tropical cyclone size, translation speed and rainfall significantly account for proportions of the predictive power, while wind speed is not significant.

(a)	Wind Speed		Radius		Translation Speed	
No Lag	**Maximum**	**Mean**	**Maximum**	**Mean**	**Maximum**	**Mean**
Minimum	0.022	0.026	0.013	0.037	0.001	-0.011
Mean	0.025	0.026	***0.253****	***0.345****	0.033	0.001
90th percentile	0.035	0.034	***0.335****	***0.433****	0.029	0.000
95th percentile	0.034	0.052	***0.316****	***0.380****	0.094	0.026
%pixels > 1mg/m3	0.019	0.025	***0.240****	***0.340****	0.008	-0.002
Maximum	-0.015	0.002	-0.005	-0.022	0.023	0.143

(b)	Wind Speed		Radius		Translation Speed	
8 Day Lag	**Maximum**	**Mean**	**Maximum**	**Mean**	**Maximum**	**Mean**
Minimum	0.174	**0.262***	0.093	0.122	0.029	0.001
Mean	0.167	0.184	***0.207****	0.185	0.067	0.041
90th percentile	0.151	0.169	***0.271****	***0.235****	0.054	0.027
95th percentile	0.166	0.176	***0.202****	0.151	0.077	0.072
%pixels > 1mg/m3	0.179	0.183	***0.262****	***0.219****	0.043	0.024
Maximum	0.003	0.003	0.060	0.088	0.065	0.062

(c)	Wind Speed		Radius		Translation Speed	
16 Day Lag	**Maximum**	**Mean**	**Maximum**	**Mean**	**Maximum**	**Mean**
Minimum	0.052	0.062	0.003	0.000	-0.047	-0.081
Mean	0.126	0.181	***0.369****	***0.370****	0.095	0.099
90th percentile	0.053	0.103	***0.248****	***0.242****	0.065	0.103
95th percentile	0.113	0.159	***0.343****	***0.351****	0.109	0.108
%pixels > 1mg/m3	0.142	***0.195****	***0.439****	***0.404****	0.072	0.098
Maximum	0.007	0.000	0.079	0.056	***0.227****	***0.190****

Table 5: The r^2 values of the single factor regressions with the independent variables of tropical cyclone wind speed, size (radius), and translation speed and the chlorophyll *a* dependent variables at (a) no time lag, (b) 8-day time lag, (c)16-day time lag. Significant regression values ($p < 0.05$) are presented in bold and italics, with a star. Size (radius) has a strong positive correlation with chlorophyll a at all three time lags, but it is predominantly strongest at the 16-day time lag, particularly for the mean and % > 1mg/m^3.

Figures

Figure 1

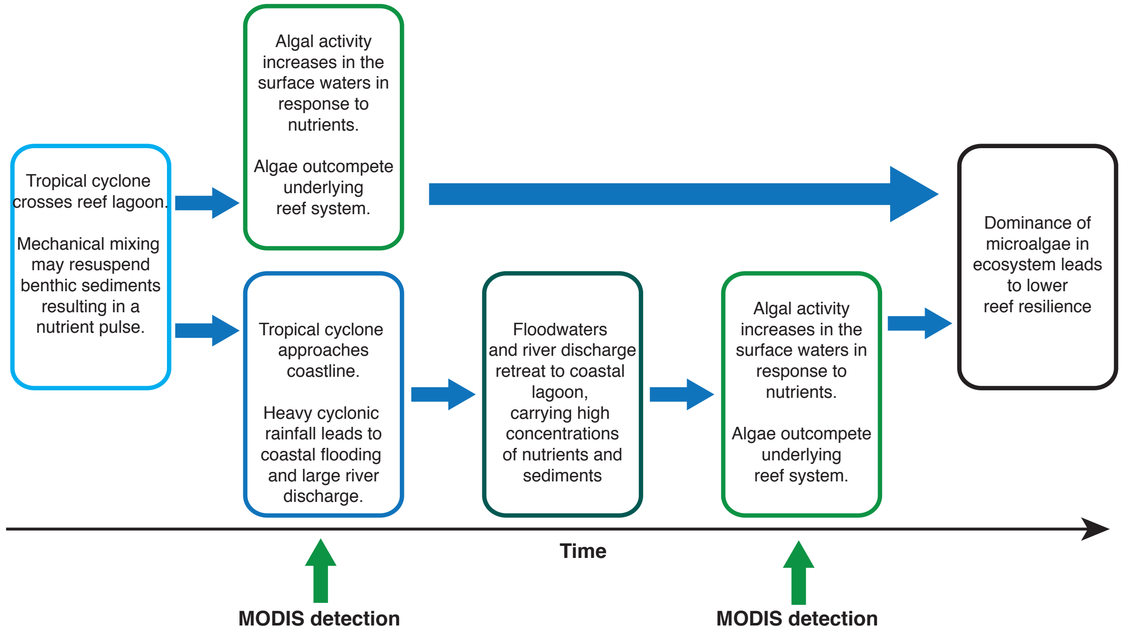

Figure 1: Postulated mechanisms by which a chlorophyll a response can be detected remotely following tropical cyclone activity.

Figure 2

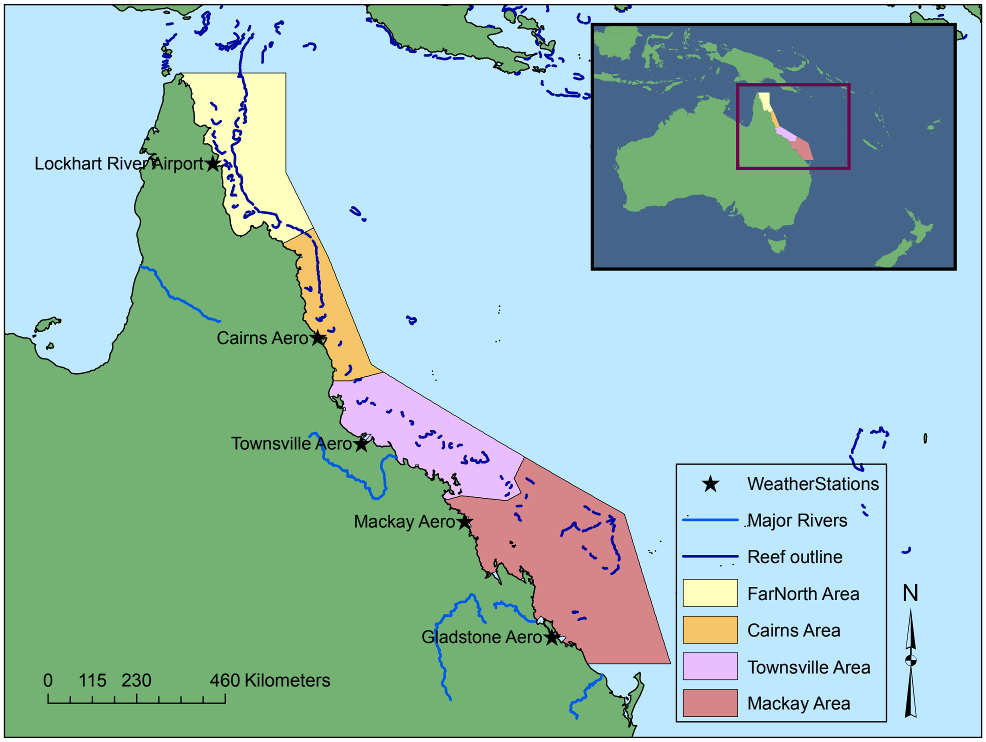

Figure 2: Great Barrier Reef study area and its designated regions (colored zones). Major reef areas and atolls are outlined in dark blue and major rivers are shown in light blue. The locations of the coastal weather stations are denoted by stars.

Figure 3

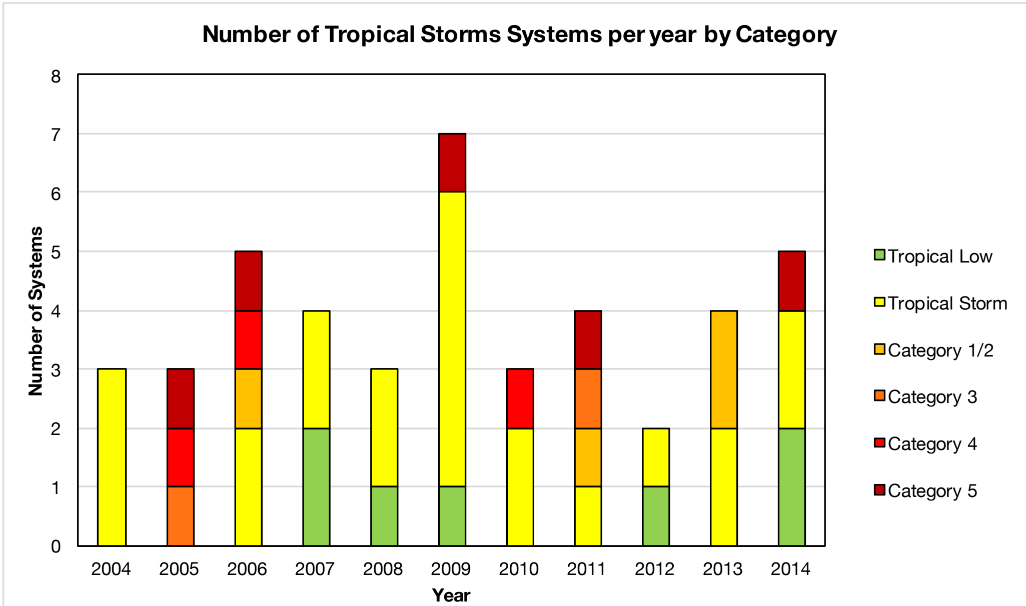

Figure 3: Tropical storms systems by year separated by Saffir Simpson wind based intensity index. The total number of events in the study period is 43. The storms within a year may overlap in time and thus not produce unique effects on the water quality.

Figure 4

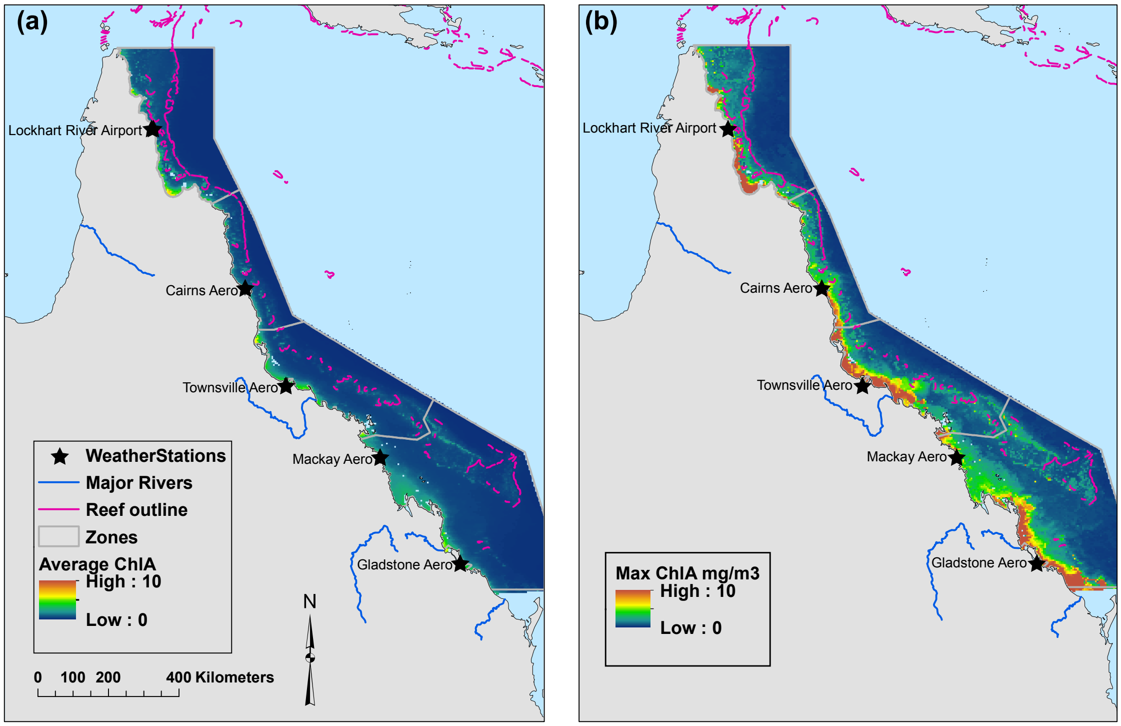

Figure 4: (a) Average and (b) maximum chlorophyll a concentration, recorded over the 10-year period. Green denotes the 1mg m^{-3} threshold and yellow and brown denotes exceeding the 1mg m^{-3} threshold. White pixels denote insufficient clear days to obtain a reliable value.

Figure 5

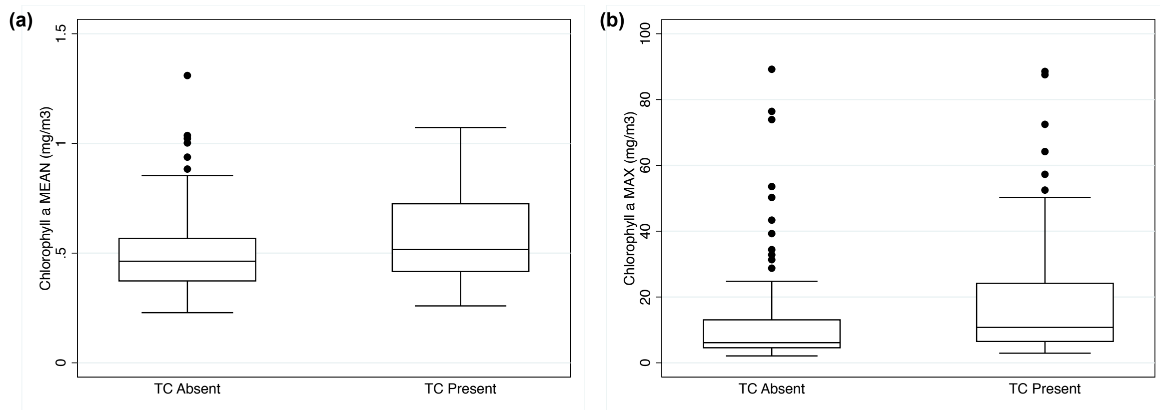

Figure 5: (a) The spread of the mean chlorophyll *a* measured over the whole Great Barrier Reef during each time period over the 10-years binned by whether there was a tropical cyclone present or absent in the previous 8-day period. (b) The spread of maximum chlorophyll *a* values recorded over the Great Barrier Reef binned by whether there was a tropical cyclone present or absent in the previous 16-day period.

Figure 6

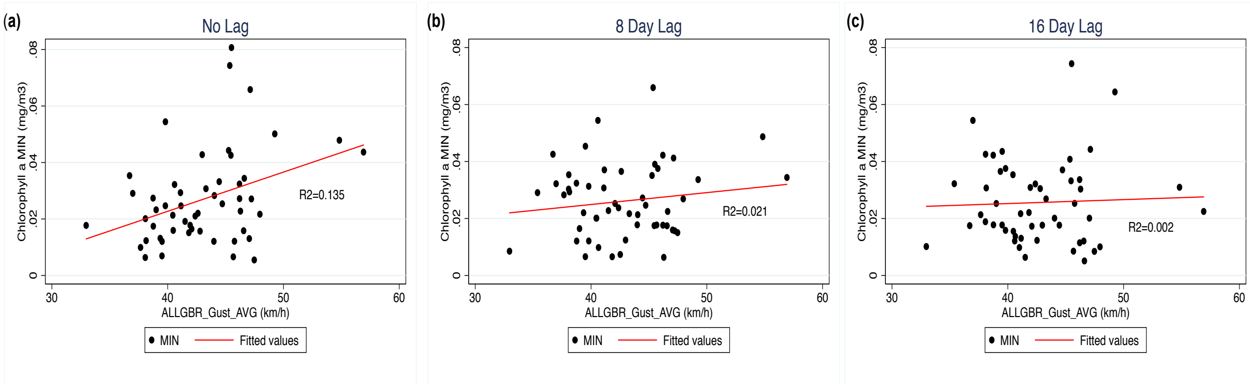

Figure 6: the minimum chlorophyll *a* concentration over the Great Barrier Reef against the average coastal gust speed recorded over the time period during tropical activity at a) no time lag b) 8-day time lag c) 16-day time lag to tropical cyclone activity. The line of best fit for the scatter plot is given in red and the r^2 value given against the line. The strongest correlation is at no time lag and there is no notable correlation thereafter.

Figure 7

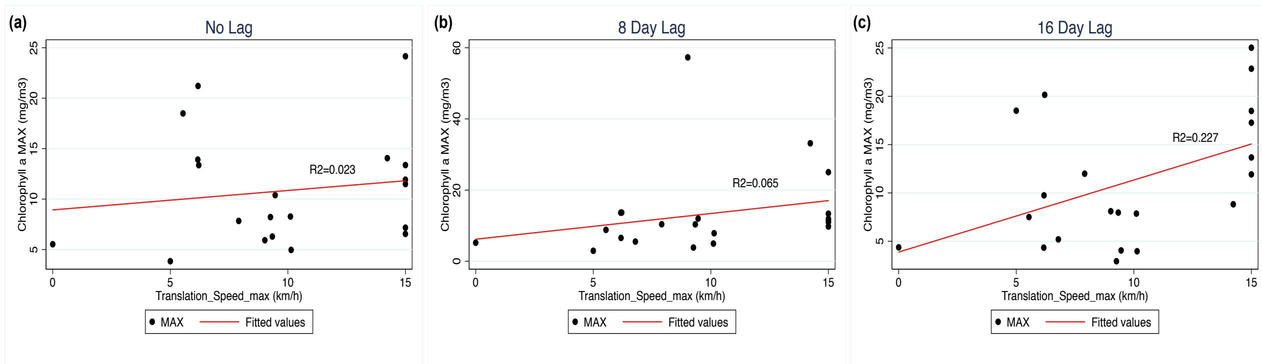

Figure 7: the maximum chlorophyll *a* concentration over the Great Barrier Reef against the maximum of the tropical cyclone translation speed over the time period at a) no time lag b) 8-day time lag c) 16-day time lag to tropical cyclone activity. The line of best fit for the scatter plot is given in red and the r^2 value given against the line. The r^2 values and p-value significance can be found in Table 5. The translation speed cannot explain chlorophyll a variance at the shorter time scales, but over 2 weeks, there is a strong positive correlation.

Figure 8

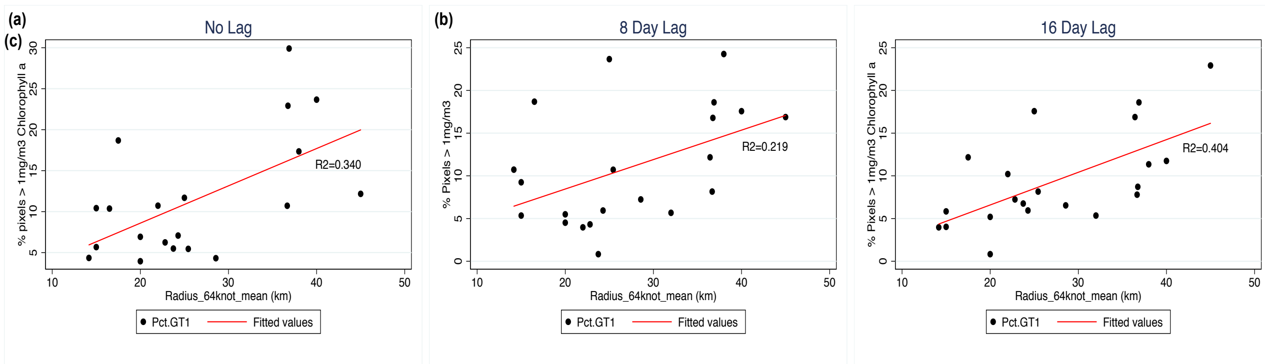

Figure 8: the % of pixels that exceed the 1mg m^{-3} threshold over the Great Barrier Reef against the average of the tropical size (radius) over the time period at a) no time lag b) 8-day time lag c) 16-day time lag to tropical cyclone activity. The line of best fit for the scatter plot is given in red and the r^2 value given against the line. The r^2 values and p-value significance can be found in Table 5. The strongest correlation is at the 16-day time lag. But the positive linear relationship is sustained from no time lag to the 16-day time lag and for many of the important measures of chlorophyll a such as the mean, extremes, or % of pixels > 1mg m^{-3}.

Figure 9

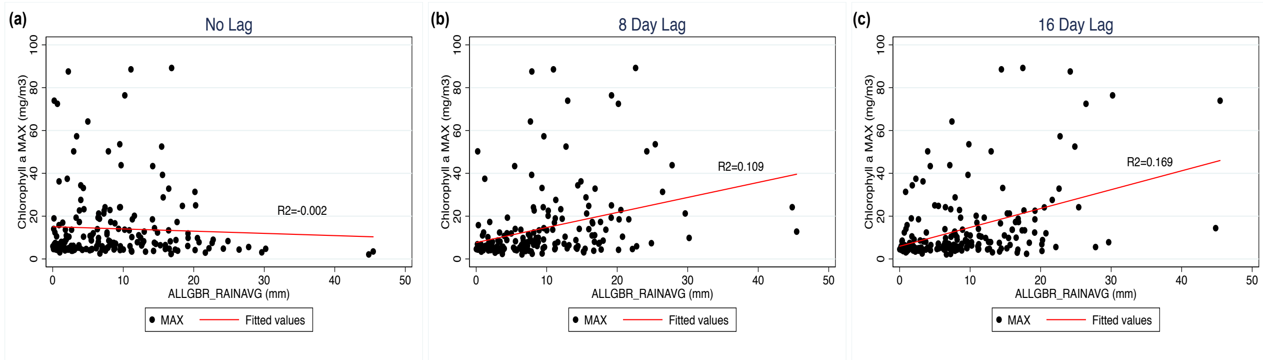

Figure 9: the maximum chlorophyll *a* concentration over the Great Barrier Reef against the average rainfall measured along the coastline for the whole 10-year study period at a) no time lag b) 8-day time lag c) 16-day time lag to rainfall activity. The line of best fit for the scatter plot is given in red and the r^2 value given against the line. The positive correlation is found at the 8-day time lag increases to the 16-day time lag.

CHAPTER TWO

FACTORS AFFECTING THE SIMULATED TRAJECTORY AND INTENSIFICATION OF TROPICAL CYCLONE YASI (2011)

CHELSEA L. PARKER[*1,2], AMANDA H. LYNCH[1,2], AND PRISCILLA A. MOONEY[3]

[1]Department of Earth, Environmental and Planetary Sciences, Brown University, Providence, RI, 02912, USA

[2]Institute at Brown for Environment and Society, Brown University, Providence, RI, 02912, USA

[3]National Center for Atmospheric Research, Boulder, CO, USA

Published in its current form in Atmospheric Research:
http://doi.org/10.1016/j.atmosres.2017.04.002

Abstract

This study investigates the sensitivity of the simulated trajectory, intensification, and forward speed of Tropical Cyclone Yasi to initial conditions, physical parameterizations, and sea surface temperatures. Yasi was a category 5 storm that made landfall in Queensland, Australia in February 2011. A series of simulations were performed using WRF-ARW v3.4.1 driven by ERA-Interim data at the lateral boundaries. To assess these simulations, a new simple skill score is devised to summarize the deviation from observed conditions at landfall. The results demonstrate the sensitivity to initial condition resolution and the need for a new initialization dataset. Ensemble testing of physics parameterizations revealed strong sensitivity to cumulus schemes, with a trade-off between trajectory and intensity accuracy. The Tiedtke scheme produces an accurate trajectory evolution and landfall location. The Kain Fritsch scheme is associated with larger errors in trajectory due to a less active shallow convection over the ocean, leading to warmer temperatures at the 700mb level and a stronger, more poleward steering flow. However, the Kain Fritsch scheme produces more accurate intensities and translation speeds. Tiedkte-derived intensities were weaker due to suppression of deep convection by active shallow convection. Accurate representation of the sea surface temperature through correcting a newly discovered SST lag in reanalysis data or increasing resolution of SST data can improve the simulation. Higher resolution increases relative vorticity and intensity. However, the sea surface boundary had a more pronounced effect on the simulation with the Tiedtke scheme due to its moisture convergence trigger and active shallow convection over the tropical ocean.

Keywords

Australia; Weather Research and Forecasting (WRF) model; tropical cyclone; Yasi; initial conditions; cumulus parameterization; sea surface temperature.

1. Introduction

During the last two decades, the northeast coastal regions of Australia have experienced increased total rainfall and more frequent heavy rainfall (Alexander et al. 2007, Lynch et al. 2008). Since 2003, a number of intense TCs have affected the area (Great Barrier Reef Marine Park Authority 2011a; Beeden et al. 2015); in contrast with previous decades (1970-2003), when there were no TCs greater than category 1 on the Saffir-Simpson scale (category 3 on the Australian scale) recorded in the area (Puotinen et al. 1997, Puotinen 2007). For this region, during this time period, it is perceived that the frequency of total tropical cyclone (TC) events has increased (Great Barrier Reef Marine Park Authority 2011a; Beeden et al. 2005), while the proportion of high intensity storms has also increased (Nicholls et al. 1998; Alexander et al. 2007; Holland and Bruyère 2013). However, analyzing trends in TC intensity and frequency to the present day has been confounded by the availability, quality, and temporal range of historical data (Landsea et al. 2010, Kuleshov et al. 2010, Walsh et al. 2012), particularly in the South Pacific (Walsh et al. 2012; Walsh et al. 2016).

The possible response of TCs to predicted climate change is still an active area of inquiry. The outstanding questions include, the extent to which intensity will reach the theoretical potential maximum and whether there will be a significant change in genesis location and trajectories (e.g. Walsh et al. 2016). Numerical modeling studies using global-scale General Circulation Models are computationally intensive and may not capture environmental conditions favorable for TC genesis and development. The horizontal resolution of these models (from ~100 to 300 km for the CMIP5 models down to ~50 km for the new generation of models [Walsh et al. 2016]) has thus far been inadequate to accurately capture the short-term variability of intense TCs given that high resolution meteorological forcing cannot be supplied by the coarse grid (Walsh 2004, Lynn et al. 2009, Walsh et al. 2016). Regional climate models and climate downscaling techniques are needed to resolve realistic TC intensities, life cycles, and structures such as size and eyewalls (Lynn et al. 2009; Lackmann 2015). The majority of regional studies have focused on the Atlantic basin (Walsh et al. 2012). However, studies have demonstrated that there may be substantial variations in the response of TCs to climate change across basins particularly in terms of frequency and intensity (e.g. Oouchi et al. 2006; Walsh et al. 2006). Previous studies dedicated to the South Pacific and Australia region, have focused on the statistics of overall changes to TCs in the basin (e.g. frequency [Lavender and Walsh 2011], interannual variability of frequency [Walsh 2015], genesis location [Walsh and Katzfey 2000; Nguyen and Walsh 2001], trajectory [Lavender and Walsh 2011], and intensity [Walsh and Ryan 2000]). Accurate representations of TC systems and their characteristics at relatively coarse horizontal grid resolutions (e.g. 12km) in this region are essential for future studies exploring the sensitivity of TCs to climate change forcing. This study acts as a precursor to such studies and assesses the skill and sensitivity of simulating TC-scale characteristics at horizontal resolutions typically used in regional climate studies (12-15km [Jacob et al. 2014]). The findings provide valuable information for initial conditions, physical parametrizations, and surface boundary conditions which can be used for simulating TC-scale characteristics (such trajectory, intensity, and forward speed) in the Australia region.

TC Yasi was one of the most powerful TCs to affect the Great Barrier Reef and the Queensland coastal region (Great Barrier Reef Marine Park Authority 2011b). Cyclogenesis began just northeast of Fiji on January 29 2011. Yasi tracked westward across roughly 3500km of ocean in five days to make landfall at Mission Beach, Queensland, in the early hours of February 3, 2011 (local time) (Figure 1). Within its lifecycle, the system rapidly intensified from a category 3 to a category 5 storm in just 36 hours, covering a distance of roughly 1800km (Australian Bureau of Meteorology [BOM] 2011). The destructive winds were estimated to have affected 13% of the Great Barrier Reef and the economic impacts on tourism, agriculture and coal exports were significant (Queensland Government 2012). Storm intensity was maintained for a considerable distance inland, contributing to further flooding and wind damage over a wide swath of productive agricultural land and World Heritage wilderness regions (AON Benfield 2011). The agricultural losses in Queensland were estimated at AUD$1 billion (AON Benfield 2011). Total damage and cost to insurers makes Yasi the costliest TC to have affected Australia (Reuters, 2015) due to its anomalously large size, intense wind speeds, and heavy rainfall (particularly inland after landfall). Given Yasi's intensity and destructive capacity, it is important to test the sensitivity and accuracy of this system at a regional model resolution.

The Advanced Research Weather Research and Forecasting model (hereafter, WRF) is a mesoscale numerical weather prediction model. Numerous studies have demonstrated that WRF is suitable for simulating TC events primarily in the Northern Hemisphere (e.g. Davis et al. 2008, Abarca and Corbosiero 2011). Efforts have been made to optimize the model setup, and to demonstrate how parameterizations affect the simulation of TCs. Fierro et al. (2009) and Gentry and Lackmann (2010) concluded that increasing horizontal grid spacing (up to 1km) increases accuracy of simulated central pressure and TC processes, particularly in the eyewall. This study assesses the ability of WRF at a coarse horizontal resolution of 12km to simulate the intensity and TC lifecycle.

The choice of cumulus parameterization scheme (hereafter CU) influences many aspects of simulation skill including trajectory, landfall time, structure, intensity, precipitation patterns, and accumulation bias (e.g. Wang and Seaman 1997; Gallus 1999; Prater and Evans 2002; Zhang et al. 2011; Nasrollahi et al. 2012; Shepherd and Walsh 2016). Of particular interest to this study, Nasrollahi et al. (2012) found that the Betts-Miller-Janjić (BMJ) CU scheme yielded the most accurate TC trajectory; while Prater and Evans (2002) found that BMJ caused TC track recurvature too early, and the Kain Fritsch CU scheme reproduced the most accurate trajectory. However, Torn and Davis (2012) found that the Kain Fritsch scheme produced a large track bias and the Tiedtke scheme produced the trajectory closest to observed. Furthermore, Shepherd and Walsh (2016) discussed that the Kain Fritsch and Tiedtke schemes produced relatively similar trajectories. This study aims to reconcile the sensitivity of the TC Yasi trajectory to the CU parameterization in the chosen WRF set up. Simulated intensity is also highly sensitive to CU scheme, where BMJ (Prater and Evans 2002) and the Tiedtke schemes yield TCs weaker than observed, but the Kain Fritsch scheme has produced more accurate deepening and intensities in the literature (e.g. Torn and Davis 2012; Shepherd and Walsh 2016). This study considers the accuracy of intensity representation to further inform model configuration for TC simulation at this resolution, in this basin. Nasrollahi et al. (2012) found that several combinations of CU with microphysics schemes were adequate in simulating landfall time. Landfall time may be affected by trajectory and the relative location of the coastline, therefore this study considers TC translation speed over the TC lifecycle up to landfall. The sensitivity of translation speed to model set up and parameters has not previously been addressed in depth in the literature. Translation speed is an important TC characteristic to consider as it can affect the ground relative wind speeds (Shapiro 1983), storm surge (Peng et al. 2004; Weisberg and Zheng 2006; Rego and Li 2009; Irish and Resio 2010), and the duration of TC-like conditions experienced at any one location.

The microphysics scheme (hereafter MP) can particularly affect simulated intensity (Tao et al. 2011) and precipitation (Nasrollahi et al. 2012). Some studies concluded that modeled trajectory may not be significantly sensitive to MP parameterization (e.g., Yang and Ching, 2005; Zhu and Zhang, 2006; Li and Pu, 2008; Tao et al., 2011). However, others (Fovell and Su 2007; Fovell et al. 2009; Nasrollahi et al. 2012) found that trajectory can be particularly sensitive to the MP parameterization due to the sensitivity of the TC size and outer winds to the MP scheme. Therefore, analyzing the sensitivity of trajectory and intensity to the MP scheme will be included in the physics testing ensemble in this study. Different planetary boundary layer parameterization schemes (hereafter PBL) can alter intensity evolution and structural characteristics (e.g. Braun and Tao 2000; Li and Pu, 2008; Smith and Thomsen 2010; Bao et al. 2012). In particular, the choice of PBL scheme can result in differences of up to 19hPa in simulated sea level pressure (SLP) in just a 30h forecast period (Li and Pu 2008). Therefore, the effect of the PBL, particularly on the simulated intensity, will be considered in the testing of a physics parameterization ensemble.

Previous work has explored the sensitivity of TC simulations in WRF to initial condition datasets (e.g. Mohanty et al. 2010) and initial condition time (e.g. Mohanty et al. 2010; Shepherd and Walsh 2016). Shepherd and Walsh (2016) showed that trajectories can be sensitive to initial condition time, however they are more sensitive to the CU parameterization. Mohanty et al. (2010) demonstrated that simulated intensity and vorticity maxima are sensitive to the chosen initial and boundary condition data set. Furthermore, it has been shown that improved initial conditions from data assimilation can particularly improve the representation of intensity (Li and Pu 2008; Torn and Davis 2012). Alternatively, nudging could be applied to the model until cyclone genesis, which would constrain the model to be more consistent with observations. However, there are issues concerning the impact of nudging strength on model internal variability (Glisan et al., 2013). Therefore, this study focuses on testing the effect of initial conditions with differing resolutions on the outcome of the TC simulation on this relatively coarse grid.

TC development and intensity are closely related to and controlled by sea surface temperature (SST) (e.g. Schade and Emanuel 1999; Ramsay and Sobel 2011; Bruyère et al. 2012). Therefore, some studies have explored the response of WRF TC simulations to variations in the SSTs boundary conditions. Miglietta et al. (2011) demonstrated that as SST increases, so does the simulated intensity (depth of the minimum pressure) and the persistence of the symmetric warm core. Davis et al. (2008) found that the rate of intensification of Atlantic hurricanes in WRF was particularly sensitive to the SST field and the treatment of mixing feedback and ocean cooling. Mooney et al. (2016) also found that the treatment of the Atlantic SST in the model dictated the accuracy and relative development of the TC-induced cold wake, and therefore the subsequent effect on TC intensity through interaction with the reduced SSTs. This study however, explores whether the simulated TC characteristics, such as intensity and trajectory, can be improved on this grid through improvements in the physical representation of the SSTs in the model or through increasing the resolution of the SST boundary condition data.

The results from the literature discussed thus far have been from studies of TC systems in the Northern Hemisphere. Aside from recent work by Shepherd and Walsh (2016), to the best of the authors' knowledge, no other studies have assessed the simulation of TC events in the Western South Pacific region with WRF, and further improvements need to be made for TC simulations in a regional model set up in this region. While forecasts were able to predict the trajectory of TC Yasi accurately, they were unable to capture the intensification, particularly into landfall (Reeder et al. 2012). This study assesses the ability of the WRF model to capture the characteristics of TC Yasi at a relatively coarse horizontal grid resolution, testing the sensitivity of the simulation to (1) initial conditions, (2) physical parameterizations, and (3) sea surface temperature (SST) boundary conditions.

2. Methods

2.1. Model configuration

The mesoscale numerical weather prediction model WRF-ARW version 3.4.1 (Skamarock et al. 2008) was configured with static two-way nesting for two domains of 36- and 12-km grid spacing (Figure 2). Higher resolutions of horizontal grid spacing may improve the simulation accuracy of intensity in strong TCs, and physical processes such as eyewall replacement (e.g. Gentry and Lackmann 2010), and rapid intensification (e.g. Davis et al. 2008). However, studies have shown that a 12km grid spacing is sufficient for reproducing sub-system-scale structures such as eye-wall asymmetries and spiral bands (Done et al. 2013). Therefore, we have used the 12km spacing in order to carry out a large number of exploratory simulations to address the sensitivity of TC representation in regional climate models, which typically have grid spacings of 10-15 km (Jacob et al. 2014). Both domains are centered on latitude 16.018°S and longitude 156.382°E. All simulations have 28 vertical levels and the model top pressure level was set to 50 hPa. The impacts of increased vertical resolution and pressure level distribution were investigated in a similar method as employed by Ma et al. (2012). These factors did not significantly affect the simulation skill as to warrant increased vertical resolution for the remainder of the simulations (see Table 2 Run numbers 9, 10, 11, 12).

All simulations spanned 96 hours to capture the main intensification period and landfall of TC Yasi. Initialization was at 00:00 UTC January 31 2011 and runs lasted until 00:00 UTC February 4 2011. Lateral boundary conditions were provided by the pressure level data products from the European Centre for Medium-Range Weather Forecasts (ECMWF) Re-Analysis Interim (hereafter ERA-I) data set (Dee et al. 2011).

The data are at 6-hourly intervals, 0.7° spatial resolution, and have 37 atmospheric levels. Surface data at 6-hourly intervals were also used.

2.2. Initial Conditions

While others have tested simulation sensitivity to initial condition time (e.g. Shepherd and Walsh 2016), this study tested sensitivity to initial condition spatial resolution. We compared two initialization techniques: (1) the ERA-I data as both boundary and initial conditions, and (2) a high resolution initial condition dataset in conjunction with ERA-I boundary conditions. For the new technique, we obtained a high-resolution data set from the BOM TC operational forecast model Australian Community Climate and Earth System Simulator-Tropical Cyclone (ACCESS-TC) (Puri et al. 2010, 2013; Davidson et al. 2014). The data is at 0.11° horizontal resolution with 50 vertical level for January 31, 2011, at 00:00 UTC. We converted the data file into WRF intermediate file format and read it in with the ERA-I data during data pre-processing to create a new forcing file for the initial time step. Figure 3 demonstrates the difference between the SLP data in the ERA-I and the ACCESS-TC data for initializing Yasi. The ACCESS-TC file did not cover the whole WRF domain, but extends from -7 : -25°N and 142 : 171°E (Figure 3b). Therefore, ERA-I data was used to fill in the initial condition data in areas of the domain where ACCESS-TC data was absent. After initialization, ERA-I provides the boundary conditions. The simulations were compared in terms of intensity over the TC life cycle (central pressure and wind speed), translation speed, trajectory, and landfall location.

2.2.1 Sensitivity to Initial Conditions

Blending high-resolution ACCESS-TC data with the coarser ERA-I data produced a notably different track (Figure 4) and a more intense TC system (deeper central pressure and elevated wind speeds (Figure 5). Figure 4 demonstrates that there is a discrepancy between the observed IBTrACS (Knapp et al. 2010) trajectory and the trajectory present in the ERA-I reanalysis data which may be due to the coarse resolution (0.7°) of the ERA-I data. This highlights that error is introduced with the boundary condition dataset and the large scale forcing. Figure 4 also shows a disparity between the trajectory simulated by WRF with the ERA-I only conditions and the observed trajectory in the ERA-I data. This disparity may be attributed to uncertainties introduced through the WRF numerical modeling technique, such as parametrization choice and internal variability. Figure 4 also shows that initializing with ACCESS causes the trajectory to deviate further poleward from observed data (IBTrACS and ERA-I), and the system makes landfall ~100km further south than the simulation with just ERA-I for initial and boundary conditions (Table 2, Run 5 and 6). This suggests that there are additional uncertainties introduced by the ACCESS initialization data. However, the trajectory evolution with the ACCESS initialization is more consistent with observations, while the ERA-I only simulation demonstrates erroneous sinuosity compared to observations. Furthermore, the simulations where ERA-I provides both the initial and boundary conditions (Table 2, Run 1 and Run 5) produced a much faster translation speed compared to observed, affecting the simulation skill.

In preliminary analyses (not shown), initializing the WRF simulations earlier or later with the ERA-I only data for boundary and initial conditions did not improve the simulation. This is consistent with results from Shepherd and Walsh (2016) where there was some sensitivity to initialization time, but a greater sensitivity to other factors such as physical parameterizations. Furthermore, it has been found that increasing simulation lead time (≥72 hours before landfall) can result in greater landfall location errors (Mohanty et al. 2010). Therefore, we continued our investigation of the sensitivity to initial condition resolution, with one initialization time.

Despite the increased trajectory deviation, Table 2 demonstrates that initializing with ACCESS increases the intensity and reduces the pressure error at landfall (compare Runs 1 and 2 and Runs 5 and 6). Figure 3b demonstrates there is a defined vortex structure with increasing intensity towards the eye, reaching pressures of 980hPa, in the analysis data provided by the ACCESS-TC (0.11° horizontal resolution) initial condition file. Figure 3a shows that the pressure structure and intensity is comparatively not as well defined in the ERA-I (0.7° horizontal resolution) reanalysis data at this early stage of the event. This difference was fundamental for enabling the development of a more intense system (particularly the sea level pressure). We found that initializing with the higher resolution ACCESS-TC data, with no CU, MP, or PBL schemes reduces the error index from 1.20 to 0.88 through reduced deviations in all metrics (Table 2, Run 1 to Run 2, no CU, MP, PBL enabled). The simulated TCs are still very weak compared to observations regardless of initialization technique if no parameterization schemes are prescribed (Figure 5a). When physics parameters are prescribed (e.g. CU1 MP5 PBL1) but simulations differ by the initialization data method, using the ACCESS-TC data improves the skill score from 1.12 to 0.77 by reducing central pressure and translation speed errors (compare Runs 5 and 6, Table 2). Figure 5b shows that with the CU1, MP5, PBL1, the ACCESS initialization data results in TC intensification at a rate greater than observed and maximum intensity is reached too early in the simulation. However, with this initialization, the rate of intensification, the SLP values, and intensity at landfall are more realistic and comparable to observations in contrast with the weaker system (higher central pressure values) achieved with ERA-I only. It is important to accurately capture TC intensity, particularly at landfall given potential damage to coastal areas. These results demonstrate a technique to improve translation speed and intensity simulation on a model setup with grid spacing of 36 / 12 km without increasing horizontal or vertical resolution, saving computational costs and time. Consequently, this initialization method is used for the sensitivity tests that follow.

2.3. Physical parameterizations

We performed an ensemble of simulations using a range of physical parameterization configurations, using otherwise identical model setups, boundary and initial conditions, and run times. The ensemble members included varying the sub-grid scale convection (CU), moist microphysics (MP), planetary boundary layer (PBL) schemes, the use of a surface flux coefficient, and a 1-dimensional ocean mixed layer model (OML) (see Table 1).

The CU parameterization simulates the effects of sub-grid scale cumulus convection on heat and moisture tendencies and rainfall (Skamarock et al. 2008). Most

CU parameterizations include shallow convection, where cumulus clouds that are not deep enough to produce precipitation transport air from the mixed layer across the boundary layer inversion (Torn and Davis 2012). The overall effect is to transport moisture upwards and heat downwards (Torn and Davis 2012). In this way, these CU parameterizations vertically redistribute heat and moisture regardless of latent heating from precipitation (Nasrollahi et al. 2012). However, the closure mechanisms and activation of shallow and deep convection varies by scheme, affecting their representation of vertical heat and moisture. A total of five CU schemes were used in this ensemble (see Table 1).

The MP scheme represents the effects of grid resolved moisture physics on the atmospheric heat and moisture tendencies, the vertical flux of precipitation, and the sedimentation process (Skamarock et al. 2008). Five MP schemes were used in this ensemble (see Table 1).

The PBL scheme parameterizes turbulent exchanges of heat, moisture and momentum and thus governs vertical diffusion and mixing in the lower atmosphere. Two PBL schemes were tested in this ensemble (see Table 1).

Previous studies (Emanuel 1995; Braun and Tao 2000; Bao et al. 2002; Davis et al. 2008) have shown that the surface flux coefficient (ISFTCFLX), and the use of a one-dimensional ocean mixed layer model (OML) can influence the model’s ability to simulate the TC inner core structure, eye size, and intensity. Thus, bulk surface drag coefficients and energy exchange parameterizations have been developed in WRF for TCs over the ocean surface. The ISFTCFLX (Garratt 1994; Donelan et al. 2004) option was included in some ensemble members to test its effect. This parameterization has reduced surface drag compared to the original Charnock (1955) formulation. Furthermore, there is a potential negative feedback of wind-driven ocean mixing on TC intensity. Strong TC winds drive oceanic turbulence which is one of the dominant mechanisms for cooling the sea surface during a TC event. This cooling occurs in the vicinity of the storm and reduces the amount of heat and moisture available to the TC which in turn limits its intensity (Mooney et al. 2016). This first order negative feedback can be represented by coupling a simple one-dimensional ocean mixed layer (OML) to the atmosphere within WRF (Emanuel et al. 2004). Some studies (e.g. Davis et al. 2008) have demonstrated that this coupling can improve the simulation of TC intensity and the rate of intensification, particularly in simulations where intensity was over estimated (central pressures too low) before coupling. Thus, the available OML (Pollard et al. 1972) was tested as part of the parameterization sensitivity ensemble.

Other physical parameterizations that were held constant are as follows: shortwave radiation is calculated by the Dudhia scheme (Dudhia 1989); longwave radiation fluxes are calculated by the RRTM scheme (Mlawer et al. 1997); surface layer is from the MM5 Monin-Obukov scheme (Monin and Obukhov 1954); land surface processes and structure are defined by the Unified Noah Land Surface Model (Chen and Dudhia 2001; Ek et al. 2003; Tewari et al. 2004); and SSTs are fixed for the duration of the simulations unless otherwise stated.

2.4. Sea Surface Temperature Boundary Conditions

Lastly, we directly tested the sensitivity of the simulation to four different representations of SST boundary condition. (1) Daily ERA-I SSTs were provided to WRF at regular intervals (SST updating). (2) One dimensional OML (in isolation from using ISFTCFLX) was employed while allowing ERA-I SST updating. Further details of simulating TC interactions with SSTs using ERA-I and the one-dimensional OML model are described in Mooney et al. (2016). (3) Lag-corrected ERA-I SSTs, updated every 24-hrs. (4) Finally, the sensitivity to a higher resolution auxiliary SST dataset was tested.

Detailed analysis of the ERA-I data by the authors has revealed that the ERA-I SSTs are lagging the atmospheric variables by 30 hours in the reanalysis data since 2009. Figure 6 of the SST fields on Feb 2 2011, demonstrates the uncorrected compared to the 30-hour ERA-I corrected data (Figure 6 a, b). Once this SST lag has been corrected for, there are cooler SSTs beneath the path of the storm (Figure 6b) that more closely resemble the SST values and distribution present in the Operational Sea Surface Temperature and Sea Ice Analysis (OSTIA, Stark 2007) SST data set that is used for the ERA-I Reanalysis (6c). A TC-induced SST cold wake would be expected trailing an intense TC such as Yasi (Dare and McBride 2011; Mooney et al. 2016) but is largely missing from the ERA-I data before the lag correction (Figure 6a). The 30-hour lag is further evident in Figure 6e which shows the evolution of the SSTs averaged over a 2° x 2° area centred on 155°E, 15°S. Figure 6e demonstrates that the SSTs values in the ERA-I reanalysis data are lagging the OSTIA observed SST values by 30h and when this time lag is corrected for, the ERA-I SST values then align with the OSTIA values. Therefore, we have tested the effect of this lag-corrected SST representation, for scenario 3 of the surface boundary condition testing.

For the fourth SST scenario with a higher resolution SST, we used the blended Microwave Optimally Interpolated SST product (hereafter referred to as REMSS) (REMSS 2013) which are daily means available on a global grid of 9km spacing. We temporally interpolated the REMSS SST data into 6-hourly intervals and assimilated it into the lower boundary forcing during pre-processing to create new forcing files for the simulation. Figure 6 demonstrates that the resolution of the REMSS dataset (6d) captures more structure and detail in the SST field, particularly the area of the cold wake and some warmer SST pockets in the coastal lagoon that are absent in the ERA-I data even with lag fixed (6b). The SST sensitivity scenarios tested are summarized in Table 1 (last column). Each of these non-static SST scenarios provides a more accurate representation of the true SSTs, and therefore improve the interaction between the TC and the sea surface. We have examined whether including these improvements to the lower boundary conditions increases the simulation skill.

2.5. Analysis methods

Individual realizations of Yasi were assessed in terms of trajectory, landfall location, life cycle intensity (central pressure and wind speed), intensity at landfall, and translation speed. To easily compare the individual realizations, we created a new simple skill score metric using the following parameters: (1) the deviation in landfall central pressure from observed (hPa); (2) the deviation in the average translation speed of the system up to landfall (km/h); and (3) the deviation in landfall location from observed (km). The error index for each ensemble simulation was calculated by normalized root-mean-square error of the listed parameters using Equation 1. The value chosen to normalize each parameter was the largest recorded deviation for the given parameter in all of the simulations tested.

$$Equation\ 1: Simulation\ Skill = \sqrt{\left(\frac{\Delta LandfallPressure}{77.170\ (hPa)}\right)^2 + \left(\frac{\Delta TranslationSpeed}{19.920\ (\frac{km}{h})}\right)^2 + \left(\frac{\Delta LandfallLocation}{256.476\ (km)}\right)^2}$$

This calculation considers equally the landfall location (trajectory), central pressure (intensity), and translation speed (forward speed), allowing the simulation skill of WRF and the different combinations of physical parameterizations to be evaluated. The lowest error index indicates the most accurate simulation in the ensemble. A comprehensive list of parameter deviations and error indices for each ensemble member are given in Table 2. Skill scores inherently simplify complex datasets, but do provide a method for easily comparing a large number of ensemble members. Our skill score calculation is primarily based on TC conditions at landfall, which could be considered a narrow focus. However, it is pertinent to use landfall characteristics to calculate skill given the relationship with potential coastal damage. In addition, the use of the translation speed term in the calculation of the index considers an aspect of the TC lifecycle from initialization up to landfall, and so is not just a characteristic of the ensemble members at landfall. Furthermore, the spread in the ensemble results (e.g. trajectories in Figure 7) suggests that the spread in results at landfall is representative of the spread in the ensemble members throughout the simulations of the TC lifecycles. The spread in skill scores of the ensemble members was also explored using a multivariate analysis of variance (ANOVA). For the ANOVA, the changes in CU, MP, PBL, ISFTCFLX, OML, and vertical resolution are selected as the independent predictor variables, with error index score as the dependent variable. These analyses explore the mechanisms that produce the large spread between realizations.

3. Results and Discussion

3.1 Sensitivity to Physics Parameterizations

As expected, prescribing any CU, MP and PBL parameterizations (instead of default of none) greatly improved the simulation performance, and were crucial to producing TC-like wind speed and pressure evolution over these simulations (compare Figure 5a-5b). Using parameterizations reduced the error index, particularly in terms of the pressure and translation speed deviation (see Table 2).

The choice of CU, MP, PBL, ISFTCFLX, OML, and vertical resolution parameterizations significantly ($p = 0.01$) accounted for ~91% of error index variance calculated using multivariate ANOVA. The CU and MP are the only parameterizations to individually account for the variance in error index significantly in one-way ANOVAs. MP parameterization variation accounted for 46% of the error index variation ($p = 0.03$) while CU parameterizations explained 66% of the variance ($p = 0.0005$). Therefore, this analysis focuses primarily on the effect of the CU and MP parameterizations on the simulation.

As with other studies (e.g. Wang and Seaman 1997; Gallus 1999; Prater and Evans 2002; Zhang et al. 2011; Nasrollahi et al. 2012; Shepherd and Walsh 2016), analysis of the ensemble members highlights a distinct sensitivity of the simulation to the cumulus parameterization. Our results demonstrate a trade-off between simulating either the trajectory or intensity accurately with the choice of CU. As the simulations progress and landfall approaches, some ensemble members diverge significantly from the observed trajectory and landfall location (Figure 7). CU parameterization choices strongly influence the clustering of trajectories (Figure 7). Our independent findings did not support those of Nasrollahi et al. (2012) where BMJ produced the most accurate trajectory, or Shepherd and Walsh (2016) where there was little difference in the trajectories from the Kain Fritsch or Tiedtke schemes. Instead, our results confirm those of Torn and Davis (2012) where the ensemble members that utilize the Tiedtke parameterization (CU6, Figure 7, red) resulted in a trajectory much closer to observed than those using other parameterizations. It is particularly apparent in our results that the members with the Kain Fritsch CU scheme (CU1, Figure 7, green) systematically track further poleward, making landfall from 135 to 215km further south than observed. Though the simulations with no CU scheme prescribed (Figure 7, black) achieve a more accurate landfall location than those members with the Kain Fritsch scheme (CU1, Figure 7, green), the simulated trajectory through the lifecycle up to landfall is still markedly displaced southwards (which is not captured by the index calculation). The Grell Devenyi (CU3) and Grell 3D ensemble (CU5) schemes (Table 2 Runs: 7 and 8 respectively) simulated accurate translation speeds. However, their trajectories and landfall locations fall between those simulated using the Tiedtke and Kain Fritsch schemes.

Previous studies (e.g. Torn and Davis 2012) have shown that shallow convection over the tropical oceans is poorly represented in the Kain Fritsch scheme and may result in a warm temperature bias at the 700mb level, with associated steering flow bias. Figure 8 shows the average temperature and wind at the 700mb level over the entire 96 hours of a simulation, with Kain Fritsch (Figure 8a) and Tiedtke (Figure 8b) CU schemes. The Kain Fritsch scheme simulates temperatures ~1°C (and up to 2°C) warmer than the Tiedtke scheme. The Kain Fritsch scheme also produces a difference in the average flow, likely steering the system further poleward (Figure 8c). The active shallow convection over tropical ocean (where the moisture flux through the cloud base is assumed to be equivalent to surface moisture flux in the Tiedtke scheme (Torn and Davis 2012)) produces cooler temperatures at the 700mb level and an average flow that moves predominately east-west (Figure 8b). As discussed by Shepherd and Walsh (2016), beta drift (Holland 1983) can add an additional southward component of motion to the steering flow to westward moving TCs in the Southern Hemisphere. Figure 9 demonstrates that the radius of 64 knot winds was notably larger with the Kain Fritsch scheme (solid green line, Figure 9) during the main intensification period up to landfall than with the Tiedtke scheme (dashed green lines Figure 9). The larger TC size with the Kain Fritsch scheme could account for the greater drift of the system polewards due to a stronger beta effect (Holland 1983), in addition to the steering flow.

When considering both the calculated landfall location distance deviation and pressure deviation of the simulations from observed (Table 2), it is clear that while changes to ensemble members such as MP scheme, PBL scheme, vertical resolution, ISFTCFLX, and OML did have some effect on the outcome of the simulation, the CU parameterization remains the greatest influence particularly in terms of the resulting intensity and trajectory. Figure 10 depicts the landfall pressure deviation against the landfall distance deviation for each ensemble member. Ensemble members employing the Tiedtke scheme (CU6, Figure 10 red) cluster at the lowest landfall deviation values, indicating that this scheme is best for producing accurate trajectories. However, this scheme produces relatively high landfall pressure deviations, indicating systematically weaker TCs. Conversely, ensemble members employing the Kain Fritsch scheme (CU1, Figure 10 green) cluster at lower pressure deviations, demonstrating that this scheme achieves a more realistic pressure (and thus intensity at landfall). However, the Kain Fritsch scheme produces a relatively large landfall location deviation (greater than 130km). Therefore, there appears to be a trade-off between employing the Kain Fritsch and Tiedtke CU parameterizations that has not previously been discussed for this grid, in this location. The Tiedtke scheme produces the most accurate trajectories, while the Kain Fritsch scheme produces the most accurate intensities. Other schemes produce intermediate results (with much higher overall error indices). The significant degree of CU-dependent clustering observed indicates that these differences are systematic effects, and are not simply due to model internal variability.

Figure 9 demonstrates that the Kain Fritsch scheme (CU1, solid line) produced lower pressure values (closer to observed values of SLP, in red) and therefore a more intense system than the Tiedtke scheme which lacked deepening and intensification (CU6, dashed line) throughout the lifecycle up to landfall. These results support the intensity differences discussed in Shepherd and Walsh (2016). The active shallow convection of the Tiedtke scheme over the tropical ocean allows vertical advection of evaporation from the ocean surface and upward transport of moisture across the boundary layer (Torn and Davis 2012). However, the shallow convection can reduce the deep convective mass flux and buoyancy, resulting in reduced TC intensification rate (Torn and Davis 2012). This reduction would account for the reduced central pressure achieved by the ensemble members with the Tiedtke scheme in this study. Conversely, without the shallow convection over the tropical oceans (Torn and Davis 2012), the Kain Fritsch scheme may be less likely to reduce the deep convective mass flux and allow intensification rate increase resulting in systems with greater intensity.

To further evaluate the Tiedtke and Kain Fritsch schemes, we investigate the accuracy of translation speed, as well as the overall error indices. As seen in Table 2, ensemble members employing the Kain Fritsch scheme had systematically lower deviations in translation speed than those employing the Tiedtke scheme. However, the Kain Fritsch ensemble members have larger overall error indices than the Tiedtke ensemble members, indicating that these error indices are dominated by deviations in trajectory.

Changing the MP parameterization with an otherwise fixed model configuration (compare Runs 9, 13, 14, and 15 in Table 2) did affect the outcome of the error index calculation. However, discerning the effect may be somewhat difficult, as the dominant influence of the shallow convection scheme in the CU parameterization can mask that of the MP scheme (Torn and Davis 2012). Notably, the WSM 5-class scheme (MP4) results in a reduced error index, primarily due to improving the simulated trajectory and landfall deviation (Table 2, Run 13). However, the Ferrier new Eta scheme

(MP5) results in the lowest error index through reduced translation speed error and pressure deviation (Table 2, Run 9). We chose to continue further simulations with the Ferrier scheme (MP5) because it is designed for computational efficiency.

The choice of CU and MP scheme influenced the simulation sensitivity to other parameterizations such as the PBL, ISFTCFLX, and OML in the ensemble members. The results did not demonstrate a consistent effect of the PBL on the calculated skill score nor a consistent improvement when employing the ISFTCFLX in this ensemble setup. Therefore, the YSU PBL scheme with no ISTCFLX surface drag coefficient setup was chosen for further simulations. The YSU PBL is a first order closure scheme (Noh et al. 2003) and is often less biased toward excessive mixing (Braun and Tao 2000) and so is favored from this ensemble.

The ensemble members with the Kain Fritsch CU scheme are comparatively the most successful at simulating intensity evolution and pressure at landfall. However, as with the ACCESS-TC forecasts (Reeder et al. 2012), none of our model configurations thus far were able to reproduce the maximum observed intensity of TC Yasi or maintain intensity towards landfall. For almost all ensemble members, the minimum in central pressure occurred too early over the open ocean around 08:00 UTC on February 1, 2011, and then weakened towards landfall. This under-representation of intensity could be expected with a relatively coarse horizontal resolution of 12km (Gentry and Lackmann 2010). However, TC intensity is strongly linked to SSTs (Schade and Emanuel 1999; Ramsay and Sobel 2011). Therefore, we have tested the simulation sensitivity to the SST boundary condition. In particular, the sensitivity to the SST dataset resolution and SST interaction with the atmosphere, which will now be discussed.

3.2. Sensitivity to SST Boundary Conditions

In previous simulations, the SSTs were constant throughout the entire simulation. However, this is physically unrealistic as TCs interact with the ocean surface, cooling surface temperatures within hours of their arrival (Dare and McBride 2011; Mooney et al. 2016). This is particularly important for TC intensity, as cooling near the cyclone reduces heat and moisture available to the system, thus dampening the intensity. Therefore, non-static SST boundary conditions may improve the simulations. Here, we investigate the sensitivity of Yasi simulations to four different representations of SST (detailed in Section 2.4): (1) daily SSTs derived from ERA-I, (2) active interaction between TC and SST via a 1-D ocean mixed layer model, (3) daily SSTs derived from ERA-I with 30hr lag corrected, and (4) 6-hourly SSTs derived from higher resolution REMSS data. A change in the spatial distribution and representation of the SSTs could be important for controlling the intensification of TC Yasi, particularly in the coastal lagoon area (Bosart et al. 2000; Hong et al. 2000; and Mainelli et al. 2008).

Figure 11c and d show that allowing SST to update during the simulation and then making further changes to the SST representation, results in significant deviations in the SSTs observed under the center of the TC systems (compare colored lines to black line). The simulations of TC Yasi with the Kain Fritsch scheme are relatively insensitive to the changes made to the SST boundary. The trajectories (Figure 11 a) and intensities (Figure

11 e) are relatively stable (see also Table 2, Runs 33-37) with the results from the simulations tightly clustered. The changes to the SST representation have a common effect of reducing landfall location error slightly and increasing intensity. The increased intensity is particularly notable for the ERA-I lag fix scenario (Figure 11e green) and may be attributed to the increased SST values under the storm particularly between 25h and 45h of simulation time (Figure 11c).

Given the same changes to the SST boundary, simulated trajectories with the Tiedtke scheme show a slightly larger spread (Table 2, Runs 28-32; Figure 11 b). The different SSTs encountered by the TC (Figure 11 d) contribute to comparatively greater differences in intensity through the TC lifecycle, with significant increases in intensity of up to ~10hPa from 30h to landfall (Figure 11 f). The tested scenarios should improve the physical representation of the TC-ocean interaction and improve the representation of the TC-induced cool wake in the WRF simulation. The ocean interaction and cold wake did not dampen or reduced TC intensity as may have been expected, but in fact increases intensity from the fixed SST simulation for both CU schemes (Figure 11e,f). This may be attributed to the forward speed of Yasi which enabled the system to interact with warmer SSTs (Figure 11 c,d) ahead of the TC-induced cold wake.

In the Tiedtke scheme, deep and shallow convection are both governed by moisture flux (Qiao and Liang 2015). Convection is activated when moisture convergence exceeds a limit of boundary layer turbulent moisture flux (Qiao and Liang 2015). The Tiedtke scheme may therefore have greater sensitivity to changes in the boundary SSTs (and the associated evaporation and moisture) than the Kain Fritsch scheme, which is triggered by column convective instability and parcel temperature (Qiao and Liang 2015). As discussed in section 3.1, the Tiedtke scheme has a more appropriate and active treatment of shallow oceanic convection where the moisture flux through the cloud base is assumed to be equivalent to surface moisture flux (Torn and Davis 2012). The shallow convection allows vertical advection of evaporation from the ocean surface and upward transport of moisture across the boundary layer (Torn and Davis 2012). This shallow convection parameterization is appropriate for tropical oceans, even during hurricane winds, and may account for the greater sensitivity to the SST boundary conditions over the ocean. Conversely, the Kain Fritsch scheme performs better over land surfaces, but its inadequate representation of shallow convection over tropical oceans may make it less responsive to changes in the SST boundary (Torn and Davis 2012).

Table 2 shows that the intensity at landfall is sensitive to the SSTs. The ERA-I lag fix improved intensity for the Kain Fritsch scheme (Figure 11e) but the higher resolution REMSS SSTs improve the simulated intensity regardless of the CU scheme used. This increased intensity is primarily responsible for improving the error index. We focus this discussion on the Tiedtke simulations as the improvement in intensity is more evident. From time step 42 to 60, the simulated TC tracked over warmer SST values using REMSS SSTs (Figure 11 d red line) than when using the ERA-I SSTs (Figure 11 d other colors). The increased SST gradient destabilizes the overlying atmosphere and increases the upper limit of TC intensity (Vecchi and Soden 2007). The surface fluxes of heat and moisture, and vigorous convection increase in concert with SST values. Vertical mass flux and acceleration are subsequently enhanced and the inward mass convergence results in enhanced vorticity convergence and vortex stretching. Upper-level thermal expansion develops along with the upper-level vortex intensification. These system-scale changes cause increases in relative vorticity and rapid intensification of the TC system (Garner et al. 2009). Figure 12 demonstrates that with both the Kain Fritsch and Tiedtke schemes, the REMSS SST data set acted to increase the relative vorticity at the 500hPa level. For the Kain Fritsch scheme (Figure 12a), the increased values of relative vorticity are tightly confined around the TC eye. There was a greater system-scale response of the relative vorticity to altered SST forcing with the Tiedtke scheme (Figure 12b). There were more discernible changes in values within the eye and over the whole cross section of the system for this CU scheme, further indicating a greater sensitivity to the change in the SST boundary condition.

At higher grid spacing, where convection is explicitly resolved, it is expected that simulation responses to SST changes would be influenced by the PBL schemes. Li and Pu (2008, 2009) showed that, for hurricane Emily, CU were the most influential at 9km grid spacing whereas the PBL schemes were the most influential at grid spacing of 3km. This demonstrates that at the convection resolving scales, PBL schemes are an important consideration while at the grid spacing used in this study, the CU are more influential.

4. Conclusions

Tropical Cyclone Yasi was a rapidly-intensifying and long-lived category 5 system, the first to cross the Queensland coastline in nearly a century. It is important to improve the representation of such TC cases on a relatively coarse grid to inform model configuration for future regional climate simulations. While the results from sensitivity testing on this grid may not translate to future simulations over long time periods, the results could be used in future simulations of extreme events. Yasi's maximum intensity and intensity evolution towards landfall proved difficult to simulate with the numerical weather model (WRF) in a 36km and 12km nested domain configuration. However, this study successfully represents the TC's characteristics on this grid using ERA-Interim data as boundary conditions, ACCESS-TC high resolution data for initialization, optimized physics parameterizations after ensemble testing, and a high-resolution SST boundary condition after SST sensitivity testing.

This study finds a distinct simulation sensitivity to the spatial resolution of the initial conditions. Results demonstrated that the simulation accuracy (particularly the intensity and translation speed) of TCs at the horizontal resolution of 36 / 12 km and with 28 vertical levels can be improved with an accurate and high resolution initial condition field. This is advantageous, as it is computationally cheaper than other methods, such as increasing model resolution (e.g. Gentry and Lackmann 2010; Shepherd and Walsh 2016) or large scale data assimilation (e.g. Torn and Davis 2012). This initialization method and model setup may be valuable to future regional climate studies that require large numbers of simulations to explore the response of TC dynamics over long time scales.

Of the physical parameterizations tested, the Yasi simulations were particularly sensitive to the cumulus parameterization, resulting in a trade-off between accurately simulating trajectory or accurately simulating intensity. The Tiedtke scheme supported a skillful trajectory evolution and landfall location, but a propagation speed faster than observed, and an overall weaker system. Conversely, the Kain Fritsch scheme simulated track and landfall location poorly, but the simulations produced more accurate intensities and translation speeds over the TC lifecycle. Several of these differences can be attributed to the CU schemes' representation of shallow convection over the tropical ocean. The Kain Fritsch scheme lacked shallow convection, leading to warmer temperatures at 700 hPa, and ultimately a poleward bias in the average steering flow. The more active shallow convection of the Tiedtke scheme resulted in more accurate steering flows but reduced deep convective mass flux, and subsequently, intensity. These findings may inform the physics parameterization choices for future studies of TC dynamics at this resolution, depending on whether intensity or trajectory is the primary focus.

No simulation on this grid, regardless of configuration, was able to successfully reproduce the 929 hPa minimum central pressure of Yasi, or it's intensification towards landfall. The correction of a newly discovered 30h lag in SSTs in the ERA-I reanalysis data reduced the trajectory error for simulations with the Tiedtke schemes and intensity errors with Kain Fritsch. However, the inclusion of a high-resolution, daily SST product improved the track, landfall location, and intensity of the TC simulation for both CU schemes. Altering the SST forcing resulted in a greater change to simulated intensity with the Tiedtke scheme due to heightened alteration in the relative vorticity in response to the added thermal energy in the boundary condition. The greater sensitivity of the Tiedtke scheme stems from the moisture convergence trigger function and the more active shallow convection over the tropical ocean than the Kain Fritsch scheme. The differing sensitivities of the scheme to the surface forcing may be an important consideration when selecting a cumulus parameterization in a model setup for future studies, particularly those that consider climate change forcing.

SST sensitivity simulations demonstrate that additional warming in the boundary condition resulted in increased TC intensity. It follows that providing accurate SSTs is essential to accurately simulating intensity, particularly towards landfall. Additional warming may have been present in the coastal lagoon during TC Yasi due to the East Australian Current (EAC), a "broad, warm tongue of water that extends southwards" (Ridgway 2007) and transports warm equatorial water into the Coral Sea (Lough 1998). The EAC exhibits non-linearity and large inter-annual variability (Foster et al. 2014), and a warm phase may not have been captured in the SST data in this region due to poor resolution, measurement error, and systematic cool bias of satellite data over Australia (particularly during times of high cloud prevalence in the summer season) (Foster et al. 2014). If SSTs were indeed underestimated during Yasi, our SST boundary condition simulations suggest that this could account for the underestimation of TC intensity through the coastal lagoon into landfall. The resolution and accuracy of SST data will also be very important in future TC intensity simulations and predictions, given that SSTs have been rising in this region already (Hughes et al. 2003; Foster et al. 2014) and will likely continue with climate change forcings (Hughes et al. 2003).

Acknowledgements

The authors would like to thank Todd Arbetter at the Institute for Environment and Society at Brown University for invaluable assistance in pre-processing and post-processing; Henry Johnson for assistance implementing WRF on Brown University's

Center for Computing and Visualization; Noel Davidson at the Australian Bureau of Meteorology for the high resolution initialization data and advice; Jung-Eun Lee at Brown University, and Greg Holland at the National Center of Atmospheric Research for helpful discussion; and Daniel P Moriarty III at Brown University for assistance in editing the manuscript. This work was funded by Brown University. NCAR is sponsored by the National Science Foundation.

5. References

Abarca, S. F., & Corbosiero, K. L. (2011). Secondary eyewall formation in WRF simulations of Hurricanes Rita and Katrina (2005). Geophysical Research Letters, 38(7).

Alexander, L. V., Hope, P., Collins, D., Trewin, B., Lynch, A., & Nicholls, N. (2007). Trends in Australia's climate means and extremes: a global context. Australian Meteorological Magazine, 56(1), 1-18.

AON Benfield, (2011) http://thoughtleadership.aonbenfield.com/Documents/201103_ab_if_tropical_cyclone_yasi_recap.pdf

Australian Bureau of Meteorology, (2011) [http://www.bom.gov.au/cyclone/history/yasi.shtml];

Bao, J. W., Gopalakrishnan, S. G., Michelson, S. A., Marks, F. D., & Montgomery, M. T. (2012). Impact of Physics Representations in the HWRFX on Simulated Hurricane Structure and Pressure-Wind Relationships. Monthly Weather Review, 140(10), 3278-3299.

Bao, J. W., Michelson, S. A., & Wilczak, J. M. (2002). Sensitivity of numerical simulations to parameterizations of roughness for surface heat fluxes at high winds over the sea. Monthly weather review, 130(7), 1926-1932.

Beeden R, Maynard J, Puotinen M, Marshall P, Dryden J, Goldberg J, et al. (2015). Impacts and Recovery from Severe Tropical Cyclone Yasi on the Great Barrier Reef. PLoS ONE 10(4): e0121272. doi:10.1371/journal.pone.0121272

Bosart, L. F., Bracken, W. E., Molinari, J., Velden, C. S., & Black, P. G. (2000). Environmental influences on the rapid intensification of Hurricane Opal (1995) over the Gulf of Mexico. Monthly weather review, 128(2), 322-352.

Braun, S. A., & Tao, W. K. (2000). Sensitivity of high-resolution simulations of Hurricane Bob (1991) to planetary boundary layer parameterizations. Monthly Weather Review, 128(12), 3941-3961.

Bruyère, C. L., Holland, G. J., & Towler, E. (2012). Investigating the use of a genesis potential index for tropical cyclones in the North Atlantic basin. *Journal of Climate*, *25*(24), 8611-8626.

Charnock, H. (1955). Wind stress on a water surface. *Quarterly Journal of the Royal Meteorological Society*, *81*(350), 639-640.

Chen, F., & Dudhia, J. (2001). Coupling an advanced land surface-hydrology model with the Penn State-NCAR MM5 modeling system. Part I: Model implementation and sensitivity. Monthly Weather Review, 129(4), 569-585.

Dare, R. A., & McBride, J. L. (2011). Sea surface temperature response to tropical cyclones. Monthly Weather Review, 139(12), 3798-3808.

Davidson, N. E., Xiao, Y., Ma, Y., Weber, H. C., Sun, X., Rikus, L. J., ... & Fraser, J. (2014). ACCESS-TC: Vortex specification, 4DVAR initialization, verification, and structure diagnostics. Monthly Weather Review, 142(3), 1265-1289.

Davis, C., Wang, W., Chen, S. S., Chen, Y., Corbosiero, K., DeMaria, M., ... & Xiao, Q. (2008). Prediction of landfalling hurricanes with the Advanced Hurricane WRF model. Monthly Weather Review, 136(6), 1990-2005.

Dee, D. P., and Coauthors, (2011): The ERA-Interim reanalysis: Configuration and performance of the data assimilation system. Quart. J. Roy. Meteor. Soc., 137, 553–597.

Done, J.M., Holland, G.J., Bruyère, C.L., Leung, L.R., and Suzuki-Parker, A., 2013: Modeling high-impact weather and climate: Lessons from a tropical cyclone perspective. Climatic Change, doi: 10.1007/s10584-013-0954-6

Donelan, M. A., Hamilton, J., & Hui, W. H. BK Haus, N. Reul, WJ Plant, M. Stiassnie, HC Graber, OB Brown, and ES Saltzman, (2004): On the limiting aerodynamic roughness of the ocean in very strong winds. *Geophys. Res. Lett*, *31*, L18306.

Dudhia, J. (1989). Numerical study of convection observed during the winter monsoon experiment using a mesoscale two-dimensional model. *Journal of the Atmospheric Sciences*, *46*(20), 3077-3107.

Ek, M. B., Mitchell, K. E., Lin, Y., Rogers, E., Grunmann, P., Koren, V., ... & Tarpley, J. D. (2003). Implementation of Noah land surface model advances in the National Centers for Environmental Prediction operational mesoscale Eta model. *Journal of Geophysical Research: Atmospheres (1984–2012)*, *108*(D22).

Emanuel, K. A. (1995). Sensitivity of tropical cyclones to surface exchange coefficients and a revised steady-state model incorporating eye dynamics. Journal of the Atmospheric Sciences, 52(22), 3969-3976.

Emanuel, K., DesAutels, C., Holloway, C., & Korty, R. (2004). Environmental control of tropical cyclone intensity. *Journal of the atmospheric sciences*, *61*(7), 843-858.

Ferrier, B. S. (1994). A double-moment multiple-phase four-class bulk ice scheme. Part I: Description. *Journal of the atmospheric sciences*, *51*(2), 249-280.

Ferrier, B. S., Y. Jin, Y. Lin, T. Black, E. Rogers, and G. DiMego, (2002). Implementation of a new grid-scale cloud and rainfall scheme in the NCEP Eta Model. Preprints, 15th Conf. on Numerical Weather Prediction, San Antonio, TX, Amer. Meteor. Soc., 280–283.

Fierro, A. O., Rogers, R. F., Marks, F. D., & Nolan, D. S. (2009). The impact of horizontal grid spacing on the microphysical and kinematic structures of strong tropical cyclones simulated with the WRF-ARW model. Monthly Weather Review, 137(11), 3717-3743.

Foster, S. D., Griffin, D. A., & Dunstan, P. K. (2014). Twenty Years of High-Resolution Sea Surface Temperature Imagery around Australia: Inter-Annual and Annual Variability. PloS one, 9(7), e100762.

Fovell, R. G., & Su, H. (2007). Impact of cloud microphysics on hurricane track forecasts. Geophysical Research Letters, 34(24).

Fovell, R. G., Corbosiero, K. L., & Kuo, H. C. (2009). Cloud microphysics impact on hurricane track as revealed in idealized experiments. Journal of the Atmospheric Sciences, 66(6), 1764-1778.

Gallus Jr, W. A. (1999). Eta simulations of three extreme precipitation events: Sensitivity to resolution and convective parameterization. Weather and forecasting, 14(3), 405-426.

Garner, S. T., Held, I. M., Knutson, T., & Sirutis, J. (2009). The roles of wind shear and thermal stratification in past and projected changes of Atlantic tropical cyclone activity. *Journal of Climate*, *22*(17), 4723-4734.

Garratt, J. R. (1994). The atmospheric boundary layer. Cambridge university press.

Gentry, M. S., & Lackmann, G. M. (2010). Sensitivity of simulated tropical cyclone structure and intensity to horizontal resolution. Monthly Weather Review, 138(3), 688-704.

Glisan, J. M., Gutowski Jr, W. J., Cassano, J. J., & Higgins, M. E. (2013). Effects of spectral nudging in WRF on Arctic temperature and precipitation simulations. *Journal of Climate*, *26*(12), 3985-3999.

Great Barrier Reef Marine Park Authority (2011a), Extreme Weather and the Great Barrier Reef, 2011, GBRMPA, Townsville.

Great Barrier Reef Marine Park Authority (2011b), Impacts of tropical cyclone Yasi on the Great Barrier Reef: a report on the findings of a rapid ecological impact assessment, July 2011, GBRMPA, Townsville.

Grell, G. A. (1993). Prognostic evaluation of assumptions used by cumulus parameterizations. *Monthly Weather Review*, *121*(3), 764-787.

Grell, G. A., & Dévényi, D. (2002). A generalized approach to parameterizing convection combining ensemble and data assimilation techniques. Geophysical Research Letters, 29(14), 38-1.

Holland, G. J. (1983). Tropical cyclone motion: Environmental interaction plus a beta effect. Journal of the Atmospheric Sciences, 40(2), 328-342.

Holland, G., & Bruyère, C. L. (2013). Recent intense hurricane response to global climate change. Climate Dynamics, 1-11.

Hong, S. Y., & Lim, J. O. J. (2006). The WRF single-moment 6-class microphysics scheme (WSM6). *J. Korean Meteor. Soc*, *42*(2), 129-151.

Hong, S. Y., Dudhia, J., & Chen, S. H. (2004). A revised approach to ice microphysical processes for the bulk parameterization of clouds and precipitation. Monthly Weather Review, 132(1), 103-120.

Hong, S. Y., Noh, Y., & Dudhia, J. (2006). A new vertical diffusion package with an explicit treatment of entrainment processes. *Monthly Weather Review*, *134*(9), 2318-2341.

Hong, X., Chang, S. W., Raman, S., Shay, L. K., & Hodur, R. (2000). The interaction between Hurricane Opal (1995) and a warm core ring in the Gulf of Mexico. Monthly Weather Review, 128(5), 1347-1365.

Hughes, L. (2003). Climate change and Australia: trends, projections and impacts. Austral Ecology, 28(4), 423-443.

Irish, J. L., & Resio, D. T. (2010). A hydrodynamics-based surge scale for hurricanes. Ocean Engineering, 37(1), 69-81.

Jacob, D., J. Petersen, J., Eggert, B., Alias, A., Christensen, O.B., Bouwer, L.M., Braun, A., Colette, A., Deque, M., Georgievski, G., Georgopoulou, E., Gobiet, A., Menut, L., Nikulin, G., Haensler, A., Hempelmann, N., Jones, C., Keuler, K., Kovats, S., Kroner, N., Kotlarski, S., Kriegsmann, A., Martin, E., van Meijgaard, R., Moseley, C., Pfeifer, S., Preuschmann, S., Radermacher, C., Radtke, K., Rechid, D., Rounsevell, M., Samuelsson, P., Somot, S., Soussana, J-F., Teichmann, C., Valentini, R., Vautard, R., Weber, B. & Yiou, P. (2014). EURO-CORDEX: new high-resolution climate change projections for European impact research. *Regional Environmental Change*, *14*(2), 563-578.

Janjić, Z. I. (1994). The step-mountain eta coordinate model: Further developments of the convection, viscous sublayer, and turbulence closure schemes. *Monthly Weather Review*, *122*(5), 927-945.

Janjić, Z. I. (2002). Nonsingular implementation of the Mellor–Yamada level 2.5 scheme in the NCEP Meso model. *NCEP office note*, *437*, 61.

Kain, J. S. (1993). Convective parameterization for mesoscale models: The Kain Fritsch scheme. *The representation of cumulus convection in numerical models, Meteor. Monogr*, *46*, 165-170.

Kain, J.S., (2004): The Kain–Fritsch convective parameterization: An update. *J. Appl. Meteor. Climatol.*, **43**, 170–181.

Kain, J.S., and J.M. Fritsch, (1990): A one-dimensional entraining detraining plume model and its application in convective parameterization. *J. Atmos. Sci.*, **47**, 2784–2802.

Kessler, E. (1969). On the distribution and continuity of water substance in atmospheric circulation. Meteorological Monograph, 10.
Knapp, K. R., Kruk, M. C., Levinson, D. H., Diamond, H. J., & Neumann, C. J. (2010). The international best track archive for climate stewardship (IBTrACS) unifying tropical cyclone data. *Bulletin of the American Meteorological Society*, *91*(3), 363-376.
Kuleshov, Y., Fawcett, R., Qi, L., Trewin, B., Jones, D., McBride, J., & Ramsay, H. (2010). Trends in tropical cyclones in the South Indian Ocean and the South Pacific Ocean. Journal of Geophysical Research: Atmospheres, 115(D1).
Lackmann, G. M. (2015). Hurricane Sandy before 1900 and after 2100. Bulletin of the American Meteorological Society, 96(4), 547-560
Landsea, C. W., Vecchi, G. A., Bengtsson, L., & Knutson, T. R. (2010). Impact of duration thresholds on Atlantic tropical cyclone counts. Journal of Climate, 23(10), 2508-2519.
Lavender, S. L., & Walsh, K. J. E. (2011). Dynamically downscaled simulations of Australian region tropical cyclones in current and future climates. Geophysical Research Letters, 38(10).
Li X, Pu Z. (2009). Sensitivity of numerical simulations of the early rapid intensification of Hurricane Emily to cumulus parameterization schemes in different model horizontal resolutions. *J. Meteorol. Soc. Japan* 87 403–421.
Li, X., & Pu, Z. (2008). Sensitivity of numerical simulation of early rapid intensification of Hurricane Emily (2005) to cloud microphysical and planetary boundary layer parameterizations. *Monthly Weather Review*, *136*(12), 4819-4838.
Lough, J. M. (1998). Coastal climate of northwest Australia and comparisons with the Great Barrier Reef: 1960 to 1992. Coral Reefs, 17(4), 351-367.
Lynch, A., Nicholls, N., Alexander, L., & Griggs, D. (2008). Defining the impacts of climate change on extreme events. Garnaut Climate Change Review.
Lynn, B. H., Healy, R., & Druyan, L. M. (2009). Investigation of Hurricane Katrina characteristics for future, warmer climates. Climate Research, 39(1), 75-86.
Ma, Z., Fei, J., Huang, X., & Cheng, X. (2012). Sensitivity of tropical cyclone intensity and structure to vertical resolution in WRF. Asia-Pacific Journal of Atmospheric Sciences, 48(1), 67-81.
Mainelli, M., DeMaria, M., Shay, L. K., & Goni, G. (2008). Application of oceanic heat content estimation to operational forecasting of recent Atlantic category 5 hurricanes. Weather and Forecasting, 23(1), 3-16.
Miglietta, M. M., Moscatello, A., Conte, D., Mannarini, G., Lacorata, G., & Rotunno, R. (2011). Numerical analysis of a Mediterranean ‘hurricane’over south-eastern Italy: sensitivity experiments to sea surface temperature. *Atmospheric Research*, *101*(1), 412-426.
Mlawer, E. J., Taubman, S. J., Brown, P. D., Iacono, M. J., & Clough, S. A. (1997). Radiative transfer for inhomogeneous atmospheres: RRTM, a validated correlated-k model for the longwave. Journal of geophysical research, 102(D14), 16663-16.
Mohanty, U. C., Osuri, K. K., Routray, A., Mohapatra, M., & Pattanayak, S. (2010). Simulation of Bay of Bengal tropical cyclones with WRF model: Impact of initial and boundary conditions. *Marine Geodesy*, *33*(4), 294-314.
Monin, A. S., & Obukhov, A. (1954). Basic laws of turbulent mixing in the surface layer of the atmosphere. Contrib. Geophys. Inst. Acad. Sci. USSR, 151, 163-187.
Mooney, P. A., Gill, D. O., Mulligan, F. J., & Bruyère, C. L. (2016). Hurricane simulation using different representations of atmosphere–ocean interaction: the case of Irene (2011). Atmospheric Science Letters, 17(7), 415-421.
Nakanishi, M., & Niino, H. (2009). Development of an improved turbulence closure model for the atmospheric boundary layer. 気象集誌, 87(5), 895-912.

Nasrollahi, N., AghaKouchak, A., Li, J., Gao, X., Hsu, K., & Sorooshian, S. (2012). Assessing the Impacts of Different WRF Precipitation Physics in Hurricane Simulations. Weather and Forecasting, 27(4), 1003-1016.

Nguyen, K. C., & Walsh, K. J. E. (2001). Interannual, decadal, and transient greenhouse simulation of tropical cyclone–like vortices in a regional climate model of the South Pacific. *Journal of Climate*, *14*(13), 3043-3054.

Nicholls, N., Landsea, C., & Gill, J. (1998). Recent trends in Australian region tropical cyclone activity. Meteorology and Atmospheric Physics, 65(3-4), 197-205.

Noh, Y., Cheon, W. G., Hong, S. Y., & Raasch, S. (2003). Improvement of the K-profile model for the planetary boundary layer based on large eddy simulation data. *Boundary-layer meteorology*, *107*(2), 401-427.

Oouchi, K., Yoshimura, J., Yoshimura, H., Mizuta, R., Kusunoki, S., & Akira, N. O. D. A. (2006). Tropical cyclone climatology in a global-warming climate as simulated in a 20 km-mesh global atmospheric model: Frequency and wind intensity analyses. Journal of the Meteorological Society of Japan. Ser. II, 84(2), 259-276.

Peng, M., Xie, L., & Pietrafesa, L. J. (2004). A numerical study of storm surge and inundation in the Croatan–Albemarle–Pamlico Estuary System. Estuarine, Coastal and Shelf Science, 59(1), 121-137

Pollard, R. T., Rhines, P. B., & Thompson, R. O. (1972). The deepening of the wind-mixed layer. Geophysical & Astrophysical Fluid Dynamics, 4(1), 381-404.

Prater, B. E., & Evans, J. L. (2002). Sensitivity of modeled tropical cyclone track and structure of hurricane Irene (1999) to the convective parameterization scheme. Meteorology and Atmospheric Physics, 80(1-4), 103-115.

Puotinen, M. L. (2007). Modelling the risk of cyclone wave damage to coral reefs using GIS: a case study of the Great Barrier Reef, 1969–2003. International Journal of Geographical Information Science, 21(1), 97-120.

Puotinen, M. M., Done, T. T., & Skelley, W. (1997). An atlas of tropical cyclones in the Great Barrier Reef region: 1969-1997.

Puri, K., Dietachmayer, G., Steinle, P., Dix, M., Rikus, L., Logan, L., ... & Bermous, I. (2013). Implementation of the initial ACCESS numerical weather prediction system. Aust. Meteorol. Oceanogr. J, 63, 265-284.

Puri, K., Xiao, Y., Sun, X., Lee, J., Engel, C., Steinle, P., ... & Bowen, R. (2010). Preliminary results from Numerical Weather Prediction implementation of ACCESS. CAWCR Research Letters, 5, 15-22.

Qiao, F., & Liang, X. Z. (2015). Effects of cumulus parameterizations on predictions of summer flood in the Central United States. Climate Dynamics, 45(3-4), 727-744.

Queensland Government (2012). Budget Strategy and Outloook 2011-2012, 70 pp, Accessed January 5 2015. [http://www.budget.qld.gov.au/current-budget/budget-papers/index.php]

Ramsay, H. A., & Sobel, A. H. (2011). Effects of relative and absolute sea surface temperature on tropical cyclone potential intensity using a single-column model. Journal of Climate, 24(1), 183-193.

Reeder, M. J., Davidson, N. E., Bishop, C. H., Kepert, J. D., Steinle, P., Tory, K. J., ... & Chen, Y. J. (2012). Annual Report FY2012 ONRBAA09-012.

Rego, J. L., & Li, C. (2009). On the importance of the forward speed of hurricanes in storm surge forecasting: A numerical study. Geophysical Research Letters, 36(7).

REMSS (2013) accessed September 1 2013 [http://www.remss.com/sst/microwave_oi_sst_data_description.html]

Reuters (2015) Cyclone Yasi to cost insurers AUS $3.5 bln forecaster. [Available online at http://www.reuters.com/article/2011/02/03/insured-losses-yasi-idUSLDE7121NR20110203]

Ridgway, K. R. (2007). Long-term trend and decadal variability of the southward penetration of the East Australian Current. Geophysical Research Letters, 34(13).

Schade, L. R., & Emanuel, K. A. (1999). The ocean's effect on the intensity of tropical cyclones: Results from a simple coupled atmosphere-ocean model. Journal of the atmospheric sciences, 56(4), 642-651.

Shapiro, L. J. (1983). The asymmetric boundary layer flow under a translating hurricane. Journal of the Atmospheric Sciences, 40(8), 1984-1998.

Shepherd, T. J., & Walsh, K. J. (2016) Sensitivity of hurricane track to cumulus parameterization schemes in the WRF model for three intense tropical cyclones: impact of convective asymmetry. Meteorology and Atmospheric Physics, 1-30.

Skamarock, W. C., Klemp, J. B., Dudhia, J., Gill, D. O., & Barker, D. M. (2005). Coauthors, 2008: A description of the Advanced Research WRF version 3. NCAR Tech. Note NCAR/TN-475+ STR, 113.

Smith, R. K., & Thomsen, G. L. (2010). Dependence of tropical-cyclone intensification on the boundary layer representation in a numerical model. Quarterly Journal of the Royal Meteorological Society, 136(652), 1671-1685.

Smith, R. K., Montgomery, M. T., & Thomsen, G. L. (2013). Sensitivity of tropical-cyclone models to the surface drag coefficient in different boundary-layer schemes. Quarterly Journal of the Royal Meteorological Society.

Stark, J. D., Donlon, C. J., Martin, M. J., & McCulloch, M. E. (2007, June). OSTIA: An operational, high resolution, real time, global sea surface temperature analysis system. In *Oceans 2007-Europe* (pp. 1-4). IEEE.

Tao, W. K., Shi, J. J., Chen, S. S., Lang, S., Lin, P. L., Hong, S. Y., ... & Hou, A. (2011). The impact of microphysical schemes on hurricane intensity and track. Asia-Pacific Journal of Atmospheric Sciences, 47(1), 1-16.

Tewari, M., Chen, F., Wang, W., Dudhia, J., LeMone, M. A., Mitchell, K., ... & Cuenca, R. H. (2004, January). Implementation and verification of the unified NOAH land surface model in the WRF model. In *20th conference on weather analysis and forecasting/16th conference on numerical weather prediction* (pp. 11-15).

Thompson, G., Field, P. R., Rasmussen, R. M., & Hall, W. D. (2008). Explicit forecasts of winter precipitation using an improved bulk microphysics scheme. Part II: Implementation of a new snow parameterization. Monthly Weather Review, 136(12), 5095-5115.

Thompson, G., Rasmussen, R. M., & Manning, K. (2004). Explicit forecasts of winter precipitation using an improved bulk microphysics scheme. Part I: Description and sensitivity analysis. Monthly Weather Review, 132(2), 519-542.

Tiedtke, M., (1989): A comprehensive mass flux scheme for cumulus parameterization in large-scale models. *Mon. Wea. Rev.*, **117**, 1779–1800.

Torn, R.D. & Davis, D.A. (2012): The Influence of Shallow Convection on Tropical Cyclone Track Forecasts. *Mon. Wea. Rev.*, **140**, 2188–2197.

Vecchi, G. A., & Soden, B. J. (2007). Effect of remote sea surface temperature change on tropical cyclone potential intensity. Nature, 450(7172), 1066-1070.

Walsh, K. (2004). Tropical cyclones and climate change: unresolved issues. *Climate Research*, *27*(1), 77-83.

Walsh, K. (2015). Fine resolution simulations of the effect of climate change on tropical cyclones in the South Pacific. Climate Dynamics, 45(9-10), 2619-2631.

Walsh, K. J., & Katzfey, J. J. (2000). The impact of climate change on the poleward movement of tropical cyclone-like vortices in a regional climate model. Journal of Climate, 13(6), 1116-1132.

Walsh, K. J., & Ryan, B. F. (2000). Tropical cyclone intensity increase near Australia as a result of climate change. Journal of Climate, 13(16), 3029-3036

Walsh, K. J., McBride, J. L., Klotzbach, P. J., Balachandran, S., Camargo, S. J., Holland, G., ... & Sugi, M. (2016). Tropical cyclones and climate change. Wiley Interdisciplinary Reviews: Climate Change, 7(1), 65-89.

Walsh, K. J., McInnes, K. L., & McBride, J. L. (2012). Climate change impacts on tropical cyclones and extreme sea levels in the South Pacific—A regional assessment. Global and Planetary Change, 80, 149-164.

Wang, W., & Seaman, N. L. (1997). A comparison study of convective parameterization schemes in a mesoscale model. Monthly Weather Review, 125(2), 252-278.

Wang, Y. (2002). An Explicit Simulation of Tropical Cyclones with a Triply Nested Movable Mesh Primitive Equation Model: TCM3. Part II: Model Refinements and Sensitivity to Cloud Microphysics Parameterization*. Monthly weather review, 130(12), 3022-3036.

Weisberg, R. H., & Zheng, L. (2006). Hurricane storm surge simulations for Tampa Bay. Estuaries and Coasts, 29(6), 899-913.

Yang, M. J., & Ching, L. (2005). A modeling study of Typhoon Toraji (2001): Physical parameterization sensitivity and topographic effect. *Terr. Atmos. Oceanic Sci*, *16*, 177-213.

Zhang, C., Wang, Y., & Hamilton, K. (2011). Improved Representation of Boundary Layer Clouds over the Southeast Pacific in ARW-WRF Using a Modified Tiedtke Cumulus Parameterization Scheme. Monthly Weather Review, 139(11), 3489-3513.

Zhu, T., & Zhang, D. L. (2006). Numerical simulation of Hurricane Bonnie (1998). Part II: Sensitivity to varying cloud microphysical processes. *Journal of the atmospheric sciences*, *63*(1), 109-126.

Tables

Table 1

Cumulus Parameterisation	Microphysics Scheme	Planetary Boundary Layer	Surface Flux	Sea Surface
None (CU0)	None (CU0)	None (CU0)	None	Fixed
Kain Fritsch (CU1 Kain and Fritsch 1990; Kain 1993; Kain 2004)	Kessler (MP1) (Kessler 1969)	YSU (PBL1) (Hong et al. 2006)	Surface flux coefficient (ISFTCFLX)	SST Updating with ERA-I
Betts Miller Janjic (CU2) (Janjic 1994)	WSM 5-class (MP4) (Hong et al. 2004)	MYNN 2.5 level TKE closure (PBL5) (Janic 2002; Nakanishi and Niino 2009)		1D Ocean Mixed Layer (OML) with ERA-I
Grell Devenyi Ensemble (CU3) (Grell and Devenyi 2002)	Ferrier new eta (MP5) (Ferrier 1994; Ferrier et al. 2002)			SST Updating with ERA-I Lag Fix
Grell 3D Ensemble (CU5) (Grell 1993; Grell and Devenyi 2002)	WSM 6-class graupel (MP6) (Hong and Lim 2006)			SST Updating with REMSS
Tiedtke (CU6) (Tiedtke 1989; Zhang et al. 2011)	Thompson (MP8) (Thompson et al. 2004, 2008).			

Table 1: The schemes that were tested in the physics parameterization ensemble. CU schemes are listed in column 1, MP in column 2, PBL in column 3, the surface flux in column 4. The details and differences of the SST sensitivity simulations are given in the last column.

Table 2

Run	Run Name	Landfall Pressure deviation from 929 (hPa)	Translation Speed Deviation from 32.93 (km/h)	Landfall Distance deviation from 146.11°E, 17.87°S (km)	Error Index
1	ERA CU0MP0PBL0	77	11.0	93	1.20
2	ERABOM CU0MP0PBL0	59	4.9	87	0.88
3	ERABOM CU2MP4PBL1	28	2.6	98	0.55
4	ERABOM CU0MP5PBL1	27	4.8	110	0.60
5	ERA CU1MP5PBL1	29	19.9	87	1.12
6	ERABOM CU1MP5PBL1	17	0.8	188	0.77
7	ERABOM CU3MP5PBL1	40	-0.3	74	0.59
8	ERABOM CU5MP5PBL1	34	0.6	122	0.65
9	ERABOM CU6MP5PBL1	24	2.2	33	0.36
10	ERABOM CU6MP5PBL1vert33	29	1.2	21	0.39
11	ERABOM CU6MP5PBL1vert55	30	8.3	9	0.57
12	ERABOM CU6MP5PBL1vert56	28	2.0	33	0.40
13	ERABOM CU6MP4PBL1	25	4.0	9	0.38
14	ERABOM CU6MP8PBL1	34	2.7	33	0.47
15	ERABOM CU6MP6PBL1	26	2.9	25	0.38
16	ERABOM CU6MP6PBL1isflx	29	3.7	17	0.42
17	ERABOM CU6MP6PBL1isflxOML	26	3.2	17	0.38
18	ERABOM CU6MP6PBL5isflxOML	35	3.6	58	0.54
19	ERABOM CU6MP5PBL5isflxOML	37	0.8	36	0.50
20	ERABOM CU6MP5PBL1isflxOML	35	2.9	84	0.58
21	ERABOM CU6MP5PBL1isflx	30	2.6	39	0.44
22	ERABOM CU1MP5PBL1isflxOML	21	1.3	168	0.71
23	ERABOM CU1MP6PBL1isflxOML	22	1.5	200	0.83
24	ERABOM CU1MP6PBL1isflx	21	1.4	216	0.89
25	ERABOM CU1MP6PBL1	20	1.1	216	0.88
26	ERABOM CU1MP6PBL5isflxOML	26	1.9	135	0.63
27	ERABOM CU2MP1PBL1isflxOML	38	5.2	256	1.15
28	ERABOM CU6MP5PBL1	27	3.8	25	0.41
29	ERABOM CU6MP5PBL1sstupdate	28	1.6	68	0.45
30	ERABOM CU6MP5PBL1OML	26	2.2	67	0.44
31	ERABOM CU6MP5PBL1LAGFIX	28	2.0	33	0.40
32	ERABOM CU6MP5PBL1REMSS	22	1.7	25	0.31
33	ERABOM CU1MP5PBL1	17	0.4	194	0.79
34	ERABOM CU1MP5PBL1sstupdate	17	0.7	172	0.71
35	ERABOM CU1MP5PBL1OML	18	0.8	183	0.75
36	ERABOM CU1MP5PBL1LAGFIX	17	0.9	188	0.77
37	ERABOM CU1MP5PBL1REMSS	16	1.0	172	0.71

Table 2: Details of the initialization, physics parameterization, and SST boundary condition set up of each ensemble run (column 1). The resulting deviation of the

simulated landfall pressure (hPa, rounded to the nearest whole number); translation speed (km/h, rounded to one decimal place); landfall location (km, rounded to nearest whole number) compared to observations; and the error index from the root mean square error calculation (rounded to two decimal places) are provided in columns 2-5.

List of figures

Figure 6: The SST data on February 2nd, 2011 12h UTC when Yasi is nearing landfall provided by (a) the ERA-Interim 6 hourly surface data, (b) the ERA-Interim 6 hourly surface data when the 30-hour lag is corrected for, (c) the OSTIA SST that the ERA-I reanalysis data uses and (d) the 1°x1° resolution REMSS MW OI SST daily data set. Yasi's simulated trajectory using each of these SST scenarios and the Tiedtke CU is overlain on each plot with a black line. (e) shows the average SST over a 2°x2° box centered on 155°E and 15°S over time for the data from ERA-I reanalysis, OSTIA data, and from ERA-I with 30-hour lag fixed. The line plot shows the 30-hour lag in SSTs between ERA-I and OSTIA data and that when ERA-I values are corrected by 30 hours they match the OSTIA observations.

Figure 7: Simulated TC trajectories from each member in the physics sensitivity ensemble, color-coded by the CU parameterization scheme utilized. Observed trajectory is depicted by white circle marker and the landfall location by the large "X". The clustering of like colors and thus the effect of the cumulus schemes on the trajectory is apparent.

Figure 8: the simulated temperature and wind speeds at the 700mb level averaged over the 96 hours of the simulation with the TC trajectory overlain for (a) the Kain Fritsch scheme and (b) the Tiedtke scheme (corresponding to Table 2, Runs 6 and 9 respectively). (c) The difference in the average temperature and wind fields at 700mb between the two schemes calculated by Kain Fritsch – Tiedtke.

Figure 9: The simulated minimum SLP (red) and the average radius (from the four quadrants of the TC of 64knot winds (green) simulated at each time step through the simulation with using CU1MP5PBL1 (solid lines, corresponding to Table 2, Run 6)

compared to CU6MP5PBL1 (dashed lines, corresponding to Table 2, Run 9) parameterizations. The observed timing and SLP at landfall is marked with red X. The Kain Fritsch scheme (CU1, solid line) results in a much lower SLP (greater intensity) and greater radius of 64knot winds (larger TC) than with the Tiedtke scheme (CU6).

Figure 10: Scatterplot of physics sensitivity ensemble members based on their landfall distance anomaly and landfall pressure anomaly compared to observed (marked by the black X at 0, 0). The ensemble runs are represented by color according to the CU parameterization and symbol shape represents the MP scheme utilized in the simulation. The clustering of like colors and thus cumulus schemes is apparent. Details of each ensemble member set up, landfall distance, timing, and pressure anomaly and the corresponding calculated skill score are given in Table 2.

Figure 11: The sensitivity of the simulations to different representations of the sea surface 1) ERA-I SSTs do not vary temporally 2) updating the SSTs from ERA-I every day, 3) allowing the TC to cool the ocean surface with a 1-D ocean mixed layer model, 4) updating the SSTs from ERA-I but fixing the 30hr lag in ERA-I, and 5) using SSTs from REMSS which have a higher spatial resolution than the SSTs from ERA-I. Sensitivity of the trajectories when employing the Kain Fritsch (a) and Tiedtke (b) schemes. The SST temperature under the eye of the storm at every time step through the simulation for the Kain Fritsch (c) and Tiedtke (d) members. The minimum sea level pressure recorded at every time step through the simulations with Kain Fritsch (e) and Tiedtke (f). The red X denotes the observed SLP at landfall of Yasi. Figures a, c, e correspond with Table 2 Runs 33-37 and figures b, d, f show Table 2 Runs 28-32.

Figure 12: The calculated difference in the simulated relative vorticity fields at the 500hPa level at time step 50 with REMSS SST – the ERA-I SST when using (a) Kain Fritsch cumulus scheme and (b) Modified Tiedtke scheme. Using the REMSS SST increases relative vorticity with both physics parameterizations, indicating vortex stretching and increased intensity. For the Kain Fritsch scheme (a), the change is confined around the eye, while there is a greater change within the eye and over the whole cross section of the system in response to the altered SSTs with the Tiedtke scheme (b). The simulations depicted correspond with Table 2, Runs 29, 32, 34, 37.

Captioned Figures

Fig.1

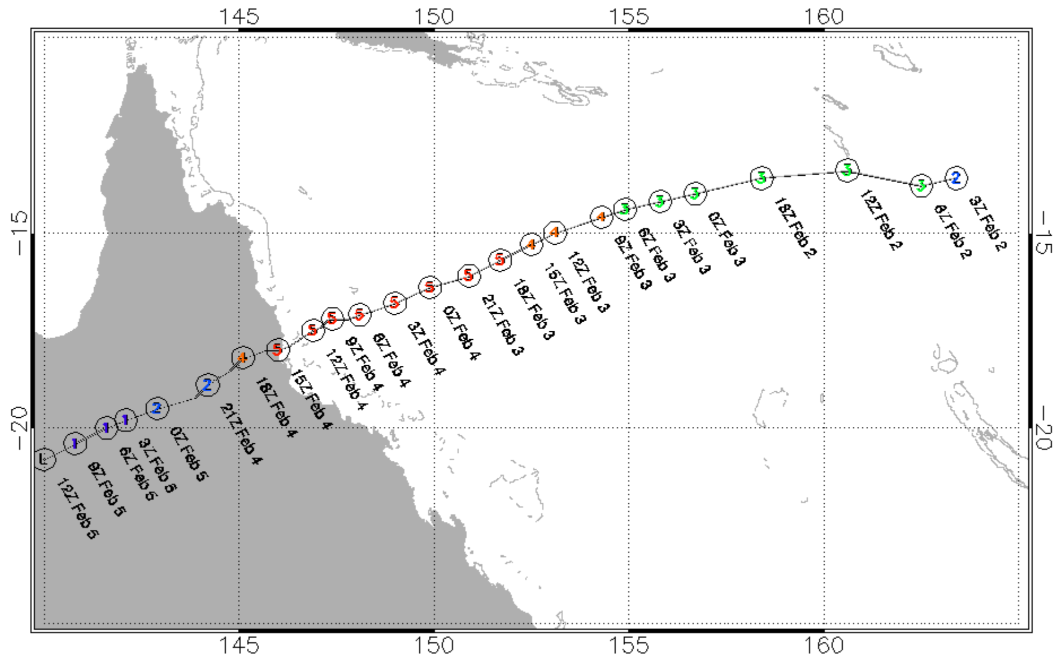

Figure 1: The trajectory and category evolution of TC Cyclone Yasi plotted from observations provided by the Australian Bureau of Meteorology (BOM), 2011 from 03Z February 2nd to 12Z February 5th UTC. Yasi intensifies to a category 5 system in the Coral Sea and remains at this category up to the time of landfall.

Fig.2

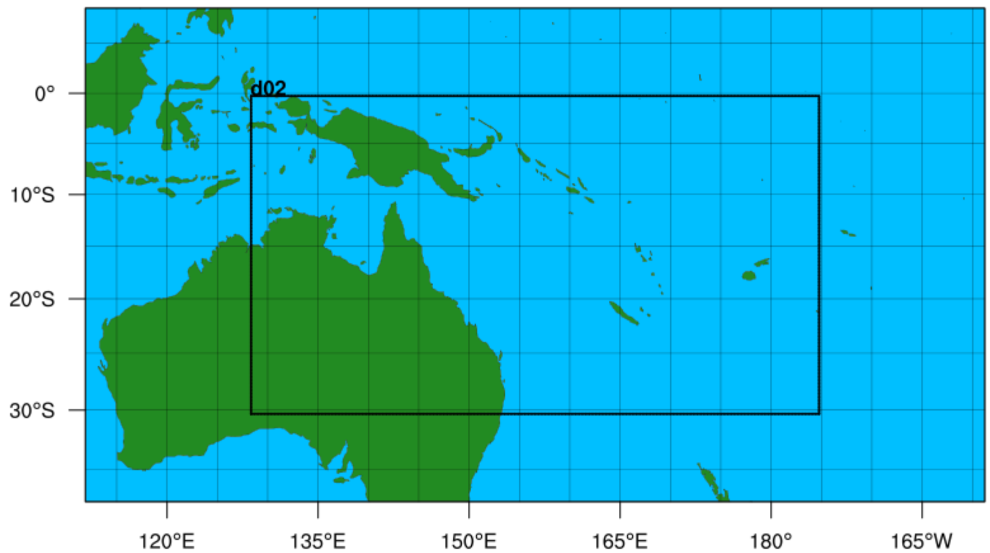

Figure 2: The 2-domain nested WRF-ARW v3.4.1 set up: d01 has 36km horizontal grid spacing and d02 has 12km resolution.

Fig. 3

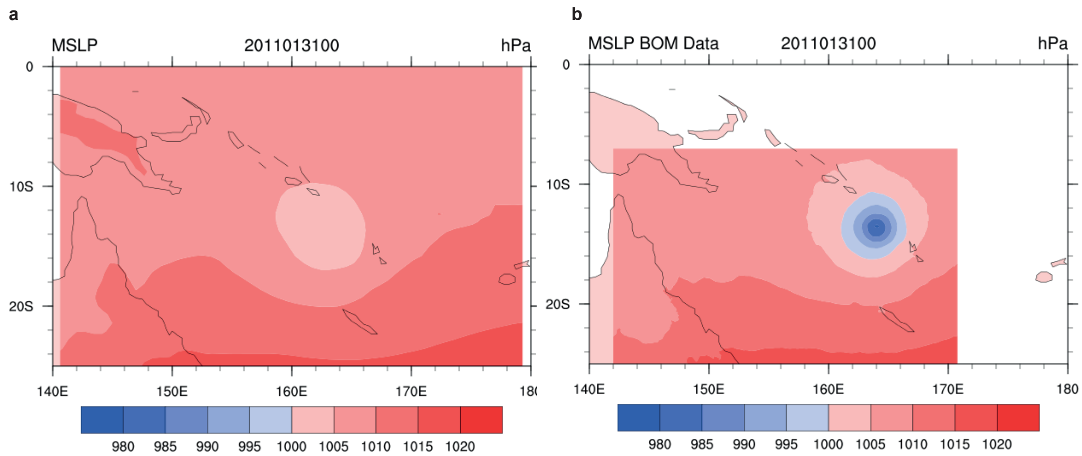

Figure 3: The sea level pressure (SLP) data in the initial condition data set of (a) ERA-Interim reanalysis and (b) the BOM 4km ACCESS-TC analysis file at January 31 2011 00UTC. The high resolution BOM data (b) manages to capture the structure and SLP change associated with TC Yasi that is largely missing from the ERA-I file (a).

Fig. 4

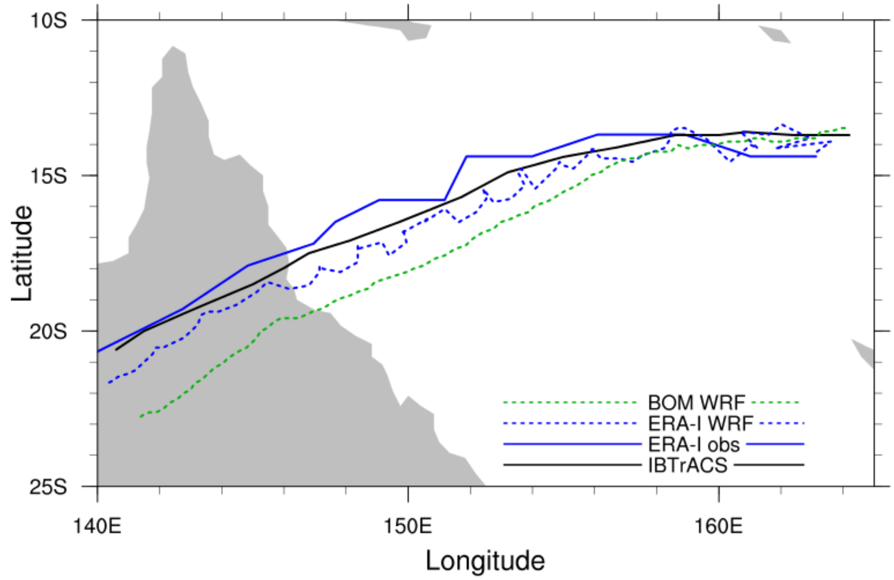

Figure 4: A comparison of the trajectories from observed data (IBTrACS solid black line), from the ERA-I reanalysis data (solid blue line) to the WRF simulated trajectories when using the ERAI data for lateral and boundary conditions (dashed blue line) or ERAI with ACCESS (BOM) initial conditions with CU1MP5PBL1 physics prescribed (corresponding to Table 2 Runs 5 and 6).

Fig. 5

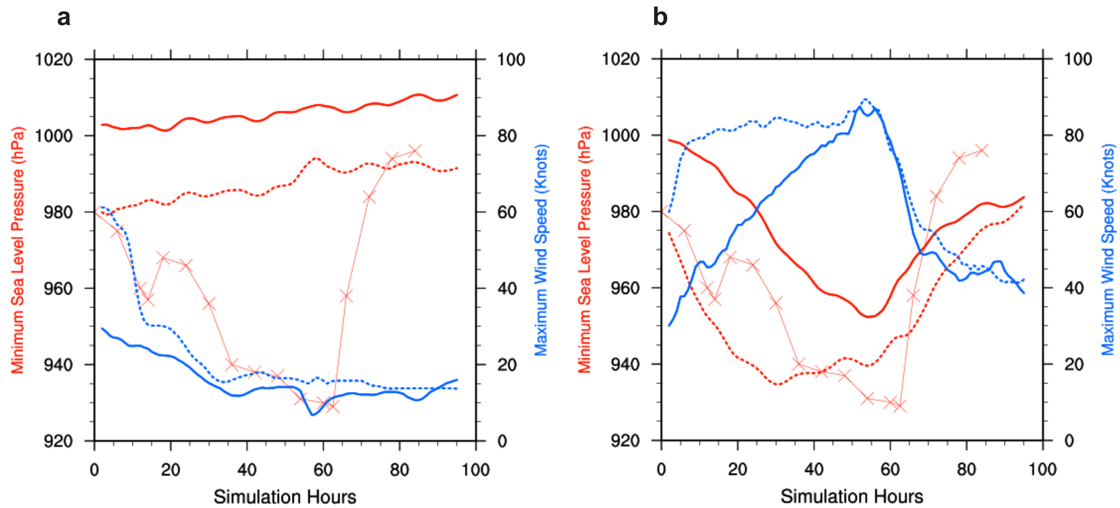

Figure 5: The minimum sea level pressure (SLP, red) and maximum recorded wind speeds (blue) at each time step through the simulations with just ERA-I initialization (solid lines) compared with initializing with ERA-I and the BOM data (dashed lines). The observed SLP evolution is depicted in red with 'x' markers. Initializing with the BOM data reduces the SLP and increases the simulated wind speeds when no physics parameterizations are employed (a, corresponding to Table 2, Runs 1 and 2), and when CU1 MP5 PBL1 physics are employed (b, corresponding to Table 2, Runs 5 and 6).

Fig. 6

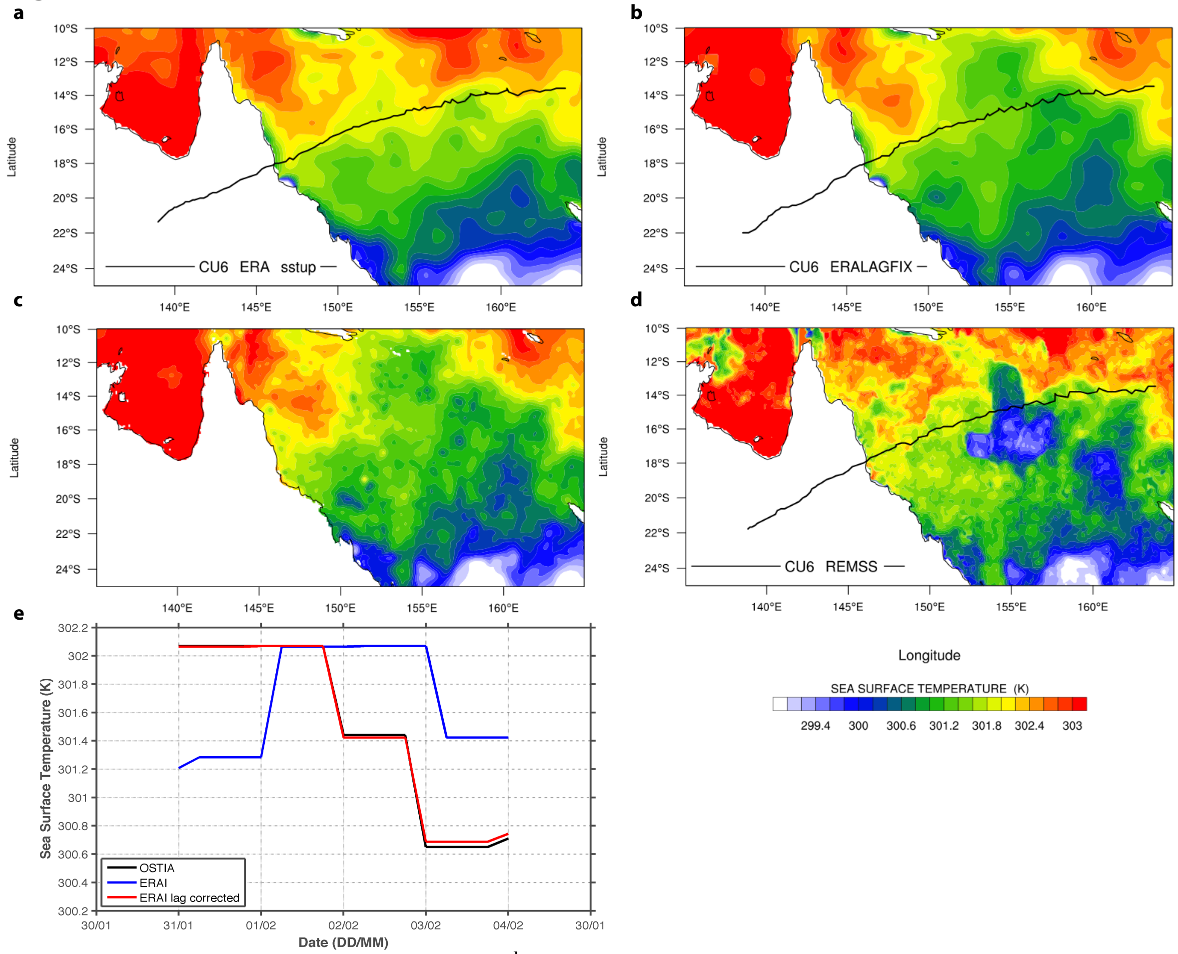

Figure 6: The SST data on February 2nd, 2011 12h UTC when Yasi is nearing landfall provided by (a) the ERA-Interim 6 hourly surface data, (b) the ERA-Interim 6 hourly surface data when the 30-hour lag is corrected for, (c) the OSTIA SST that the ERA-I reanalysis data uses and (d) the 1°x1° resolution REMSS MW OI SST daily data set. Yasi's simulated trajectory using each of these SST scenarios and the Tiedtke CU is overlain on each plot with a black line. (e) shows the average SST over a 2°x2° box centered on 155°E and 15°S over time for the data from ERA-I reanalysis, OSTIA data, and from ERA-I with 30-hour lag fixed. The line plot shows the 30-hour lag in SSTs between ERA-I and OSTIA data and that when ERA-I values are corrected by 30 hours they match the OSTIA observations.

Fig. 7

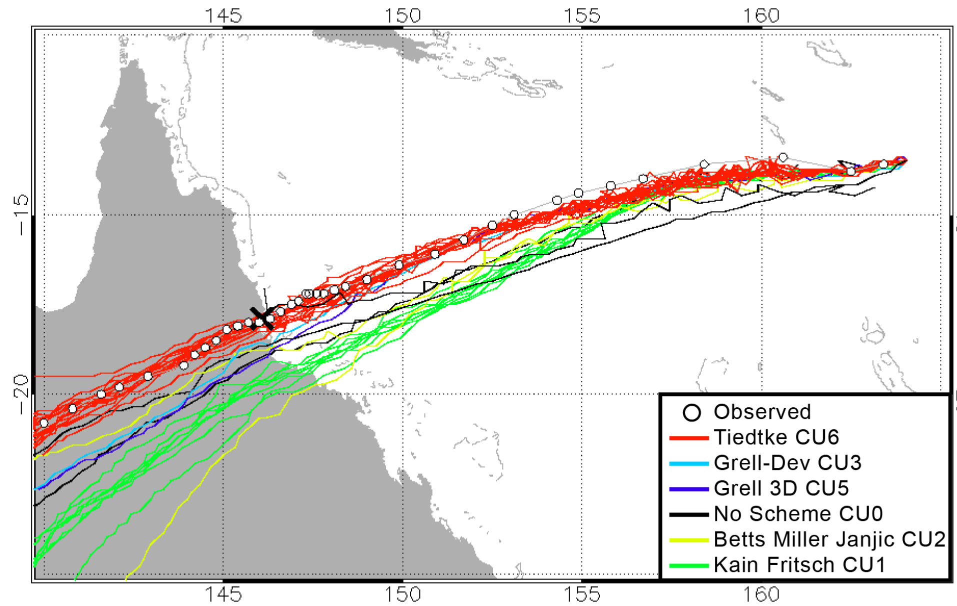

Figure 7: Simulated TC trajectories from each member in the physics sensitivity ensemble, color-coded by the CU parameterization scheme utilized. Observed trajectory is depicted by white circle marker and the landfall location by the large "X". The clustering of like colors and thus the effect of the cumulus schemes on the trajectory is apparent.

Fig 8.

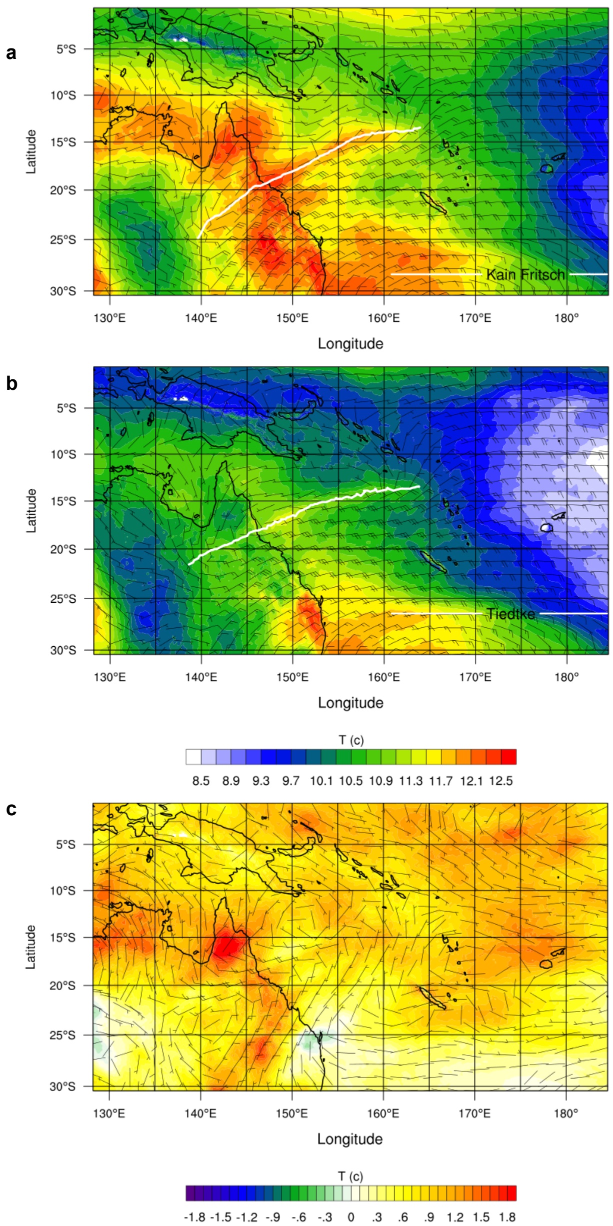

Figure 8: the simulated temperature and wind speeds at the 700mb level averaged over the 96 hours of the simulation with the TC trajectory overlain for (a) the Kain Fritsch scheme and (b) the Tiedtke scheme (corresponding to Table 2, Runs 6 and 9 respectively). (c) The difference in the average temperature and wind fields at 700mb between the two schemes calculated by Kain Fritsch – Tiedtke.

Fig. 9

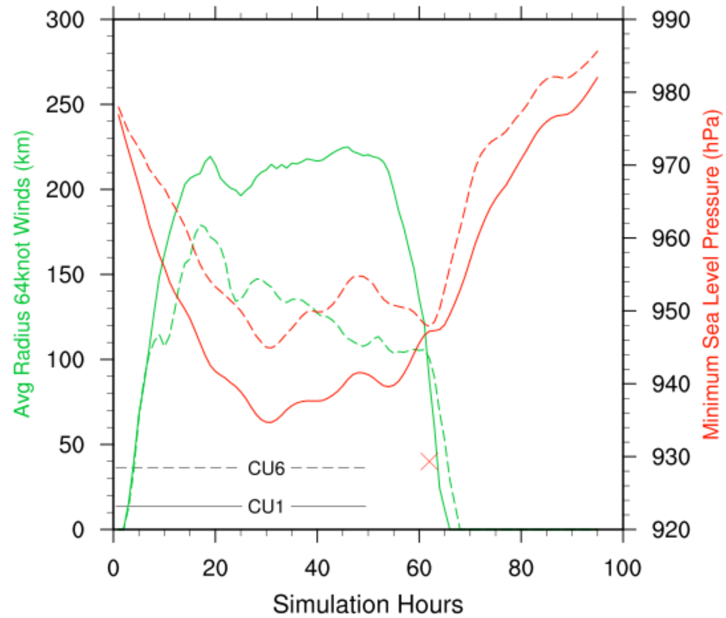

Figure 9: The simulated minimum SLP (red) and the average radius (from the four quadrants of the TC of 64knot winds (green) simulated at each time step through the simulation with using CU1MP5PBL1 (solid lines, corresponding to Table 2, Run 6) compared to CU6MP5PBL1 (dashed lines, corresponding to Table 2, Run 9) parameterizations. The observed timing and SLP at landfall is marked with red X. The Kain Fritsch scheme (CU1, solid line) results in a much lower SLP (greater intensity) and greater radius of 64knot winds (larger TC) than with the Tiedtke scheme (CU6).

Fig. 10

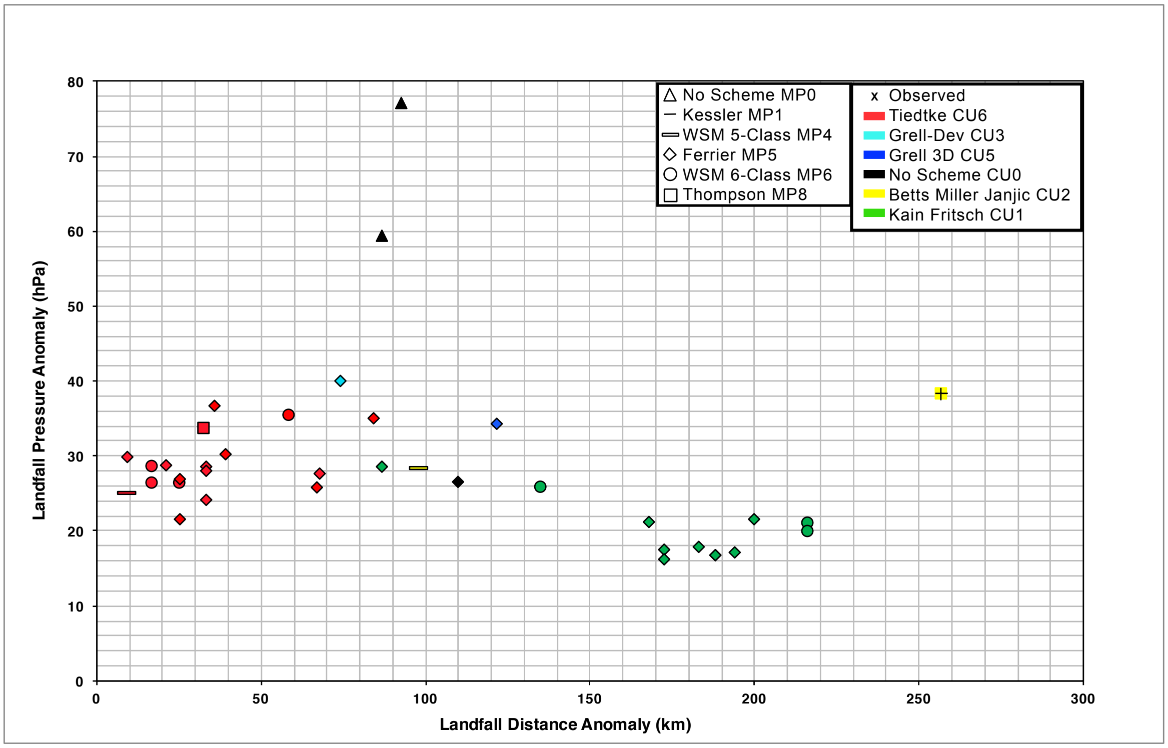

Figure 10: Scatterplot of physics sensitivity ensemble members based on their landfall distance anomaly and landfall pressure anomaly compared to observed (marked by the black X at 0, 0). The ensemble runs are represented by color according to the CU parameterization and symbol shape represents the MP scheme utilized in the simulation. The clustering of like colors and thus cumulus schemes is apparent. Details of each ensemble member set up, landfall distance, timing, and pressure anomaly and the corresponding calculated skill score are given in Table 2.

Fig 11.

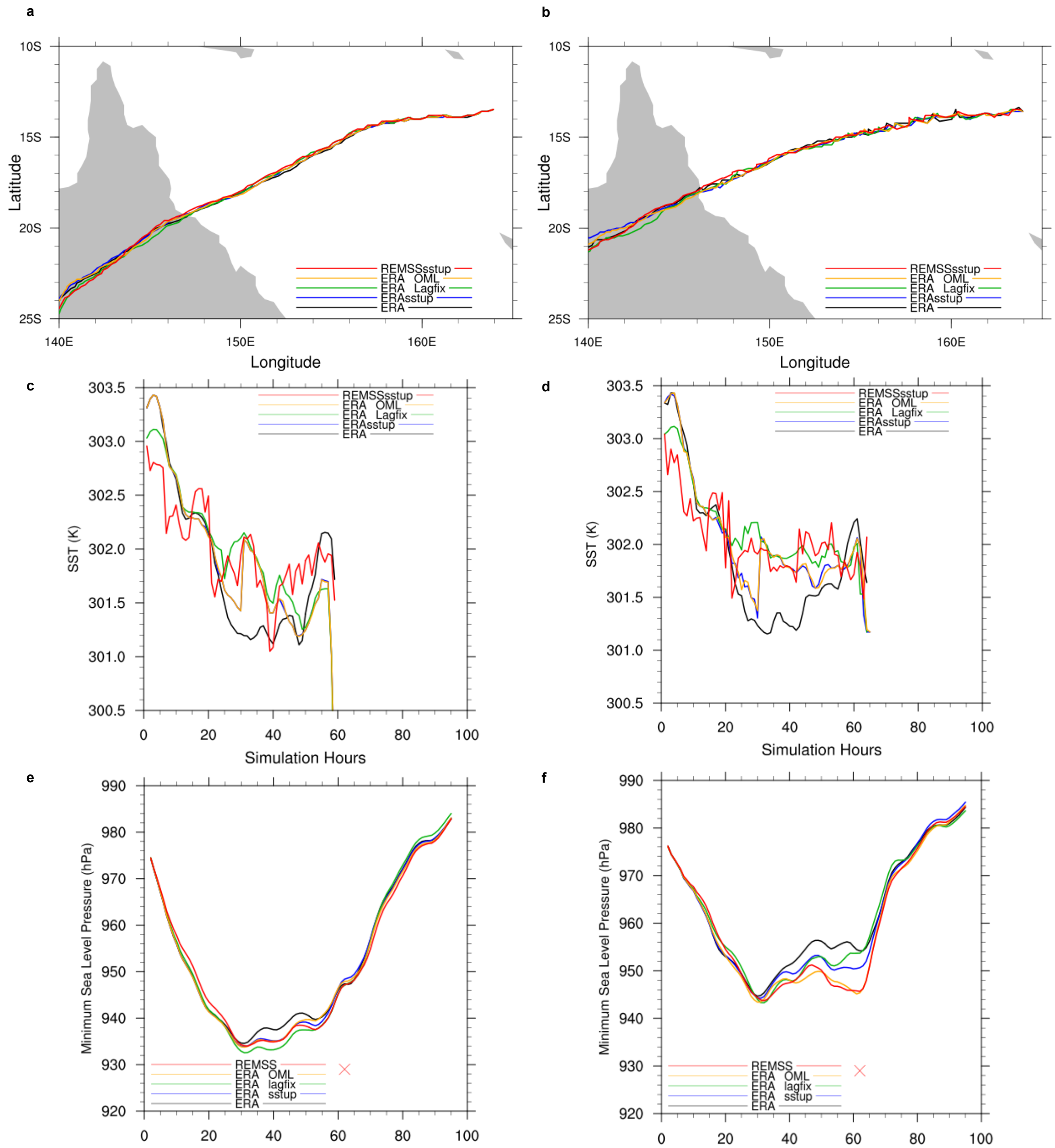

Figure 11: The sensitivity of the simulations to different representations of the sea surface 1) ERA-I SSTs do not vary temporally 2) updating the SSTs from ERA-I every day, 3) allowing the TC to cool the ocean surface with a 1-D ocean mixed layer model, 4) updating the SSTs from ERA-I but fixing the 30hr lag in ERA-I, and 5) using SSTs from REMSS which have a higher spatial resolution than the SSTs from ERA-I. Sensitivity of the trajectories when employing the Kain Fritsch (a) and Tiedtke (b) schemes. The SST

temperature under the eye of the storm at every time step through the simulation for the Kain Fritsch (c) and Tiedtke (d) members. The minimum sea level pressure recorded at every time step through the simulations with Kain Fritsch (e) and Tiedtke (f). The red X denotes the observed SLP at landfall of Yasi. Figures a, c, e correspond with Table 2 Runs 33-37 and figures b, d, f show Table 2 Runs 28-32.

Fig. 12

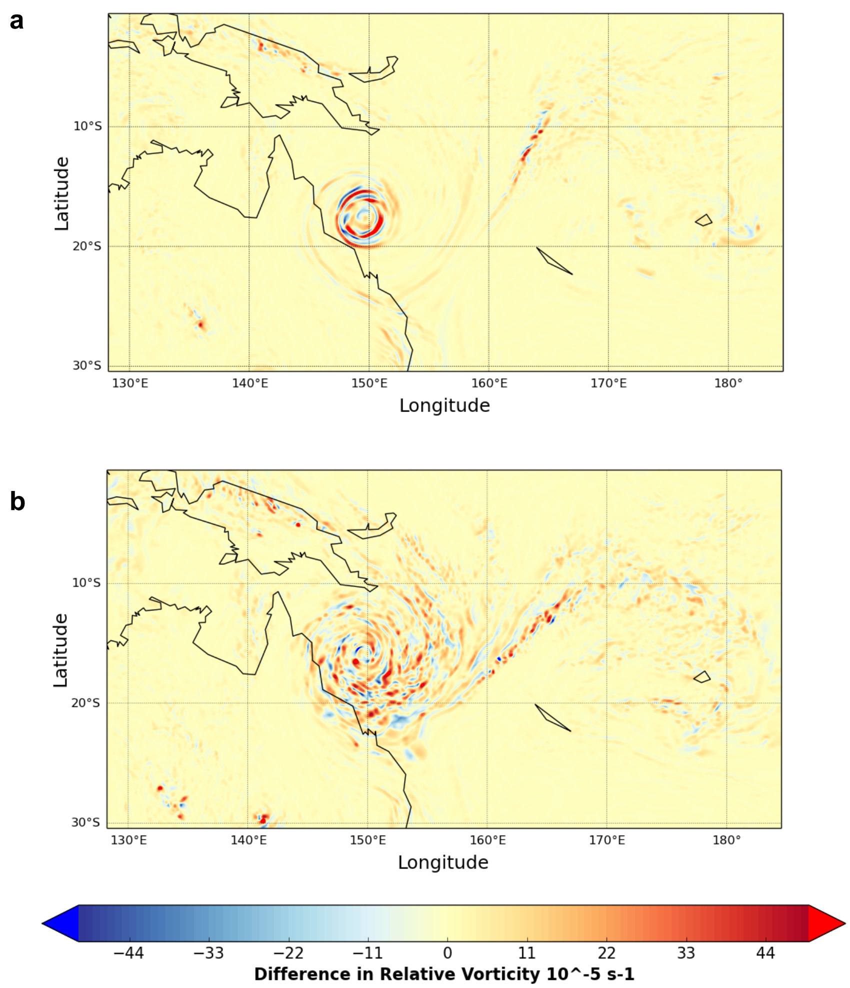

Figure 12: The calculated difference in the simulated relative vorticity fields at the 500hPa level at time step 50 with REMSS SST – the ERA-I SST when using (a) Kain Fritsch cumulus scheme and (b) Modified Tiedtke scheme. Using the REMSS SST increases relative voriticity with both physics parameterizations, indicating vortex stretching and increased intensity. For the Kain Fritsch scheme (a), the change is confined around the eye, while there is a greater change within the eye and over the whole cross section of the system in response to the altered SSTs with the Tiedtke scheme (b). The simulations depicted correspond with Table 2, Runs 29, 32, 34, 37.

CHAPTER THREE

THE RESPONSE OF LAND-FALLING TROPICAL CYCLONE CHARACTERISTICS TO PROJECTED CLIMATE CHANGE IN NORTHEAST AUSTRALIA

CHELSEA L. PARKER[1,2*], CINDY L. BRUYÈRE[3,4], AND PRISCILLA A. MOONEY[3]

[1]*Department of Earth, Environmental, and Planetary Sciences, Brown University, Providence RI 02912*

[2]*Institute at Brown for Environment and Society, Providence RI 02912*

[3]*National Center for Atmospheric Research, Boulder CO 80301*

[4]*Environmental Sciences and Management, North-West University, South Africa*

Submitted in its current form to:
Climate Dynamics

Abstract

Land-falling tropical cyclones along the Queensland coastline can result in serious and widespread damage. However, the effects of climate change on cyclone characteristics such as intensity, trajectory, rainfall, and especially translation speed and size are not well-understood. This study explores the relative change in the characteristics of three case study intense tropical cyclones using the Weather Research and Forecasting Model and the future climate downscaled from the Community Earth System Model through a pseudo global warming technique. Results demonstrate a consistent response of increasing intensity through reduced central pressure (up to 10hPa) and increased wind speeds (5-10% on average). The responses of other characteristics were variable and governed by either the original intensity and size of the cyclone or the change in the steering flow. The smallest and weakest case could undergo the greatest change in response to the climate perturbation, with the largest proportional increase in intensity and rainfall, and a 40% size increase. The predicted change in the 500mb winds with climate change varied monthly. The predominant flow steered the April case equatorward and increased the translation speed, but shifted the January and February cases poleward with little change to the translation speed. The predicted changes have serious implications for damage to coastal settlements, infrastructure, and ecosystems through high wind speeds, storm surge, rainfall, and potentially increased size of some systems. The results highlight the importance of case study based approaches and the need for a greater number of cases to be examined.

1. Introduction

Tropical cyclone (TC) activity in the Queensland area of Australia often results in serious and widespread damage (AON Benfield 2011). Settlements, livelihoods, and ecosystems supporting high biodiversity in Queensland are vulnerable to TC activity (Anderson-Berry 2003). TC events in the area are associated with damage to buildings and key infrastructure (Stewart 2003; Ginger et al. 2007); forested areas (Laurence and Curran 2008; Turton 2008); agriculture (AON Benfield 2011); and the Great Barrier Reef ecosystem (Puotinen 2007; Fabricius et al. 2008; De'ath et al. 2012). Much of this damage is associated with specific TC characteristics, such as the maximum sustained wind speed which inflicts significant damage to buildings and infrastructure (Stewart 2003; Ginger et al. 2007), and causes coral breakage and dislodgement in the reef community (Done 1992; Puotinen 2007; Fabricius et al. 2008). Other important characteristics include the TC size, associated rainfall, and TC trajectory. The TC size determines the area encompassed by the TC's circulation and thus the total destructive capacity (Merrill 1984; Powel and Reinhold 2007; Knaff 2014). TC-associated rainfall and storm surge are often the most damaging aspects of TCs (Walsh 2004) and can determine catchment flooding damage (McInnes et al. 2002) and pollutant runoff to coastal ecosystems (Preen et al. 1995; Davies and Eyre 2005; Devlin and Brodie 2005; Mitchell et al. 2005; Parker et al. 2017a). The importance of the TC trajectory cannot be understated, as it dictates the areas that will experience TC conditions. Significant damage will result if the TC strikes densely populate areas along the coast.

To understand the relationship between TCs and climate change, it is important to first understand the historical data. However, quantifying and analyzing historical trends in TC intensity and frequency has been confounded by the availability, quality, and temporal range of historical data (Landsea et al. 2010; Kuleshov et al. 2010; Walsh et al. 2012). This analysis has been particularly problematic in the South Pacific (Walsh et al. 2012; Walsh et al. 2016) where there have been fewer studies and opposing trends have been found (e.g. Kuleshov et al. 2010; Holland and Bruyère 2013). The identification of trends related to the mean climate state is specifically complicated by the strong variability of TC activity with the El Niño Southern Oscillation (ENSO) regime. However, it has been suggested that during the last two decades, the northeast coastal regions of Australia have experienced significantly increased total rainfall, more frequent heavy rainfall, and more intense TC events (Alexander et al. 2007). Since 2003, a number of named TCs have affected the Great Barrier Reef area (Beeden et al. 2015); including Ingrid (2005); Monica (2006); Larry (2006); Hamish (2009); Ului (2010); Yasi (2011); Ita (2014); and Marcia (2015). This contrasts with the previous decades (1970-2003), when there were no TCs greater than Category 1 (Saffir-Simpson scale) recorded in the Great Barrier Reef / Coral Sea area (Puotinen et al. 1997; Puotinen 2007). This recent TC activity compared to historical records has led to speculation that changes to TC frequency and intensity are already occurring in this area (Beeden et al. 2015). This perceived trend is supported by findings suggesting that the prevalence of Category 4 and 5 hurricanes has already increased by ~25-30% per °C of global warming since 1975, balanced by a decrease in category 1 and 2 (Holland and Bruyère 2013).

Regional and global scale atmospheric numerical models have been used to explore the future of TC activity in a changing climate. While there is a range of predictions given different models and warming scenarios, the majority of studies suggest there will be a decrease in total TCs globally but a further intensification of TCs with climate change (Bengtsson et al. 2007; Sugi et al. 2009; Bell et al. 2013; Emanuel 2013). Global studies predict a shift in the distribution of TCs toward increased incidence of category 4 and 5 TCs and a decrease in weaker systems (Bender et al. 2010; Knutson et al. 2010; Done et al. 2012; Holland and Bruyère 2013).

The majority of regional studies have primarily focused on Atlantic TCs (Walsh et al. 2012) and predict that while total numbers may decrease, intense systems are likely to increase in power dissipation and destructive potential (e.g. Emanuel 2005; Emanuel 2006; Yamada et al. 2010) and may double in frequency with each 1°C of climate warming (e.g. Bender et al. 2010; Done et al. 2012). However, studies have shown that there can be substantial variations in the response of TCs to climate change across ocean basins (e.g. Oouchi et al. 2006; Walsh et al. 2016). In the Southern Hemisphere and Australia, the sparse results have limited the confidence in the predicted relationships between both historical and future TC activity considering climate change (Walsh et al. 2012).

The few studies that have focused on the Southern Hemisphere and Australia regions also found that the overall frequency of TCs and frequency of weaker storms may decrease (Emanuel et al. 2008; Lavender and Walsh 2011; Walsh et al. 2012; Walsh 2015), perhaps more acutely than the global average (Sugi and Yoshimura 2012; Walsh et al. 2016). However, an increase in the power dissipation and intensity of Southern

Hemisphere TCs is likely (Emanuel et al. 2008), along with increasing intensity and an increase in the percentage of most severe TCs specifically in the Australia region (Walsh and Ryan 2000; Walsh et al. 2004; Leslie et al. 2007; Lavender and Walsh 2011; Abbs 2012). The previous studies that examined the response of TCs to climate change in northeastern Australia have examined the statistics of the overall change to TC frequency (Lavender and Walsh 2011), inter-annual variability of TC frequency (Walsh 2015), genesis location (Walsh and Katzfey 2000; Nguyen and Walsh 2001), trajectory (Lavender and Walsh 2011), and intensity (Walsh and Ryan 2000).

Unlike previous studies of Australia, this work explores the response of TC characteristics to climate change forcing in northeastern Australia using a Pseudo Global Warming (PGW) technique. The PGW technique (Schär et al. 1996; Hara et al. 2008; Kawase et al. 2009; Ramussen et al. 2011; and Yoshikane et al. 2012) calculates the differences in environmental variables between current and future climates. The calculated changes (climate change delta) are then added to the boundary and initial condition of simulations of the current climate to represent a possible future climate scenario.

Previous studies have used the PGW approach to examine the response of idealized (Hill and Lackmann 2011) and real world TCs from the North Atlantic region to climate change, including Hurricane Katrina (August 2005) (Lynn et al. 2009) and Hurricane Sandy (October 2012) (Lackmann 2015). These studies demonstrate that the response of some TC characteristics to climate change were consistent, while others were not. For example, all studies demonstrated significant cyclone intensification (decreased sea level pressures (SLPs) up to 14hPa) with climate perturbation. However, precipitation associated with the idealized TCs and Hurricane Sandy increased with climate change by up to 30% (Hill and Lackmann 2011; Lackmann 2015), while no significant change was found in Hurricane Katrina's precipitation (Lynn et al. 2009). For the idealized storms and Hurricane Sandy, lower tropospheric potential vorticity increased with climate change (Hill and Lackmann 2011; Lackmann 2015). For Hurricane Katrina, maximum winds after landfall were prolonged (Lynn et al. 2009). However, Katrina's average wind speeds and radius of strong winds both decreased in the climate change scenario (Lynn et al. 2009). These previous studies found that the changes in TC trajectories were governed by the response of the steering flow to climate perturbation. For Sandy, the track consistently deviated further poleward and eastward compared to the current climate (Lackmann 2015). However, Katrina's trajectory response to climate change varied over time in the future, as future simulations were run for every decade from 2020 to 2090 (Lynn et al. 2009).

The details from these previous studies suggest that while there are several robust and uniform responses of TCs to climate change forcing (i.e. intensity increase), there are variations in the responses of other characteristics, depending on the TC case. Given the variability in response of cases to PGW in the Atlantic and the known heterogeneity in response of TCs to climate change in varying ocean basins, it is valuable to explore and reconcile how the characteristics of TCs in the western South Pacific will respond to the future climate. The case study events chosen caused notable damage to the Queensland area of Australia in the current climate. It is therefore pertinent to investigate how their characteristics may change if these types of synoptic weather patterns were to occur again in the future. Specifically, we investigate the response of damaging characteristics (i.e.

central pressure, maximum wind speed, trajectory, size, translation speed, and rainfall) to climate change perturbation. The characteristics of size and translation speed have not been explored in detail in the literature but can be important for predicting resultant damage to infrastructure (Czajkowski and Done 2014; Done et al. 2014) and reef ecosystems (Puotinen 2007).

2. Methods

2.1 Case Studies

To explore the response of TC characteristics to climate change forcing, we have chosen to carry out simulations with the three most recent intense TCs affecting the northeastern coastline of Australia: TC Yasi (2011); TC Ita (2014); and TC Marcia, (2015). TC Yasi (Figure 1a) was a category 5 system with a lowest-recorded central pressure of 929 hPa, maximum sustained wind speeds of 135 knots, and an associated 5m storm surge (Queensland Government 2012). Yasi made landfall near Mission Beach (see Figure 2 for locations of places affected) on February 3, 2011, damaging over 15% of the Great Barrier Reef through its lifecycle (Beeden et al. 2015). The economic impacts on tourism, coal exports, and agriculture were also substantial (Queensland Government 2012), with agricultural losses alone estimated at AUD$1 billion (AON Benfield 2011). Yasi is the costliest TC to have affected Australia (Reuters, 2015), and this was due to its anomalously large size, intense wind speeds, and heavy rainfall (particularly inland after landfall).

TC Ita (Figure 1b) was a category 5 system with a minimum central pressure of 930 hPa, with sustained wind speeds of up to 140 knots. Ita was an intense TC that developed unusually late in the TC season, and made landfall at Cape Flattery (Figure 2) on April 12 2014. It caused AUD$1.1 billion of economic loss, primarily through damage to sugar cane crop (AON Benfield, 2014). The area sustained structural and agricultural damage principally from the high wind speeds and heavy rainfall. A decline in coral cover (Ceccarelli et al. 2016) and seagrass in the Cairns-Cooktown region (Figure 2) (Authority, Great Barrier Reef Marine Park 2015) was recorded after the passage of TC Ita. High winds cause wave action that breakages and dislodges corals from the reef substrate (Massel and Done 1993; Puotinen 2007). The heavy rainfall over the catchment results in increased river discharge and runoff into the reef lagoon. The flood plumes carry high concentrations of nutrients and sediments which reduce water quality and negatively affect corals through inhibition of photosynthesis (Devlin and Schaffelke 2009); decrease in calcification rates (Devlin and Schaffelke 2009); increase in competition with phytoplankton and algal activity (Fraser and Currie 1996; Furnas et al. 2005; Brodie et al. 2010); and smothering, resulting in coral bleaching and mortality (Anthony and Fabricius 2000; Fabricius and Wolanski 2000).

TC Marcia (Figure 1c) was a relatively compact category 5 system which achieved a minimum central pressure of 932 hPa and maximum sustained wind speeds of 116 knots after a period of unprecedented, rapid intensification (Australian Government, Bureau of Meteorology 2015). The genesis region and trajectory of Marcia was further poleward than other cases. The system made landfall near Shoalwater Bay (Figure 2) on February 20, 2015 and negatively affected the southern coast of Queensland. Structural damage to housing was recorded at Yeppoon and Rockhampton (Figure 2) (Australian Government, Bureau of Meteorology 2015) and other inshore areas south of Mackay (Figure 2) (Authority, Great Barrier Reef Marine Park 2016) from wind gusts. A large storm surge resulted in significant beach erosion and structural damage, and the TC-associated rainfall lead to flooding in three river catchments (Australian Government, Bureau of Meteorology 2015). The estimated cost of Marcia was ~$750 million AUD (Carroll and Authority 2015).

2.2 WRF Model Set-up

The mesoscale numerical weather prediction model Weather Research and Forecasting (WRF-ARW) version 3.4.1 (Skamarock et al. 2008) was configured with fixed two-way nesting for two domains of 36- and 12-km grid spacing. A higher resolution of horizontal grid spacing may be necessary for modeling accurate central pressure and TC processes, particularly in the eyewall (e.g. Gentry and Lackmann 2010). However, it has been shown that 12km grid spacing is sufficient for reproducing the main TC structure (Done et al. 2013), lifecycle, and characteristics of interest to this study (Parker et al. 2017b). Therefore, we used the 12km spacing (as configured in Parker et al. [2017b]) to balance resolution requirements and computational efficiency, conducting many exploratory simulations in a regional climate set up (Jacob et al. 2014). The domain extents and locations vary by case study and are shown in Figure 3. The domains are determined based on the trajectory of the case and the area covered by the available initial condition data. All simulations have 36 vertical levels, with higher resolution in the planetary boundary layer to better resolve the TC. TC Yasi is initialized on January 31

2011 at 00:00h UTC and simulations last 96 hours. TC Ita is initialized on April 7 2014 at 12:00h UTC and simulations last 120 hours. TC Marcia is initialized on February 20 2015 at 12:00h UTC and simulations last 72 hours. The initialization times were selected to allow sufficient time for TC development but also to provide initial conditions that resulted in accurate simulations of trajectory and TC lifecycle in the current climate.

Boundary conditions were provided by the pressure level data products from the European Centre for Medium-Range Weather Forecasts (ECMWF) Re-Analysis Interim (hereafter ERA-I) data set (Dee et al. 2011). ERA-I data are available at 6-hour intervals, with 0.7° spatial resolution, and 37 atmospheric levels. While this resolution was sufficient for the boundary conditions, previous research (Parker et al. [2017b]) has shown that higher resolution initial conditions can substantially improve the representation of the TC, particular intensity, in simulations using a 12km grid spacing. Thus, we generated initial conditions from the Australian Community Climate and Earth System Simulator-Tropical Cyclone (ACCESS-TC) (Puri et al. 2010, 2013; Davidson et al. 2014), which has a finer horizontal grid spacing of 0.11° with 50 vertical levels. We converted the ACCESS-TC data file into WRF intermediate file format and blended it with the ERA-I data to create initial conditions for the entire domain. Boundary conditions are provided by ERA-I alone after the initialization time step. The sea surface temperatures (SSTs) provided by the boundary conditions are fixed for the duration of the simulations.

The following physical parameterizations were used for the WRF simulations: RRTMG shortwave and longwave radiation schemes (Iacono et al. 2008), MM5 Monin-Obukov surface layer scheme (Monin and Obukhov 1954), Unified Noah Land Surface

Model (Chen and Dudhia 2001; Ek et al. 2003; Tewari et al. 2004) for land surface processes and structure, the Yonsei University planetary boundary layer scheme (Hong et al. 2006), the Ferrier new Eta microphysics parameterization (Ferrier 1994; Ferrier et al. 2002), and the Kain Fritsch scheme for cumulus parameterization (Kain and Fritsch 1990; Kain 1993; Kain 2004). These parameterizations were chosen due to suitability for TC simulations on this grid, in this region. Many of the choices were informed by ensemble testing of the TC Yasi simulation sensitivity to physical parameterizations (Parker et al. 2017b).

The WRF simulations for each case study under current climate conditions used the lateral and initial conditions described above. All simulations utilized the WRF digital filter initialization (DFI) procedure (Lynch and Huang 1992, 1994; Chen and Huang 2006). DFI fully balances the wind fields at the initial time using an adiabatic backward and diabatic forward integration (Lackmann 2015). The procedure is critical to this study as it helps to smooth the disturbance to the system when adding the climate change delta from the PGW technique.

2.3 Pseudo Global Warming Technique

General Climate Models (GCMs) are the main tools for projecting the effect of anthropogenic climate change. However, long time scale studies from seasons to years are computationally intensive and may not capture environmental conditions favorable for TC genesis and development. Furthermore, the current horizontal resolution of GCMs (from ~100 to 300 km for the CMIP5 models down to ~50 km for the new generation of high-resolution models [Walsh et al. 2016]) has thus far been inadequate to accurately capture the short-term variability of intense TCs given that high resolution meteorological forcing cannot be supplied by the GCM coarse grid (Walsh 2004; Lynn et al. 2009; Walsh et al. 2016). This study uses a pseudo global warming (PGW based on the methods developed by Schär et al. [1996]; Hara et al. [2008]; Kawase et al. [2009]; Ramussen et al. [2011]; and Yoshikane et al. [2012]) downscaling technique to create a future climate scenario and investigate the response of intense TC characteristics to predicted climate change forcing. The PGW approach allows us to focus on time scales of days to a week, simulate an environment known to be conducive to and support TC development (in the current climate), and use a regional model set up that can accurately capture TC characteristics. The PGW technique creates a simulation where the boundary conditions retain the realistic sub-daily variability in the ERA-I data for a TC to develop, but also include the climate change delta that is predicted from current climate to future (2070-2100) (as discussed by Lynn et al. 2009). We can then isolate and examine TC-specific responses to the same environment but perturbed by the predicted larger-scale changes to the environment (Lackmann 2015). As discussed in Section 1, the PGW method has been used to investigate the response of idealized TCs (Hill and Lackmann 2011) and real-world TCs in the Atlantic (Lynn et al 2009; Lackmann 2015) to climate change forcing. However, to our knowledge, this PGW approach has not been used to investigate the response of Southern Hemisphere or Australian TC characteristics to climate change forcing. Given variability in response of cases to PGW in the Atlantic, and the possible heterogeneity in response of TCs to climate change regionally (discussed in Section 1), this study provides novel insights into the response of TCs to climate change in this region that have not previously been captured.

To create a future climate scenario using the PGW technique, a monthly climate change delta (ΔCC) is calculated for pressure, geopotential height, relative humidity, temperature, horizontal winds, surface pressure, mean sea level pressure, soil moisture, soil temperature, sea surface temperature, and skin temperature. Each ΔCC is added to its corresponding variable in the current boundary and initial conditions of the regional model to represent the effect of predicted climate change on the environment. This is summarized in Eq 1,

$$Equation\ 1: X_{future\ climate} = X_{current\ climate} + Monthly\ \Delta \mathrm{CC}_X$$

where X is the variable, e.g. pressure, and ΔCC_X is the climate change delta for the variable X. An example of the technique for pressure (P) in the Yasi case is given in Eq. 2.

$$Equation\ 2: P_{future} = P_{current} + January\ \Delta \mathrm{CC}_P$$

In this study, the climate change delta (ΔCC) is created by subtracting the current climate simulated by the Community Earth System Model (CESM) 20th Century simulations from the future climate predicted by the CESM simulations of the 8.5 Representative Concentration Pathway (RCP) (Eq. 3).

$$Equation\ 3: \Delta CC = Average\ Future\ Climate(2071 - 2100) - Average\ Current\ Climate(1976 - 2005)$$

We calculate the current climate as the monthly averages of the climate variables over the constructed domains (Figure 3) from 1976-2005 of the 20th century simulations. The future climate is calculated as the monthly average of climate variables over the TC domains (Figure 3) from 2071-2100 of the RCP 8.5 scenario simulations. The CESM data used is the global bias-corrected (Bruyère et al. 2014) Coupled Model Intercomparison Project (CMIP) output to support WRF/MPAS research (Monaghan et al. 2014). We use thirty-year average climatologies from both time periods to smooth decadal oscillation signals in the climate system. For each of the three cases, we calculated a month-averaged delta at every grid point, at every vertical level, over both domains in the regional WRF set up. This resulted in 3-dimensional deltas for the variables of pressure, geopotential height, relative humidity, temperature, and horizontal winds, and 2-dimensional deltas for surface pressure, mean sea level pressure, soil moisture, soil temperature, sea surface temperature, and skin temperature. The January, February, and April climate change deltas were added to the current climate boundary and initial conditions for the Yasi, Marcia, and Ita case studies respectively to create the future climate scenario to be simulated (Equations 2 and 3). Model CO_2 is increased from the model default of 379ppm (present day levels) to 935ppm (the atmospheric CO_2 concentration roughly predicted by the year 2070 (Riahi et al. 2011) for the future scenario simulations. Simulations in this scenario represent 'future' versions of the TCs where the large scale thermodynamic conditions correspond roughly to those predicted 100 years in the future but with synoptic weather patterns similar to chosen present day events.

The approach used in this study based on the PGW technique and CESM predicted climate has implicit assumptions. This method assumes that a TC vortex structure could exist in the future climate and essentially seeds a vortex in the domain at the start of the simulation. The thermodynamic changes were applied to the TCs after genesis and the early parts of TC development. Therefore, this study does not investigate the likelihood or dynamics of genesis, nor the effect of thermodynamic change on early TC development in a future environment. Instead, the study focuses on how the characteristics of TCs (with vortices similar to intense TCs of the present-day), during the main phase of intensification and landfall, may respond to changes in the environmental variables of the climate if they were to occur in the future. This study uses only the CESM predicted climate and does not consider the CMIP ensemble spread of future climate forecasts to calculate the ΔCC for PGW. However, it has been shown that CESM produces physically realistic results (Sillmann et al. 2013), and falls around the median of the CMIP5 model spread of error in present day representations and future forecasts (Knutti et al. 2013). Furthermore, Lackmann (2015) demonstrates that the responses of Atlantic Hurricane Sandy (2012) to future climate perturbations are robust when using the PGW technique and the climate predictions of five different GCMs from the CMIP ensemble. Therefore, for this study we find it satisfactory to use the CESM simulations to derive the climate change delta. Representative Concentration Pathway (RCP) 8.5 (Riahi et al. 2011) is the highest greenhouse gas emissions scenario with CO_2 concentrations up to three times year 2000 values. These predictions are based on a scenario with a lack of policy changes to reduce emissions, high population, and continued heavy reliance on fossil fuels. While there are more conservative RCP scenarios, this study aims to explore the response of the TC characteristics to the climate perturbation caused by the maximum greenhouse gas scenario currently predicted.

2.4 Scenarios Tested

Each case study is simulated in both the current and future climate scenario three times. Within each climate scenario, the simulations differ by the digital filter initialization (DFI) time length. DFI is initialized for 1, 2, or 3 hours in order to produce variable initial conditions for the full WRF simulation and thereby facilitate the testing of a small ensemble of initial conditions. The ensemble of simulations allows us to explore whether the changes to the TC characteristics are an artefact of model internal variability when making alterations to the model or a true response to the changes in the boundary conditions.

2.5 Analysis Techniques

Trajectory is assessed by finding the latitude and longitude at the point of minimum sea level pressure (i.e. the location of the eye) at every time step. Intensity evolution is analyzed through maximum recorded wind speeds and minimum sea level pressure along the simulated cyclone track. Forward motion is assessed as the average of the hourly translation speed (km/h) from the start of the simulation until the time step of landfall. Size is designated to be the radius of the 34, 56, and 64 knot winds averaged from all four quadrants of the storm at each time step through the simulation. Average and maximum TC-associated rainfall (mm) are calculated from precipitation within a 500km radius of the TC track. The maximum is indicative of the activity in the most active quadrant of the TC. The changes to the characteristics given the climate forcing are assessed through direct comparison for each case study and also through calculating percentage change for each characteristic.

3. Results

While simulations of the chosen case studies under current climate conditions can accurately simulate many of the TC characteristics, there are some limitations due to model resolution. In particular, the current climate simulations underestimate maximum TC intensity by ~7hPa for Yasi, ~20hPa for Ita, and especially ~49Pa for TC Marcia. Observations demonstrate that Marcia was a compact system that intensified from 980hPa to 932hPa in 18 hours and weakened to 980hPa again over the following 12 hours (IBTrACS data Knapp et al. [2010]). At this resolution, the model was not able to capture this rapid intensification and weakening. We consider that, within the constraints of the model ability, the simulations are representative of possible TC systems in the current climate. Given the noted inaccuracies, we base the following analyses primarily on the relative change of the simulated TC characteristics in the future environment.

3.1 Trajectory and Translation Speed

Trajectory changes are an important component of TC response to climate change, because they could alter which areas are negatively affected by TC conditions, including areas that have not been affected previously. The trajectories of Yasi and Marcia shift poleward and eastward in response to the climate change perturbation, in accordance with similar findings in the literature (Walsh and Katzfey 2000; Lackmann 2015). The Ita case, however, does not follow this trend.

As discussed in the Atlantic study of Hurricane Katrina (2005) by Lynn et al. (2009), trajectory deviations can be caused by the anomalies in the zonal steering flow. Analysis suggests that the small poleward shift for Yasi (Figure 4a) is caused by the wind delta field applied to the case (Figure 5a). The poleward and eastward shift in the Marcia trajectory (Figure 4c) in the future climate can also be attributed to the steering flow delta forcing (Figure 5c). This poleward shift supports similar findings of a poleward shift of Atlantic hurricane Sandy (2012) by 2100 (Lackmann 2015) and a predicted general poleward extension of TC trajectories in the Australia region (Walsh and Katzfey 2000; Nguyen and Walsh 2001). However, with future climate perturbation, the Ita trajectory moves ~4° equatorward (Figure 4b). This trajectory leads the system to move back over the ocean (after the first landfall) and make landfall for a second time towards the end of the simulation (Figure 4b). Some studies have suggested that greater SST warming along the Equator compared to areas further poleward (Collins et al. 2010) could lead to equatorward shift in TC formation and trajectory (Oouchi et al. 2006). However, the SST delta used in this study demonstrates the opposite spatial pattern, with greater warming towards the poles (Figure 4). Instead, our analysis suggests that the Ita trajectory migration behavior is due to the April steering flow delta (Figure 5b) added to the case for the future scenario. The April wind delta is predominantly to the west and northwest in the area of TC activity (near the northeastern coastline, Figure 5b). In contrast, the wind direction is towards the southeast in the January and February deltas for the Yasi and Marcia cases respectively (Figure 5a and c). Variations in the conditions of the steering flow also resulted in large deviations in the trajectory response of Atlantic hurricane Katrina (2005) in the future climate (Lynn et al. 2009). The initial condition ensemble of simulations using DFI initialization demonstrates that the divergence in the Ita trajectory is robust given the two climate scenarios (not shown). Results indicate that the trajectory alterations are also driven by the size change response of each case to the climate perturbation, which will be discussed in the Section 3.2.

The response of TC translation speed to climate change has not been comprehensively addressed in the literature. We found that the climate change perturbation induces only minimal changes to the translation speed for Yasi and Marcia (Table 1). However, there is, on average, a 26% increase in the translation speed of TC Ita in the future climate scenario (Table 1). This increase supports a similar theoretical increase in translation speed proposed by Walsh and Katzfey (2000) for Australian TCs in a future climate. Analysis again suggests that this translation speed increase is driven by the wind delta added to the Ita case study. The April wind delta vector is larger than calculated for January or February (Figure 5b compared to 4a, c) and results in an increase in the forward motion of TC Ita.

The relationship between changing translation speed and damage is complex. An increased translation speed may decrease the risk of damage as the exposure time to TC-conditions, such as strong winds, would decrease (e.g. Czajkowski and Done 2014; Puotinen 2007). However, increases to translation speed also increase the ground-relative wind speeds (Shapiro 1983) experienced by coastal ecosystems and settlements and therefore heighten the risk of damage. While it has been suggested that increasing the translation speed may reduce storm surge height and flood inundation (Peng et al. 2004; Weisberg and Zheng 2006), this relationship is likely non-linear (Irish and Resio 2010).

Resonance can occur for certain translation speeds (Rego and Li 2009), whereby increasing translation speed increases peak surge heights by up to 40% (Rego and Li 2009). Despite flooding a narrower section of the coast, a TC with an increased translation speed would move quickly across the shoreline potentially generating higher surges (Rego and Li 2009). Increased surge height can result in negative effects such as coastal erosion and nutrient and sediment leaching into coastal waterways (Parker et al. 2017a). The relationship between translation speed and storm surge is important to consider further as storm surge has been named as one of the most damaging aspects of TCs (Walsh 2004), but is beyond the scope of this study.

3.2 Size

Similar to translation speed, the change to TC size with climate change has not been widely explored or analyzed in the literature. Increasing size would increase the area affected by TC-associated winds, storm surge, and rainfall. Increasing TC size may thus increase the total destructive capacity (Merrill 1984; Powel and Reinhold 2007; Knaff 2014). Our results demonstrate that there is not a consistent response of the TC size to the future climate scenario. While there was a decrease in radius of 34 knot winds for Ita from the current to future climate (Figure 6b, Table 1), which agreed with the previous finding of radius decrease for Atlantic hurricane Katrina (2005) (Lynn et al. 2009); there was no discernible size change in Yasi until the very end of the simulation (Figure 6a, Table 1); and a significant increase in radius for the Marcia case in response to the future climate (Figure 6c, Table 1). These patterns are mirrored when considering size change of the cases through the radius of the 56 knot and 64 knot winds (not shown).

The results point towards a saturation condition in the future climate as suggested by Holland and Bruyère (2013). The increase in size and intensity is effectively limited by the cap in potential intensity with climate change (Emanuel 1987). Therefore, large, intense systems may only be able to increase modestly in size and intensity in the future climate. However, weaker and smaller systems can undergo rapid intensification and greater relative change to reach higher intensities and larger sizes and resemble Category 3-4 systems (Holland and Bruyère 2013).

Marcia is the smallest and weakest case in this study. This is evident in the weaker wind speeds (blue solid lines) and slower intensification rate (solid red lines) in the current climate for Marcia (Figure 6f) compared to Yasi and Ita (Figure 6d, e) and also the substantial difference in the radius of 34 knot winds at the start of the current climate simulation (solid green line Figure 6a, b, c). The saturation theory accounts for the lack of size increase in the larger, intense systems Yasi and Ita in the future climate scenario as well as the 40% average size increase of Marcia case, with an increase of greater than 100% early in its life cycle (Table 1). The initial size and intensity of the Marcia case and the larger SST perturbation experienced given the poleward trajectory (Figure 4c), accounts for the significant size increase found for Marcia as well as the larger percentage change in characteristics such as SLP, wind speed, and rainfall compared to Yasi and Ita (Table 1).

The size changes and the beta effect (Holland 1983) also contribute to the trajectory changes discussed in Section 3.1. With only minimal changes in size for the Yasi case (Figure 6a, green lines), there would not be large trajectory shift due to a beta effect change with the climate perturbation. Whereas, the increase in size for Marcia (Figure 6c, green line) increases the beta effect and the tendency of the system to move poleward (Holland 1983), resulting in a larger trajectory deviation than for Yasi in the future climate. Furthermore, as the Ita case predominantly decreased in size with the future climate perturbation (Figure 6b, Table 2), the beta effect weakened, resulting in a reduced tendency for the system to track poleward (Holland, 1983).

3.3 Intensity

Intensity changes which alter wind speeds and storm surges would have a significant implication for potential damage to coastal buildings and infrastructure (McInnes et al. 2003; Stewart 2003; Ginger et al. 2007), and ecosystems (e.g. the Great Barrier Reef [Done 1992]; [Puotinen 2007]; [Fabricius et al. 2008]) in this region. For all three cases, the future climate perturbation acts to increase intensity. Minimum sea level pressure decreases on average 3.5-5 hPa, with a maximum increase of up to ~10hPa, indicating more intense systems in the climate change scenario (Table 1; Figure 6d, e, f). The relative change in intensity is in good agreement with previous studies, which found decreases in SLP on the order of 8-14 hPa (Knutson and Tuleya 2004; Lynn et al. 2009; Hill and Lackmann 2011). Increasing intensity may have an effect on storm surge damage, as McInnes et al. (2003) have shown that with decreasing SLP and rising sea levels there will be more frequent damaging storm surge events in the Cairns region of Australia.

With the climate change perturbation, maximum recorded wind speeds tend towards higher values. We find an average increase of ~4.5-9% (Table 1, Figure 6d, e, f) in maximum wind speeds for all three cases. For TC Marcia, the proportional change in wind speed was greatest, with a maximum increase of 31% (Table 1, Figure 6f) which occurred after landfall. Maximum winds were also prolonged after landfall with Atlantic hurricane Katrina (2005) in the future climate (Lynn et al. 2009). The trajectory change and oscillation between land and ocean of the Ita case (Figure 5b) greatly alters the intensity characteristics in the future climate scenario (Figure 6e). Importantly, the change brings about a secondary peak in maximum wind speeds (Figure 6e) and therefore a secondary potential for damage.

The results of the initial condition ensemble for each TC case, in each scenario, demonstrate that the changes to the TC characteristics are a true response to the boundary condition perturbation and not an artefact of model internal variability (where a response is induced through any change to the model configuration). We have highlighted this in Figure 6d, e, f where the dashed lines compared to the solid lines portray a clear clustering of the TC intensity characteristics in the simulations with the same climate scenario (regardless of DFI initialization field), and a distinct separation of the characteristics given different climate forcings. While we do not formally present results from a physics parameterization ensemble, we have found the same relative change in TC intensity characteristics given climate perturbation when varying the cumulus and microphysics schemes. Furthermore, Lackmann (2015) also found a consistent average response of Hurricane Sandy to climate forcing regardless of varying the cumulus, microphysics, or planetary boundary layer parameterizations. Therefore, for this study we conclude that the calculated relative changes are robust.

Analysis of the PGW delta suggests that the intensity increase with climate change is attributed to the thermodynamic changes and the SST delta added to the boundary conditions (as discussed by Lynn et al. 2009). In the regions of TC activity, the SST perturbation for each case ranges from around +2° to +3° K (Figure 4a, b, c). Increased SSTs are associated with increased water vapor in the lower troposphere (Trenberth 2005, Trenberth et al. 2005). The increase in thermal energy and latent heat exchange, and the change to the SST gradient (particularly towards the northeastern coastline) would increase TC intensity. SST increases can lead to concurrent increases in the surface fluxes of heat and moisture, and vigorous convection. Increased SST gradients can destabilize the overlying atmosphere and increase the upper limit of TC intensity (Vecchi and Soden 2007). Vertical mass flux and acceleration are subsequently enhanced and the inward mass convergence results in enhanced vorticity convergence and vortex stretching. Upper-level thermal expansion develops along with the upper-level vortex intensification. These system-scale changes cause increases in relative vorticity and rapid intensification of the TC system (Garner et al. 2009). The SST increase varies temporally and spatially, being greater for the January and February months (Figure 4a,c) and towards the Pole (Figure 4). The more southerly trajectory of Marcia exposes the system to an area of greater SST increases (+2.6 to 3°K) than the other two cases in the future scenario. This SST delta, in addition to the greater potential change for a smaller and weaker system in the future environment (as discussed), accounts for the proportionally greater increase in intensity observed for this case.

In addition to surface boundary changes, the future scenario perturbs the vertical profile of the atmosphere. Figure 7 demonstrates that the average environment over the domain at the beginning of the simulation (for Yasi) is warmer and moister throughout the atmosphere in the future climate, as expected with the increasing SSTs (Trenberth 2005, Trenberth et al. 2005). These changes will increase the energy available for atmospheric convection for the development of TCs (Trenberth 2005). Indeed, we calculated a notable increase in Convective Available Potential Energy (CAPE) over the domain in the future scenario. There was a 47% increase in the future environment (for the January Yasi case Figure 7) and up to 100% increase in CAPE in the environment for Ita with the April climate change delta. Knutson and Tuleya (2004) found an aggregate 21% increase in CAPE in a high CO_2 environment and enhanced CAPE is consistent with theories suggesting a relationship between higher CAPE and warmer climates (e.g. Renno and Ingersoll 1996). The increase in CAPE in the vertical profile increases the potential for enhanced moist convection and thus TC development (Trenberth 2005) and greater TC intensification in the future environment (Knutson and Tuleya 2004), as was demonstrated by the cases in this study.

3.4 Rainfall

Significant increases in rainfall amounts may increase damage through catchment flooding (McInnes et al. 2002) and nutrient and sediment leaching into the coastal lagoon causing a decline in water quality (Davies and Eyre 2005; Mitchell et al. 2005; Stieglitz 2005; Brodie 2012; Parker et al. 2017a). Results show that the TC-associated rainfall increases considerably with the future perturbation in the Yasi and Marcia cases. However, on average, rainfall decreases in the Ita case.

Calculations reveal that the maximum and average rainfall in the 500km radius around the eye of Yasi increase ~15% on average, but the increases can be up to 61 and 42% respectively (Table 1, Figure 6g). Previous studies of idealized TCs (e.g. Knutson and Tuleya 2004; Hill and Lackmann 2011), also found increases of 10-30% in precipitation around the TC inner core (100km around the center). Increasing instances of heavy precipitation are expected with climate warming (Pall et al. 2007) due to increasing atmospheric water vapor content (Allen and Ingram 2002). According to the Clausius-Clapeyron relationship, the atmosphere vapor capacity increases with temperatures with a global-mean water vapor rate of increase in of 7.5% per °K of warming (Held and Soden 2006). When convection and condensation do occur, more water precipitates out of the atmosphere with an associated increase in condensational heating, driving stronger TCs (Lackmann 2015). For Marcia, there is an even greater increase in the TC-associated rainfall. Maximum and average rainfall around the eye increase, on average, 46% and 31% respectively, but the increase can be up to 91% and 83% respectively at individual time steps (Table 1, Figure 6i). This heightened response is again attributed to the greater TC intensity change to climate forcing for a weaker original system, and the larger SST change in the location of the Marcia trajectory (Figure 4c).

The measures of Ita-associated rainfall decreased on average in the future climate scenario (Table 1, Figure 6h). While this is unexpected given the increase in the SST (Figure 4b) and the increase in environmental moisture (Figure 7), the decrease in rainfall is attributed to the system's smaller size (Figure 6b) and faster translation speed (Table 2) across the open ocean. It has been previously suggested that maximum potential rainfall associated with TC activity is often inversely proportional to the system's translation speed (Elsner and Kara 1999). The potential decrease in flooding risk from decreased rainfall is in contrast to the possible increase in flood risk posed by the translation speed changes to Ita (Section 3.1).

4. Discussion and Conclusions

For the three tropical cyclone case studies modeled, environmental perturbations supplied by a Pseudo Global Warming technique result in overall increased intensity, with sea level pressures reduced by up to ~10 hPa (~4-5hPa, on average) and maximum wind speeds increased by up to 31% (5-10% on average). However, not all the TC characteristics responded to the climate forcing uniformly across the three cases. While we found a poleward and eastward trajectory shift for Yasi and Marcia (similar to findings from Walsh and Katzfey [2000] and Lackmann [2015]), the Ita case responded to the future climate with an equatorward trajectory shift (supporting predictions by Oouchi et al. 2006) and a substantial increase in translation speed (supporting conjecture by Walsh and Katzfey 2000). Similarly, while the rainfall associated with Yasi and Marcia increased notably, mirroring findings by Knutson and Tuleya (2004) and Hill and Lackmann (2011), rainfall unexpectedly decreased during the Ita future simulation.

We attribute the unique responses of Ita to the differences in April steering flow delta added to this case, which is substantially different to the January and February wind delta field added to the other two cases. For Ita, steering flow shifted the trajectory equatorward, increased translation speed, and therefore decreased precipitation. Although changes to TC translation speed with climate change forcings have not previously been studied in great detail, our results showed a unique average 26% increase in translation speed of Ita with climate change.

Leslie et al. (2007) found a proportionally larger increase in the number of intense TCs affecting the western South Pacific later in the TC season in the future climate. With this prediction, there would be an increase in the number of systems that respond to climate change forcing similarly to TC Ita. However, more work is needed to explore seasonal trends with climate change to increase confidence in this prediction. Furthermore, the findings in this study highlight the need for greater confidence and consensus in the GCM predictions of changes to the large-scale environmental steering flow in the future climate.

We found consistent, proportionally larger changes to Marcia's characteristics with climate perturbation, including a unique 40% average increase in size not previously found in other studies. We attribute the greater changes to the larger SST delta in the region of Marcia's track, and the potential for weaker, smaller systems to undergo rapid intensification in the future environment to resemble category 3 or 4 systems (Holland and Bruyère 2013). A weaker system such as Marcia would not reach the potential intensity cap and saturation, which would restrict the intensification and growth of originally intense systems such as Yasi and Ita (Holland and Bruyère 2013). While previous PGW studies have considered only large (e.g. Hurricane Sandy [Lackmann 2015]) or intense (e.g. Hurricane Katrina [Lynn et al. 2009]) TC systems, the large relative changes exhibited by Marcia highlight the need to consider the response of weaker, smaller TCs to climate change and how risks may be consequently altered.

The possible responses of TC characteristics with potential climate change forcing have significant implications for the northeastern region of Australia. Increasing intensity (decreasing SLP) and alterations in translation speed may increase TC-associate storm surge. Increases in wind speed, rainfall, and translation speed can result in increased coastal damage to buildings, infrastructure, and important coastal ecosystems such as the Great Barrier Reef. Changing trajectories would alter the areas in the path of the storm and negatively affected by TC conditions, including areas that previously may not have been affected. Furthermore, increasing the size of the system would increase the area affected by TC-associated winds, storm surge, and rainfall.

The results presented in this study should be interpreted carefully, given the small sample-size of case studies as well as the assumptions inherent to the methodology and model set up (discussed Section 2.3). This methodology used 30-year averages of the current and future climate to calculate the climate delta in order to remove decadal oscillations and consider the response to the change in the mean state. However, this study does not address the large uncertainties surrounding the GCM predictions of the ENSO response to climate change (Walsh et al. 2012; Chand et al. 2013; Diamond et al. 2013; Dowdy 2014). It is important to note that a shift in the mean state or more frequent oscillations towards El Niño or La Niña like conditions would inhibit or promote TC development respectively in this region. Nevertheless, differences in current and future simulations may be amplified with longer integration times (Lackmann 2015), which suggests that the relative responses to climate change reported here may be underestimated. Additionally, these simulations underestimate intensity and absolute values of intensity and risk may in fact be much greater in the future. Furthermore, the effects of climate change on TC characteristics presented here will likely be acting in concert with population growth, increasing urbanization, agricultural intensification (Hughes et al. 2015), and other changes associated with climate such as sea level rise. Both the vulnerability and resultant negative consequences could thus increase with climatic change.

The results in this study demonstrated novel responses of TC characteristics to climate change in this basin not captured by the Atlantic PGW studies or more generalized Australia region studies. Our findings emphasize that not all TCs respond in the same way to climate perturbation and some responses may be dependent on time-of-year and the monthly delta applied, along with the size and intensity of the original case. These differences highlight the merit of a case study based approach, which considers multiple cases with differing characteristics in the current climate, in concert with the PGW technique. However, these differences also suggest that a greater number of cases needs to be studied in order to identify trends and outliers of the responses in TC characteristics to climate change.

Acknowledgements

The authors would like to thank Amanda Lynch at Brown University, James Done, and Greg Holland at the National Center for Atmospheric Research (NCAR) for very helpful discussion of the results; Noel Davidson at the Australian Bureau of Meteorology for the high-resolution ACCESS initialization data and advice; and Daniel P Moriarty III at Brown University for assistance in editing the manuscript. Computational work was supported by NCAR and the Yellowstone supercomputing facilities. This work was funded by Brown University and in part by NCAR summer visitor program. NCAR is sponsored by the National Science Foundation.

5. References

Abbs, D. (2012). The impact of climate change on the climatology of tropical cyclones in the Australian region. Retrieved September, 5, 2014.

Alexander, L. V., Hope, P., Collins, D., Trewin, B., Lynch, A., & Nicholls, N. (2007). Trends in Australia's climate means and extremes: a global context. Australian Meteorological Magazine, 56(1), 1-18.

Allen, M. R., & Ingram, W. J. (2002). Constraints on future changes in climate and the hydrologic cycle. Nature, 419(6903), 224-232.

Anderson-Berry, L. J. (2003). Community vulnerability to tropical cyclones: Cairns, 1996–2000. Natural Hazards, 30(2), 209-232.

Anthony, K. R., & Fabricius, K. E. (2000). Shifting roles of heterotrophy and autotrophy in coral energetics under varying turbidity. Journal of experimental marine biology and ecology, 252(2), 221-253.

AON Benfield, (2011) [http://thoughtleadership.aonbenfield.com/Documents/201103_ab_if_tropical_cyclone_yasi_recap.pdf]

AON Benfield (2014). April 2014 Global Catastrophe Recap. Accessed October 31 2016. [http://thoughtleadership.aonbenfield.com/Documents/20140507_if_april_global_recap.pdf]

Australian Government, Bureau of Meteorology 2015. Severe Tropical Cyclone Marcia. Accessed Jan 31 2017. [http://www.bom.gov.au/cyclone/history/marcia.shtml]

Authority, Great Barrier Reef Marine Park (2015). Marine Monitoring Program results for 2013-2014: summary report.

Authority, Great Barrier Reef Marine Park (2016). Marine Monitoring Program summary report: results for 2014-2015.

Beeden R, Maynard J, Puotinen M, Marshall P, Dryden J, Goldberg J, et al. (2015). Impacts and Recovery from Severe Tropical Cyclone Yasi on the Great Barrier Reef. PLoS ONE 10(4): e0121272. doi:10.1371/journal.pone.0121272

Bell, R., Strachan, J., Vidale, P. L., Hodges, K., & Roberts, M. (2013). Response of tropical cyclones to idealized climate change experiments in a global high-resolution coupled general circulation model. Journal of Climate, 26(20), 7966-7980.

Bender, M. A., Knutson, T. R., Tuleya, R. E., Sirutis, J. J., Vecchi, G. A., Garner, S. T., & Held, I. M. (2010). Modeled impact of anthropogenic warming on the frequency of intense Atlantic hurricanes. Science, 327(5964), 454-458.

Bengtsson, L., Hodges, K. I., Esch, M., Keenlyside, N., Kornblueh, L., LUO, J. J., & Yamagata, T. (2007). How may tropical cyclones change in a warmer climate?. Tellus a, 59(4), 539-561.

Brodie, J. E., Kroon, F. J., Schaffelke, B., Wolanski, E. C., Lewis, S. E., Devlin, M. J., ... & Davis, A. M. (2012). Terrestrial pollutant runoff to the Great Barrier Reef: an update of issues, priorities and management responses. Marine Pollution Bulletin, 65(4), 81-100.

Brodie, J., Schroeder, T., Rohde, K., Faithful, J., Masters, B., Dekker, A., ... & Maughan, M. (2010). Dispersal of suspended sediments and nutrients in the Great Barrier Reef lagoon during river-discharge events: conclusions from satellite remote sensing and concurrent flood-plume sampling. Marine and Freshwater Research, 61(6), 651-664.

Bruyère, C. L., Done, J. M., Holland, G. J., & Fredrick, S. (2014). Bias corrections of global models for regional climate simulations of high-impact weather. Climate dynamics, 43(7-8), 1847-1856.

Carroll, F., & Authority, Q. R. (2015). Building it back better to reduce risks after multiple disaster events. In Queensland Reconstruction Authority, Queensland, presented to the Floodplain Management Association National Conference.

Ceccarelli DM, Emslie MJ, Richards ZT (2016). Post-Disturbance Stability of Fish Assemblages Measured at Coarse Taxonomic Resolution Masks Change at Finer Scales. PLoS ONE 11(6): e0156232. doi:10.1371/journal.pone.0156232

Chand, S. S., L. McBride, J., Tory, K. J., Wheeler, M. C., & Walsh, K. J. (2013). Impact of different ENSO regimes on southwest Pacific tropical cyclones. Journal of Climate, 26(2), 600-608.

Chen, F., & Dudhia, J. (2001). Coupling an advanced land surface-hydrology model with the Penn State-NCAR MM5 modeling system. Part I: Model implementation and sensitivity. Monthly Weather Review, 129(4), 569-585.

Chen, M., & Huang, X. Y. (2006). Digital filter initialization for MM5. Monthly weather review, 134(4), 1222-1236.

Collins, M., An, S. I., Cai, W., Ganachaud, A., Guilyardi, E., Jin, F. F., ... & Vecchi, G. (2010). The impact of global warming on the tropical Pacific Ocean and El Niño. Nature Geoscience, 3(6), 391-397.

Czajkowski, J., & Done, J. (2014). As the wind blows? Understanding hurricane damages at the local level through a case study analysis. Weather, climate, and society, 6(2), 202-217.

Davies, P. L., & Eyre, B. D. (2005). Estuarine modification of nutrient and sediment exports to the Great Barrier Reef Marine Park from the Daintree and Annan River catchments. Marine Pollution Bulletin, 51(1), 174-185.

De'ath, G., Fabricius, K. E., Sweatman, H., & Puotinen, M. (2012). The 27–year decline of coral cover on the Great Barrier Reef and its causes. Proceedings of the National Academy of Sciences, 109(44), 17995-17999.

Deloitte Access Economics (2013), Economic contribution of the Great Barrier Reef, Great Barrier Reef Marine Park Authority, Townsville.

Devlin, M. J., & Brodie, J. (2005). Terrestrial discharge into the Great Barrier Reef Lagoon: nutrient behavior in coastal waters. Marine Pollution Bulletin, 51(1), 9-22.

Devlin, M., & Schaffelke, B. (2009). Spatial extent of riverine flood plumes and exposure of marine ecosystems in the Tully coastal region, Great Barrier Reef. Marine and Freshwater Research, 60(11), 1109-1122.

Diamond, H. J., Lorrey, A. M., & Renwick, J. A. (2013). A southwest Pacific tropical cyclone climatology and linkages to the El Niño–Southern Oscillation. Journal of Climate, 26(1), 3-25.

Done, T. J. (1992). Effects of tropical cyclone waves on ecological and geomorphological structures on the Great Barrier Reef. Continental Shelf Research, 12(7), 859-872.

Done, J.M., Holland, G.J., Bruyère, C.L., Leung, L.R., and Suzuki-Parker, A., 2013: Modeling high-impact weather and climate: Lessons from a tropical cyclone perspective. Climatic Change, doi: 10.1007/s10584-013-0954-6

Done, J. M., Ge, M., Holland, G. J., & Bruyère, C. L. (2014, May). Future changes in Gulf of Mexico hurricane wave climatology. In Offshore Technology Conference. Offshore Technology Conference.

Dowdy, A. J. (2014). Long-term changes in Australian tropical cyclone numbers. Atmospheric Science Letters, 15(4), 292-298.

Ek, M. B., Mitchell, K. E., Lin, Y., Rogers, E., Grunmann, P., Koren, V., ... & Tarpley, J. D. (2003). Implementation of Noah land surface model advances in the National Centers for Environmental Prediction operational mesoscale Eta model. *Journal of Geophysical Research: Atmospheres (1984–2012)*, *108*(D22).

Elsner, J. B., & Kara, A. B. (1999). Hurricanes of the North Atlantic: Climate and society. Oxford University Press.

Emanuel, K. (2006). Climate and tropical cyclone activity: A new model downscaling approach. Journal of Climate, 19(19), 4797-4802.

Emanuel, K., Sundararajan, R., & Williams, J. (2008). Hurricanes and global warming: Results from downscaling IPCC AR4 simulations. Bulletin of the American Meteorological Society, 89(3), 347.

Emanuel, K. A. (2013). Downscaling CMIP5 climate models shows increased tropical cyclone activity over the 21st century. Proceedings of the National Academy of Sciences, 110(30), 12219-12224.

Fabricius, K. E., De'Ath, G., Puotinen, M. L., Done, T., Cooper, T. F., & Burgess, S. C. (2008). Disturbance gradients on inshore and offshore coral reefs caused by a severe tropical cyclone. Limnology and Oceanography, 53(2), 690-704.

Fabricius, K. E., & Wolanski, E. (2000). Rapid smothering of coral reef organisms by muddy marine snow. Estuarine, Coastal and Shelf Science, 50(1), 115-120.

Ferrier, B. S. (1994). A double-moment multiple-phase four-class bulk ice scheme. Part I: Description. *Journal of the atmospheric sciences*, *51*(2), 249-280.

Ferrier, B. S., Y. Jin, Y. Lin, T. Black, E. Rogers, and G. DiMego, (2002). Implementation of a new grid-scale cloud and rainfall scheme in the NCEP Eta Model. Preprints, 15th Conf. on Numerical Weather Prediction, San Antonio, TX, Amer. Meteor. Soc., 280–283.

Fraser, R. H., & Currie, D. J. (1996). The species richness-energy hypothesis in a system where historical factors are thought to prevail: coral reefs. American Naturalist, 138-159.

Furnas, M., Mitchell, A., Skuza, M., & Brodie, J. (2005). In the other 90%: phytoplankton responses to enhanced nutrient availability in the Great Barrier Reef Lagoon. Marine pollution bulletin, 51(1), 253-265.

Garner, S. T., Held, I. M., Knutson, T., & Sirutis, J. (2009). The roles of wind shear and thermal stratification in past and projected changes of Atlantic tropical cyclone activity. Journal of Climate, 22(17), 4723-4734.

Gentry, M. S., & Lackmann, G. M. (2010). Sensitivity of simulated tropical cyclone structure and intensity to horizontal resolution. Monthly Weather Review, 138(3), 688-704.

Ginger, J. D., Henderson, D. J., Leitch, C. J., & Boughton, G. N. (2007). Tropical Cyclone Larry: Estimation of wind field and assessment of building damage. Australian Journal of Structural Engineering, 7(3), 209-224.

Hara, M., Yoshikane, T., Kawase, H., & Kimura, F. (2008). Estimation of the impact of global warming on snow depth in Japan by the pseudo-global-warming method. Hydrological Research Letters, 2, 61-64.

Held, I. M., & Soden, B. J. (2006). Robust responses of the hydrological cycle to global warming. Journal of Climate, 19(21), 5686-5699.

Hill, K. A., & Lackmann, G. M. (2011). The impact of future climate change on TC intensity and structure: A downscaling approach. Journal of Climate, 24(17), 4644-4661.

Holland, G., & Bruyère, C. L. (2013). Recent intense hurricane response to global climate change. Climate Dynamics, 1-11.

Holland, G. J. (1983). Tropical cyclone motion: Environmental interaction plus a beta effect. Journal of the Atmospheric Sciences, 40(2), 328-342.

Hong, S. Y., Noh, Y., & Dudhia, J. (2006). A new vertical diffusion package with an explicit treatment of entrainment processes. Monthly Weather Review, 134(9), 2318-2341.

Hughes, T. P., Day, J. C., & Brodie, J. (2015). Securing the future of the Great Barrier Reef. Nature Climate Change, 5(6), 508-511.

Iacono, M. J., Delamere, J. S., Mlawer, E. J., Shephard, M. W., Clough, S. A., & Collins, W. D. (2008). Radiative forcing by long-lived greenhouse gases: Calculations with the AER radiative transfer models. Journal of Geophysical Research: Atmospheres, 113(D13).

Irish, J. L., & Resio, D. T. (2010). A hydrodynamics-based surge scale for hurricanes. Ocean Engineering, 37(1), 69-81.

Jacob, D., J. Petersen, J., Eggert, B., Alias, A., Christensen, O.B., Bouwer, L.M., Braun, A., Colette, A., Deque, M., Georgievski, G., Georgopoulou, E., Gobiet, A., Menut, L., Nikulin, G., Haensler, A., Hempelmann, N., Jones, C., Keuler, K., Kovats, S., Kroner, N., Kotlarski, S., Kriegsmann, A., Martin, E., van Meijgaard, R., Moseley, C., Pfeifer, S., Preuschmann, S., Radermacher, C., Radtke, K., Rechid, D., Rounsevell, M., Samuelsson, P., Somot, S., Soussana, J-F., Teichmann, C., Valentini, R., Vautard, R., Weber, B. & Yiou, P. (2014). EURO-CORDEX: new high-resolution climate change projections for European impact research. *Regional Environmental Change*, *14*(2), 563-578.

Kain, J. S. (1993). Convective parameterization for mesoscale models: The Kain Fritsch scheme. *The representation of cumulus convection in numerical models, Meteor. Monogr*, *46*, 165-170.

Kain, J.S., (2004): The Kain–Fritsch convective parameterization: An update. *J. Appl. Meteor. Climatol.*, **43**, 170–181.

Kain, J.S., and J.M. Fritsch, (1990): A one-dimensional entraining detraining plume model and its application in convective parameterization. *J. Atmos. Sci.*, **47**, 2784–2802.

Kawase, H., Yoshikane, T., Hara, M., Kimura, F., Yasunari, T., Ailikun, B., ... & Inoue, T. (2009). Intermodel variability of future changes in the Baiu rainband estimated by the pseudo global warming downscaling method. Journal of Geophysical Research: Atmospheres, 114(D24).

Knaff, J. A., Longmore, S. P., & Molenar, D. A. (2014). An objective satellite-based tropical cyclone size climatology. Journal of Climate, 27(1), 455-476.

Knapp, K. R., Kruk, M. C., Levinson, D. H., Diamond, H. J., & Neumann, C. J. (2010). The international best track archive for climate stewardship (IBTrACS) unifying tropical cyclone data. *Bulletin of the American Meteorological Society*, *91*(3), 363-376.

Knutson, T. R., McBride, J. L., Chan, J., Emanuel, K., Holland, G., Landsea, C., ... & Sugi, M. (2010). Tropical cyclones and climate change. Nature Geoscience, 3(3), 157-163.

Knutson, T. R., & Tuleya, R. E. (2004). Impact of CO2-induced warming on simulated hurricane intensity and precipitation: Sensitivity to the choice of climate model and convective parameterization. Journal of Climate, 17(18), 3477-3495.

Knutti, R., Masson, D., & Gettelman, A. (2013). Climate model genealogy: Generation CMIP5 and how we got there. Geophysical Research Letters, 40(6), 1194-1199.

Kuleshov, Y., Fawcett, R., Qi, L., Trewin, B., Jones, D., McBride, J., & Ramsay, H. (2010). Trends in tropical cyclones in the South Indian Ocean and the South Pacific Ocean. Journal of Geophysical Research: Atmospheres, 115(D1).

Lavender, S. L., & Walsh, K. J. E. (2011). Dynamically downscaled simulations of Australian region tropical cyclones in current and future climates. Geophysical Research Letters, 38(10).

Lackmann, G. M. (2015). Hurricane Sandy before 1900 and after 2100. Bulletin of the American Meteorological Society, 96(4), 547-560.

Landsea, C. W., Vecchi, G. A., Bengtsson, L., & Knutson, T. R. (2010). Impact of duration thresholds on Atlantic tropical cyclone counts. Journal of Climate, 23(10), 2508-2519.

Laurance, W. F., & Curran, T. J. (2008). Impacts of wind disturbance on fragmented tropical forests: a review and synthesis. Austral Ecology, 33(4), 399-408.

Leslie, L. M., Karoly, D. J., Leplastrier, M., & Buckley, B. W. (2007). Variability of tropical cyclones over the southwest Pacific Ocean using a high-resolution climate model. Meteorology and Atmospheric Physics, 97(1-4), 171-180.

Lynch, P., & Huang, X. Y. (1992). Initialization of the HIRLAM model using a digital filter. Monthly Weather Review, 120(6), 1019-1034.

Lynch, P., & Huang, X. Y. (1994). Diabatic initialization using recursive filters. Tellus A, 46(5).

Lynn, B. H., Healy, R., & Druyan, L. M. (2009). Investigation of Hurricane Katrina characteristics for future, warmer climates. Climate Research, 39(1), 75-86.

Massel, S. R., & Done, T. J. (1993). Effects of cyclone waves on massive coral assemblages on the Great Barrier Reef: meteorology, hydrodynamics and demography. Coral Reefs, 12(3-4), 153-166.

McInnes, K. L., Hubbert, G. D., Abbs, D. J., & Oliver, S. E. (2002). A numerical modelling study of coastal flooding. Meteorology and Atmospheric Physics, 80(1-4), 217-233.

McInnes, K. L., Walsh, K. J. E., Hubbert, G. D., & Beer, T. (2003). Impact of sea-level rise and storm surges on a coastal community. Natural Hazards, 30(2), 187-207.

Merrill, R. T. (1984). A comparison of large and small tropical cyclones. Monthly Weather Review, 112(7), 1408-1418.

Mitchell, C., Brodie, J., & White, I. (2005). Sediments, nutrients and pesticide residues in event flow conditions in streams of the Mackay Whitsunday Region, Australia. Marine Pollution Bulletin, 51(1), 23-36.

Monaghan, A. J., D. F. Steinhoff, C. L. Bruyere, and D. Yates. 2014. NCAR CESM Global Bias-Corrected CMIP5 Output to Support WRF/MPAS Research. Research Data Archive at the National Center for Atmospheric Research, Computational and Information Systems Laboratory. http://dx.doi.org/10.5065/D6DJ5CN4. Accessed† 01 Jun 2015.

Monin, A. S., & Obukhov, A. (1954). Basic laws of turbulent mixing in the surface layer of the atmosphere. Contrib. Geophys. Inst. Acad. Sci. USSR, 151, 163-187.

Nguyen, K. C., & Walsh, K. J. E. (2001). Interannual, decadal, and transient greenhouse simulation of tropical cyclone–like vortices in a regional climate model of the South Pacific. *Journal of Climate*, *14*(13), 3043-3054.

Oouchi, K., Yoshimura, J., Yoshimura, H., Mizuta, R., Kusunoki, S., & Akira, N. O. D. A. (2006). Tropical cyclone climatology in a global-warming climate as simulated in a 20 km-mesh global atmospheric model: Frequency and wind intensity analyses. Journal of the Meteorological Society of Japan. Ser. II, 84(2), 259-276.

Pall, P., Allen, M. R., & Stone, D. A. (2007). Testing the Clausius–Clapeyron constraint on changes in extreme precipitation under CO2 warming. Climate Dynamics, 28(4), 351-363.

Parker, C. L., Lynch, A. H., Spera, S. A., and Spangler, K. R. (2017a): The Relationship between Tropical Cyclone Activity, Nutrient Loading, and Algal Blooms over the Great Barrier Reef, Biogeosciences Discuss., doi:10.5194/bg-2017-23, in review, 2017.

Parker, C.L., Lynch, A.H., Mooney, P.A. (2017b) "Factors Affecting the Trajectory and Intensification of Tropical Cyclone Yasi (2011)". Atmospheric Research. http://doi.org/10.1016/j.atmosres.2017.04.002

Peng, M., Xie, L., & Pietrafesa, L. J. (2004). A numerical study of storm surge and inundation in the Croatan–Albemarle–Pamlico Estuary System. Estuarine, Coastal and Shelf Science, 59(1), 121-137.

Powell, M. D., & Reinhold, T. A. (2007). Tropical cyclone destructive potential by integrated kinetic energy. Bulletin of the American Meteorological Society, 88(4), 513.

Preen, A. R., Long, W. L., & Coles, R. G. (1995). Flood and cyclone related loss, and partial recovery, of more than 1000 km 2 of seagrass in Hervey Bay, Queensland, Australia. Aquatic Botany, 52(1), 3-17.

Puotinen, M. M., Done, T. T., & Skelley, W. (1997). An atlas of tropical cyclones in the Great Barrier Reef region: 1969-1997.

Puotinen, M. L. (2007). Modelling the risk of cyclone wave damage to coral reefs using GIS: a case study of the Great Barrier Reef, 1969–2003. International Journal of Geographical Information Science, 21(1), 97-120.

Queensland Government (2012). Budget Strategy and Outloook 2011-2012, 70 pp, Accessed January 5 2015. [http://www.budget.qld.gov.au/current-budget/budget-papers/index.php]

Rasmussen, R., Liu, C., Ikeda, K., Gochis, D., Yates, D., Chen, F., ... & Miller, K. (2011). High-resolution coupled climate runoff simulations of seasonal snowfall over Colorado: a process study of current and warmer climate. Journal of Climate, 24(12), 3015-3048.

Rego, J. L., & Li, C. (2009). On the importance of the forward speed of hurricanes in storm surge forecasting: A numerical study. Geophysical Research Letters, 36(7).

Rennó, N. O., & Ingersoll, A. P. (1996). Natural convection as a heat engine: A theory for CAPE. *Journal of the Atmospheric Sciences*, *53*(4), 572-585.

Reuters (2015) Cyclone Yasi to cost insurers AUS $3.5 bln forecaster. [Available online at http://www.reuters.com/article/2011/02/03/insured-losses-yasi-idUSLDE7121NR20110203]

Riahi, K., Rao, S., Krey, V., Cho, C., Chirkov, V., Fischer, G., ... & Rafaj, P. (2011). RCP 8.5—A scenario of comparatively high greenhouse gas emissions. Climatic Change, 109(1-2), 33-57.

Schär, C., Frei, C., Lüthi, D., & Davies, H. C. (1996). Surrogate climate-change scenarios for regional climate models. Geophysical Research Letters, 23(6), 669-672.

Shapiro, L. J. (1983). The asymmetric boundary layer flow under a translating hurricane. Journal of the Atmospheric Sciences, 40(8), 1984-1998.

Sillmann, J., Kharin, V. V., Zhang, X., Zwiers, F. W., & Bronaugh, D. (2013). Climate extremes indices in the CMIP5 multimodel ensemble: Part 1. Model evaluation in the present climate. Journal of Geophysical Research: Atmospheres, 118(4), 1716-1733.

Skamarock, W. C., Klemp, J. B., Dudhia, J., Gill, D. O., & Barker, D. M. (2005). Coauthors, 2008: A description of the Advanced Research WRF version 3. NCAR Tech. Note NCAR/TN-475+ STR, 113.

Stewart, M. G. (2003). Cyclone damage and temporal changes to building vulnerability and economic risks for residential construction. Journal of Wind Engineering and industrial aerodynamics, 91(5), 671-691.

Stieglitz, T. (2005). Submarine groundwater discharge into the near-shore zone of the Great Barrier Reef, Australia. Marine Pollution Bulletin, 51(1), 51-59.

Sugi, M., & Yoshimura, J. (2012). Decreasing trend of tropical cyclone frequency in 228-year high-resolution AGCM simulations. Geophysical Research Letters, 39(19).

Sugi, M., Murakami, H., & Yoshimura, J. (2009). A reduction in global tropical cyclone frequency due to global warming. Sola, 5, 164-167.

Tewari, M., Chen, F., Wang, W., Dudhia, J., LeMone, M. A., Mitchell, K., ... & Cuenca, R. H. (2004, January). Implementation and verification of the unified NOAH land surface model in the WRF model. In *20th conference on weather analysis and forecasting/16th conference on numerical weather prediction* (pp. 11-15).

Tiedtke, M., (1989): A comprehensive mass flux scheme for cumulus parameterization in large-scale models. Mon. Wea. Rev., 117, 1779–1800.

Trenberth, K. (2005). Uncertainty in hurricanes and global warming. Science, 308(5729), 1753-1754.

Trenberth, K. E., Fasullo, J., & Smith, L. (2005). Trends and variability in column-integrated atmospheric water vapor. Climate dynamics, 24(7-8), 741-758.

Turton, S. M. (2008). Landscape-scale impacts of Cyclone Larry on the forests of northeast Australia, including comparisons with previous cyclones impacting the region between 1858 and 2006. Austral Ecology, 33(4), 409-416.

Vecchi, G. A., & Soden, B. J. (2007). Effect of remote sea surface temperature change on tropical cyclone potential intensity. Nature, 450(7172), 1066-1070.

Walsh, K. J., & Katzfey, J. J. (2000). The impact of climate change on the poleward movement of tropical cyclone–like vortices in a regional climate model. Journal of Climate, 13(6), 1116-1132.

Walsh, K. J. E., Nguyen, K. C., & McGregor, J. L. (2004). Fine-resolution regional climate model simulations of the impact of climate change on tropical cyclones near Australia. Climate Dynamics, 22(1), 47-56.

Walsh, K. (2004). Tropical cyclones and climate change: unresolved issues. Climate Research, 27(1), 77-83.
Walsh, K. J., & Ryan, B. F. (2000). Tropical cyclone intensity increase near Australia as a result of climate change. Journal of Climate, 13(16), 3029-3036.
Walsh, K. J., McInnes, K. L., & McBride, J. L. (2012). Climate change impacts on tropical cyclones and extreme sea levels in the South Pacific—A regional assessment. Global and Planetary Change, 80, 149-164.
Walsh, K. (2015). Fine resolution simulations of the effect of climate change on tropical cyclones in the South Pacific. Climate Dynamics, 45(9-10), 2619-2631.
Walsh, K. J., McBride, J. L., Klotzbach, P. J., Balachandran, S., Camargo, S. J., Holland, G., ... & Sugi, M. (2016). Tropical cyclones and climate change. Wiley Interdisciplinary Reviews: Climate Change, 7(1), 65-89.
Weisberg, R. H., & Zheng, L. (2006). Hurricane storm surge simulations for Tampa Bay. Estuaries and Coasts, 29(6), 899-913.
Yamada, Y., Oouchi, K., Satoh, M., Tomita, H., & Yanase, W. (2010). Projection of changes in tropical cyclone activity and cloud height due to greenhouse warming: Global cloud-system-resolving approach. Geophysical Research Letters, 37(7).
Yoshikane, T., Kimura, F., Kawase, H., & Nozawa, T. (2012). Verification of the performance of the pseudo-global-warming method for future climate changes during June in East Asia. SOLA, 8(0), 133-136.
Zhang, C., Wang, Y., & Hamilton, K. (2011). Improved Representation of Boundary Layer Clouds over the Southeast Pacific in ARW-WRF Using a Modified Tiedtke Cumulus Parameterization Scheme. Monthly Weather Review, 139(11), 3489-3513.

6. Tables

Change in Characteristic Future - Current		Yasi	Ita	Marcia
Change in Sea Level Pressure (up to landfall)	Mean	-4.85 hPa	-3.57 hPa	-5.00 hPa
	Maximum	-8.14 hPa	-11.85 hPa	-9.55 hPa
% Change in maximum Wind Speed	Mean	4.94%	4.52%*	9.40%
	Maximum	17.11%	13.90%*	31.37%
% Change in Size	Mean	2.96%	-6.90%*	39.95%
	Maximum	65.06%	8.58%*	157.95%
% Change in average Translation Speed (up to landfall)		2.36%	25.84%	-6.03%
% Change in average Rainfall in area around eye	Mean	14.33%	-10.14%	31.16%
	Maximum	41.93%	28.81%	83.46%
% Change in maximum Rainfall in area around eye	Mean	16.07%	-5.43%	45.75%
	Maximum	61.12%	25.58%	90.54%

Table 1: the calculated change in the TC characteristics from the current to the future climate for all three cases. The changes are calculated as future – current for the simulations of the cases with DFI of 2 hours. The values for Ita marked with an asterisk (*) were calculated from the percentage changes up to landfall of the future case. The large deviations in the trajectories and life cycle of the case in the different scenarios after landfall would have skewed the calculations.

7. Figures

Figure 1

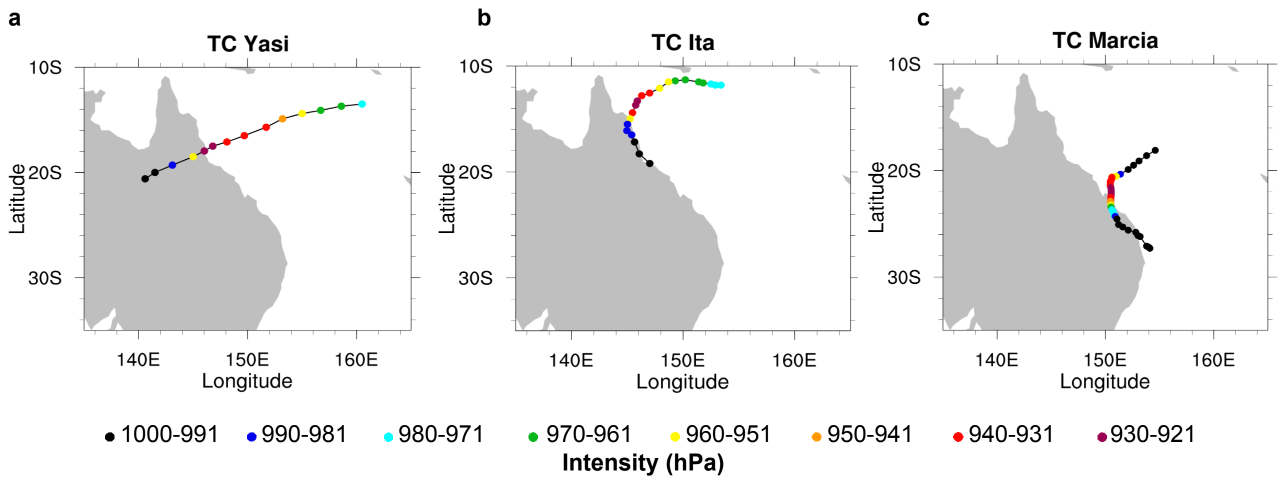

Figure 1: Observed trajectories and intensities of the case study cyclones for the chosen duration of simulations.

Figure 2

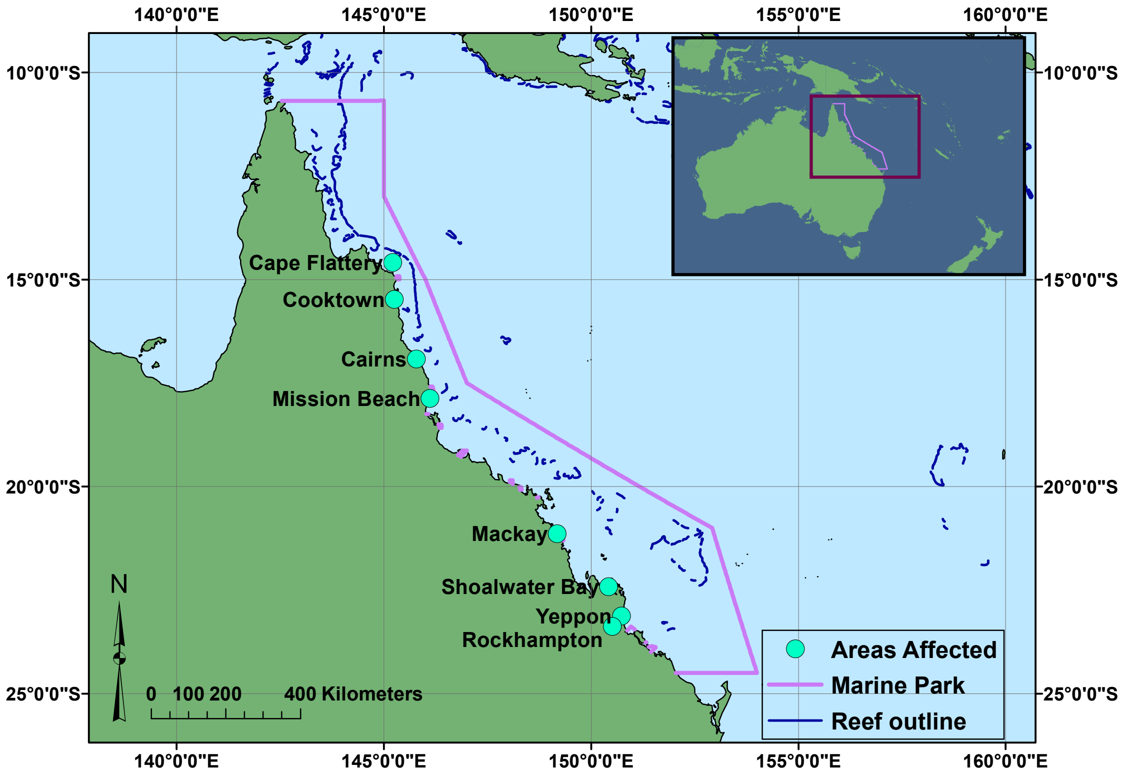

Figure 2: Map of the Queensland area showing the coastal areas affected by the cases and the neighboring Great Barrier Reef Marine Park.

Figure 3

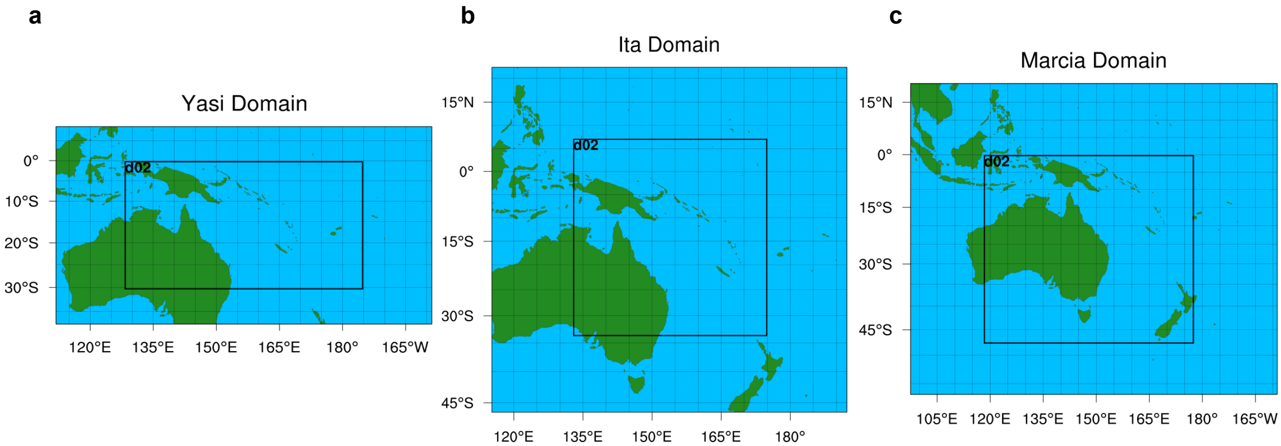

Figure 3: WRF v3.4.1 domain configuration for each of the case studies. The outer domains have 36 km horizontal grid spacing and the inner domains have 12 km (labelled d02).

Figure 4

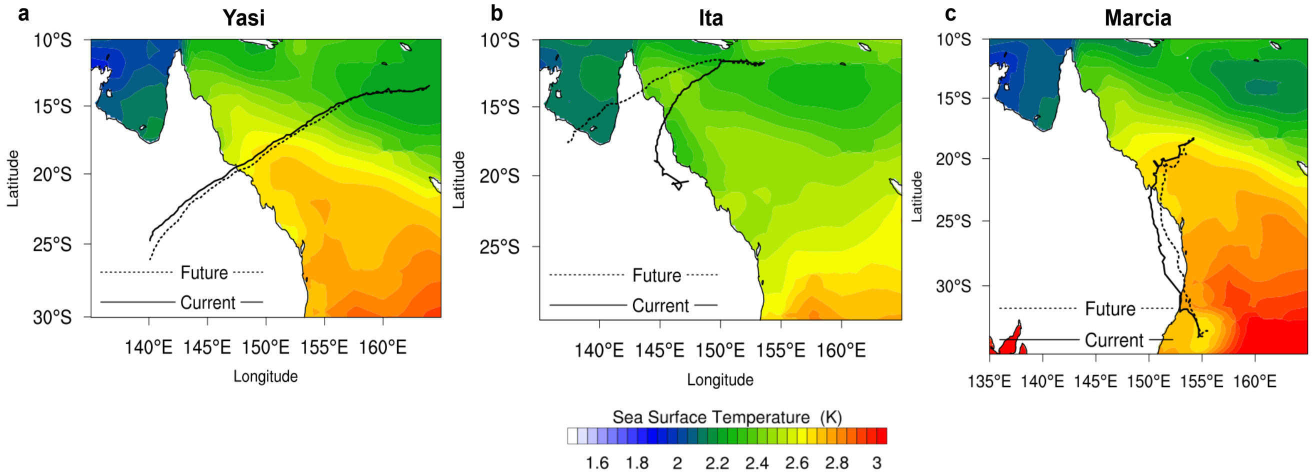

Figure 4: The a) January, b) April, and c) February monthly sea surface temperature delta (°K) component of the climate change delta added to the boundary and initial conditions of the current climate simulations to create the future climate scenario. Overlain, are the trajectories given the current climate scenario (solid line) and future climate scenario (dashed line).

Figure 5

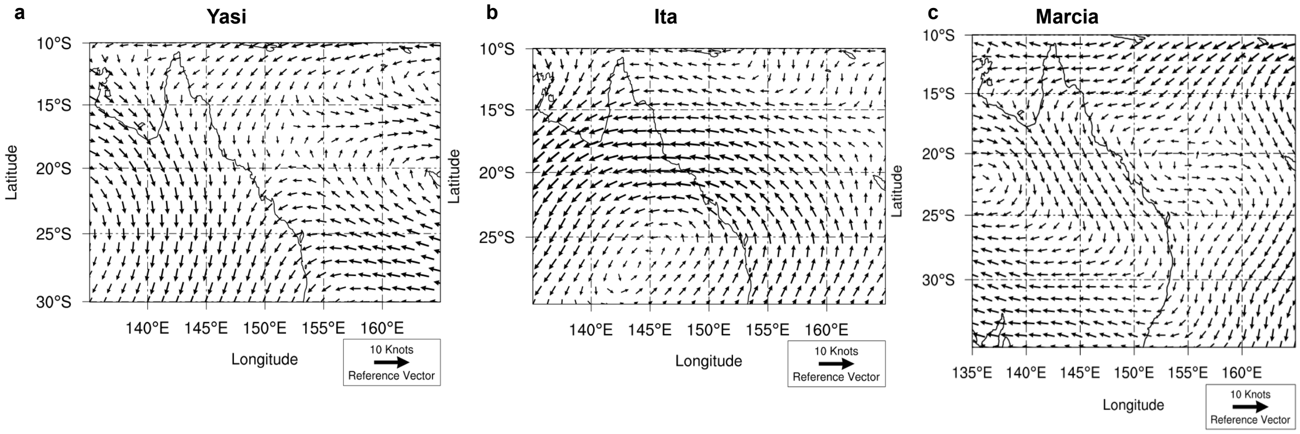

Figure 5: the a) January, b) April, c) February vectors of the 500mb wind delta calculated from CESM climatology that were added to the simulations in the future scenarios.

Figure 6

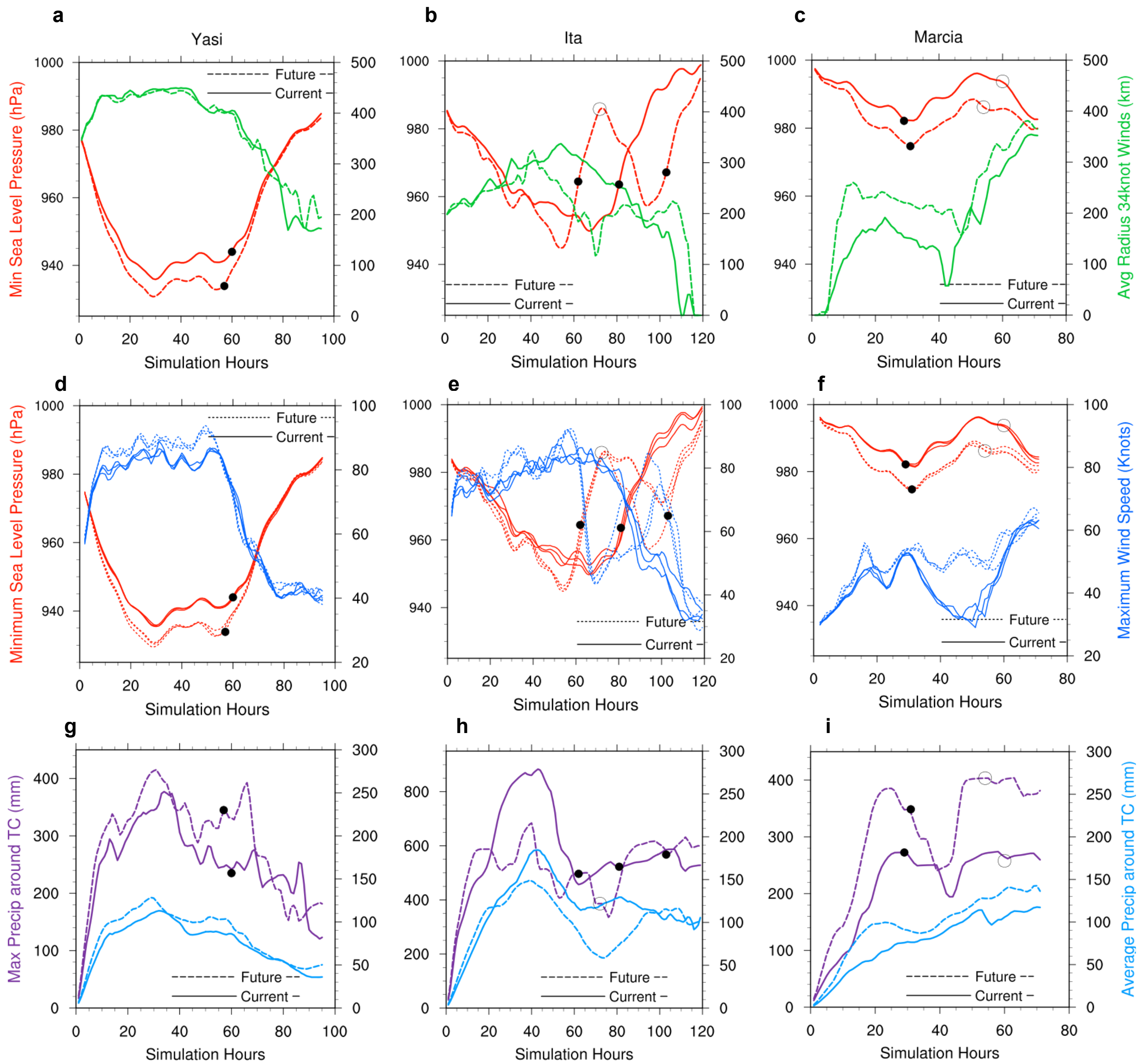

Figure 6: (a), (b), (c) the SLP (red) and average radius of 34 knot winds in all four quadrants of the storm (green) evolution given the current climate (solid line) and future climate (dashed lines). (d), (e), (f) the SLP (red) and wind speed change (blue). Each case study is run in each scenario three times with differing initial conditions produced by running DFI for different lengths of time. (g), (h), (i) the average (cyan) and maximum

(purple) recorded rainfall (mm) in a 480 x 480 km box around the eye through the simulation given current climate (solid line) and future climate (dashed line). The filled markers denote the time of landfall for each simulation, and the open marker (where present) shows when the system returned to the ocean.

Figure 7

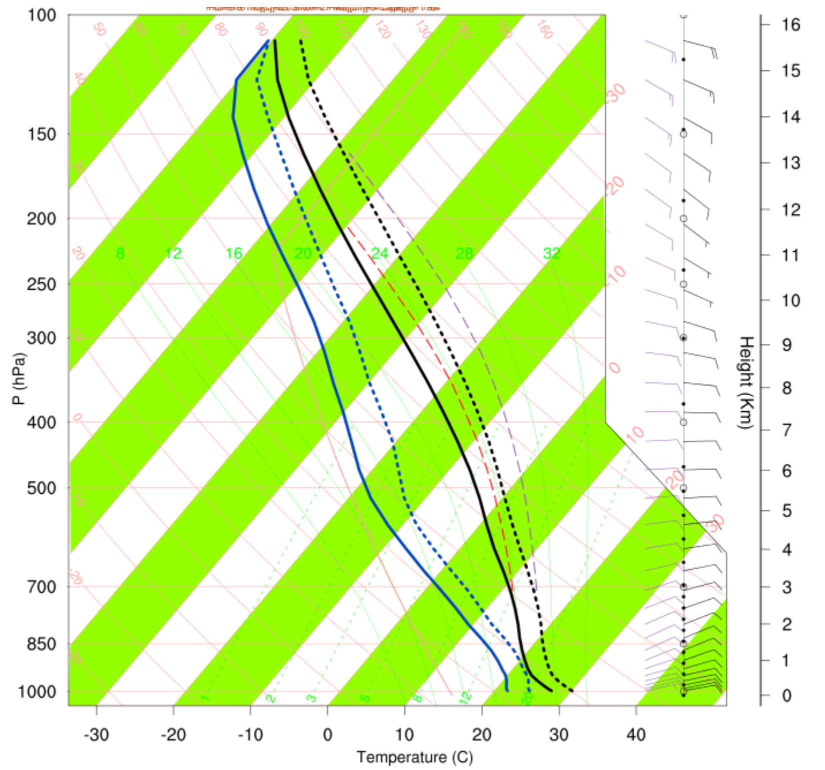

Figure 7: The environmental vertical profile of the air temperature (black), dew point (blue), convective available potential energy (CAPE red and grey dashed lines), and wind speed (barbs) averaged over the inner domain at the first-time step of the simulation for Yasi. The current climate temperatures are solid lines; the future are dotted lines. The current climate CAPE is the area under the red dashed line, future CAPE is the area under the grey dashed line. The current climate wind speed is given in black barbs and future in grey barbs.

CHAPTER FOUR

TROPICAL CYCLONES, CLIMATE CHANGE, AND THE GREAT BARRIER REEF: A SYNTHESIS

CHELSEA L. PARKER[1,2*]

[1]*Department of Earth, Environmental, and Planetary Sciences, Brown University, Providence RI 02912*

[2]*Institute at Brown for Environment and Society, Providence RI 02912*

1. Introduction

As coastal development and population density have increased, so too has vulnerability to Tropical Cyclones (TCs) (Henderson-Sellers et al. 1998). TCs are associated with significant monetary losses from damages to infrastructure, agricultural, and ecosystems as well as significant losses of life. TCs are natural but powerful phenomena. As low pressure systems, their development, intensification, and maintenance are driven by the convergence of warm, moist air from the ocean surface, expansional cooling, and latent heat release (Emanuel 1991; Walsh et al. 2016). Therefore, it is thought that potential changes to the global climate (oceanic and atmospheric warming) from anthropogenic forcing could induce a response in various TC characteristics, affecting their intensity and potential to cause harm to both human communities and natural ecosystems.

There is a large body of work exploring how TCs will respond to climate change using a variety of methods from statistical to dynamical analyses, and regional to global numerical modeling. However, the scientific community has yet to reach a consensus on many aspects of how TCs will respond to climate change. TC parameters have been found to respond differently to the same climate change forcings across different ocean basins and TC categories. Exploring TC response to future climate has been confounded by the implicit assumptions, difficulties, and errors in forecasting techniques.

The primary assumption in this work is the prediction of future emission pathways and the resultant global radiative forcing. Moreover, a number of uncertainties are introduced through the use of models as a tool. Although sophisticated, global and regional numerical models are still approximations of the real world, with many inherent assumptions and simplifications, resulting in a wide range of climatological responses to an identical forcing. A major source of uncertainty is introduced through physical parameterizations in the models, such as cumulus parameterization (e.g. Murakami et al. 2014). In analyzing results from such models, there are assumptions that the interactions, feedbacks and responses of the climate system to forcings are accurately represented. Determining whether to use an ensemble mean prediction of the future climate or favor certain models over others may introduce bias and uncertainties.

Additionally, though model resolution has greatly improved over recent decades, it is still a barrier for comprehensive TC simulation and analysis (Murakami et al. 2014). The resolutions of general circulation models (GCMs) to date (from ~100 to 300 km for the CMIP5 models down to ~50 km for the new generation of high-resolution models [Walsh et al. 2016]) have been relatively too low to accurately resolve the short-term variability of individual TC systems. Long time-scale simulations are computationally intensive and can present an initial condition problem for TC simulation and a boundary condition problem due to drift. The finer horizontal grid resolution of regional models increases the ability to accurately simulate TC-scale characteristic response to climate change. However, regional models require initial and boundary conditions (typically from coarse resolution data e.g. GCMs or reanalysis data) which can introduce error into the simulation and uncertainty to the outcome. Therefore, estimations of error and bias need to be taken into account when analyzing model predictions which leads to doubt in the results.

Finally, GCMs not only vary in their prediction of the large-scale environment, but also in the spatial distribution and gradients of changes to variables such as sea surface temperatures (SSTs) which will affect TC future potential intensity (Emanuel 2005; Walsh et al. 2016). GCMs also differ in their predictions of the changes to oscillations such as the El Niño Southern Oscillation (ENSO) in the future climate (Walsh et al. 2016). There is currently no consensus on the future mean state of the Pacific or the timing and frequency of ENSO oscillations about the mean (Hoerling and Kumar 2003). ENSO variability is an important control on TC genesis, frequency, and intensity in the South Pacific but also in other basins such as the Atlantic through teleconnections (Nguyen and Walsh 2001; Walsh 2004).

The scientific literature has been primarily focussed on global average studies or regional studies of the North Atlantic and the North Pacific. The body of evidence demonstrating the response of TCs to climate change in the western South Pacific and the northeast of Australia is relatively small. This discussion synthesizes the current knowledge and understanding (including findings from the author) of the ways in which TCs will respond to predicted climate change in the western South Pacific and Australia region and what implications these changes will have on the Great Barrier Reef (GBR).

2. Tropical Cyclone Intensity

Under climate change conditions, mean and maximum TC intensity may increase on the order of 5%/°C of global warming (Emanuel 2000; Knutson et al. 2010). Studies in the literature have established a theoretical understanding of TC intensity, the maximum potential intensity (MPI) theory (e.g. Holland 1997; Emanuel et al. 2004). A TC maximum potential intensity (MPI) can be calculated from the change to the SSTs and thus the energy available in the atmosphere for TC intensification through the latent heat engine mechanism (Emanuel 1991; Walsh et al. 2016). Given a 3-4°C increase in SSTs, we could expect a 20-40hPa decrease in the central pressure and ~15-25% increase in wind speeds (Walsh and Ryan 2000). While studies demonstrate that simulated systems do intensify in response to climate change, they usually fail to reach the predicted intensity change (e.g. Walsh and Ryan 2000). Walsh and Ryan (2000) found up to 13% increase in wind speed of the most intense systems with 2xCO_2 forcing. Parker et al. (2017a) found on average a ~5hPa and a 12hPa maximum decrease in central pressure over the lifecycle of TC systems by 2070-2100 with ~2.5xCO_2 forcing (predicted by the Representative Concentration Pathway 8.5, [Riahi et al. 2011]). This corresponded to an average increase in maximum wind speeds of 5-10% but a maximum of 30% increase was found for a TC system that was smaller and weaker in the current climate. Dynamical changes in the future environment such as vertical wind shear may limit the ability of the storms to reach the MPI in response to the thermodynamic changes (Walsh and Ryan 2000; Walsh 2004). Furthermore, some studies suggest that future ocean surface warming may be dampened in the South Pacific compared to the global average (Knutson et al. 2010; Vecchi and Wittenberg 2010). Therefore, the increase in TC MPI would be dampened.

Increases in TC-induced storm surges with climate change may be caused by a combination of sea level rise and increases in TC intensity (specifically wind speeds (Lin et al. 2012). McInnes et al. (2003) predicted a substantial increase in the frequency of storm surge event in the Cairns region of Australia with future sea level rise, which is exacerbated when considering an increase in TC intensity (decrease in central pressure of 10hPa ±5hPa). Even with no change to TC characteristics such as intensity, the TC-associated storm surge would still increase with sea level rise (Knutson et al. 2010; Walsh et al. 2016) and coastal environments need to plan to mitigate these effects.

Increasing TC-associated rainfall rates is also a robust prediction of the response to climate change in numerical models concurrent with increasing intensity (Christensen et al. 2013; Villarini et al. 2014; Scoccimarro et al. 2014). Projected increases in TC rainfall typically range from 5 to 25%, although results can vary somewhat between different TC basins (Knutson et al. 2015). Walsh and Ryan (2000) calculated an increase of 25% in the peak TC-precipitation in Australia by 2050 and Nguyen and Walsh (2001) a 2-fold increase in positive TC-rainfall anomalies off the NE coast of Australia by 2061-2090. Parker et al. (2017a) found that precipitation change with climate change by 2070-2100 was dependent on the TC case. On average, rainfall increases by ~15% in a large area around the eye of a large, intense TC, in agreement with the literature. However, the average increases for smaller, weaker TC systems are over 30%, and the percentage change for maximum values was even greater. Precise quantitative changes depend on the details of the TC precipitation metric chosen between studies. Nonetheless, an increase in storm-relative rainfall rates in a warmer climate is a confident prediction of the effects of future climate on TCs (Knutson et al. 2010) given the predicted increase in water-vapor content of the tropical atmosphere (Allen and Ingram 2002; Held and Soden 2006).

2.1 Implications for the Great Barrier Reef

Spanning 350,000 km^2 in area and extending more than 2,300 km along Australia's northeastern coast, the Great Barrier Reef Marine Park (GBR) encompasses the world's largest coral reef ecosystem (Stoeckl et al. 2011; Great Barrier Reef Marine Park Authority 2017). The location and extent of the GBR are demonstrated in Figure 1. The park is home to over 3000 coral reefs and 1600 fish species, and was added to the World Heritage List in 1981. The GBR annually generates approximately AUS$5.7 billion and 69,000 full-time-equivalent jobs for Australia's economy (Deloitte Access Economics 2013). Despite protection efforts, the GBR is still subject to many local- and global-scale stressors associated with a myriad of negative impacts and long-term consequences. TCs that cross the GBR are a local scale disturbance that can damage the reef ecosystems through primary mechanisms such as coral breakage or secondary effects such as reduced water quality.

Waves from TC winds directly affect the density, structure and local distribution of coral assemblages through damage and dislodgement (Massel and Done 1993). Damage can range from minor breakage of individual coral colonies, to coral dislodgement from the reef substratum, to stripping all living coral off entire reef slopes (Puotinen et al. 1997; Puotinen 2007). Mechanical damage is governed by the magnitude and duration of high-energy wind and waves (Puotinen 2007). Increases in TC average and maximum wind speeds with climate change would therefore increase the wave and kinetic energy available for mechanical damage of coral assemblages. Soft coral species (e.g. Acropora sp.), tall, complex hard coral species (e.g. Staghorn corals) (Souter et al. 2010), and species not attached to firm substrate (Massel and Done 1993) are most susceptible to damage or dislodgement. Furthermore, mortality from wave damage is greatest for coral assemblages at shallow depths (3m) (Massel and Done 1993; Puotinen 2007). Therefore, TCs in the future climate could result not only in reduced total coral cover but also a decrease in species richness and a shift in species composition to mostly massive corals (e.g. Porites sp.) firmly attached to the substrate at depths greater than 3m. Systems with this composition would support a reduced fish density and biodiversity. Fabricius et al. (2008) predicted that an increase in TC intensity by half a category would result in a 50-60% greater reduction in coral cover compared to present day effects. A 10% increase in maximum wind speeds of TCs with climate change (Parker et al. 2017a) would shift TCs a half to a whole category higher by 2070-2100, implying a 50-120% greater resultant reduction in coral cover (Fabricius et al. 2008).

TC-associated wind speed increase may also increase the resuspension of benthic substrates in the water column (Marra et al. 1990; Larcombe and Carter 2004; Wolanksi et al. 2005) with an associated pulse of nutrients to the surface from reef pore water (Furnas 1989). These nutrients and sediments could reduce water quality and facilitate phytoplankton blooms outcompeting benthic coral organisms (Parker et al. 2017b). Chlorophyll *a* concentrations are commonly used as a proxy for water quality in the GBR (Brodie and Furnas 1994; Brodie et al. 1997, 2007; Furnas and Brodie 1996; Steven et al. 1998). Given the relationships found between water quality and TC characteristics by

Parker et al. (2017b), a 10% increase in maximum wind speeds of intense TCs with climate change (Parker et al. 2017a) could result in ~19-24% increase the minimum and background chlorophyll *a* concentrations (Parker et al. 2017b), suggesting a reduced water quality in the future climate (see Figure 2).

In the current literature, we have the highest confidence in the predicted future increases in TC-associated rainfall and storm surge. High volumes of rainfall decrease the salinity of the water column, resulting in salinity-induced stress for the organisms adapted to 35ppt salinity (Smith and Buddermeier, 1992). Ultimately, reduced salinity disrupts the crucial zooxanthellae-coral host relationship and causes coral bleaching and die-off in the reef ecosystems (Smith and Buddermeier, 1992, Sweatman et al., 2007). With robust predictions of increases in TC-associated rainfall in the future climate, an increase in salinity stress and rainfall related bleaching is expected.

Heavy rainfall also results in large river discharges and runoff from the GBR catchment into the lagoon, resulting in high concentrations of nutrients and sediment loads to the GBR (Davies and Eyre 2005; Mitchell et al. 2005; Stieglitz 2005; Hoegh-Guldberg et al. 2011; Brodie 2012b) and an associated reduction in water quality (Parker et al. 2017b). Poor water quality can inhibit photosynthesis in the benthic coral organisms (Devlin and Schaffelke 2009), decrease calcification rates (Devlin and Schaffelke 2009), increase competition between surface photosynthetic organisms and typical benthic reef producers and builders below [Fraser and Currie 1996; Furnas et al. 2005; Brodie et al. 2010]), and can cause smothering leading to coral bleaching and mortality (Anthony and Fabricius 2000; Fabricius and Wolanski 2000). With increasing rainfall rates related to climate change, runoff and river discharge will increase, resulting in greater reduction in water quality. A 25% increase in precipitation associated with intense TCs (Walsh and Ryan 2000) could result in a 15-20% increase in the maximum values of chlorophyll *a* over the GBR (Parker et al. 2017b) during times of TC activity in the future climate (Figure 3), indicating more extreme decreases in water quality.

Storm surge is often considered the most damaging aspect of TCs (Walsh 2004) particularly for coastal infrastructure and communities (McInnes et al. 2002; 2003). With increasing TC-associated storm surge with climate change, coastal inundation (McInnes et al. 2002; 2003) and coastal erosion will increase. The retreat of coastal flood waters and the coastal erosion would provide increased sediment and nutrient loading to the reef lagoon and reduce water quality as described above.

3. Tropical Cyclone Size

Several studies have concluded that TC-induced damages are correlated with size and translation speed, not simply intensity (wind speed) alone (Puotinen 2007; Czajkowski and Done 2014; Done et al. 2014). Predicting impacts requires explicit consideration of changes in size and translation speed with climate change. However, physical factors such as TC size are difficult to measure with confidence in the current horizontal grid spacing of global models. Furthermore, unlike for TC intensity, there is currently no theoretical understanding of how TC size responds to temperature forcing and future climate change. Therefore, the possible change to TC size with climate change is not well-documented in the literature either globally or in the Australia region. Recent work by Parker et al. (2017a) has begun to address the sensitivity of TC size to climate change. They found that while the size of large, intense TC systems was relatively insensitive to climate forcing, a smaller, weaker system increased in radius on average 40% through the TC lifecycle in the future climate. There may be a saturation point in the future climate (effectively capped by maximum potential intensity), where larger, more intense systems can only increase in size and intensity a relatively small amount before reaching this saturation (Holland and Bruyère 2013). However, smaller and weaker TCs have the capacity for a greater relative change in response to the large increase in dynamic and thermodynamic forcing with climate change (Parker et al. 2017a).

3.1 Implications for the Great Barrier Reef

Increasing the TC size would increase the area encompassed by the TC's circulation and thus the area affected by TC-associated winds, storm surge, and rainfall (which are also likely to increase as discussed in Section 2). Therefore, the total destructive capacity of the TC may increase with the size (Merrill 1984; Powel and Reinhold 2007; Knaff 2014). The area where coral breakage and dislodgement could occur will increase (Puotinen 2007). Additionally, Parker et al. (2017b) demonstrated a strong positive correlation between TC size and chlorophyll *a* (as a proxy for reduction in water quality). As TC size increases, so too does the area that nutrients and sediments are extracted from and subsequently delivered to the surface waters of the GBR. With a 40% increase in TC size of smaller systems (Parker et al. 2017a), there could be a doubling (45 to 50% increase) of the reef area where water quality is reduced (i.e an increase in the area where chlorophyll *a* exceeds a threshold of 1mg/m^3 Parker et al. 2017b) (see Figure 4). A larger reef area would then be subjected to this poorer water quality. Parker et al. 2017b also demonstrates a positive correlation between TC size and extreme measures of chlorophyll *a*, detrimental to reef health. As will be discussed in Section 5, the negative consequences of size increases of this magnitude may be mitigated by a decrease in the frequency of the weaker systems that are susceptible to this size increase in the future climate. Parker et al. (2017b) demonstrate that size, and the area that nutrients can be extracted from, are the most important TC characteristics in determining the changes in water quality over the reef. However, the future changes to the characteristic of TC size are among the most uncertain in the literature.

4. Tropical Cyclone Genesis Location, Trajectory, and Translation Speed

Walsh (2004) discussed that genesis regions in the southwest Pacific are unlikely to change. The minimum SST or threshold temperature required for development of deep convection (that is necessary for TC formation) may increase (Dutton et al. 2000; Johnson and Xie 2010; Walsh et al. 2012, Evans and Waters 2012) given the greater stability in the tropical atmosphere in the future climate. Therefore, there may be no geographical expansion of area undergoing deep convection and TC genesis unless there are large-scale changes in ENSO (Walsh 2004). However, numerical simulations in some studies found a poleward shift in genesis region in the southwest Pacific (Nguyen and Walsh 2001; Leslie et al. 2007; Lavender and Walsh 2011). Specifically, Leslie et al. (2007) found a poleward shift of over 2° for the genesis region. A poleward shift can be attributed to changes in vertical velocity and relative vorticity associated with a weakening of tropical circulation in the future climate (Lavender and Walsh 2011). Therefore, a poleward shift in genesis region is possible with climate change.

There are also varied predictions of the response of TC trajectories to climate change forcing. Walsh and Katzfey (2000) simulated poleward extension of trajectories (south of 15°S) in eastern Australia given a warmer environment, and Lavender and Walsh (2011) found a poleward shift in the zone of dissipation, demonstrating that trajectories reach further south. Nguyen and Walsh (2001) also found a slight increase in the occurrence of TCs at latitudes greater than 30°S and the average latitude for TC occurrence shifts 0.9° poleward in a 3xCO_2 environment. A poleward shift in trajectory may be caused by a combination of increased SSTs and evaporation rates at higher latitudes, and more southward and less eastward steering winds in the future climate (Walsh and Katzfey 2000). Instrumental records have demonstrated that SSTs along the northeast coast of Australia have increased 0.12°C per decade since 1950 in the region of 10.5° to 29.5°S, with greater warming in the higher latitudes than the lower (Lough 2008). Models suggest that with an intensifying East Australian Current, this warming pattern along the Eastern coastline will continue with climate change (Cai et al. 2005, Cai 2006). Northern SSTs could be 0.5°C and southern SSTs 1.5-2°C warmer along the coastline within the next 100 years (Lough 2008). Walsh et al. 2004 found an increase in TC occurrence further south than 25°S but could not conclude that there was significant evidence for a poleward shift in trajectory in this region in response to greenhouse conditions. Some studies have conversely predicted greater SST warming along the equator compared to further poleward, (Collins et al. 2010) which would suggest an equatorward shift in the TC formation and trajectory (Oouchi et al. 2006).

Most recently, Parker et al. (2017a) found a variation in response of the TC trajectories that was primarily dependent on the change to the environmental steering flow with climate change (and not SSTs). Cases early in the TC season (January and February) were steered further poleward with the future climate perturbation (supporting results of Walsh and Katzfey 2000). However, a TC from later in the season (April), encountered a different change in the predominant environmental wind field and was steered equatorward to make landfall ~4° further north. Therefore, there is currently a lack of consensus and understanding in the literature of how TC trajectory will respond to climate change in the southwestern Pacific. To address trajectory changes we need greater certainty in the predicted changes to SST and wind steering patterns in this basin.

As discussed in Section 3, TC-related damages can be attributed to TC translation speed as well as other TC characteristics. Observations suggest that annual storm duration and average storm peak wind speed may have increased in recent history in the North Atlantic and North Pacific (by up to 60% and 50% respectively, Emanuel 2005). Theoretically stronger storms may take longer to reach greater peak winds and longer to dissipate, therefore stronger storms may last longer (Emanuel, 2005). However, Walsh and Katzfey (2000) conjectured that the change to steering winds may cause Australian systems to track polewards at a greater speed, therefore leading to a reduction in lifecycle duration. As with TC size, the response of TC translation speed to climate change has not been explored in great detail in the literature.

Recent work by Parker et al. (2017a) demonstrates that the translation speeds of the TC cases early in the TC season (storms that tracked further poleward) were relatively insensitive to climate change perturbation. However, a TC developing late in the season (April) tracked further equatorward and had an average increase in translation speed of 25% and a shortened duration. This alteration was attributed to the change in steering winds with climate forcing. This finding supports the theoretical conjecture of increasing translation speed and shortened duration (Walsh and Katzfey 2000). More extensive work is needed to address the possible changes to TC duration and translation speed in the western South Pacific. In particular, there needs to be an increase in the confidence of the projected changes to the environmental steering flows.

4.1 Implications for the Great Barrier Reef

The uncertainty surrounding the predictions of the geographical response of TC genesis location and trajectory to climate change inherently results in uncertainty for the implications to the reef environment. If there is a poleward shift in genesis location and trajectories in the future climate, then TC will tend to affect reefs communities towards the south of the GBR, including areas that may currently have little interaction with TCs (e.g. reefs at 25°S or greater). The population density is greater in Southern Queensland, therefore there may be increased pollutant concentrations leached and loaded into the reef lagoon during the TC-associated precipitation and storm surge of the systems tracking towards this area (see Figure 1). Water quality may therefore be reduced further through the mechanisms described in Section 2.1.

The change in risk associated with a change in translation speed is complex. An increased translation speed may decrease the risk of damage to the reef as the exposure time to TC-conditions, such as strong winds, would decrease (Puotinen 2007). However, increases to translation speed may increase the ground-relative wind speeds (Shapiro 1983) experienced by the reef ecosystems, and therefore heighten the maximum wave energy and the risk of breakage and dislodgement. While it has been suggested that increasing the translation speed may reduce storm surge height and flood inundation (Peng et al. 2004; Weisberg and Zheng 2006), this relationship may be non-linear (Irish and Resio 2010). Resonance may occur for certain translation speeds (Rego and Li 2009), whereby increasing translation speed increases peak surge heights by up to 40% (Rego and Li 2009). Despite flooding a narrower section of the coast, a TC with an increased translation speed would move quickly across the shoreline potentially generating higher surges (Rego and Li 2009). Increased surge height may result in greater coastal erosion and nutrient and sediment leaching into coastal waterways (Parker et al. 2017b). A 25% increase in translation speed (Parker et al. 2017a) could result in a 13-18% increase in the maximum recorded chlorophyll *a* concentrations over the reef lagoon and thus a decrease in water quality (Parker et al. 2017b) (Figure 5). However, maximum potential rainfall associated with TC activity is often inversely proportional to the system's translation speed (Elsner and Kara 1999) and the water quality degradation may be mitigated by a decrease in the rainfall runoff and river discharge. Therefore, in the future climate, the risk of reef damage from increasing translation speed may be governed by a balance between increased ground relative wind speed, decreased duration of exposure, decreased precipitation, and increased surge height.

5. Tropical Cyclone Frequency

Studies and model simulations are beginning to reach a consensus, predicting a decrease in global frequency with a warming climate (Emanuel 2013). The extent of the decrease in TC frequency to increased greenhouse gases depends on model resolution, with finer-resolution models showing stronger decreases in TC numbers (Bell et al. 2013; Walsh et al. 2016). There remains some disagreement between models regarding frequency projections for individual basins (Walsh 2004; Knutson et al. 2010; Camargo 2013). However, a decrease in TC activity with climate change is also predicted for the Southern Hemisphere (Nguyen and Walsh 2001; Walsh et al. 2012; Walsh 2015). The prediction of decreasing mean counts in the Southern Hemisphere is more robust than for other ocean basins (Knutson et al. 2010; Murakami et al. 2012), and the overall decrease may, in fact, be augmented here compared to the global average (Sugi et al. 2012; Tory et al. 2013; Walsh et al. 2016). Predictions vary from a 5-40% reduction in TCs in the area (Walsh et al. 2012). Lavender and Walsh (2011) found a 30% decrease in the number of TCs by 2100 in the Australia region, and Walsh (2015) found a 22% decrease in TC numbers in the western South Pacific by the end of the century.

The decreasing frequency may be explained by several possible changes in the environmental variables where TCs develop: (1) an increase in tropical atmosphere stability, a slow-down in tropical circulation, and a weakening Walker Circulation (Held and Soden 2006), making it more difficult for storms to develop (Sugi et al. 2002). This is caused by increasing saturation deficit in the free troposphere (Emanuel 2013). (2) Drying in the middle troposphere with climate change leading to a decrease in TC formation (Emanuel et al. 2008). (3) An increase in vertical velocity in the equatorial Pacific, leading to compensating subsidence in the adjacent TC formation regions of the South Pacific, resulting in TC formation suppression (Walsh 2015). (4) Increasing vertical shear of horizontal winds and so inhibition of TC formation (Nguyen and Walsh 2001; Emanuel 2013). Mechanism (1) is predicted by most models (Walsh et al. 2012) and is likely the cause of the robust prediction of frequency decrease. The relative SST hypothesis may also be important in determining future TC rates. Upper tropospheric temperatures reflect average tropical SSTs leading to a stable atmosphere. However, local SST changes may lead to local changes in stability. Local changes may therefore have a greater influence over TC formation rates (Vecchi and Soden 2007) than the average tropical SSTs.

The number of very strong TCs is more important for estimating damage or risk than measures such as mean intensity or total TC numbers (Christensen et al. 2013). With climate change, there may be an increase in the number of intense TC systems both globally and in the western South Pacific (Knutson et al. 2010; Emanuel 2013; Holland and Bruyère 2013) with a potential doubling of Category 4-5 systems for each 1°C of global warming (Bender et al. 2010; Done et al. 2012). Leslie et al. (2007) simulated a 22% increase in the most intense (Category 3-5) TCs in the southwest Pacific by 2050. Lavender and Walsh (2011) found an increase in the percentage of the most intense TCs in the Australia region balanced by decreases in the percentage of mid-intensity systems. Numerical simulations by Walsh et al. (2004) suggest up to a 56% increase in TC numbers with maximum wind speeds over 30 m/s and a 26% increase in number of storms with central pressures under 970hPa. TC formation may be suppressed by changes to the environment as discussed above, resulting in a decline in overall frequency. However, if conditions are sufficient to enable the genesis of a system, the TC can reach a greater intensity in the future climate as discussed in Section 2. Interestingly, Leslie et al. (2007) found that the number of intense TCs double in the last two months of the season with enhanced GHGs. This may be important given that Parker et al. (2017a) demonstrated that environmental forcings with climate change vary through the season and ultimately affect the TC response. Possible temporal variations in frequency changes need to be addressed in greater detail.

5.1 Interaction with the Great Barrier Reef

With the predicted decrease in overall TC frequency with climate change, the return period of TC disturbance on reef environments would be reduced. This would increase the recovery time between events and increase ecosystem resilience. However, observations demonstrate that TC damage increases non-linearly with intensity (Pielke and Landsea 1998). Power dissipation and damage have been calculated to increase with the cube of wind speed (Emanuel 2005). Therefore, the negative consequences to reef environments discussed in Section 2.1 are likely to increase in the future climate through a combination of increased TC maximum intensity and wind speed when they are able to develop (Section 2) and an increase in frequency of the most intense systems (Section 5).

Coral reef ecosystems naturally have resilience to natural stressors such as TCs. A monitoring study demonstrated that after a storm event in 1988 that reduced coral cover from 80 to 10% on a shallow reef in the southern GBR, the coral community was able to recover to pre-storm levels in ~10 years (Halford et al. 2004). However, the resistance and resilience of the GBR has already been and will continue to be reduced by global stresses such as increasing oceanic temperatures, ocean acidification, and sea level rise, as well as local stresses such as overfishing, dredging, and degraded water quality (Hoegh-Guldberg et al. 2007; Hughes et al. 2015) and intense TCs may occur more frequently.

Increased re-occurrence of TC-induced damage and dislodgement and long-lasting episodes of degraded water quality over the reef in addition to other stressors, can reduce total coral cover, coral species richness (Fabricius and De'ath 2004; Fabricius 2005), and reef rugosity (Hoegh-Guldberg et al. 2007). Fish density and biodiversity will subsequently decrease (Hoegh-Guldberg et al. 2007). With reduced resilience and more frequent and destructive intense events, coral cover will rebound more slowly and competitive interactions with macroalgae will increase in frequency and duration (Hoegh-Guldberg et al. 2007). Eventually, reefs may reach a tipping point and shift from a coral-dominated to a macroalgal-dominated ecosystem (Fabricius and De'ath 2004; Hoegh-Guldberg et al. 2007; Devlin and Schaffelke 2009; Brodie et al. 2010). This phase shift can cause further mortality of corals and reef organisms (McClanahan et al. 2005; Smith et al. 2006) and would no longer support high biodiversity or provide the same ecosystem services. The new state would have its own resilience and stability inhibiting the re-establishment of a coral-state community (Hoegh-Guldberg et al. 2007). Furthermore, resilience to future disturbances and stressors can be further reduced following this phase shift (Lapointe 1997; McCook 1999), creating a negative feedback effect.

Reef building corals have long generation times and low genetic diversity, leading to very slow adaptation rates (Hoegh-Guldberg et al. 2007). It is thought that coral reef environments will not be able to adapt at the rate of climatic change to shift to geographic regions out of the path of TC activity or to areas with reduced thermal stress (Hoegh-Guldberg et al. 2007; Poloczanska et al. 2007).

6. Concluding Remarks and Future Work

There is growing confidence in modeled responses of tropical cyclone (TC) characteristics to climate change in the western South Pacific. It is likely that total TC frequency will decrease, but the number of intense TCs will increase. Furthermore, the maximum TC intensity (sea level pressure and wind speed) of those that do occur will increase. However, the intensity increase may not reach the maximum potential due to increased wind shear. TC-associated precipitation and storm surge are also likely to increase significantly with climate change. These changes to TC frequency and intensity will increase damage to reef areas through amplified breakage and dislodgement, as well as reductions in water quality driven primarily through storm surge and rainfall runoff and river discharge. With these local disturbances in addition to anthropogenic-induced stresses including rising ocean temperatures and acidification, overfishing, and dredging, reef resilience will decline, potentially to the point of phase shifts to macro-algal dominated communities. Furthermore, there are concerns that water quality reduction over the GBR with climate change may be further exacerbated by increasing coastal population density, land use change, and more intensive agriculture and fossil fuel industry (Hughes et al. 2015).

There is growing evidence for a number of other responses in TC characteristics with climate change, with the potential for significant implications for the local ecosystems. However, there is still uncertainty associated with these predictions. Smaller and weaker systems may be highly sensitive to future climate forcing, resulting in increases in size. Size is the dominant cause of TC-related water quality degradation, however there is a lack of theoretical understanding in how TC size will respond to climate change perturbation. There is also the potential for TC translation speed to increase, but this is governed by the predominant steering flow and may be dependent on the timing of the TC in the season. Furthermore, studies suggest a poleward shift in both genesis location and trajectory, which would shift the risk of disturbance to reefs to the south of the Great Barrier Reef. However, there have been disparate findings where trajectories shift equatorward. These inconsistencies in predictions arise primarily from differences in the SSTs and steering flow fields in the models.

It remains a priority to reduce the uncertainties in the 21st Century projections of the mean magnitude and patterns of change of regional SST patterns and environmental steering flow. There is also a need to improve predictions of the ENSO which exerts control over TC genesis region, trajectory, and frequency in the western South Pacific. Parker et al. (2017a) have demonstrated that a case study and climate change downscaling approach is appropriate for exploring the unique responses of TC characteristics to climate change. However, a larger number of cases need to be tested in this way with a wider range of climate forcings to begin to discern the patterns and outliers of the responses to climate change.

It is important for the scientific community to reach a consensus on future trends for mitigation and planning purposes for coastal communities and ecosystems. Additionally, TC activity may play an important role in oceanic thermohaline circulation, with important feedbacks to the regional and global climate (Emanuel 2001). The estimates of TC-induced transport response are still uncertain (Bueti et al. 2014), but TCs may account for a significant fraction of the ocean poleward heat flux (Emanuel 2001). The fraction could potentially be up to 15% (Sriver and Huber 2007) and may increase with increasing TC intensity in the future climate. However, and the effect is complicated and highly sensitive to SST patterns (Emanuel 2001; Sriver and Huber 2007) and will be similarly sensitive to the SST patterns in the future climate.

While TCs and increases in ocean temperature and acidification cannot be prevented locally, agencies and communities can reduce local pressures in order to assist reef resistance and resilience against the stressors that cannot be controlled. Several studies have stated that local pressures need to be reduced or eradicated to improve reef resilience for its long-term survival (Folke et al. 2004; Great Barrier Reef Marine Park Authority 2014; Hughes et al. 2015). Areas that are highly prone to TCs may be targeted for protection from human pressures that can be mitigated, such as overfishing (Puotinen 2007). The Queensland Government should continue to improve reef water quality over the GBR by reducing runoff, erosion, fertiliser loss, and nutrient and sediment leaching into the lagoon from coastal lands through programs such as the Reef Water Quality

Protection Plan (Department of Premiers and Cabinet 2013a) and the Paddock to Reef program (Department of Premiers and Cabinet 2013b). Urban and agricultural areas in catchments that drain into the GBR lagoon will need to be particularly vigilant in reducing leaching as urbanization and agricultural intensification continue. Substantial buffer zones should be created to reduce this leaching. If TC trajectories do track further south and ocean temperature increase is comparatively greater at higher latitudes, it may also be prudent to focus protection on northern reefs which may have a greater chance of survival (Lough 2008).

Parker et al. (2017b) found that TC-associated river discharge, and rainfall and storm surge runoff likely dominate over wind mixing and resuspension in deteriorating water quality over the GBR. However, detailed work with a larger dataset, storm surge height data, and stream gauge data still needs to be carried out to further assess the mechanisms of TC-induced water quality reduction. With a better understanding of the mechanism, predictions for future water quality reduction over the reef with climate change will be more robust. Future work could also quantify the time taken for nutrient and sediment loading to enter the reef lagoon after a TC disturbance and the most vulnerable zones. This information could aid mitigation efforts that reduce runoff and leaching such as the extent and location of buffer zone development.

This discussion has focussed on the response of TCs to climate change in the western South Pacific, and the implications to the Great Barrier Reef. While the predicted TC response to climate change varies between ocean basins (Walsh et al. 2016), there is similar growing evidence for an increase in maximum intensity (Sugi et al. 2009; Bell et al. 2013; Emanuel 2013) and increasing frequency of the most intense systems in the Atlantic and North Pacific (Bender et al. 2010; Knutson et al. 2010; Holland and Bruyère 2013). TCs in these regions can affect coral reef environments, such as the reefs found in the Caribbean and the South China Sea. Many of these reefs also neighbor large coastal populations and suffer from local anthropogenic stresses such as over fishing and poor water quality. In some areas, the interaction between TC activity and anthropogenic stressors has led to more widespread damage than experienced by the Great Barrier Reef (e.g. Caribbean reefs [Hughes 1994; Gardner et al. 2005; Mumby et al. 2007]). Therefore, the discussion here could be applicable to other reef areas and help to target future research and management strategies.

7. References

Allen, M. R., & Ingram, W. J. (2002). Constraints on future changes in climate and the hydrologic cycle. Nature, 419(6903), 224-232.

Anthony, K. R., & Fabricius, K. E. (2000). Shifting roles of heterotrophy and autotrophy in coral energetics under varying turbidity. Journal of experimental marine biology and ecology, 252(2), 221-253.

Bell, R., Strachan, J., Vidale, P. L., Hodges, K., & Roberts, M. (2013). Response of tropical cyclones to idealized climate change experiments in a global high-resolution coupled general circulation model. Journal of Climate, 26(20), 7966-7980.

Bender, M. A., Knutson, T. R., Tuleya, R. E., Sirutis, J. J., Vecchi, G. A., Garner, S. T., & Held, I. M. (2010). Modeled impact of anthropogenic warming on the frequency of intense Atlantic hurricanes. Science, 327(5964), 454-458.

Brodie, J. E., Kroon, F. J., Schaffelke, B., Wolanski, E. C., Lewis, S. E., Devlin, M. J., ... & Davis, A. M. (2012). Terrestrial pollutant runoff to the Great Barrier Reef: an update of issues, priorities and management responses. Marine Pollution Bulletin, 65(4), 81-100.

Brodie, J. J., Furnas, M. M., Stevens, A., Trott, L. L., Pantus, F. F., & Wright, M. M. (1997, January). Monitoring chlorophyll in the Great Barrier Reef lagoon: trends and variability. In Proceedings of the 8th International Coral Reef Symposium, Panama, 24-29 June 1996-pages: 1: 797-802. Smithsonian Tropical Research Institute.

Brodie, J., & Furnas, M. (1994). Long term monitoring programs for eutrophication and the design of a monitoring program for the Great Barrier Reef. In Proceedings of the 7th International Coral Reef Symposium (Vol. 1, pp. 77-84).

Brodie, J., De'Ath, G., Devlin, M., Furnas, M., & Wright, M. (2007). Spatial and temporal patterns of near-surface chlorophyll a in the Great Barrier Reef lagoon. Marine and Freshwater Research, 58(4), 342-353.

Brodie, J., Schroeder, T., Rohde, K., Faithful, J., Masters, B., Dekker, A., ... & Maughan, M. (2010). Dispersal of suspended sediments and nutrients in the Great Barrier Reef lagoon during river-discharge events: conclusions from satellite remote sensing and concurrent flood-plume sampling. Marine and Freshwater Research, 61(6), 651-664.

Bueti, M. R., Ginis, I., Rothstein, L. M., & Griffies, S. M. (2014). Tropical cyclone–induced thermocline warming and its regional and global impacts. Journal of Climate, 27(18), 6978-6999.

Cai, W. (2006). Antarctic ozone depletion causes an intensification of the Southern Ocean super-gyre circulation. Geophysical Research Letters, 33(3).

Cai, W., Shi, G., Cowan, T., Bi, D., & Ribbe, J. (2005). The response of the Southern Annular Mode, the East Australian Current, and the southern mid-latitude ocean circulation to global warming. Geophysical Research Letters, 32(23).

Camargo, S. J. (2013). Global and regional aspects of tropical cyclone activity in the CMIP5 models. Journal of Climate, 26(24), 9880-9902.

Christensen, J. H., Kanikicharla, K. K., Marshall, G., & Turner, J. (2013). Climate phenomena and their relevance for future regional climate change.

Collins, M., An, S. I., Cai, W., Ganachaud, A., Guilyardi, E., Jin, F. F., ... & Vecchi, G. (2010). The impact of global warming on the tropical Pacific Ocean and El Niño. Nature Geoscience, 3(6), 391-397.

Czajkowski, J., & Done, J. (2014). As the wind blows? Understanding hurricane damages at the local level through a case study analysis. Weather, climate, and society, 6(2), 202-217.

Davies, P. L., & Eyre, B. D. (2005). Estuarine modification of nutrient and sediment exports to the Great Barrier Reef Marine Park from the Daintree and Annan River catchments. Marine Pollution Bulletin, 51(1), 174-185.

Deloitte Access Economics (2013), Economic contribution of the Great Barrier Reef, Great Barrier Reef Marine Park Authority, Townsville.

Department of Premiers and Cabinet, (2013a). Reef Water Quality Protection Plan, 2013, For the Great Barrier Reef World Heritage Area and adjacent catchments. Queensland Department of Premiers and Cabinet. The State of Queensland and the Commonwealth of Australia. www.reefplan.qld.gov.au.

Department of Premiers and Cabinet, (2013b). Paddock to Reef Integrated Monitoring, Modelling and Reporting Program, Reef Water Quality Protection Plan, 2013-2018. Queensland Department of Premiers and Cabinet. The State of Queensland and the Commonwealth of Australia. www.reefplan.qld.gov.au.

Devlin, M., & Schaffelke, B. (2009). Spatial extent of riverine flood plumes and exposure of marine ecosystems in the Tully coastal region, Great Barrier Reef. Marine and Freshwater Research, 60(11), 1109-1122.

Done, J. M., Ge, M., Holland, G. J., & Bruyère, C. L. (2014, May). Future changes in Gulf of Mexico hurricane wave climatology. In Offshore Technology Conference. Offshore Technology Conference.

Done, J. M., Holland, G. J., Bruyère, C. L., Leung, L. R., & Suzuki-Parker, A. (2015). Modeling high-impact weather and climate: lessons from a tropical cyclone perspective. Climatic Change, 129(3-4), 381-395.

Done, T. J. (1992). Effects of tropical cyclone waves on ecological and geomorphological structures on the Great Barrier Reef. Continental Shelf Research, 12(7), 859-872.

Dutton, J. F., Poulsen, C. J., & Evans, J. L. (2000). The effect of global climate change on the regions of tropical convection in CSM1. Geophysical research letters, 27(19), 3049-3052.

Elsner, J. B., & Kara, A. B. (1999). Hurricanes of the North Atlantic: Climate and society. Oxford University Press.

Emanuel, K. (2001). Contribution of tropical cyclones to meridional heat transport by the oceans. Journal of Geophysical Research: Atmospheres, 106(D14), 14771-14781.

Emanuel, K. (2005). Increasing destructiveness of tropical cyclones over the past 30 years. Nature, 436(7051), 686-688.
Emanuel, K. A. (1991). The theory of hurricanes. Annual Review of Fluid Mechanics, 23(1), 179-196.
Emanuel, K. A. (2013). Downscaling CMIP5 climate models shows increased tropical cyclone activity over the 21st century. Proceedings of the National Academy of Sciences, 110(30), 12219-12224.
Emanuel, K., DesAutels, C., Holloway, C., & Korty, R. (2004). Environmental control of tropical cyclone intensity. Journal of the atmospheric sciences, 61(7), 843-858.
Emanuel, K., Sundararajan, R., & Williams, J. (2008). Hurricanes and global warming: Results from downscaling IPCC AR4 simulations. Bulletin of the American Meteorological Society, 89(3), 347.
Evans, J. L., & Waters, J. J. (2012). Simulated relationships between sea surface temperatures and tropical convection in climate models and their implications for tropical cyclone activity. Journal of Climate, 25(22), 7884-7895.
Fabricius, K. E. (2005). Effects of terrestrial runoff on the ecology of corals and coral reefs: review and synthesis. Marine pollution bulletin, 50(2), 125-146.
Fabricius, K. E., & De'Ath, G. (2004). Identifying ecological change and its causes: a case study on coral reefs. Ecological Applications, 14(5), 1448-1465.
Fabricius, K. E., & Wolanski, E. (2000). Rapid smothering of coral reef organisms by muddy marine snow. Estuarine, Coastal and Shelf Science, 50(1), 115-120.
Fabricius, K. E., De'Ath, G., Puotinen, M. L., Done, T., Cooper, T. F., & Burgess, S. C. (2008). Disturbance gradients on inshore and offshore coral reefs caused by a severe tropical cyclone. Limnology and Oceanography, 53(2), 690-704.
Folke, C., Carpenter, S., Walker, B., Scheffer, M., Elmqvist, T., Gunderson, L., & Holling, C. S. (2004). Regime shifts, resilience, and biodiversity in ecosystem management. Annu. Rev. Ecol. Evol. Syst., 35, 557-581.
Fraser, R. H., & Currie, D. J. (1996). The species richness-energy hypothesis in a system where historical factors are thought to prevail: coral reefs. American Naturalist, 138-159.
Furnas, M. M. (1989, January). Cyclonic disturbance and a phytoplankton bloom in a tropical shelf ecosystem. In Red Tides: Biology, Environmental Science and Toxicology. Proceedings of the First International Symposium on Red Tides held November 10-14, 1987, in Takamatsu, Kagawa Prefecture, Japan-pages: 273-276. Elsevier Science Publishing Co., Inc.
Furnas, M. M., & Brodie, J. J. (1996). Current status of nutrient levels and other water quality parameters in the Great Barrier Reef. Downstream Effects of Land Use-pages: 9-21.
Furnas, M., Mitchell, A., Skuza, M., & Brodie, J. (2005). In the other 90%: phytoplankton responses to enhanced nutrient availability in the Great Barrier Reef Lagoon. Marine pollution bulletin, 51(1), 253-265.
Gardner, T. A., Cote, I. M., Gill, J. A., Grant, A., & Watkinson, A. R. (2005). Hurricanes and Caribbean coral reefs: impacts, recovery patterns, and role in long‐term decline. Ecology, 86(1), 174-184.
Great Barrier Reef Marine Park Authority (2017). Facts About the Great Barrier Reef. [Accessed online 18 March 17] http://www.gbrmpa.gov.au/about-the-reef/facts-about-the-great-barrier-reef
Great Barrier Reef Marine Park Authority. (2014) "Great barrier reef outlook report 2014." http://elibrary.gbrmpa.gov.au/jspui/handle/11017/2855
Halford, A., Cheal, A. J., Ryan, D., & Williams, D. M. (2004). Resilience to large-scale disturbance in coral and fish assemblages on the Great Barrier Reef. Ecology, 85(7), 1892-1905.

Held, I. M., & Soden, B. J. (2006). Robust responses of the hydrological cycle to global warming. Journal of Climate, 19(21), 5686-5699.
Henderson-Sellers, A., Zhang, H., Berz, G., Emanuel, K., Gray, W., Landsea, C., ... & McGuffie, K. (1998). Tropical cyclones and global climate change: A post-IPCC assessment. Bulletin of the American Meteorological Society, 79(1), 19-38.
Hoegh-Guldberg, O., Andréfouët, S., Fabricius, K., Diaz-Pulido, G., Lough, J., Marshall, P., & Pratchett, M. S. (2011). Vulnerability of coral reefs in the tropical Pacific to climate change. Vulnerability of tropical Pacific fisheries and aquaculture to climate change. Secretariat of the Pacific Community, Noumea, 251-296.
Hoegh-Guldberg, O., Mumby, P. J., Hooten, A. J., Steneck, R. S., Greenfield, P., Gomez, E., ... & Knowlton, N. (2007). Coral reefs under rapid climate change and ocean acidification. Science, 318(5857), 1737-1742.
Hoerling, M., & Kumar, A. (2003). The perfect ocean for drought. Science, 299(5607), 691-694.
Holland, G. J. (1997). The maximum potential intensity of tropical cyclones. Journal of the atmospheric sciences, 54(21), 2519-2541.
Holland, G., & Bruyère, C. L. (2013). Recent intense hurricane response to global climate change. Climate Dynamics, 1-11.
Hughes, T. P. (1994). Catastrophes, phase shifts, and large-scale degradation of a Caribbean coral reef. Science-AAAS-Weekly Paper Edition, 265(5178), 1547-1551.
Hughes, T. P., Day, J. C., & Brodie, J. (2015). Securing the future of the Great Barrier Reef. Nature Climate Change, 5(6), 508-511.
Irish, J. L., & Resio, D. T. (2010). A hydrodynamics-based surge scale for hurricanes. Ocean Engineering, 37(1), 69-81.
Johnson, N. C., & Xie, S. P. (2010). Changes in the sea surface temperature threshold for tropical convection. Nature Geoscience, 3(12), 842-845.
Knaff, J. A., Longmore, S. P., & Molenar, D. A. (2014). An objective satellite-based tropical cyclone size climatology. Journal of Climate, 27(1), 455-476.
Knutson, T. R., McBride, J. L., Chan, J., Emanuel, K., Holland, G., Landsea, C., ... & Sugi, M. (2010). Tropical cyclones and climate change. Nature Geoscience, 3(3), 157-163.
Knutson, T. R., Sirutis, J. J., Zhao, M., Tuleya, R. E., Bender, M., Vecchi, G. A., ... & Chavas, D. (2015). Global projections of intense tropical cyclone activity for the late twenty-first century from dynamical downscaling of CMIP5/RCP4. 5 scenarios. Journal of Climate, 28(18), 7203-7224.
Lapointe, B. E. (1997). Nutrient thresholds for bottom-up control of macroalgal blooms and coral reefs. Limnol. Oceanogr, 44, 1586-1592.
Larcombe, P., & Carter, R. M. (2004). Cyclone pumping, sediment partitioning and the development of the Great Barrier Reef shelf system: a review. Quaternary Science Reviews, 23(1), 107-135.
Lavender, S. L., & Walsh, K. J. E. (2011). Dynamically downscaled simulations of Australian region tropical cyclones in current and future climates. Geophysical Research Letters, 38(10).
Leslie, L. M., Karoly, D. J., Leplastrier, M., & Buckley, B. W. (2007). Variability of tropical cyclones over the southwest Pacific Ocean using a high-resolution climate model. Meteorology and Atmospheric Physics, 97(1-4), 171-180.
Lin, N., Emanuel, K., Oppenheimer, M., & Vanmarcke, E. (2012). Physically based assessment of hurricane surge threat under climate change. Nature Climate Change, 2(6), 462-467.
Lough, J. M. (2008). Shifting climate zones for Australia's tropical marine ecosystems. Geophysical Research Letters, 35(14).
Marra, J., Bidigare, R. R., & Dickey, T. D. (1990). Nutrients and mixing, chlorophyll and phytoplankton growth. Deep Sea Research Part A. Oceanographic Research Papers, 37(1), 127-143.

Massel, S. R., & Done, T. J. (1993). Effects of cyclone waves on massive coral assemblages on the Great Barrier Reef: meteorology, hydrodynamics and demography. Coral Reefs, 12(3-4), 153-166.

McClanahan, T. R., Steneck, R. S., Pietri, D., Cokos, B., & Jones, S. (2005). Interaction between inorganic nutrients and organic matter in controlling coral reef communities in Glovers Reef Belize. Marine Pollution Bulletin, 50(5), 566-575.

McCook, L. J. (1999). Macroalgae, nutrients and phase shifts on coral reefs: scientific issues and management consequences for the Great Barrier Reef. Coral reefs, 18(4), 357-367.

McInnes, K. L., Hubbert, G. D., Abbs, D. J., & Oliver, S. E. (2002). A numerical modelling study of coastal flooding. Meteorology and Atmospheric Physics, 80(1-4), 217-233.

McInnes, K. L., Walsh, K. J. E., Hubbert, G. D., & Beer, T. (2003). Impact of sea-level rise and storm surges on a coastal community. Natural Hazards, 30(2), 187-207.

Merrill, R. T. (1984). A comparison of large and small tropical cyclones. Monthly Weather Review, 112(7), 1408-1418.

Mitchell, C., Brodie, J., & White, I. (2005). Sediments, nutrients and pesticide residues in event flow conditions in streams of the Mackay Whitsunday Region, Australia. Marine Pollution Bulletin, 51(1), 23-36.

Mumby, P. J., Hastings, A., & Edwards, H. J. (2007). Thresholds and the resilience of Caribbean coral reefs. Nature, 450(7166), 98-101.

Murakami, H. (2014). Tropical cyclones in reanalysis data sets. Geophysical Research Letters, 41(6), 2133-2141.

Nguyen, K. C., & Walsh, K. J. E. (2001). Interannual, decadal, and transient greenhouse simulation of tropical cyclone–like vortices in a regional climate model of the South Pacific. Journal of Climate, 14(13), 3043-3054.

Oouchi, K., Yoshimura, J., Yoshimura, H., Mizuta, R., Kusunoki, S., & Akira, N. O. D. A. (2006). Tropical cyclone climatology in a global-warming climate as simulated in a 20 km-mesh global atmospheric model: Frequency and wind intensity analyses. Journal of the Meteorological Society of Japan. Ser. II, 84(2), 259-276.

Parker, C. L., Lynch, A. H., Spera, S. A., and Spangler, K. R. (2017b): The Relationship between Tropical Cyclone Activity, Nutrient Loading, and Algal Blooms over the Great Barrier Reef, Biogeosciences Discuss., doi:10.5194/bg-2017-23, in review, 2017.

Parker, C.L., Bruyère, C.L., Mooney, P.A. (2017a) "The Response of Land-Falling Tropical Cyclone Characteristics to Projected Climate Change in Northeast Australia". *In Review* Climate Dynamics.

Peng, M., Xie, L., & Pietrafesa, L. J. (2004). A numerical study of storm surge and inundation in the Croatan–Albemarle–Pamlico Estuary System. Estuarine, Coastal and Shelf Science, 59(1), 121-137.

Pielke Jr, R. A., & Landsea, C. W. (1998). Normalized hurricane damages in the United States: 1925–95. Weather and Forecasting, 13(3), 621-631.

Poloczanska, E. S., Babcock, R. C., Butler, A., Hobday, A. J., Hoegh-Guldberg, O., Kunz, T. J., ... & Richardson, A. J. (2007). Climate change and Australian marine life. Oceanography and marine biology, 45, 407.

Powell, M. D., & Reinhold, T. A. (2007). Tropical cyclone destructive potential by integrated kinetic energy. Bulletin of the American Meteorological Society, 88(4), 513.

Puotinen, M. L. (2007). Modelling the risk of cyclone wave damage to coral reefs using GIS: a case study of the Great Barrier Reef, 1969–2003. International Journal of Geographical Information Science, 21(1), 97-120.

Puotinen, M. M., Done, T. T., & Skelley, W. (1997). An atlas of tropical cyclones in the Great Barrier Reef region: 1969-1997.

Rego, J. L., & Li, C. (2009). On the importance of the forward speed of hurricanes in storm surge forecasting: A numerical study. Geophysical Research Letters, 36(7).

Riahi, K., Rao, S., Krey, V., Cho, C., Chirkov, V., Fischer, G., ... & Rafaj, P. (2011). RCP 8.5—A scenario of comparatively high greenhouse gas emissions. Climatic Change, 109(1-2), 33-57.
Scoccimarro, E., Gualdi, S., Villarini, G., Vecchi, G. A., Zhao, M., Walsh, K., & Navarra, A. (2014). Intense precipitation events associated with landfalling tropical cyclones in response to a warmer climate and increased CO2. Journal of climate, 27(12), 4642-4654.
Shapiro, L. J. (1983). The asymmetric boundary layer flow under a translating hurricane. Journal of the Atmospheric Sciences, 40(8), 1984-1998.
Smith, J. E., Shaw, M., Edwards, R. A., Obura, D., Pantos, O., Sala, E., ... & Rohwer, F. L. (2006). Indirect effects of algae on coral: algae-mediated, microbe-induced coral mortality. Ecology letters, 9(7), 835-845.
Smith, S. V., & Buddemeier, R. W. (1992). Global change and coral reef ecosystems. Annual Review of Ecology and Systematics, 23, 89-118.
Souter, P., Willis, B. L., Bay, L. K., Caley, M. J., Muirhead, A., & Van Oppen, M. J. H. (2010). Location and disturbance affect population genetic structure in four coral species of the genus Acropora on the Great Barrier Reef. Marine Ecology Progress Series, 416, 35-45.
Sriver, R. L., & Huber, M. (2007). Observational evidence for an ocean heat pump induced by tropical cyclones. Nature, 447(7144), 577-580.
Steven, A. D. L., Pantus, F., Brooks, D., & Trott, L. (1998). Long-term chlorophyll monitoring in the Great Barrier Reef Lagoon: status report 1, 1993-1995. Great Barrier Reef Marine Park Authority.
Stieglitz, T. (2005). Submarine groundwater discharge into the near-shore zone of the Great Barrier Reef, Australia. Marine Pollution Bulletin, 51(1), 51-59.
Stoeckl, N., Hicks, C. C., Mills, M., Fabricius, K., Esparon, M., Kroon, F., ... & Costanza, R. (2011). The economic value of ecosystem services in the Great Barrier Reef: our state of knowledge. Annals of the New York Academy of Sciences, 1219(1), 113-133.
Sugi, M., & Yoshimura, J. (2012). Decreasing trend of tropical cyclone frequency in 228-year high-resolution AGCM simulations. Geophysical Research Letters, 39(19).
Sweatman, H. H., Thompson, A. A., Delean, S. S., Davidson, J. J., & Neale, S. S. (2007). Status of near-shore reefs of the Great Barrier Reef 2004.
Sweatman, H., Thompson, A., Neale, S., & Thomson, D. (2006). 5. Inshore Coral Reefs Monitoring.
Tory, K. J., Chand, S. S., McBride, J. L., Ye, H., & Dare, R. A. (2013). Projected changes in late-twenty-first-century tropical cyclone frequency in 13 coupled climate models from phase 5 of the Coupled Model Intercomparison Project. Journal of Climate, 26(24), 9946-9959.
Vecchi, G. A., & Soden, B. J. (2007). Effect of remote sea surface temperature change on tropical cyclone potential intensity. Nature, 450(7172), 1066-1070
Vecchi, G. A., & Wittenberg, A. T. (2010). El Niño and our future climate: where do we stand? Wiley Interdisciplinary Reviews: Climate Change, 1(2), 260-270.
Villarini, G., Lavers, D. A., Scoccimarro, E., Zhao, M., Wehner, M. F., Vecchi, G. A., ... & Reed, K. A. (2014). Sensitivity of tropical cyclone rainfall to idealized global-scale forcings. Journal of climate, 27(12), 4622-4641.
Walsh, K. (2004). Tropical cyclones and climate change: unresolved issues. Climate Research, 27(1), 77-83.
Walsh, K. (2015). Fine resolution simulations of the effect of climate change on tropical cyclones in the South Pacific. Climate Dynamics, 45(9-10), 2619-2631.
Walsh, K. J. E., Nguyen, K. C., & McGregor, J. L. (2004). Fine-resolution regional climate model simulations of the impact of climate change on tropical cyclones near Australia. Climate Dynamics, 22(1), 47-56.

Walsh, K. J., & Katzfey, J. J. (2000). The impact of climate change on the poleward movement of tropical cyclone–like vortices in a regional climate model. Journal of Climate, 13(6), 1116-1132.

Walsh, K. J., & Ryan, B. F. (2000). Tropical cyclone intensity increase near Australia as a result of climate change. Journal of Climate, 13(16), 3029-3036.

Walsh, K. J., McBride, J. L., Klotzbach, P. J., Balachandran, S., Camargo, S. J., Holland, G., ... & Sugi, M. (2016). Tropical cyclones and climate change. Wiley Interdisciplinary Reviews: Climate Change, 7(1), 65-89.

Walsh, K. J., McInnes, K. L., & McBride, J. L. (2012). Climate change impacts on tropical cyclones and extreme sea levels in the South Pacific—A regional assessment. Global and Planetary Change, 80, 149-164.

Weisberg, R. H., & Zheng, L. (2006). Hurricane storm surge simulations for Tampa Bay. Estuaries and Coasts, 29(6), 899-913.

Wolanski, E., Fabricius, K., Spagnol, S., & Brinkman, R. (2005). Fine sediment budget on an inner-shelf coral-fringed island, Great Barrier Reef of Australia. Estuarine, Coastal and Shelf Science, 65(1), 153-158.

8. Figures

Figure 1

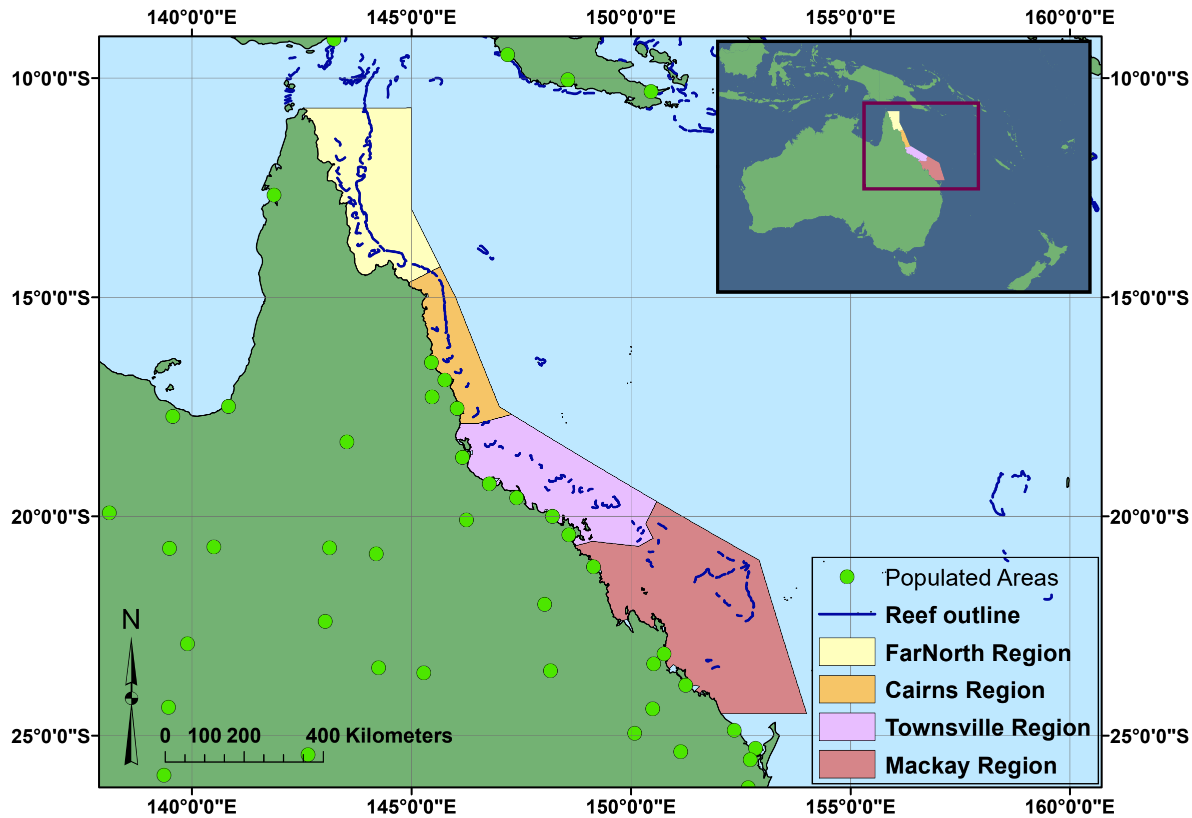

Figure 1: This map demonstrates the location and extent of the Great Barrier Reef on the northeast coastline of Australia. The zoning of the Great Barrier Reef Marine Park and the location of populated areas along the Queensland coastline are also shown here for context.

Figure 2

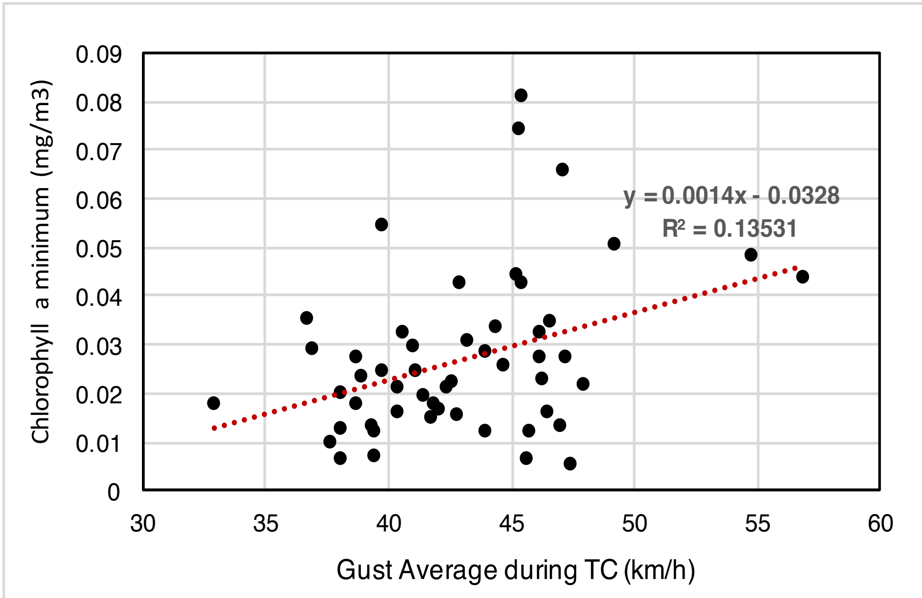

Figure 2: the relationship between the average wind gust during TC activity and the minimum chlorophyll *a* concentrations recorded from satellite data over the whole of the Great Barrier Reef Marine Park over a 10-year period (from results of Parker et al. (2017b)).

Figure 3

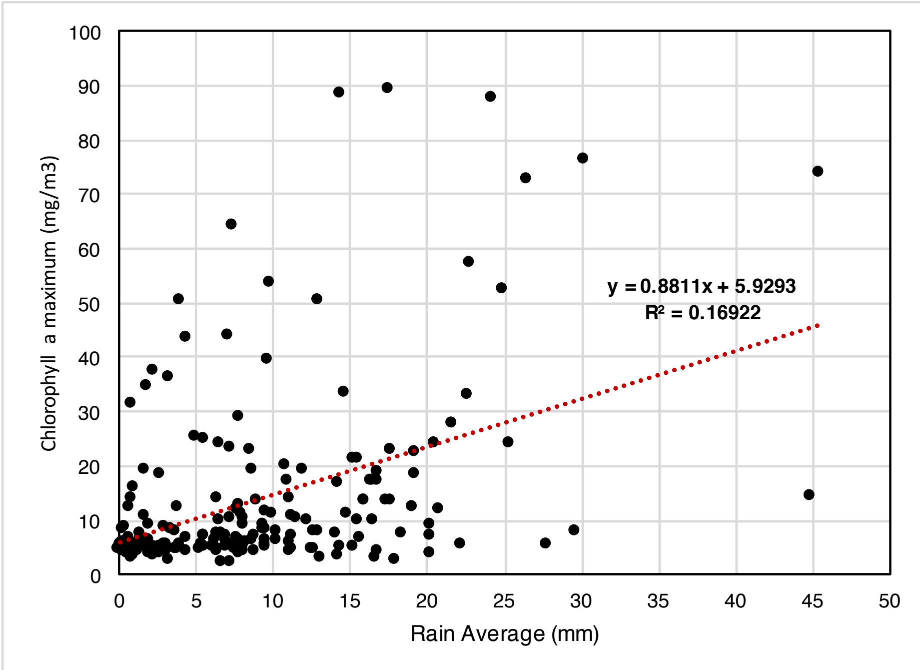

Figure 3: the relationship between the average daily rainfall and the maximum chlorophyll *a* concentrations recorded from satellite data over the whole of the Great Barrier Reef Marine Park over a 10-year period (from results of Parker et al. (2017b)).

Figure 4

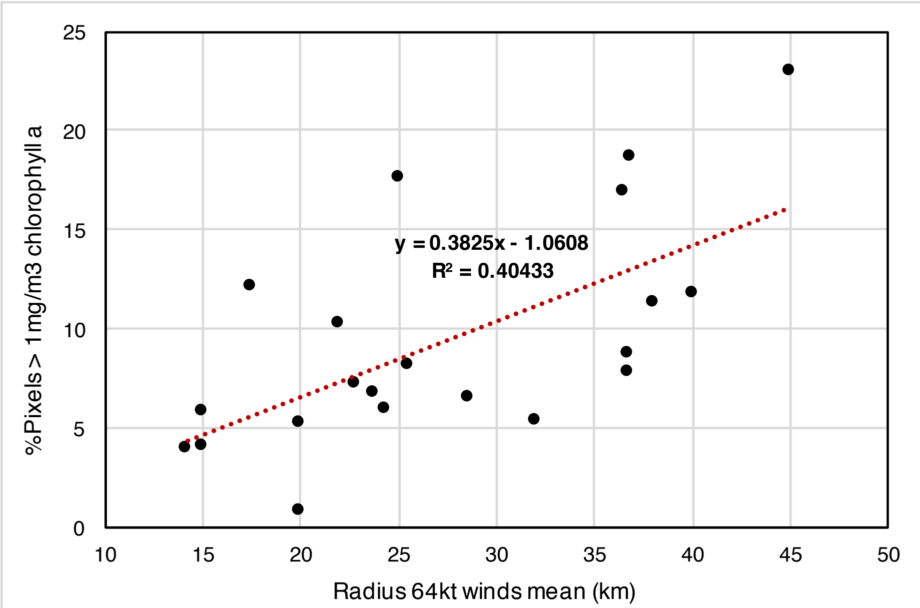

Figure 4: the relationship between the average radius of 64 knot winds (a measure of TC size) and the percentage of observed pixels that are greater than a threshold of $1mg/m^3$ chlorophyll *a* concentration at a 16-day lag from the TC activity. The percentage is calculated from the number of pixels observed from satellite data over the whole of the Great Barrier Reef Marine Park over a 10-year period (from results of Parker et al. (2017b)).

Figure 5

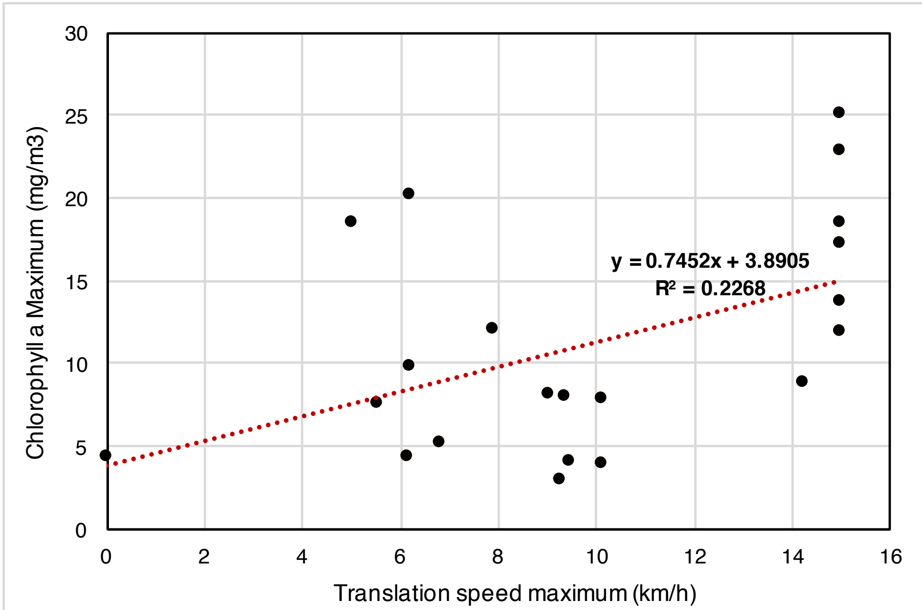

Figure 5: the relationship between the maximum translation speed of a TC and maximum chlorophyll *a* concentration recorded at a 16-day lag from the TC activity. The chlorophyll *a* data is retreived from satellite data over the whole of the Great Barrier Reef Marine Park over a 10-year period (from results of Parker et al. (2017b)).

METHODOLOGY: WEATHER RESEARCH AND FORECASTING MODEL

1. The WRF Model

The Weather Research and Forecasting model (WRF) is developed and maintained by the National Center for Atmospheric Research (NCAR). It is a mesoscale numerical weather prediction system used for research and forecasting. It has two dynamical cores, one for idealized simulations and one for real data cases (Advanced Research WRF [ARW]). The governing equations of dynamical cores control the evolution of resolved fluid-dynamical processes. WRF-ARW uses fully compressible nonhydrostatic equations, terrain-following vertical coordinates, a staggered grid (Arakawa C-grid, where variables such as zonal and meridional wind are recorded at the corners of the grid boxes and variables such as temperature are recorded at the center), and scalar flux conservation (where flux is multiplied by velocity) (Skamarock et al. 2008). This thesis employs the WRF-ARW to explore the dynamics and characteristics of case study tropical cyclones that affected the Queensland coastline of Australia.

WRF is competitive in the analyzing and predicting tropical cyclones and is especially appropriate for simulating trajectories and intensities, compared to other operational forecasts (Davis et al. 2008; Bassill 2014). WRF is able to simulate asymmetries within the cyclone and spiral bands (Done et al. 2013), and when configured at fine horizontal grid spacing, can capture important processes in the eyewall (Gentry and Lackmann 2010) such as eye-eyewall mixing events, and secondary eyewall formation (Abarca and Corbosiero 2011). However, the model has demonstrated excessive intensification prior to landfall, insufficient momentum exchange with the surface, and struggles to capture periods of rapid intensification (Davis et al. 2008).

These problems suggest that there are still improvements to be made for the simulation of tropical cyclones with WRF.

The WRF model has great flexibility in terms of user-defined options such as horizontal and vertical resolution, domain size, nesting, input data for boundary and initial conditions, and physical parameterizations. This flexibility enables WRF to be tailored to fit the research question at hand and improve the simulation of the feature of interest. Conversely, the vast number of options may be a drawback as initial model set up can become complex and large amounts of time and computational resources can be invested in tailoring and fine-tuning the model. As a regional model, WRF is more computationally efficient than global, general circulation models. Numerous simulations can be carried out at high resolutions relatively easily, making WRF ideal for analyzing tropical cyclones, which cannot be resolved by coarser global models (Walsh et al. 2016). However, in the regional model configuration, WRF requires lateral boundary conditions as well as initial conditions. Simulations are therefore constrained by the availability and accuracy of prior forecasts, reanalysis data, or simulations from global models.

As has been suggested, understanding and learning to use the WRF model efficiently has a steep learning curve. In order to complete this thesis, a large number of simulations to explore, test, and fine-tune the model for simulating TCs in the western South Pacific / Queensland area were necessary. Much of this preliminary work does not feature in Chapters 2 and 3, as it is not well-suited for publication. To preserve a record of this preliminary work, it is documented here. While the following discussion does not include an exhaustive list of all the simulations run, it demonstrates the range of WRF parameters explored and tested to facilitate the resulting Chapters of this thesis.

2. Domain and Simulation Configuration

The first configuration for simulating cyclones in the western South Pacific consisted of one relatively narrow domain, with 45km horizontal resolution, and a simulation time of 18 days (to capture the lifecycles of tropical cyclones Anthony and Yasi that occurred in January of 2011). We then tested a wider domain to include a broader field of the large-scale flow and the area of genesis around Fiji, particularly to improve the simulated trajectories. This domain configuration was then used to conduct a 57-day simulation to explore tropical cyclone activity produced by the model over ~2 months, and a 10-day simulation to focus on the simulation of intense cyclone Yasi alone. The representation of Yasi in the WRF simulation was poor in terms of intensity and trajectory, and detailed analyses revealed a number of causes. (1) The simulation was initialized before the system's genesis resulting in an initial condition problem for the model, (2) the horizontal resolution of 45km was too coarse to resolve important processes and characteristics of tropical cyclones, and (3) the input data (NCEP data see Table 2) was also at a coarse resolution and could have presented a boundary and initial condition problem for the simulation. In response to these findings, we tested a wider domain, with 36km horizontal grid spacing and a nested domain of 12km grid spacing, a higher resolution input dataset (see Table 2), and a simulation time of 4-days (beginning after cyclogenesis). The simulation time focuses on the intensification and landfall portion of the TC's lifecycle. A configuration with a third domain nested within the second (with a grid spacing of 4km) was also tested. This configuration did not significantly improve the simulation. Therefore, we decided that it was more computationally efficient to continue with a 2-domain configuration at 36 and 12km resolutions. Nesting is necessary so that the low-resolution outermost domain can be large enough to capture large-scale flow, while the high-resolution innermost domains can be smaller and be bounded by the area of interest. This nested approach significantly reduces computation time while preserving the ability to resolve processes of interest. Nesting is also necessary to reduce the resolution gradient between the resolution of the input data and the inner most nest.

For cyclone Ita (April 2014) we tested two initialization times and simulation durations and two different domain sizes to explore the effect on the simulation. For cyclone Marcia (February 2015) we also tested two different simulation lengths to find the necessary time period to capture intensification and landfall of the event. A summary of these configuration tests and changes are shown in Table 1.

Cyclone Case	Number of Domains	Resolution (km)	Longitudinal Extent of D01	Latitudinal Extent of D01	Simulation Length (days)
Yasi	1	45	140°E - 175°E	10°S - 29°S	18
Yasi	1	45	138°E - 176°W	0° - 29°S	18
Yasi	1	45	138°E - 176°W	0° - 29°S	57
Yasi	1	45	138°E - 176°W	0° - 29°S	10
Yasi	2	36/12	112°E - 171°W	8°N - 37°S	4
Yasi	3	36/12/4	112°E - 171°W	8°N - 37°S	4
Ita	2	36/12	115°E - 168°W	22°N - 47°S	5
Ita	2	36/12	115°E - 168°W	22°N - 47°S	4
Ita	2	36/12	113°E - 152°W	20°N - 38°S	5
Marcia	2	36/12	98°E - 171°W	20°N - 55°S	5
Marcia	2	36/12	98°E - 171°W	20°N - 55°S	3

Table 1: the domain and simulation configurations tested and utilized for this thesis.

Additionally, we explored the effect of vertical resolution on the simulation by testing different numbers (27, 33, 35, 55, 56) of vertical levels, as well as the distribution of those levels within the atmosphere. We also tested the use of damping, smaller time steps and adaptive time stepping when the model encountered Courant-Friedrichs-Lewy

(CFL) errors, fine input stream for data input into the WRF model, and Digital Filter Initialization to fully balance the wind fields at the initial time before the full simulation.

We began our model set up and fine-tuning in Spring 2012 with the latest version of WRF, version 3.4.1. However, an updated version of WRF is released ~ every 6 months. In June 2015, we ran test simulations in WRF version 3.6.1, but after several problems decided to continue with v3.4.1 for ease and continuity for the simulations in this thesis. We do not anticipate that the WRF model version has a significant effect on the overall results in the chapters of this thesis.

3. Boundary and Initial Condition Data

Preliminary simulations used the NCEP/NCAR reanalysis-1 data (Kalnay et al. 1996) that is available at 6 hourly intervals, 17 pressure levels, and 2.5°x2.5° horizontal grid resolution as input data for boundary and initial conditions. We also tested simulations where we increased the sea surface temperature (SST) field in the NCEP boundary data by +1, +2, +2.5°K in the WRF pre-processing stage to explore the response of the cyclones to increases in thermal energy from the ocean surface. As mentioned in Section 2, analysis demonstrated that the simulation of tropical cyclone Yasi could have been improved by using an input data set with higher resolution that provides more detail and structure of the cyclone for the boundary conditions. Therefore, we transitioned to using the European Centre for Medium-Range Weather Forecasts (ECMWF) Re-Analysis Interim (ERA-I) data set (Dee et al. 2011) as input data for boundary conditions. ERA-I data are available at 6-hour intervals, with 0.7° horizontal grid resolution, and 37 atmospheric pressure levels. We found significant improvement in the simulations and proceeded with ERA-I as the input data. Our analysis revealed that SST values lag the atmospheric variables in the ERA-I reanalysis data set by 30-hours. Therefore, we reprocessed the input data in the WRF pre-processing stage to create new forcing files to explore the response of the cyclone simulation to the fixed SST lag.

We found that simulations of Yasi's intensity were still lacking in this domain with ERA-I boundary condition (see Chapter 2 for full discussion). Therefore, we utilized the high-resolution blended microwave optimally interpolated SST product (REMSS) (REMSS 2013) as an auxiliary SST data set to replace the SST variable of the ERA-I boundary conditions. The REMSS is a daily data set with 9km horizontal resolution and again we reprocessed the input data in WRF pre-processing to incorporate this auxiliary data to create new forcing files for the WRF simulation. The inclusion of this SST dataset increased simulated intensity slightly (see Chapter 2 for full discussion). We also tested scenarios with the REMSS SST boundary alter by +1°K over the whole domain or just in the coastal region to explore the response of the cyclone to increased thermal energy and to steep SST gradients towards landfall. A summary of the input data used to create the boundary for the WRF simulations is given in Table 2.

Data Source	Resolution	Variables	Additional modification
NCEP	2.5° x 2.5°	ALL	SST +1, +2, +2.5°K across domain
ERA-I	0.7° x 0.7°	ALL	SST 30-hour time lag corrected
REMSS	9km x 9km	SST	SST +1°K across domain. SST +1°K in the coastal region

Table 2: details of the input data sources for boundary conditions and any additional modification tested.

In addition to boundary condition manipulations, we tested two methods of initialization (as discussed in detail in Chapter 2). In the first method, the reanalysis dataset (either NCEP or ERA-I) provided both the boundary and initial conditions for the simulation. Then we tested the incorporation of a high-resolution initial condition from the tropical cyclone operational forecast model: Australian Community Climate and Earth System Simulator-Tropical Cyclone (ACCESS-TC) (Puri et al. 2010, 2013; Davidson et al. 2014). The data is at one time step for initialization and has 0.11° horizontal grid spacing and 50 vertical levels. We reprocessed the input data in WRF pre-processing to blend this data with the ERA-I data for a new initial condition forcing file for the full WRF simulation. This initialization approach improved the simulation of Yasi, particularly the intensity (see Chapter 2 for a full discussion).

4. Physical Parameterisations

Previous studies have established that tropical cyclone simulations in WRF are sensitive to the physical parameterizations chosen. After optimizing the domain set up and boundary and initial condition data for the simulations, we tested the simulation sensitivity to a variety of combinations of physical parameterizations. We varied the cumulus parameterization, the microphysics scheme, the planetary boundary layer, the radiation schemes, the surface flux with the ocean, and the representation of the SST during the simulation. The full range of options tested is shown in Table 3 and discussed in detail in Chapter 2.

Cumulus Parameterisation	Microphysics Scheme	Planetary Boundary Layer	Radiation Scheme	Surface Flux	Sea Surface
None (CU0)	None (CU0)	None (CU0)		None	Fixed
Kain Fritsch (CU1)	Kessler (MP1)	YSU (PBL1)	Dudhia Shortwave (SW1) RRTM Longwave (LW1)	Surface flux coefficient (ISFTCFLX)	SST Updating
Betts Miller Janjic (CU2)	WSM 5-class (MP4)	MYNN 2.5 level TKE closure (PBL5)	RRTMG shortwave (SW1) and longwave (LW1)		1D Ocean Mixed Layer (OML)
Grell Devenyi Ensemble (CU3)	Ferrier new eta (MP5)				
Grell 3D Ensemble (CU5)	WSM 6-class graupel (MP6)				
Tiedtke (CU6)	Thompson (MP8)				

Table 3: the schemes and parameterizations tested for simulating tropical cyclones in the western South Pacific.

5. Climate Downscaling

While tropical cyclone simulations with manipulated SSTs were interesting to explore, they do not represent the total possible change to the environment with climate perturbation in the future. Changes to factors such as wind shear and atmospheric temperature and moisture would also influence tropical cyclone development and intensification. Therefore, we decided to include the predicted changes to all variables in the future climate in the boundary conditions of the WRF simulations and examine the response of the cyclones. We used a pseudo global warming technique where the future climate scenario required a climate change delta to be added to the boundary and initial conditions of the current climate tropical cyclone simulations.

To create the climate delta, WRF pre-processing was run with 6-hourly input data from the Community Earth System Model (CESM Bruyère et al. 2014; Monaghan et al.

2014) for 1 month, 30 times with present-day input data (for years 1976-2005), and again with the future climate predicted by the Representative Concentration Pathway 8.5 (for the years 2071-2100). This was repeated for the domain set up for each of the cases, resulting in a total of 180 pre-processing runs. The present-day months were averaged and subtracted from the average of the future months creating a 3-dimensional delta for each of the climate variables. These deltas were then added to their corresponding variables in the present-day boundary and initial condition data for each case to create the WRF forcing files for the future scenario. For a full description of the pseudo global warming method, see Chapter 3.

From a series of errors, we developed a number of extra steps in this methodology. The CESM land mask was coarser than the mask in the ERA-I data which presented a problem for adding the delta to the boundary conditions. We edited the WRF variable tables and the pre-processing method to interpolate the CESM SST data up to a new ERA-I constant land mask before the pre-processing described above could occur. Furthermore, the present-day forcing files produced with ERA-I have 38 vertical levels, but the CESM delta fields have only 27 vertical levels. Therefore, we interpolated the delta fields to 38 vertical levels so that they could be added to the ERA-I fields to create new future scenario forcing files.

Additionally, we had to manually alter the coded CO_2 concentration values in the longwave and shortwave radiation modules from 379 to 935ppm. Then the dynamical core was recompiled before WRF simulations could be run. We did conduct extra simulations with the climate change delta forcing but with present day CO_2 levels and present day climate boundary conditions but future CO_2 concentrations to assess the sensitivity of cyclone simulation to the CO_2 concentration change alone (Table 4). The variation was minor and the response to the climate delta was much greater.

A number of climate delta scenarios were explored with tropical cyclone Ita (April 2014) to understand its trajectory deviation in the future climate (see Chapter 3 for discussion of trajectory change). Simulations were conducted where (1) the April delta was added to the boundary conditions; (2) April delta was added without any delta in the wind variables; (3) April delta was added without any delta in the SST; (4) January delta fields were added; and (5) no climate change delta was added but SST perturbation of +1°, 2°, and 3°K we added respectively. Table 4 shows a full range of delta scenarios tested.

Cyclone Case	Delta Month Applied	Applied to Domains	Delta Variables applied	CO_2 Concentration (ppm)
Yasi	January	D01	ALL	935
Yasi	January	D01 / D02	ALL	935
Yasi	January	D01 / D02	ALL	379
Yasi	None	None	None	935
Ita	April	D01 / D02	ALL	935
Ita	April	D01 / D02	ALL except wind	935
Ita	April	D01 / D02	ALL except SST	935
Ita	January	D01 / D02	ALL	935
Ita	SST +1,+2,+3°K	D01 / D02	Just SST	935
Marcia	February	D01 / D02	ALL	935

Table 4: the delta and model combinations tested to explore the cyclone response to possible future scenarios.

6. Summary

For our research questions, we utilized a regional model for computational efficiency and to use horizontal grid spacing appropriate for resolving tropical cyclone processes. We chose the WRF model given its demonstrated skill in tropical cyclone simulation and the computational support provided by NCAR. In order to optimize WRF simulations of case study tropical cyclones that affected the Queensland area of Australia, we conducted a number of exploratory simulations. We tested geographical extent of the domain, the horizontal and vertical grid spacing, the use of nesting, damping, adaptive time stepping, and digital filter initialization. We also tested the simulation sensitivity to the resolution of the data sets used to create boundary and initial conditions and the physical parameterization schemes. After this preliminary work, we found a simulation configuration suitable for analyzing cyclone systems in the area and could examine their response to climate change. The pseudo global warming technique to create a future climate scenario required a large number of WRF pre-processing runs and interpolation methods to add a climate change delta to the boundary and initial conditions of the current climate simulations. This technique allowed us to investigate the response of tropical cyclone-like vortices of the present day to possible future changes to environmental conditions.

7. References

Abarca, S. F., & Corbosiero, K. L. (2011). Secondary eyewall formation in WRF simulations of Hurricanes Rita and Katrina (2005). Geophysical Research Letters, 38(7).

Bassill, N. P. (2014). Accuracy of early GFS and ECMWF Sandy (2012) track forecasts: Evidence for a dependence on cumulus parameterization. Geophysical Research Letters, 41(9), 3274-3281.

Bruyère, C. L., Done, J. M., Holland, G. J., & Fredrick, S. (2014). Bias corrections of global models for regional climate simulations of high-impact weather. Climate dynamics, 43(7-8), 1847-1856.

Davidson, N. E., Xiao, Y., Ma, Y., Weber, H. C., Sun, X., Rikus, L. J., ... & Fraser, J. (2014). ACCESS-TC: Vortex specification, 4DVAR initialization, verification, and structure diagnostics. Monthly Weather Review, 142(3), 1265-1289.

Davis, C., Wang, W., Chen, S. S., Chen, Y., Corbosiero, K., DeMaria, M., ... & Reeves, H. (2008). Prediction of landfalling hurricanes with the Advanced Hurricane WRF model. Monthly Weather Review, 136(6), 1990-2005.

Dee, D. P., and Coauthors, (2011): The ERA-Interim reanalysis: Configuration and performance of the data assimilation system. Quart. J. Roy. Meteor. Soc., 137, 553–597.

Gentry, M. S., & Lackmann, G. M. (2010). Sensitivity of simulated tropical cyclone structure and intensity to horizontal resolution. Monthly Weather Review, 138(3), 688-704.

Kalnay, E., Kanamitsu, M., Kistler, R., Collins, W., Deaven, D., Gandin, L., ... & Zhu, Y. (1996). The NCEP/NCAR 40-year reanalysis project. Bulletin of the American meteorological Society, 77(3), 437-471.

Monaghan, A. J., D. F. Steinhoff, C. L. Bruyere, and D. Yates. 2014. NCAR CESM Global Bias-Corrected CMIP5 Output to Support WRF/MPAS Research. Research Data Archive at the National Center for Atmospheric Research, Computational and Information Systems Laboratory. http://dx.doi.org/10.5065/D6DJ5CN4. Accessed† 01 Jul 2015

Puri, K., Dietachmayer, G., Steinle, P., Dix, M., Rikus, L., Logan, L., ... & Bermous, I. (2013). Implementation of the initial ACCESS numerical weather prediction system. Aust. Meteorol. Oceanogr. J, 63, 265-284.

Puri, K., Xiao, Y., Sun, X., Lee, J., Engel, C., Steinle, P., ... & Bowen, R. (2010). Preliminary results from Numerical Weather Prediction implementation of ACCESS. CAWCR Research Letters, 5, 15-22.

REMSS (2013) accessed September 1 2013 [http://www.remss.com/sst/microwave_oi_sst_data_description.html]

Skamarock, W. C., Klemp, J. B., Dudhia, J., Gill, D. O., & Barker, D. M. (2005). Coauthors, 2008: A description of the Advanced Research WRF version 3. NCAR Tech. Note NCAR/TN-475+ STR, 113.

Walsh, K. J., McBride, J. L., Klotzbach, P. J., Balachandran, S., Camargo, S. J., Holland, G., ... & Sugi, M. (2016). Tropical cyclones and climate change. Wiley Interdisciplinary Reviews: Climate Change, 7(1), 65-89